Simulations of semiconductor laser using non-equilibrium Green's functions method

by

Jacek M. Miloszewski

A thesis
presented to the University of Waterloo
in fulfillment of the
thesis requirement for the degree of
Doctor of Philosophy
in
Physics

Waterloo, Ontario, Canada, 2012

I hereby declare that I am the sole author of this thesis. This is a true copy of the thesis, including any required final revisions, as accepted by my examiners.

I understand that my thesis may be made electronically available to the public.

Acknowledgements

My foremost acknowledgments go out to Dr. Marek Wartak, my thesis adviser, for inviting me to work with him and giving me the opportunity to develop this project. His help, patience, and support over the past four years are invaluable. I would also like to express my gratitude to Peter Groszkowski and Benjamin Wales for all the helpful comments to the first draft of this thesis.

Special thanks go to my my wife, parents, and sister. None of this would be possible without their faith in me, support, and love.

Abstract

A novel method of simulating edge-emitting semiconductor lasers in a non-equilibrium steady-state is developed. The simulation is based on a non-equilibrium Green's function (NEGF) method. The Dyson equation (central equation of this method) is derived and written in a basis suitable for numerical implementation. The electron-photon self-energy is derived form scratch for the case of the edge-emitting laser. Other interactions present in the simulation are phenomenological scattering and scattering due to longitudinal optical phonons. This microscopic approach significantly reduce the number of phenomenological parameters needed to simulate laser. As an example, the theory is applied to analyze quantum well laser with the effective mass Hamiltonian. The major laser characteristics such as modal gain, threshold gain, carrier and current densities are determined.

Table of Contents

Acknowledgements **iii**

Abstract **iv**

1 Introduction **1**
1.1 Motivation 1
1.2 Outline 3

2 Laser diodes **4**
2.1 Principles of semiconductor lasers 4
2.1.1 Semiconductors 4
2.1.2 Laser structure overview 5
2.1.3 Fundamentals of laser action 6
2.2 Other types of laser diodes 11
2.3 Overview of the semiconductor laser simulators 12
2.3.1 Basic components 12
2.3.2 Selected list of currently developed commercial simulators . . 13

3 Non-equilibrium Green's functions (NEGF) **15**
3.1 Preliminaries 16
3.1.1 Heisenberg and interaction pictures 16
3.1.2 Time contour 18
3.2 Definition of the NEGF 20
3.3 The Dyson equation 21
3.3.1 Hamiltonian of the system 22
3.3.2 Equation of motion for contour Green's function 25
3.3.3 Functional derivative approach 27
3.3.4 Static ion lattice, ionized impurities, and phonons 35

4 Application of NEGF to a laser diode **37**
4.1 Description of the system 37
4.2 The real-time Dyson equation in discrete basis 38
4.2.1 The Dyson equation for real-time functions 38
4.2.2 Discrete basis and temporal Fourier transform 41
4.2.3 Discretization of the Dyson equation 42
4.3 Quasiparticles and physical observables 45

4.3.1 Conduction and valence bands . . . 45
4.3.2 Charge and current densities . . . 47
4.3.3 Current conservation and power absorption/emission. . . . 48
4.4 Self-energies . . . 49
4.4.1 Electron-photon scattering . . . 50
4.4.2 Electron-phonon scattering . . . 58
4.4.3 Golizadeh scattering . . . 58

5 Numerical implementation **60**
5.1 Numerical grids of position, energy, and wavevector . . . 60
5.2 General structure of the code . . . 63
5.3 Method of solving the Poisson equation . . . 63
5.4 Application of bisection to an unstable photon Green's function loop 65
5.5 Convergence criteria and numerical simplifications . . . 66

6 Sample results and conclusions **69**
6.1 System without phonons . . . 69
6.2 System with phonons . . . 75
6.3 Summary . . . 77
6.4 Further development . . . 79

A Pictures of quantum mechanics **81**
A.1 Time evolution operators . . . 81
A.2 Interaction and Heisenberg pictures . . . 84

B Contour algebra **86**

C Functional derivative technique **92**
C.1 Functional derivatives of Green's function over external sources . . . 92
C.2 Derivation of the longitudinal self-energy and related terms . . . 94
C.3 Derivation of the transverse self-energy and related terms . . . 96

D Boundary self-energies **99**

E Polarization and electron-photon self-energy **109**
E.1 Transverse polarization . . . 109
E.2 Transverse (electron-photon) self-energy . . . 111

F List of publications **115**
F.1 Peer reviewed publications . . . 115
F.2 Conference proceedings . . . 115

Bibliography **115**

Chapter 1

Introduction

1.1 Motivation

Semiconductor lasers, also known as laser diodes, are an important part of modern devices. Because of their small manufacture costs and miniature size they are perfect choice for mass-produced optoelectronics. A mounted, ready for sale, laser diode has a typical size of only few millimeters, power output ranging from milliwatts to a couple of watts, and price somewhere between one and a few hundred dollars. Laser diodes have literally hundreds of applications. Probably the most widely known application of laser diodes is their use in optical drives (CD, DVD, Blue-ray) where they are utilized for either data reading by measuring their reflection, or to data writing by heating up organic dye layer. Other examples of applications of laser diodes are in oral surgery, where the laser is used to cut soft tissue, or in laser absorption spectrometry, which allows one to measure concentration of particles of particular substances in different gaseous mixtures. However, perhaps their most crucial application is in fiber-optic communications. Because semiconductor laser's signal is easily modulated by a changing voltage, it is an irreplaceable element of any fiber-optic network, as an electrical to optical signal transmitter.

Laser diodes have been in commercial production for many years. Currently, a variety of lasers are available with wavelengths ranging from 400 nm to over 2600 nm. The constantly changing electronics and telecommunication markets require development of new devices and improvement of already produced lasers to be more reliable, efficient, and cheaper in production. One of the major factors that affect the price of a final product is the cost of research and design. Although engineers have gathered extensive experience over the years and the fundamental physics sufficient to describe all relevant processes is already known, the physical processes in the nano-scale devices are so complex that until very recently it was almost impossible to predict device's properties before building a prototype.

First simulators provided only most basic quasi-classical calculations which were enough for larger devices (hundreds of nanometers). Quick technological progress in manufacturing technologies allowed to construct much smaller (a few nanometers) and more complex devices which require more detailed, fundamental physical models.

Almost all up-to-date simulators are based on quasi-classical methods with some

quantum corrections accounting for most crucial quantum effects. The most popular simulation technique is the drift-diffusion method. This method is derived from the Boltzman transport equation [1, 2] using the momentum expansion [3, 4]. It has been successfully used to simulate variety of lasers: heterostructure lasers [5, 6, 7, 8], quantum well lasers [9, 10, 11, 12, 13, 14, 15, 16, 17, 18], distributed feedback lasers [19, 20, 15], and surface emitting lasers [21, 22, 23].

Although computationally fast, these simulators have many disadvantages. Because they are not based on the microscopic theories, they require a huge number of experimental parameters and some of those parameters are very hard to estimate theoretically and even harder to measure experimentally. For example, Auger and radiative recombination rate parameters are available only for few III-V semiconductor materials and most of their values are 20 to 30 years old [24]. Additionally, different sources provide values for the same substance which differ even by two orders of magnitude.

Another very serious disadvantage of the most common laser simulators is the gain calculation method [25, 26, 27, 28]. Because the stimulated emission is a quantum mechanical effect, classical theory cannot be used to calculate it. Instead, the gain is calculated by solving the equilibrium quantum well problem with quasi-Fermi levels determined from the drift-diffusion equations. The gain calculated in this way has a lot of shortcomings. During the gain calculation, it is assumed that the bandedge profile is flat, while in reality it is not. When the real bandedge profile is much different form the flat band, there is a significant shift of energy levels inside the quantum well. Another problem is that this method forces artificial distinction between 2-D carriers inside quantum well and 3-D carriers outside of the well. This is very problematic when there is a large carrier concentration inside the well and the carriers occupy states near the top of the quantum well or in the barriers. Finally, the drift-diffusion assumes a parabolic, effective mass Hamiltonian, while the gain is usually calculated with many-band non-parabolic $\mathbf{k} \cdot \mathbf{p}$ Hamiltonians [29, 30, 31].

A promising answer to the demand for more precise modeling of optoelectronic devices is a quantum many-body theory tool called non-equilibrium Green's functions method (NEGF). The non-equilibrium Green's functions method has been used to successfully model resonant tunneling diodes (RTDs) [32, 33, 34, 35, 36, 37, 38], molecular junction [39], metal-oxide-semiconductor field-effect transistors (MOSFETs) [40, 41, 42, 43, 44], carbon nanotubes (CNTs) [45, 46, 47, 48], photodetectors [49, 50], light emitting diodes (LEDs) [51], and solar cells [52]. As for the lasers, NEGF method has been applied in [53, 54, 55] to calculate some properties of the laser, and by [56] to describe a special case of a quantum cascade laser. NEGF technique was also indirectly used in [57, 58] to obtain the quantum Boltzman equation for the case of an edge-emitting laser.

In this method instead of wavefunctions or density matrix, one uses Green's functions which essentially carry less information about the system but still allow for a calculation of statistical average value of any given operator. At the cost of a loss of some information, one gains the possibility for perturbative inclusion of many-body interactions such as electron-electron interaction, electron-photon interaction, etc. Contrary to the quasi-classical approaches mentioned before, NEGF allows

one to introduce many-body interactions directly from a microscopic theory instead of modeling them with semi-empirical functions and parameters. Fundamentals of this theory were developed in 1960's [32, 59, 60, 61, 62]. At that time, the huge computational power demanded by this method made it completely impractical. Using current technology it is possible to implement NEGF to accurately model semiconductor devices at small scale in equilibrium and under static non-equilibrium conditions such as steady-state current flow.

In this thesis, NEGF technique is applied to the so called semiconductor edge emitting lasers to calculate crucial characteristics such as material gain and voltage-power relationship.

1.2 Outline

In Chapter 2, a general theory of semiconductor laser is presented together with a short description of different types of semiconductor lasers, emphasizing edge emitting lasers.

Chapter 3 introduces the idea of time contour and the non-equilibrium Green's function is defined on a time contour. The Dyson equation is formally derived using functional derivative technique. Equations for Green's function and self-energies responsible for many-body interactions are obtained in very abstract, but general form.

In Chapter 4 the Dyson equation is written in discrete basis suitable for numerical implementation and formulas connecting Green's functions to crucial physical observables are derived. Final equations are provided for all relevant self-energies.

Chapter 5 contains description of the numerical implementation. The general structure of the code is presented in form of a flow diagram. A method of creating accurate numerical meshes for position, energy, and wavevector is discussed as well as convergence criteria and range of various numerical parameters.

In the final chapter, the code is used to simulate a sample single-well $Al_{0.2}Ga_{0.8}As/GaAs$ semiconductor laser. Calculations are performed for two different cases: system without phonons and system with phonons. The chapter ends with conclusions concerning accuracy and applicability of the simulator described in this work and plans for the future development.

Throughout this thesis it is assumed that the reader is familiar with fundamental concepts of non-relativistic quantum mechanics [63] and solid state physics [1].

Chapter 2

Laser diodes

This chapter presents the basic principles of laser action. It provides a short introduction to the theory of semiconductor laser diodes based on $p-i-n$ junction and describes most important laser types.

The first section contains a brief description of semiconductors and explains why they are suitable for laser manufacturing. It describes major features of an Fabry-Perot edge-emitting laser design such as formation of a $p-i-n$ junction, waveguiding effect, and mirror facets. The light generation process due to stimulated emission is explained and the idea of material gain is introduced. The section ends with a simple derivation of lasing conditions (for both phase and amplitude of the wave) and a brief discussion of emission characteristics below and above threshold.

The second section explains motivation behind construction of more complex lasers than the simple Fabry-Perot edge-emitting laser introduced in the first section. The general structure of few lasers using Bragg reflectors is shown.

The third section of this chapter provides a short overview of the currently used simulators.

2.1 Principles of semiconductor lasers

2.1.1 Semiconductors

Semiconductors are a subcategory of insulators – in the absolute zero temperature they do not conduct electrical current because all bands are either completely filled or completely empty [1]. The major criteria which is used to distinguish semiconductors from all other insulators is a small bandgap – forbidden energy between top of the highest filled band (valence band) and bottom of the lowest empty band (conduction band). The commonly accepted bandgap value below which the insulator is called semiconductor is 4 eV. Because of the bandgap, when the electrons move between bands they either emit photon (when moving from the conduction to the valence band) or absorb photon (when jumping from the valence to the conduction band). Because the bandgap is small, the emitted or absorbed photons are usually in the visible spectrum which makes semiconductors perfect for application as lasers and photodetectors.

Another crucial property of semiconductors is the possibility of changing the number and type of conduction carriers (electrons and holes) by introducing particular impurities (doping) to the crystal [1, 30, 64]. These doped semiconductors are generally known as extrinsic while undoped are called intrinsic. There are two kinds of dopants: donors and acceptors. The donor dopants release additional electrons to the conduction band, while the acceptor dopants absorb electrons from the valence band, which effectively creates holes in the valence band.

Introduction of the doping allows one to increase the number of carriers and significantly improve conductivity if there is not enough thermally excited carriers. Because the activation energies of the dopants are located very close to the bandeges, the dopants release a significant number of additional electrons or holes even in low and moderate temperatures (such as the room temperature). Additionally, manipulation with doping allows for creation of materials where electrons are dominant conduction carriers (n-type) and materials where holes are predominant carrier type (p-materials). Those two properties – small bandgap and a possibility to manipulate with type and quantity of current carriers, allow to build an extraordinary number of electronic and optoelectronic devices such as $p-n$ diodes, transistors, laser diodes, light emitting diodes, and optical amplifiers.

2.1.2 Laser structure overview

There are four major mechanisms in which carriers may move between the conduction and valence bands. These mechanisms are: spontaneous emission, stimulated emission, absorption, and non-radiative transitions form which the most dominant are defect and impurity recombination (Shockley-Read-Hall) [65, 66], and Auger [67, 68, 69] recombination. A laser utilizes stimulated emission effect: photon interacts with electron-hole pair forcing its recombination and generation of another, identical photon. The process repeats itself and the photon number grows exponentially. However for lasing action to occur, a number of conditions have to be satisfied.

It is necessary that a semiconductor material in which the electron-hole pairs are located has a direct bandgap: the bottom of the conduction band has to be at the same point of the first Brillouin zone as the top of the valence band. The majority of electrons and holes are located close to minimums of the valence and conduction bands in momentum space. Because in all recombination processes momentum has to be conserved, photon's momentum must be equal to the difference between electron's and hole's momentum. When the conduction band and the valence band are located in different points of the first Brillouin zone, the momentum difference between them is much larger than photon's momentum from the visible spectrum and the emission/absorption cannot occur.

The electron-hole pairs have to be localized in the same region of the real space (inversion of states) and because every photon created by stimulated emission causes electron-hole pair to recombine, there has to be a mechanism to sustain inversion of states. Modern laser didoes are in general $p-n$ junctions with a quantum well structure sandwiched in between p-doped and n-doped materials. The quantum well

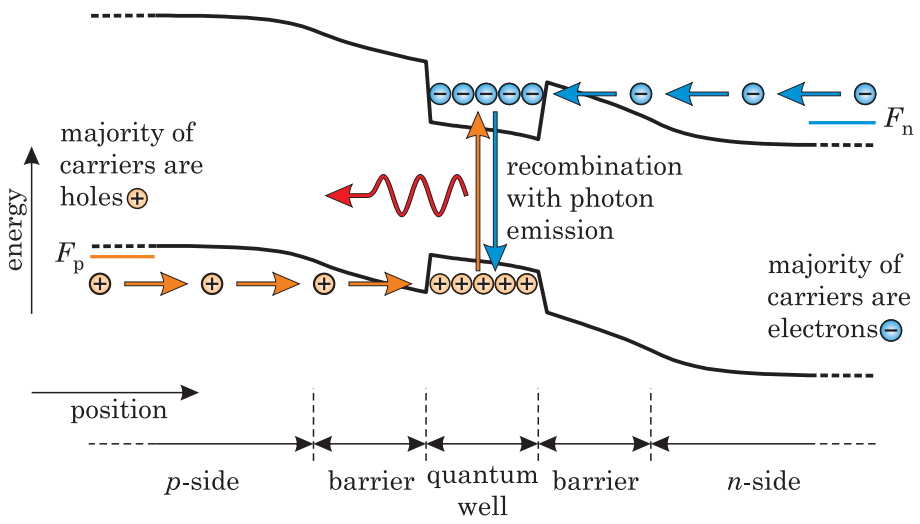

Figure 2.1: A bandedge diagram of a forward biased $p-n$ junction with a quantum well. At p-side, due to acceptor dopants, the quasi-Fermi level F_p is close to valence band edge and carriers are predominantly holes. Similarly, at n-side, F_n is close to the conduction band edge and the conduction is dominated by the electrons. Quantum well traps both types of carriers in a small space allowing for recombination to occur.

consists of a very thin (5-10 nanometers) active layer placed in between two barriers which are made of material with a higher bandgap value than the active layer. This structure ensures that when a $p-n$ junction is connected to an external bias, holes flowing from the p-side and electrons form the n-side are both trapped in the central active layer creating inversion of states and a constant current flow sustains inversion of states regardless of the ongoing stimulated emission. Figure 2.1 shows bandedge (energy at $\mathbf{k}=0$) diagram of $p-n$ junction with quantum well.

Part of electromagnetic wave has to be reflected back into the device to assure sufficient number of photons to support the stimulated emission. Along the wave propagation direction, the laser diode has a mirror on each end, which usually reflects around 30% of light back into the laser body. To prevent power propagation in two other dimensions, the light is kept inside the device ($p-n$ junction plus quantum well) by the waveguiding effect. The device is embedded in the material with lower refractive index which confines light inside the structure.

There are two main types of lasers: lasers in which light emission is perpendicular to the crystal growth direction – edge-emitting lasers, and lasers in which emission direction is the same as crystal growth direction – vertical-cavity surface-emitting lasers (VCSEL). This work focuses on edge-emitting lasers, the scheme of such a laser is presented in Fig. 2.2.

2.1.3 Fundamentals of laser action

In general, physics of the laser diode is very complex. In this section only the most basic effects are described without any derivations. Also, only steady-state condition

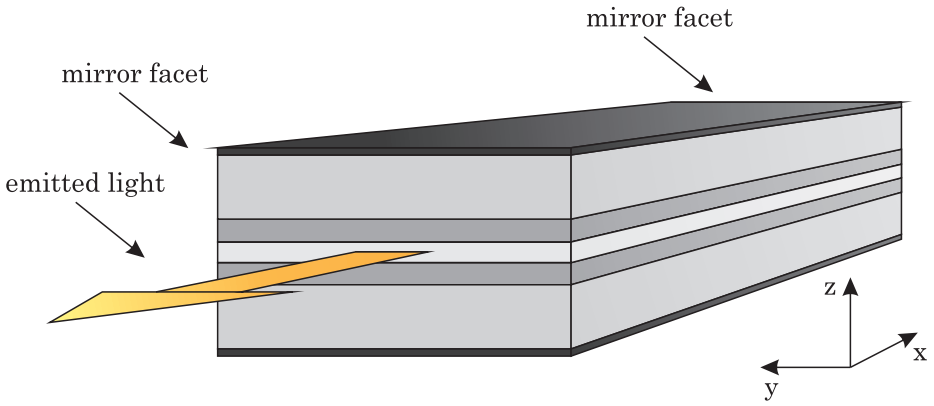

Figure 2.2: A simple scheme of edge-emitting semiconductor laser. From the top to bottom the layers are: n-side electrode, n-type material, barrier, active layer, barrier, p-type material, p-side electrode. Light is emitted in the direction perpendicular to the direction of crystal growth (z).

is considered, as it greatly simplifies the discussion of the laser action.

There are two major light generation mechanisms: spontaneous and stimulated emission [70, 64]. In laser diodes, the dominating mechanism is the stimulated emission. Because there are a lot of photons present in an active laser, one can use the classical Maxwell equations to describe the optical part of the laser action. Photons from stimulated emission have the same polarization and direction as the photons which caused the emission, and thus the *stimulated emission* can be seen as a negative absorption. In optoelectronics, a popular way to describe it is via so called material gain, which is defined as

$$g(\omega, \mathbf{r}) = -2\frac{\omega}{c}\mathrm{Im}\left(n(\omega, \mathbf{r})\right), \tag{2.1}$$

where n is refraction index.

On the other hand, the spontaneously emitted photons have random polarization and direction, and can be described classically only as a random noise added to the equations. Although in lasers the overall strength of the spontaneous emission is very small in comparison to the stimulated emission, the spontaneous emission noise has to be included in the Maxwell equations to obtain any non-trivial solution [71, 72].

In general, the material gain and absorption are position and frequency dependent. A typical material gain spectrum is shown in Fig. 2.3. It has a characteristic shape with maximum value called gain peak. Figure 2.3a shows the case in which only first levels (one in the valence band and one in the conduction band) inside the quantum well are occupied. Figure 2.3b shows situation when both first and second levels are populated.

Because the refractive index has an imaginary part, the electromagnetic wave propagating inside the device will experience exponential growth. This growth can be very non-trivial but can be calculated by solving the Maxwell equations for a particular laser geometry. A detailed discussion of this problem is provided in next chapters. Here, only a simplified version of edge-emitting laser is discussed.

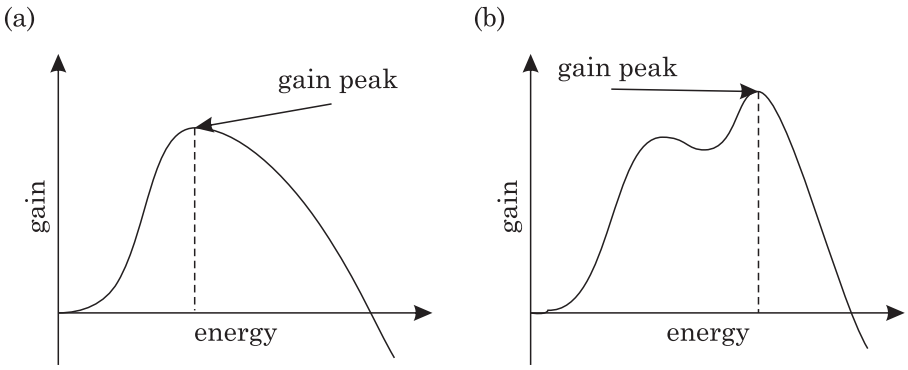

Figure 2.3: Typical material gain spectrum. (a) Spectrum of gain in quantum well, with first levels populated. (b) Spectrum with first and second levels populated.

The edge-emitting laser under consideration is presented in Fig. 2.2. It is assumed that in the propagation direction (x), it can be treated as the Fabry-Perot resonator [73, 27] which consists of a uniform cavity and two mirrors at each end of the cavity. This approximation can be used only for edge-emitting lasers as they are usually close to uniform in the light emission direction while VCSELs are highly nonuniform in the emission direction. In this case, a wave propagating throughout the cavity experiences constant exponential growth $e^{g_{\text{net}}x}$, where

$$g_{\text{net}} = g_{\text{mod}} - \alpha. \tag{2.2}$$

In the above formula, α stands for total absorption, and a modal gain g_{mod} is the modal gain (gain of power of electromagnetic wave during propagation in the laser cavity). Even in this simplified picture $g_{\text{mod}} \neq g$ because g is present only in the active layer (quantum well) and only a fraction of the wave is propagating in that region. To obtain g_{mod}, the material gain is multiplied by the confinement factor Γ which is roughly equal to ratio of power of the wave propagating in the active region to total power propagating inside the cavity

$$g_{\text{mod}} = \Gamma g. \tag{2.3}$$

The absorption coefficient α is usually assumed to be the same everywhere in the cavity and that is why it does not have to be multiplied by the confinement factor. A simple scheme of the Fabry-Perot resonator laser is shown in Fig. 2.4.

From Fig. 2.4 two resonance conditions can be deducted: one for a phase and one for an amplitude of the wave. The phase condition is easy to derive since it is obvious that for the resonance, wave inside the device has to be a standing wave satisfying

$$\lambda = \frac{2L}{m}, \tag{2.4}$$

where L is a length of the resonator, λ is a wavelength of the wave *inside the cavity*, and m is a natural number. Different wavelengths satisfying condition (2.4) are called lasing modes. An amplitude condition states that the total gain g_{net} experienced

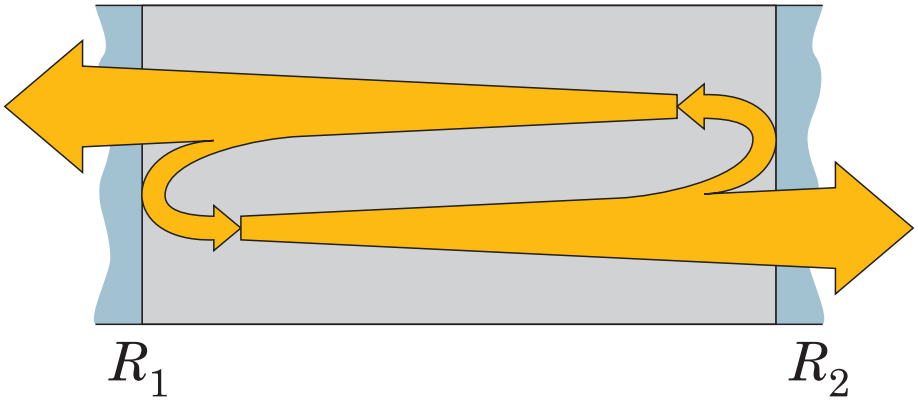

Figure 2.4: Illustration of resonance in Fabry-Perot cavity. Wave propagating inside the cavity experiences exponential growth. At two mirrors with reflectivities R_1 and R_2 part of the wave is reflected back into the device.

by the wave has to be equal to losses caused by reflection at the mirrors. This condition can be obtained using the following arguments: assume that a wave starts propagating at $x = 0$ to the right with a unit amplitude. When it reaches $x = L$ it has an amplitude of $e^{g_{\text{net}}L}$, and after the reflection is has an amplitude of $R_2 e^{g_{\text{net}}L}$. Then, after going back and reflecting again at $x = 0$ it has an amplitude of $R_1 R_2 e^{2g_{\text{net}}L}$. For the stimulated emission to be sustained, the wave after making such round trip has to have exactly the same amplitude as it had at the beginning, this means that $R_1 R_2 e^{2g_{\text{net}}L} = 1$. Thus, the second resonance condition is

$$g_{\text{net}} = \alpha_{\text{mirror}} = \frac{1}{2L} \ln \frac{1}{R_1 R_2}. \tag{2.5}$$

In general, both types of emission depend on the averaged number of carriers (inversion of population) inside the active region. Carriers can be added by increasing the forward bias across the device and thus increasing the injection current. For low currents, the condition (2.5) is not satisfied, and the spontaneous emission is the dominant process. When the injection current increases, more carriers are inside the active region and the spontaneous emission rate slowly increases. When the current (and thus carrier density) reaches a so-called threshold value (I_{th}) where the total gain is equal to losses through the mirrors, the stimulated emission becomes the dominating process. In steady-state, the total gain clearly cannot be bigger than losses as the energy of the electromagnetic wave propagating inside the device would be infinite. When the injection current becomes larger than its threshold value, the carrier density, and thus the gain stay at their threshold values. This happens because when the injection current raises above the threshold, the stimulated emission rate rises accordingly and keeps the carrier density at the threshold level. That is why above the threshold, when the injection current rises, the spontaneous emission rate stays constant (it is proportional to the carrier density) but the stimulated emission rate increases. In a more general non-steady-state, the carrier density and gain can temporarily reach values above the threshold, but similarly to the steady-state case,

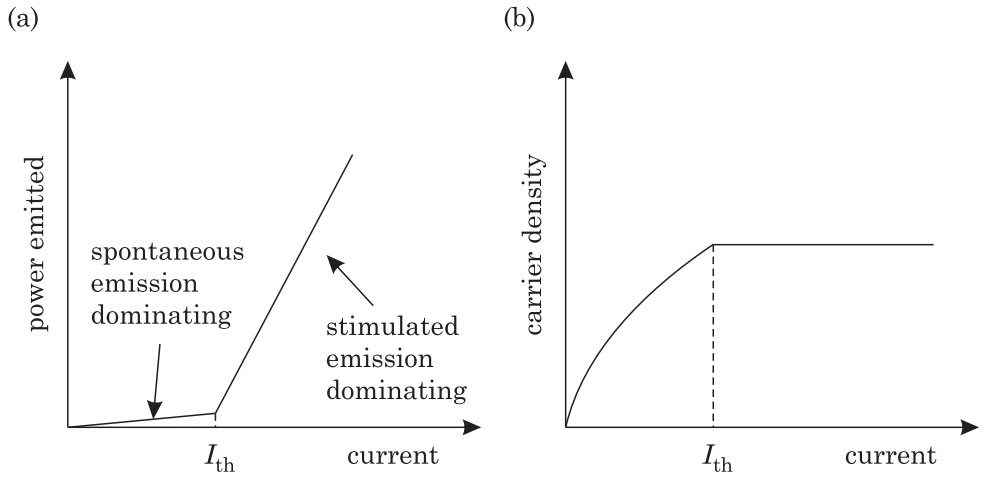

Figure 2.5: Semiconductor laser's behavior below and above the threshold. (a) Power emitted as a function of current intensity. (b) Averaged carrier density inside the active region as a function of current intensity.

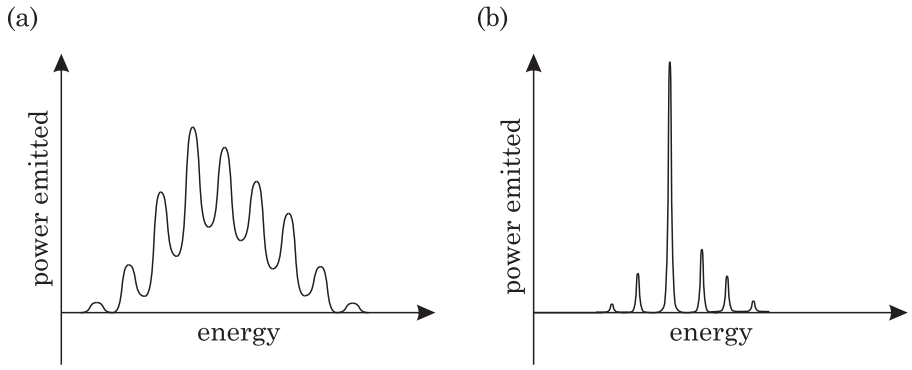

Figure 2.6: Power spectrum of laser diode. (a) Below threshold level. (b) Above threshold level.

those are quickly reduced because the stimulated emission rate also rises and hence decreases the number of carriers.

Figure 2.6 shows a power spectrum of the laser diode below and above the threshold. One can see that below the threshold, when a spontaneous emission dominates, the power spectrum is quite broad and although visible, the phase condition (2.4) is not strictly satisfied. Above the threshold, the phase condition becomes very visible and the power spectrum consists of stripes satisfying condition (2.4). Another interesting fact about the power spectrum above the threshold, is that one stripe at an energy point corresponding to gain peak becomes dominating. This happens because, above the threshold, when the second resonance condition (2.5) is satisfied for one frequency, the stimulated emission suppresses gain at other frequencies to satisfy Eq. (2.5), and in the end, the laser emits light at a single frequency only.

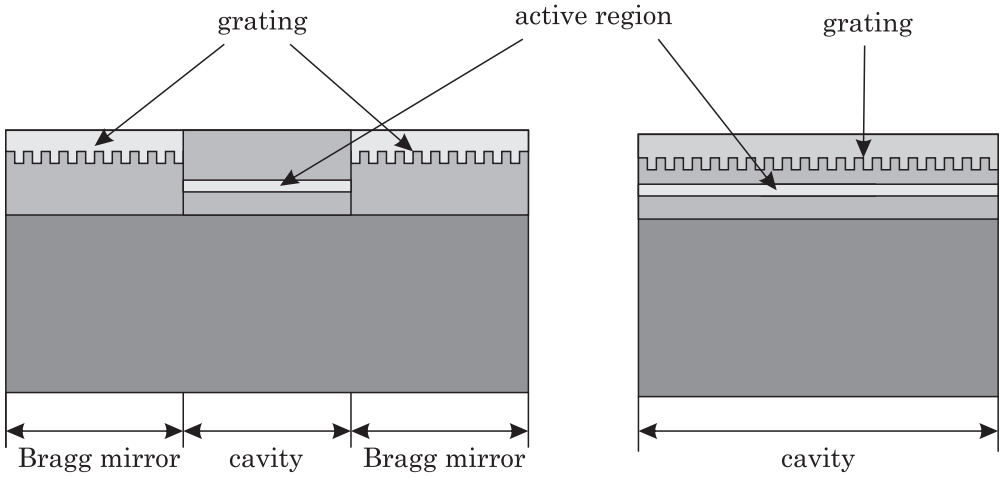

Figure 2.7: Schematics of a DBR laser (left) and DFB laser (right).

2.2 Other types of laser diodes

One of the biggest shortcomings of a Fabry-Perot laser is that there are many modes present. Although in the steady state, majority of the laser's emission is in a one dominating mode, lasers almost never operate in a steady-state. When a laser is modulated, the mode-hopping occurs: wavelength of emitted light jumps between some number of modes. This is generally an undesired effect and thus some mechanism of locking the laser at one mode is necessary. Two major types of lasers that provide better mode selectivity are: distributed Bragg reflector lasers (DBR) [74, 75, 73] and distributed feedback lasers (DFB) [76, 20, 77], both shown in Fig. 2.7.

DBR lasers are in principle very similar to standard Fabry-Perot lasers. The main difference is that there are Bragg mirrors outside of the cavity. Bragg mirrors are passive waveguides which are periodically corrugated along the propagation direction. Because of the corrugation, the refractive index of the mirror also becomes a periodic function in the propagation direction. Usually they are made by etching the surface of the waveguide and then refilling it with a material with slightly different refractive index. The corrugation has a $\lambda/(2n_{\text{eff}})$ period, where λ is intended emission wavelength (in vacuum) and n_{eff} is the effective refractive index. Bragg mirrors have high reflectivity of electromagnetic waves with the λ wavelength and a very small reflectivity of other wavelengths. This effect takes place because the wave is reflected many times at each interface, and because of the periodic design of the reflector they all have the same phase and thus add to form large reflected wave. This does not occur if the wavelength is much different than the intended emission wavelength, since reflected waves have different phases and therefore the total reflection is much smaller.

In a DFB laser the periodic corrugation is fabricated in the laser cavity itself. Both the passive and active part of the laser can be corrugated. The general principle of mode selection is identical as in DBR laser but DFB lasers are easier to manufacture and have smaller losses. However, the advantage of a DBR over DFB

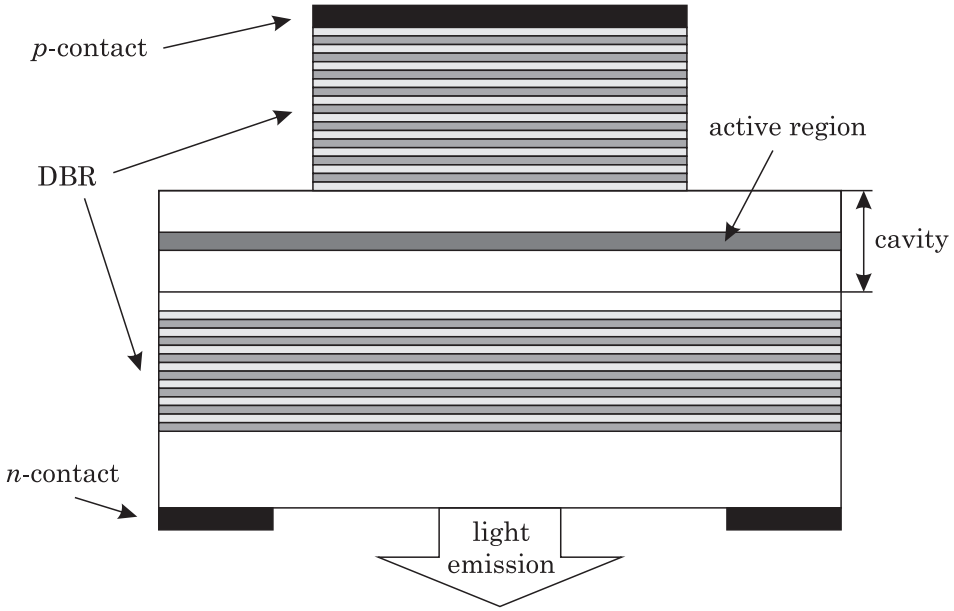

Figure 2.8: Schematic of a VCSEL laser.

laser is that in a DBR laser the reflectivity of the mirrors and thus lasing wavelength can be tuned. It is done by attaching an additional electrode to the mirror and utilizing the electro-optic effect, which allows one to modify the refractive index of the mirror with current from the additional electrode.

Distributed Bragg mirrors are also used in vertical cavity surface-emitting lasers (VCSELs) [21, 78, 24]. VCSEL is a laser in which emission of light occurs in the same direction as the crystal growth direction. It consists of two Bragg mirrors which are created by growing alternately high and low refractive index layers, each one $\lambda/\left(4n_{\text{eff}}\right)$ thick. The cavity itself is very small and modal gain is typically two orders of magnitude smaller than gain in edge-emitting laser. Laser emission is possible due to Bragg mirrors, which have to have total reflectivity of over 99.9%. Because of their short cavity they operate in a single mode only. A very important feature of VCSELs is that they can be produced in arrays on a single wafer [77] since no cleaving is necessary during the growth process. This significantly reduces the production costs and makes VCSELs increasingly popular.

2.3 Overview of the semiconductor laser simulators

2.3.1 Basic components

In general there is no one universal technique to simulate all aspects of semiconductor lasers. Majority of up-to-date simulators consists of three major parts: optical, electrical, and gain model.

Because the number of photons present during laser action is significant, the

optical part can be treated classically [64, 70]. Taking as an input parameters the geometry of the system and material gain due to stimulated emission, one can calculate field profile which can be later used to calculate photon density. There are many different methods of solving Maxwell equations for lasing system. The most popular are finite difference time-domain (FDTD) method [72], eigenmode expansion using eigenmodes that satisfy round-trip condition [20, 72], and electromagnetic Green's functions [71, 79]. The choice of the best method depends strongly on a type of the device which is simulated, and a simulation type (steady-state or signal analysis). For example, FTDT is very good when dealing with large signals but for small signals and steady-state, eigenmode expansion is much faster. On the other hand the Green's function method allows for a very realistic treatment of noise due to spontaneous emission.

As mentioned before, the most common approach to the electrical transport in the laser is the drift-diffusion method. The major advantage of this method is that it is very fast and robust. It has been in use for over three decades and it is very successful in simulating relatively large electric devices. Up-to-date drift-diffusion simulators allow for 2-D and 3D calculations with non-zero temperature gradient. The drift-diffusion model is capable of calculating carrier and current densities in the device. However, due to its quasi-classical and phenomenological nature it is very inaccurate when quantum effects have significant influence on the performance of the device.

The material gain is the most important characteristic of a laser. Because gain is purely quantum mechanical effect, one has to use a microscopic to model it [26, 70, 28, 24, 64, 72]. To calculate gain, the Schrödinger equation is solved using a single-particle Hamiltonian. Solution of the Schrödinger equation gives eigenfunctions and eigenvalues of the confined states inside the quantum well. Eigenfunctions and eigenvalues of the confined states allow to obtain gain by using Fermi golden rule. However, because the gain is so crucial in laser simulations, calculating it using only single-particle Hamiltonian is very inaccurate and many-body interactions have to be included. Modern simulators include variety of many-body corrections to the material gain. Some of them are: Hartree-Fock term, direct collision term, and electron-phonon interaction. Although these corrections increase precision of the gain model, many of them relay heavily on a number of assumptions and material parameters, and have extremely complicated analytical form.

2.3.2 Selected list of currently developed commercial simulators

PICS3D by Crosslight Software [28, 79] is one of the most sophisticated and comprehensive laser simulator available on the market. It allows to simulate very large range of lasers including DFB, DBR, VCSELs, and Fabry-Perot lasers. Optical equations are solved using 2-D scalar approximation of Helmholtz equation and electromagnetic Green's function method. Electrical transport is modeled using quasi 3D or full 3D drift-diffusion method with quantum corrections in the active region. The simulator has also state of the art gain model which uses non-parabolic Hamiltonian

and can take into account variety of many-body interactions.

Silvaco [80] provides laser simulator as an extension of its flag ship device simulation framework ATLAS. It allows to analyze VCSELs and Fabry-Perot lasers. The software provides a parabolic gain model where gain broadening is taken into account using purely phenomenological parameters and not many-body theory. Similarly as in all other commercial models carrier transport is simulated using drift-diffusion method.

DESSIS-Laser by Integrated System Engineering [81] is an extension of DESSIS device simulator. DESSIS-Laser is able so simulate Fabry-Perot lasers as well as VCSELs. It allows for non-parabolic gain model but, similarly as in the case of ATLAS, gain broadening is purely phenomenological.

LaserMOD by RSoft Design Group [82] is another advanced laser simulator. It can be used to simulate all major types of lasers. It allows for 1-D, 2-D, and quasi 3-D simulations. Gain is calculated using 8×8 Hamiltonian. Modification of gain due to many-body interactions can be taken into account by uploading gain databases from Nonlinear Control Strategies [83] which uses sophisticated quantum many-body theory to calculate gain, refractive index, and photo-luminescence spectra for semiconductor quantum wells.

HAROLD simulator made by Photon Design [84], allows for 1-D and 2-D simulation of a Fabry-Perot semiconductor laser. The gain is calculated using parabolic approximation and takes into account carrier-induced bandgap narrowing effect.

Chapter 3

Non-equilibrium Green's functions (NEGF)

Because the exact calculations in a realistic system with many particles are virtually impossible, one has to resort to perturbative methods. The non-equilibrium Green's function method allows one to deal with both a non-equilibrium system and to develop a perturbative series to account for many-body interactions. As usual, easier calculations are possible at a cost of some information loss. The Green's function of a given system allows only to calculate the average values of quantum mechanical operators, while the non-perturbative approach with a density matrix, allows one to get all the information about the system.

The first section of this chapter introduces the Heisenberg and interaction pictures of quantum mechanics and shows the motivation behind a time contour. In the second section, the contour-time Green's function is defined. Major properties of contour-time Green's function are shown and a mechanism of conversion of contour-time functions to real-time functions is provided.

The third section describes derivation of the Dyson equation which is the central equation of the theory. Functional derivative technique is used to obtain expressions for self-energies responsible for electron-electron and electron-photon interactions. At the end of this section, a method of including most significant effects of ion lattice and phonons is provided.

In general, this chapter provides only purely abstract formulation of the Dyson equation and the many-body interactions present in it. The only assumptions about the system are limited to form the Hamiltonian and the initial conditions. In this general form, the Dyson equation can describe variety of systems such as: lasers, LEDs, solar cells, RTDs, etc. Especially, the terms containing many-body interactions – self-energies, are formulated in terms of abstract equations not yet suitable for numerical implementation. However, in the next chapter those equations will serve as a framework during formulation of much more practical systems of equations for a laser.

3.1 Preliminaries

To define Green's function for a many-body system, it is necessary to use the Heisenberg picture of quantum mechanics. It holds true even for time-independent systems in equilibrium [85, 86]. The Heisenberg picture is briefly described at the beginning of this section. More details about various pictures of quantum mechanics can be found in Appendix A.

When applying the Green's function technique to a non-equilibrium system it is very convenient to introduce the so-called time contour. Introduction of the time contour significantly simplifies derivation of the Dyson equation. The idea of time contour is presented in the second part of this section in an example of a statistical average of the particle density operator in a time-dependent system.

3.1.1 Heisenberg and interaction pictures

Systems in non-equilibrium are generally time-dependent. The Hamiltonian of a given time-dependent system can be separated into static and time-dependent parts. Furthermore, one can assume that a time-dependent perturbation is turned on at some time t_0, and the total Hamiltonian can be written as

$$\hat{H}(t) = \begin{cases} \hat{H}_0 & \text{for } t < t_0 \\ \hat{H}_0 + \hat{H}_{\text{int}}(t) & \text{for } t \geq t_0 \end{cases}. \tag{3.1}$$

The boundary conditions placed on the equation of motion described by this Hamiltonian are also static until t_0 and time-dependent after t_0.

The Heisenberg picture of quantum mechanics is particularly convenient when working with time-dependent problems. In time-dependent problems the Hamiltonian has *explicit* time dependence in the Schrödinger picture and the wavefunction can not be separated into a product of position dependent function and phase factor containing time. In the Heisenberg formulation of quantum mechanics all time dependency is shifted into operators and hence the wavefunctions are independent of time.

To formally derive the Dyson equation it is necessary to formulate operators in the Heisenberg picture and then express the time-dependent operators in the interaction picture, which is yet another formulation of quantum mechanics. The interaction picture can be viewed as an intermediate formulation between the Schrödinger and the Heisenberg pictures, where only some of the time dependence is moved to operators. A detailed description of the Heisenberg and interaction pictures and relation between them is presented in Appendix A. Although operators in the interaction picture will not explicitly show up in any of the final equations, this is a necessary step in the derivation of the Dyson equation.

In this section, the following convention is used to distinguish between pictures: "I" subscript indicates the interaction picture, "H" subscript indicates the Heisenberg picture, no subscript means the Schrödinger picture. This convection applies to both operators and vector states.

Vector states and operators (which can have explicit time dependency even in the Schrödinger picture) in the interaction picture are described by the unitary transformation from the Schrödinger picture

$$|\Psi_{\mathrm{I}}(t)\rangle = e^{\frac{i}{\hbar}\hat{H}_0(t-t_0)}\,|\Psi(t)\rangle\,, \tag{3.2}$$

$$\hat{O}_{\mathrm{I}}(t) = e^{\frac{i}{\hbar}\hat{H}_0(t-t_0)}\hat{O}(t)\,e^{-\frac{i}{\hbar}\hat{H}_0(t-t_0)}. \tag{3.3}$$

In the Heisenberg picture, the states and operators can be expressed by states and operators in the interaction picture using evolution operators $\hat{S}$ and $\hat{S}^\dagger$

$$|\Psi_{\mathrm{H}}\rangle = \hat{S}^{-1}(t,t_0)\,|\Psi_{\mathrm{I}}(t)\rangle\,, \tag{3.4}$$

$$\hat{O}_{\mathrm{H}}(t) = \hat{S}^\dagger(t,t_0)\,\hat{O}_{\mathrm{I}}(t)\,\hat{S}(t,t_0)\,. \tag{3.5}$$

Operators $\hat{S}$ and $\hat{S}^\dagger$ are defined as

$$\hat{S}(t,t_0) = T_+\left[\exp\left(-\frac{i}{\hbar}\int_{t_0}^{t} dt'\,\hat{H}_{\mathrm{int,I}}(t')\right)\right], \tag{3.6}$$

$$\hat{S}^\dagger(t,t_0) = T_-\left[\exp\left(-\frac{i}{\hbar}\int_{t}^{t_0} dt'\,\hat{H}_{\mathrm{int,I}}(t')\right)\right], \tag{3.7}$$

where T_+ (T_-) is time (anti-time) ordering operator which orders time dependent operators chronologically (anti-chronologically), from left to right with decreasing (increasing) time arguments – higher (lower) times are placed to the left. Operators $\hat{S}$ and $\hat{S}^\dagger$ have the following properties

$$\hat{S}^\dagger(t_1,t_2) = \hat{S}^{-1}(t_1,t_2)\,, \tag{3.8}$$

$$\hat{S}(t,t) = \hat{1}, \tag{3.9}$$

$$\hat{S}^{-1}(t_1,t_2) = \hat{S}(t_2,t_1)\,, \tag{3.10}$$

$$\hat{S}(t_1,t_2) = \hat{S}(t_1,t_3)\,\hat{S}(t_3,t_2)\,. \tag{3.11}$$

From Eqs. (3.2) and (3.4) one can see that at $t = t_0$ all three pictures coincide and $|\Psi_{\mathrm{H}}\rangle = |\Psi_{\mathrm{I}}(t_0)\rangle = |\Psi(t_0)\rangle$.

As described in Appendix A, when the order of two Hamiltonians $\hat{H}_{\mathrm{int,I}}(t_1)$ and $\hat{H}_{\mathrm{int,I}}(t_2)$ is changed by T_+ or T_- the whole expression retains its sign i.e., Hamiltonians with different time arguments commute under time and anti-time ordering operator. However, in many-particle systems all physical Hamiltonians consist of even number of creation and annihilation operators, and one has to additionally specify their behavior under operation of time and anti-time ordering. According to [85], creation and annihilation operators under the time and anti-time ordering operator commute for bosons and anti-commute for fermions. For example, a time

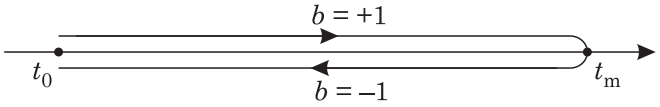

Figure 3.1: Time contour.

and anti-time ordering of a pair of operators $\hat{A}(t_1)$ and $\hat{B}(t_2)$ which can be any combination of creation and annihilation operators is

$$T_+\left[\hat{A}(t_1)\,\hat{B}(t_2)\right] = \theta(t_1-t_2)\,\hat{A}(t_1)\,\hat{B}(t_2) \mp \theta(t_2-t_1)\,\hat{B}(t_2)\,\hat{A}(t_1), \tag{3.12}$$

$$T_-\left[\hat{A}(t_1)\,\hat{B}(t_2)\right] = \theta(t_2-t_1)\,\hat{A}(t_1)\,\hat{B}(t_2) \mp \theta(t_1-t_2)\,\hat{B}(t_2)\,\hat{A}(t_1), \tag{3.13}$$

where upper $(-)$ sign refers to fermions and lower $(+)$ to bosons. It is also assumed that creation/annihilation operators for different kinds of particles always commute. For example, operators commute where one is a boson and one a fermion, or even when both are fermions of a different kind.

3.1.2 Time contour

The time contour, for the first time introduced in [62] is a tool which significantly simplifies the derivation of the Dyson equation. However, it is not absolutely necessary, and all equations can be derived using only regular time axis and time and anti-time ordering operators, although that would be a very difficult task. In this subsection, the motivation behind time contour is shown using an example of a particle density operator.

One can consider a statistical average of a particle density operator $\hat{n}_\mathrm{p} = \hat{\Psi}^\dagger\hat{\Psi}$ (spin and spatial dependency is suspended for brevity). The density of particles is named n_p to avoid confusion with quasiparticle electron density, which will be denoted as n. The statistical average $n_\mathrm{p}(t)$ can be initially written in the Schrödinger picture and then converted to the Heisenberg and interaction pictures

$$\begin{aligned} n_\mathrm{p}(t) &= \left\langle \hat{\Psi}^\dagger(t)\,\hat{\Psi}(t)\right\rangle = \left\langle \hat{\Psi}^\dagger_\mathrm{H}(t)\,\hat{\Psi}_\mathrm{H}(t)\right\rangle_0 \\ &= \left\langle \hat{S}(t_0,t)\,\hat{\Psi}^\dagger_\mathrm{I}(t)\,\hat{\Psi}_\mathrm{I}(t)\,\hat{S}(t,t_0)\right\rangle_0, \end{aligned} \tag{3.14}$$

where the subscript 0 next to the bracket $\langle\rangle$ indicates that the statistical average is calculated by taking trace of a density matrix expressed in a basis of states written in the Heisenberg picture. Construction of a statistical average in the Heisenberg representation is discussed in Appendix A.

To write Eq. (3.14) in a more compact form, one can define time contour which goes from t_0 to some arbitrary $t_\mathrm{m} > t$ (in practice, the limit $t_\mathrm{m} \to +\infty$ is taken) and then back to t_0. This contour is presented in Fig. 3.1. It is said that such contour consists of two branches: upper $b = +1$ which goes from t_0 to t_m, and lower $b = -1$,

which goes back from t_{m} back to t_0. One can also introduce the contour-time ordering operator T_{c} which works like T_+ but it orders operators along time contour. Clearly, whenever operator T_{c} orders functions of times which are on the upper branch it behaves like T_+, when all times are on the lower branch it behaves like T_-. Because operators $\hat{S}(t_1,t_2)$, where $t_2 > t_1$ depend on T_+, in the contour formalism they are located on the upper branch. On the other hand operators $\hat{S}^{\dagger}(t_1,t_2) = \hat{S}(t_2,t_1)$, where $t_2 > t_1$ depend on T_- and in the contour formalism they are located on the lower branch.

The average value of the particle density operator can be written as

$$\begin{aligned} n_{\mathrm{p}}(t) &= \left\langle \hat{S}(t_0,t)\,\hat{\Psi}_{\mathrm{I}}^{\dagger}(t)\,\hat{\Psi}_{\mathrm{I}}(t)\,\hat{S}(t,t_{\mathrm{m}})\,\hat{S}(t_{\mathrm{m}},t)\,\hat{S}(t,t_0)\right\rangle_0 \\ &= \left\langle T_+\left[\hat{S}(t_0,t_{\mathrm{m}})\,\hat{\Psi}_{\mathrm{I}}^{\dagger}(t+\delta t)\,\hat{\Psi}_{\mathrm{I}}(t)\right]\hat{S}(t_{\mathrm{m}},t_0)\right\rangle_0 \\ &= \left\langle T_{\mathrm{c}}\left[\hat{S}(t_0,t_{\mathrm{m}})\,\hat{S}^{\dagger}(t_0,t_{\mathrm{m}})\,\hat{\Psi}_{\mathrm{I}}^{\dagger}(t+\delta t,b=+1)\,\hat{\Psi}_{\mathrm{I}}(t,b=+1)\right]\right\rangle_0, \end{aligned} \tag{3.15}$$

where $t_{\mathrm{m}} > t$ is arbitrary, t in the annihilation operator was replaced by $t+\delta t$ to preserve correct order under T_+, and $b=+1$ was added to both the annihilation and creation operator to indicate that their times are located on the upper branch. The product $\hat{S}(t_0,t_{\mathrm{m}})\,\hat{S}^{\dagger}(t_0,t_{\mathrm{m}})$ is usually written as a contour evolution operator

$$\hat{S}_{\mathrm{c}}(t_0,t_{\mathrm{m}}) = \hat{S}(t_0,t_{\mathrm{m}})\,\hat{S}^{\dagger}(t_0,t_{\mathrm{m}}). \tag{3.16}$$

In the calculations of the particle density operator it was assumed that both annihilation and creation operators are located on the upper branch – this is not a unique choice. Using exactly the same procedure it can be shown that

$$n_{\mathrm{p}}(t) = \left\langle T_{\mathrm{c}}\left[\hat{S}_{\mathrm{c}}\hat{\Psi}_{\mathrm{I}}^{\dagger}(t-\delta t,b=-1)\,\hat{\Psi}_{\mathrm{I}}(t,b=-1)\right]\right\rangle_0. \tag{3.17}$$

To obtain more a compact expression, one can define the contour-time

$$\underline{t} = \{t,b\}, \tag{3.18}$$

and hence contour integral

$$\int d\underline{t} = \int_{t_0}^{t_{\mathrm{m}}} dt_{+1} + \int_{t_{\mathrm{m}}}^{t_0} dt_{-1} = \sum_{b\in\{+1,-1\}} b\int_{t_0}^{t_{\mathrm{m}}} dt_b. \tag{3.19}$$

Now, the contour evolution operator can be expressed as

$$\hat{S}_{\mathrm{c}}(t_0,t_{\mathrm{m}}) = T_{\mathrm{c}}\left[\exp\left(-\frac{i}{\hbar}\int d\underline{t}'\hat{H}_{\mathrm{int,I}}(\underline{t}')\right)\right], \tag{3.20}$$

where $\hat{H}_{\mathrm{int,I}}(t',b=+1) = \hat{H}_{\mathrm{int,I}}(t',b=-1) = \hat{H}_{\mathrm{int,I}}(t')$, and therefore the statistical average of the particle density operator is

$$n_{\mathrm{p}}(t) = \left\langle T_{\mathrm{c}}\left[\hat{S}_{\mathrm{c}}\hat{\Psi}_{\mathrm{I}}^{\dagger}\left(\underline{t}^{+}\right)\hat{\Psi}_{\mathrm{I}}(\underline{t})\right]\right\rangle_0. \tag{3.21}$$

The "+" superscript next to contour-time indicates that $\underline{t}^+$ is infinitesimally larger on contour than $\underline{t}$. A Similar procedure can be applied to any single-particle operator.

In conclusion, introduction of contour time allows one to replace operators in the Heisenberg picture with contour-time ordered operators in the interaction picture. This replacement will be crucial in the derivation of the Dyson equation for non-equilibrium Green's function.

3.2 Definition of the NEGF

From this point on, the Schrödinger picture is not going to be used any more, and most of the operators will be written in the Heisenberg picture. Because of that, and to simplify notation, the subscript "H" next to the operators in the Heisenberg picture is dropped, as well as the subscript 0 next to the statistical average brackets $\langle\rangle$.

To make the notation more compact, the following convention is used

$$\begin{aligned} k &= \{\mathbf{r}_k, \sigma_k, t_k\}, \\ \underline{k} &= \{\mathbf{r}_k, \sigma_k, \underline{t}_k\} = \{\mathbf{r}_k, \sigma_k, t_k, b_k\}, \end{aligned} \tag{3.22}$$

where contour-time is indicated as $\underline{t}_k$ and consists of two variables: real-time value t_k and branch index ($+1$ or -1), $\mathbf{r}_k$ is position vector, and σ_k is a spin index. Integrals over k and $\underline{k}$ are defined as

$$\begin{aligned} \int dk &= \sum_{\sigma_k} \int d^3 r_k \int dt_k, \\ \int d\underline{k} &= \sum_{\sigma_k} \int d^3 r_k \int d\underline{t}_k = \sum_{\sigma_k} \sum_{b} b \int d^3 r_k \int dt_b. \end{aligned} \tag{3.23}$$

For example, using the above notation any function $F(\mathbf{r}_1, \sigma_1, \underline{t}_1)$ can be written simply as $F(\underline{1})$ and

$$\sum_{\sigma_1} \int d^3 r_1 \int d\underline{t}_1 F(\mathbf{r}_1, \sigma_1, \underline{t}_1) = \int d\underline{1} F(\underline{1}). \tag{3.24}$$

The contour Green's function is defined as [62, 60, 87]

$$G(\underline{1}, \underline{2}) = \frac{1}{i\hbar} \left\langle T_{\mathrm{c}} \left[\hat{\Psi}(\underline{1}) \hat{\Psi}^{\dagger}(\underline{2}) \right] \right\rangle, \tag{3.25}$$

where the contour extents beyond the largest of two time arguments t_1 and t_2. Green's function can be converted to the interaction picture by using the same technique as in the previous section for a particle density operator

$$G(\underline{1}, \underline{2}) = \frac{1}{i\hbar} \left\langle T_{\mathrm{c}} \left[\hat{S}_{\mathrm{c}} \hat{\Psi}_{\mathrm{I}}(\underline{1}) \hat{\Psi}_{\mathrm{I}}^{\dagger}(\underline{2}) \right] \right\rangle. \tag{3.26}$$

Of course, to perform any meaningful calculations, contour Green's function has to be converted to a real-time function. By fixing branch indices b_1 and b_2, four different real-time Green's functions are obtained: lesser ($G^{<}$), greater ($G^{>}$), time ordered (G^{t}), and anti-time ordered ($G^{\bar{\mathrm{t}}}$)

$$G\left(\underline{1},\underline{2}\right)=\begin{cases} G^{<}\left(1,2\right)=-\frac{1}{i\hbar}\left\langle \hat{\Psi}^{\dagger}\left(2\right)\hat{\Psi}\left(1\right)\right\rangle , & b_1=+1,\ b_2=-1\\ G^{>}\left(1,2\right)=\frac{1}{i\hbar}\left\langle \hat{\Psi}\left(1\right)\hat{\Psi}^{\dagger}\left(2\right)\right\rangle , & b_1=-1,\ b_2=+1\\ G^{\mathrm{t}}\left(1,2\right)=\frac{1}{i\hbar}\left\langle T_{+}\left[\hat{\Psi}\left(1\right)\hat{\Psi}^{\dagger}\left(2\right)\right]\right\rangle , & b_1=+1,\ b_2=+1\\ G^{\bar{\mathrm{t}}}\left(1,2\right)=\frac{1}{i\hbar}\left\langle T_{-}\left[\hat{\Psi}\left(1\right)\hat{\Psi}^{\dagger}\left(2\right)\right]\right\rangle , & b_1=-1,\ b_2=-1 \end{cases}. \tag{3.27}$$

Properties of the components of contour Green's function defined by Eq. (3.27), and contour-time functions in general, are shown in Appendix B. It is easy to see that the Green's function from Eq. (3.27) has a general form described by Eq. (B.3) with $A_2=0$ (no singular term).

In general, the contour-time formulation is only a means to derive the Dyson equation. After the derivation is completed, final equations are converted to real-time functions and then solved.

Although functions G^{t} and $G^{\bar{\mathrm{t}}}$ are easy to get from the contour Green's function (3.25), for reasons explained in Appendix B, they are not very convenient when solving the Dyson equation. Instead of using G^{t} and $G^{\bar{\mathrm{t}}}$, one can introduce advanced (G^{A}) and retarded (G^{R}) Green's functions

$$G^{\mathrm{R}}\left(1,2\right)=G^{\mathrm{t}}\left(1,2\right)-G^{<}\left(1,2\right), \tag{3.28}$$

$$G^{\mathrm{A}}\left(1,2\right)=G^{<}\left(1,2\right)-G^{\bar{\mathrm{t}}}\left(1,2\right). \tag{3.29}$$

Because retarded and advanced functions are nothing more than linear combinations of G^{t}, $G^{\bar{\mathrm{t}}}$, and $G^{<}$, the set ($G^{<}$, $G^{>}$, G^{A}, G^{R}) has the same information about the system as ($G^{<}$, $G^{>}$, G^{t}, $G^{\bar{\mathrm{t}}}$).

Using Eqs. (B.9) and (B.10) from Appendix B, one can find that the advanced and retarded Green's functions have the following properties

$$G^{\mathrm{R}}\left(1,2\right)=\theta\left(t_1-t_2\right)\left[G^{>}\left(1,2\right)-G^{<}\left(1,2\right)\right], \tag{3.30}$$

$$G^{\mathrm{A}}\left(1,2\right)=-\theta\left(t_2-t_1\right)\left[G^{>}\left(1,2\right)-G^{<}\left(1,2\right)\right]. \tag{3.31}$$

3.3 The Dyson equation

The derivation of the Dyson equation consists of three major steps. The first step is to determine the exact form of Hamiltonian of the system. The second step is to take a time derivative from Eq. (3.25) and evaluate it using the equation of motion for an operator in the Heisenberg picture given in Appendix A. The third step is to apply a functional derivative technique [88, 60, 89, 90] to simplify the equation of motion obtained in step two.

3.3.1 Hamiltonian of the system

The Hamiltonian of a laser diode should include all of the most important interactions affecting the laser action. These are: electron-photon interaction for a radiative recombination, electron-electron interaction for Auger recombination and broadening of levels inside the quantum well, electron-impurity interaction for Shockley-Read-Hall recombination, and of course phonons which significantly affect all the mentioned above effects. Because of both conceptual complications and numerical constrains, in this work, Shockley-Read-Hall and Auger recombinations are neglected.

In the derivations in this section, the Hamiltonian is limited to only electrons and photons. Electron-phonon interaction is not included, as the addition of full (not only single-particle effective potential) electron-lattice interaction is a formidable task and it is beyond the scope of this work. Instead, at the end of this section, the influence of the static ion lattice and phonons on the system is discussed. It is shown how to modify the previously obtained equations "by hand" to account for some of the most important lattice/phonon effects.

Up to this point the only assumption about the Hamiltonian was that it consist of two parts [62, 60, 87]

$$\hat{H} = \hat{H}_0 + \hat{H}_{\text{int}}, \tag{3.32}$$

where H_0 is the unperturbed part, and H_{int} is *explicitly* time-dependent perturbation turned on at $t = t_0$.

In Eq. (3.32) $\hat{H}_0$ is the usual Hamiltonian consisting of the kinetic energy term, electron-electron interaction, current-field interaction etc. The second term in (3.32) $\hat{H}_{\text{int}}$, is a time-dependent interaction of the system with some external sources (other than a heat bath) which creates a non-equilibrium state.

Inclusion of a time-dependent perturbation $\hat{H}_{\text{int}}$ has a double purpose. The first one is that it introduces non-equilibrium conditions to the system that otherwise would be in equilibrium because it is governed by explicitly time-independent $\hat{H}_0$. Non-equilibrium conditions have to be caused by some externally controlled sources, which are not part of the system itself. That is why it is assumed that externally controlled sources are regular functions and not operators acting in the Hilbert space. Those sources have an influence on the system, but the system does not have influence on them. For example, external charges are charges located far away from the system which create a field that influences particle inside the system. However, the non-equilibrium conditions can also be introduced by time-dependent boundary conditions which are turned on at $t = t_0$.

The second purpose for $\hat{H}_{\text{int}}$ is to allow for derivation of the Dyson equation using the functional derivative approach. This is because the Dyson equation contains response functions (such as polarization) which are a system's response to a variation of externally controlled charges/currents. Those external sources play a crucial role in this derivation, and $\hat{H}_{\text{int}}$ has to have very specific form determined by interactions present in $\hat{H}_0$. For example, if $\hat{H}_0$ has electron-electron interaction via the Coulomb potential, then $\hat{H}_{\text{int}}$ must have have external charges interacting with the system via the Coulomb potential. If $\hat{H}_0$ posses a current-field (electron-photon) interaction, then $\hat{H}_{\text{int}}$ must include the interaction of an external current with the system, and

so on for every type of interaction.

If such interactions with external sources are not physically present, then all, or just some of them can be set to zero at the end of calculations. For example, in this work, all source terms in $\hat{H}_{\text{int}}$ will be set to zero at the end of calculations and non-equilibrium conditions will be imposed by the boundary conditions only.

In conclusion, the time-dependent perturbation $\hat{H}_{\text{int}}$ is used as a mathematical tool to derive the Dyson equation. It might, but not necessary has to be a real physical interaction. In case it is not physical, the boundary conditions are used to introduce a non-equilibrium state in the system.

Static (internal) Hamiltonian consists of

$$\hat{H}_0 = \hat{H}_{\text{s}} + \hat{H}_{\text{m}} + \hat{H}_{\text{f}} + \hat{H}_{\text{e-f}}. \tag{3.33}$$

The parts of unperturbed Hamiltonian are defined as follows:

1. $\hat{H}_{\text{s}}$ is a single-particle part of Hamiltonian

$$\hat{H}_{\text{s}} = \sum_{\sigma\sigma'} \int d^3r \hat{\Psi}^{\dagger}\left(\mathbf{r},\sigma,t\right)\left(t\left(\mathbf{r}\right)\delta_{\sigma,\sigma'} + u\left(\mathbf{r},\sigma,\sigma'\right)\right)\hat{\Psi}\left(\mathbf{r},\sigma',t\right), \tag{3.34}$$

   where $t\left(\mathbf{r}\right)\delta_{\sigma,\sigma'} + u\left(\mathbf{r},\sigma,\sigma'\right)$ is a single-particle Hamiltonian in first quantization with a possible spin-mixing (u) term. The operators $\hat{\Psi}$ and $\hat{\Psi}^{\dagger}$ are field annihilation and creation operators in the Heisenberg picture. If the system consist only of electrons and photons then $t\left(\mathbf{r}\right)$ is just a kinetic energy, and $u\left(\mathbf{r},\sigma,\sigma'\right) = 0$. However, for now those terms are left in a general form. They will be explicitly specified in Subsection 3.3.4 to include some of the influence of a static ion lattice, and ionized impurity on the system.

2. $\hat{H}_{\text{m}}$ is a term responsible for electron-electron interaction [85, 86]

$$\hat{H}_{\text{m}} = \frac{e^2}{2}\sum_{\sigma\sigma'}\int d^3r \int d^3r' \hat{\Psi}^{\dagger}\left(\mathbf{r},\sigma,t\right)\hat{\Psi}^{\dagger}\left(\mathbf{r}',\sigma',t\right)V\left(\mathbf{r}-\mathbf{r}'\right)\hat{\Psi}\left(\mathbf{r}',\sigma',t\right)\hat{\Psi}\left(\mathbf{r},\sigma,t\right), \tag{3.35}$$

   where the Coulomb potential is defined as

$$V\left(\mathbf{r}-\mathbf{r}'\right) = \frac{1}{4\pi\epsilon_0}\frac{1}{\left|\mathbf{r}-\mathbf{r}'\right|}. \tag{3.36}$$

3. Free electromagnetic field Hamiltonian describes the behavior of an electromagnetic field without sources [63]

$$\hat{H}_{\text{f}} = \frac{1}{2}\int d^3r \left(\epsilon_0\left(\frac{\partial\hat{\mathbf{A}}\left(\mathbf{r},t\right)}{\partial t}\right)^2 + \frac{1}{\mu_0}\left(\nabla\times\hat{\mathbf{A}}\left(\mathbf{r},t\right)\right)^2\right). \tag{3.37}$$

4. Electron-field interaction Hamiltonian is [63]

$$\hat{H}_{\text{e-f}} = -\sum_{\sigma}\int d^3r \hat{\mathbf{J}}\left(\mathbf{r},\sigma,t\right)\hat{\mathbf{A}}\left(\mathbf{r},t\right), \tag{3.38}$$

where the Coulomb gauge ($\nabla \cdot \hat{\mathbf{A}} = 0$) is chosen for the vector potential $\hat{\mathbf{A}}$, and the current operator $\hat{\mathbf{J}}$ is a sum of the paramagnetic current $\hat{\mathbf{J}}^{\nabla}$ and the diamagnetic current $\hat{\mathbf{J}}^{\mathrm{A}}$ [86]

$$\hat{\mathbf{J}}^{\nabla} = \frac{e\hbar}{2mi}\left(\left(\nabla\hat{\Psi}^{\dagger}(\mathbf{r},\sigma,t)\right)\hat{\Psi}(\mathbf{r},\sigma,t) - \hat{\Psi}^{\dagger}(\mathbf{r},\sigma,t)\left(\nabla\hat{\Psi}(\mathbf{r},\sigma,t)\right)\right), \tag{3.39}$$

$$\hat{\mathbf{J}}^{\mathrm{A}} = -\frac{e^2}{m}\hat{\mathbf{A}}(\mathbf{r},t)\,\hat{\Psi}^{\dagger}(\mathbf{r},\sigma,t)\,\hat{\Psi}(\mathbf{r},\sigma,t). \tag{3.40}$$

In the Coulomb gauge, the power of the electromagnetic plane wave (classical) is proportional to the absolute value of the squared vector potential $\mathbf{A}$. It can be shown [70] that in a usual semiconductor laser $|e\mathbf{A}| \ll |\mathbf{p}|$, where $\mathbf{p}$ is a typical momentum of a particle. In analogy with this classical picture, in this work, it is assumed that terms in the Hamiltonian proportional to $\hat{\mathbf{A}}^2$ are small in comparison with terms proportional to $e\hat{\mathbf{A}}\frac{\hbar}{i}\nabla$, and hence part of the Hamiltonian proportional to $\hat{\mathbf{A}}^2$ is neglected. It is equivalent to approximating the total current with only the paramagnetic term $\hat{\mathbf{J}}^{\nabla}$. Inserting the paramagnetic current operator (3.39) into Eq. (3.38), and using the Coulomb gauge to shift the gradient operator gives an alternative form of electron-field interaction

$$\hat{H}_{\text{e-f}} = i\hbar\frac{e}{m}\sum_{\sigma}\int d^3r\hat{\Psi}^{\dagger}(\mathbf{r},\sigma,t)\,\hat{\mathbf{A}}(\mathbf{r},t)\,\nabla\hat{\Psi}(\mathbf{r},\sigma,t). \tag{3.41}$$

The perturbation Hamiltonian (external) contains only two parts

$$\hat{H}_{\text{int}} = \hat{H}_{\text{ext}} + \hat{H}_{\text{k}}, \tag{3.42}$$

which are defined as:

1. $\hat{H}_{\text{ext}}$ describes the interaction of externally controlled carriers and currents with the system [55]

$$\hat{H}_{\text{ext}}(t) = \sum_{\sigma}\int d^3r\left(\rho_{\text{ext}}(\mathbf{r},\sigma,t)\,\hat{\phi}(\mathbf{r},t) - \mathbf{J}_{\text{ext}}(\mathbf{r},\sigma,t)\,\hat{\mathbf{A}}(\mathbf{r},t)\right), \tag{3.43}$$

where

$$\hat{\phi}(\mathbf{r},t) = -e\sum_{\sigma'}\int d^3r' V(\mathbf{r}-\mathbf{r}')\,\hat{\Psi}^{\dagger}(\mathbf{r}',\sigma',t)\,\hat{\Psi}(\mathbf{r}',\sigma',t). \tag{3.44}$$

2. $\hat{H}_{\text{k}}$ is the term describing externally controlled carriers and currents (for example their kinetic energy)

$$\hat{H}_{\text{k}} = \sum_{\sigma}\int d^3r F\left(\rho_{\text{ext}}(\mathbf{r},\sigma,t), \mathbf{J}_{\text{ext}}(\mathbf{r},\sigma,t)\right), \tag{3.45}$$

where F is some function. This term is a number and does not contain operators as externally controlled charges and currents are not part of the system. During

derivation of the Dyson equation the particular form of $\hat{H}_{\mathrm{k}}$ does not have to be specified since it will not enter the final equations. In fact, inclusion of $\hat{H}_{\mathrm{k}}$ is not necessary and many authors do not include it as all [60, 91, 55, 92]. Here, it is included only to have a complete description of the external charges and currents, and to show that it has no effect on the Dyson equation. Calculations shown in Appendix C confirm that $\hat{H}_{\mathrm{k}}$ defined by Eq. (3.45) indeed has no influence on the final equations and can be neglected.

3.3.2 Equation of motion for contour Green's function

To calculate equation of motion for Green's function it is convenient to write the Green's function defined by Eq. (3.25) using the contour step function introduced in Appendix B

$$G\left(\underline{1},\underline{2}\right)=\frac{1}{i\hbar}\left\langle T_{\mathrm{c}}\left[\hat{\Psi}\left(\underline{1}\right)\hat{\Psi}^{\dagger}\left(\underline{2}\right)\right]\right\rangle=\frac{\theta\left(\underline{t}_1,\underline{t}_2\right)}{i\hbar}\left\langle\hat{\Psi}\left(1\right)\hat{\Psi}^{\dagger}\left(2\right)\right\rangle-\frac{\theta\left(\underline{t}_2,\underline{t}_1\right)}{i\hbar}\left\langle\hat{\Psi}^{\dagger}\left(2\right)\hat{\Psi}\left(1\right)\right\rangle. \tag{3.46}$$

Now, the time derivative can be written as

$$\begin{aligned}i\hbar\frac{d}{dt}G\left(\underline{1},\underline{2}\right)&=\theta\left(\underline{t}_1,\underline{t}_2\right)\left\langle\frac{d\hat{\Psi}\left(1\right)}{dt_1}\hat{\Psi}^{\dagger}\left(2\right)\right\rangle-\theta\left(\underline{t}_2,\underline{t}_1\right)\left\langle\hat{\Psi}^{\dagger}\left(2\right)\frac{d\hat{\Psi}\left(1\right)}{dt_1}\right\rangle\\&+\frac{d\theta\left(\underline{t}_1,\underline{t}_2\right)}{dt_1}\left\langle\hat{\Psi}\left(1\right)\hat{\Psi}^{\dagger}\left(2\right)\right\rangle-\frac{d\theta\left(\underline{t}_2,\underline{t}_1\right)}{dt_1}\left\langle\hat{\Psi}^{\dagger}\left(2\right)\hat{\Psi}\left(1\right)\right\rangle.\end{aligned} \tag{3.47}$$

The above formula can be simplified using the following arguments:

1. Easy to prove anti-commutation relations for operators in the Heisenberg picture

$$\begin{aligned}&\left(\left\langle\hat{\Psi}\left(1\right)\hat{\Psi}^{\dagger}\left(2\right)\right\rangle+\left\langle\hat{\Psi}^{\dagger}\left(2\right)\hat{\Psi}\left(1\right)\right\rangle\right)_{t_1=t_2=t}\\&=\left[\hat{\Psi}\left(\mathbf{r}_1,\sigma_1,t\right),\hat{\Psi}^{\dagger}\left(\mathbf{r}_2,\sigma_2,t\right)\right]_{+}=\delta(\mathbf{r}_1-\mathbf{r}_2)\delta_{\sigma_1,\sigma_2},\end{aligned} \tag{3.48}$$

$$\left[\hat{\Psi}\left(\mathbf{r}_1,\sigma_1,t\right),\hat{\Psi}\left(\mathbf{r}_2,\sigma_2,t\right)\right]_{+}=\left[\hat{\Psi}^{\dagger}\left(\mathbf{r}_1,\sigma_1,t\right),\hat{\Psi}^{\dagger}\left(\mathbf{r}_2,\sigma_2,t\right)\right]_{+}=0. \tag{3.49}$$

2. Equation of motion for operator (not explicitly time dependent) in the Heisenberg picture from Appendix A

$$i\hbar\frac{d}{dt}\hat{O}_{\mathrm{H}}\left(t\right)=\left[\hat{O}_{\mathrm{H}}\left(t\right),\hat{H}_{\mathrm{H}}\left(t\right)\right]_{-}. \tag{3.50}$$

3. The definition of a contour delta function from Appendix B

$$\delta\left(\underline{t}_1,\underline{t}_2\right)=\frac{d}{dt_1}\theta\left(\underline{t}_1,\underline{t}_2\right). \tag{3.51}$$

In the above formulas $[]_-$ is the commutator and $[]_+$ is the anti-commutator. The equation of motion for Green's function then becomes

$$\begin{aligned} i\hbar\frac{d}{dt}G\left(\underline{1},\underline{2}\right) &= \frac{1}{i\hbar}\left\langle T_{\mathrm{c}}\left[\left[\hat{\Psi}\left(\underline{1}\right),\hat{H}\left(\underline{1}\right)\right]_-\hat{\Psi}^{\dagger}\left(\underline{2}\right)\right]\right\rangle+\delta\left(\underline{1},\underline{2}\right)\\ &= \theta\left(\underline{t}_1,\underline{t}_2\right)\frac{1}{i\hbar}\left\langle\left[\hat{\Psi}\left(1\right),\hat{H}\left(1\right)\right]_-\hat{\Psi}^{\dagger}\left(2\right)\right\rangle\\ &- \theta\left(\underline{t}_2,\underline{t}_1\right)\frac{1}{i\hbar}\left\langle\hat{\Psi}^{\dagger}\left(2\right)\left[\hat{\Psi}\left(1\right),\hat{H}\left(1\right)\right]_-\right\rangle+\delta\left(\underline{1},\underline{2}\right), \end{aligned} \tag{3.52}$$

where

$$\delta\left(\underline{1},\underline{2}\right)=\delta\left(\underline{t}_1,\underline{t}_2\right)\delta\left(\mathbf{r}_1-\mathbf{r}_2\right)\delta_{\sigma_1\sigma_2}. \tag{3.53}$$

The commutator $\left[\hat{\Psi}\left(1\right),\hat{H}\left(1\right)\right]_-$ can be evaluated by calculating commutators of each part of Hamiltonian $\hat{H}\left(1\right)$ by using standard commutator/anti-commutator properties. Anti-commutation relations for field operators in the Heisenberg picture are given by Eqs. (3.48) and (3.49). Additionally, boson and fermion operators always commute.

Partial commutators of $\left[\hat{\Psi}\left(1\right),\hat{H}\left(1\right)\right]_-$ are

$$\left[\hat{\Psi}\left(1\right),\hat{H}_{\mathrm{s}}\left(1\right)\right]_-=t\left(\mathbf{r}_1,\sigma_1\right)\hat{\Psi}\left(\mathbf{r}_1,\sigma_2,t_1\right)+\sum_{\sigma_3}u\left(\mathbf{r}_1,\sigma_1,\sigma_2\right)\hat{\Psi}\left(\mathbf{r}_1,\sigma_2,t_1\right), \tag{3.54}$$

$$\left[\hat{\Psi}\left(1\right),\hat{H}_{\mathrm{m}}\left(1\right)\right]_-=e^2\sum_{\sigma_2}\int d^3r_2V\left(\mathbf{r}_1-\mathbf{r}_2\right)\hat{\Psi}^{\dagger}\left(\mathbf{r}_2,\sigma_2,t_1\right)\hat{\Psi}\left(\mathbf{r}_2,\sigma_2,t_1\right)\hat{\Psi}\left(\mathbf{r}_1,\sigma_1,t_1\right), \tag{3.55}$$

$$\left[\hat{\Psi}\left(1\right),\hat{H}_{\mathrm{f}}\left(1\right)\right]_-=0, \tag{3.56}$$

$$\left[\hat{\Psi}\left(1\right),\hat{H}_{\text{e-f}}\left(1\right)\right]_-=i\hbar\frac{e}{m}\hat{\mathbf{A}}\left(\mathbf{r}_1,t_1\right)\nabla\hat{\Psi}\left(\mathbf{r}_1,\sigma_1,t_1\right), \tag{3.57}$$

$$\left[\hat{\Psi}\left(1\right),\hat{H}_{\mathrm{ext}}\left(1\right)\right]_-=-e\sum_{\sigma_2}\int d^3r_2V\left(\mathbf{r}_2-\mathbf{r}_1\right)\rho_{\mathrm{ext}}\left(\mathbf{r}_2,\sigma_2,t_1\right)\hat{\Psi}\left(\mathbf{r}_1,\sigma_1,t_1\right), \tag{3.58}$$

$$\left[\hat{\Psi}\left(1\right),\hat{H}_{\mathrm{k}}\left(1\right)\right]_-=0. \tag{3.59}$$

Insertion of these partial commutators into Eq. (3.52) gives the equation of motion for Green's function

$$
\begin{aligned}
&i\hbar\frac{d}{dt_1}G\left(\underline{1},\underline{2}\right)=\delta\left(\underline{1},\underline{2}\right)+t\left(\underline{1}\right)G\left(\underline{1},\underline{2}\right)+\int d\underline{3}u\left(\underline{1},\underline{3}\right)G\left(\underline{3},\underline{2}\right)\\
&+\frac{e^2}{i\hbar}\int d\underline{3}V\left(\underline{1},\underline{3}\right)\left\langle T_{\mathrm{c}}\left[\hat{\Psi}^{\dagger}\left(\underline{3}^{++}\right)\hat{\Psi}\left(\underline{3}^{+}\right)\hat{\Psi}\left(\underline{1}\right)\hat{\Psi}^{\dagger}\left(\underline{2}\right)\right]\right\rangle\\
&+\frac{e}{m}\nabla\left(\underline{1}\right)\left\langle T_{\mathrm{c}}\left[\hat{\mathbf{A}}\left(\underline{1}^{+}\right)\hat{\Psi}\left(\underline{1}\right)\hat{\Psi}^{\dagger}\left(\underline{2}\right)\right]\right\rangle-e\int d\underline{3}V\left(\underline{1},\underline{3}\right)\rho_{\mathrm{ext}}\left(\underline{3}\right)G\left(\underline{1},\underline{2}\right)
\end{aligned}
\tag{3.60}
$$

where the following notational convention is used

$$
\begin{aligned}
&t\left(\underline{1}\right)=t\left(\mathbf{r}_1\right),\\
&V\left(\underline{1},\underline{2}\right)=V\left(\mathbf{r}_1-\mathbf{r}_2\right)\delta\left(\underline{t}_1,\underline{t}_2\right),\\
&u\left(\underline{1},\underline{2}\right)=u\left(\mathbf{r}_1,\sigma_1,\sigma_2\right)\delta\left(\mathbf{r}_1-\mathbf{r}_2\right)\delta\left(\underline{t}_1,\underline{t}_2\right),\\
&\nabla\left(\underline{1}\right)=\nabla\left(\mathbf{r}_1\right)=\left(\frac{\partial}{\partial x_1},\frac{\partial}{\partial y_1},\frac{\partial}{\partial z_1}\right).
\end{aligned}
$$

The "+" subscript indicates the limit from above with respect to all continuous variables, for example for $\underline{1}^{+}$ it is defined as

$$
\underline{1}^{+}=\lim_{\underline{t}_k\rightarrow\underline{t}_1^{+}}\lim_{\mathbf{r}_k\rightarrow\mathbf{r}_1^{+}}\left(\underline{t}_k,\mathbf{r}_k,\sigma_k=\sigma_1\right), \tag{3.61}
$$

where the limit does not include spin (it is a discrete variable) and the contour-time limit is defined in Appendix B. This limit has two purposes. Because the ordering operation is not defined for identical times, in the fourth term on RHS of (3.60) its purpose is to preserve proper ordering under the chronological ordering operator in the case of identical time argument values. Note that there is no such problem for two boson operators with the same time argument (or one boson and one fermion) as those operators always commute under the time ordering operator. Also in the same term, argument $\underline{3}$ is indexed with "+" and "++" because $V\left(\underline{1},\underline{3}\right)$ contains contour delta function and overall (after integration) three field operators have the same contour time argument. In the fifth term on RHS of (3.60) the limit is used to move spatial derivative in front of the vector potential $\hat{\mathbf{A}}$.

3.3.3 Functional derivative approach

The functional derivative technique allows one to replace terms that involve field operators in Eq. (3.60) with terms (in a form of infinite series) that depend only on Green's function. It was developed for the path integral in [93] and adapted to Green's functions in [88, 61, 60]. First, the average values of field operators will be replaced by functional derivatives of Green's functions, and later it will be shown how to replace those derivatives with infinite series consisting of Green's functions. Detailed derivations of most of equations presented in this subsection can be found in Appendix C.

To apply the functional derivative technique to the equation of motion for Green's function (3.60), one has to introduce a formal distinction between the external perturbation $\hat{H}_{\mathrm{int}}\left(t,b=+1\right)$ which takes the system forward in time (the upper branch

of time contour), and $\hat{H}_{\text{int}}(t, b=-1)$ which takes the system backward in time (the lower branch of time contour) [93]. This is necessary because to derive the Dyson equation with the functional derivative technique, it is necessary to take functional derivative over external sources for each branch separately.

Because in the derivation of the equation of motion (3.60) no distinction of $\hat{H}_{\text{int}}$ between branches was made ($\hat{H}_{\text{int}}$ was the same on both branches), before inserting the result from functional derivative calculations, the limit $\hat{H}_{\text{int}}(t, b=+1) = \hat{H}_{\text{int}}(t, b=-1) = \hat{H}_{\text{int}}(t)$ is taken.

With the mentioned above distinction between the upper and lower branch, the definition of Green's function can be written as

$$G(\underline{1}, \underline{2}) = \frac{1}{i\hbar} \frac{\left\langle T_{\text{c}} \left[\hat{S}_{\text{c}} \hat{\Psi}_{\text{I}}(\underline{1}) \hat{\Psi}_{\text{I}}^{\dagger}(\underline{2}) \right] \right\rangle}{\left\langle \hat{S}_{\text{c}} \right\rangle} \Big|_{\hat{H}_{\text{int}}(t,+1)=\hat{H}_{\text{int}}(t,-1)} . \tag{3.62}$$

When the limit is taken, $\left\langle \hat{S}_{\text{c}} \right\rangle = 1$, and Eq. (3.62) becomes the same as Eq. (3.26). The denominator $\left\langle \hat{S}_{\text{c}} \right\rangle$ is necessary to normalize the expression, because after the distinction between the interaction Hamiltonian on upper and lower branches is made, the expression

$$\left\langle T_{\text{c}} \left[\hat{S}_{\text{c}} \hat{\Psi}_{\text{I}}(\underline{1}) \hat{\Psi}_{\text{I}}^{\dagger}(\underline{2}) \right] \right\rangle$$

is no longer normalized. In fact it becomes divergent [94].

This procedure can be applied not only to a Green's function but also to a statistical average of any operator $\hat{O}$

$$\left\langle \hat{O}(1) \right\rangle = \frac{\left\langle T_{\text{c}} \left[\hat{S}_{\text{c}} \hat{O}_{\text{I}}(\underline{1}) \right] \right\rangle}{\left\langle \hat{S}_{\text{c}} \right\rangle} \Big|_{\hat{H}_{\text{int}}(t,+1)=\hat{H}_{\text{int}}(t,-1)} . \tag{3.63}$$

In further calculations, for convenience, the following shorthand notation is used

$$\frac{\left\langle T_{\text{c}} \left[\hat{S}_{\text{c}} \hat{O}_{\text{I}}(\underline{1}) \right] \right\rangle}{\left\langle \hat{S}_{\text{c}} \right\rangle} \equiv \left\langle \hat{O}(\underline{1}) \right\rangle . \tag{3.64}$$

For calculations in this section and in Appendix C where intermediate steps are shown, indication of the limit $\hat{H}_{\text{int}}(t, +1) = \hat{H}_{\text{int}}(t, -1)$ is dropped to simplify the already complex notation. For example

$$\frac{\delta G(\underline{1}, \underline{2})}{\delta \rho_{\text{ext}}(\underline{3})} \Big|_{\hat{H}_{\text{int}}(t,+1)=\hat{H}_{\text{int}}(t,-1)} \equiv \frac{\delta G(\underline{1}, \underline{2})}{\delta \rho_{\text{ext}}(\underline{3})}, \tag{3.65}$$

or

$$\left\langle T_{\mathrm{c}}\left[\hat{O}\left(\underline{1}\right)\hat{O}\left(\underline{2}\right)\right]\right\rangle = \frac{\left\langle T_{\mathrm{c}}\left[\hat{S}_{\mathrm{c}}\hat{O}_{\mathrm{I}}\left(\underline{1}\right)\hat{O}_{\mathrm{I}}\left(\underline{2}\right)\right]\right\rangle}{\left\langle \hat{S}_{\mathrm{c}}\right\rangle}\Big|_{\hat{H}_{\mathrm{int}}(t,+1)=\hat{H}_{\mathrm{int}}(t,-1)}$$
$$\equiv \frac{\left\langle T_{\mathrm{c}}\left[\hat{S}_{\mathrm{c}}\hat{O}_{\mathrm{I}}\left(\underline{1}\right)\hat{O}_{\mathrm{I}}\left(\underline{2}\right)\right]\right\rangle}{\left\langle \hat{S}_{\mathrm{c}}\right\rangle}. \tag{3.66}$$

Functional derivatives over external charges and sources, necessary to get rid of the field operators in the equation of motion (3.60) are

$$\frac{\delta G\left(\underline{1},\underline{2}\right)}{\delta\rho_{\mathrm{ext}}\left(\underline{1}^{+}\right)} = -e\int d\underline{3}V(\underline{1},\underline{3})G\left(\underline{3},\underline{3}^{+}\right)G\left(\underline{1},\underline{2}\right)$$
$$-e\left(\frac{1}{i\hbar}\right)^{2}\int d\underline{3}V\left(\underline{1},\underline{3}\right)\left\langle T_{\mathrm{c}}\left[\hat{\Psi}^{\dagger}\left(\underline{3}^{++}\right)\hat{\Psi}\left(\underline{3}^{+}\right)\hat{\Psi}\left(\underline{1}\right)\hat{\Psi}^{\dagger}\left(\underline{2}\right)\right]\right\rangle, \tag{3.67}$$

and

$$\frac{\delta G\left(\underline{1},\underline{2}\right)}{\delta J_{i,\mathrm{ext}}\left(\underline{1}^{+}\right)} = \frac{1}{i\hbar}\left\langle \hat{A}_{i}\left(\underline{1}\right)\right\rangle G\left(\underline{1},\underline{2}\right) - \left(\frac{1}{i\hbar}\right)^{2}\left\langle T_{\mathrm{c}}\left[\hat{A}_{i}\left(\underline{1}\right)\hat{\Psi}\left(\underline{1}\right)\hat{\Psi}^{\dagger}\left(\underline{2}\right)\right]\right\rangle. \tag{3.68}$$

Insertion of Eqs. (3.67) and (3.68) into equation of motion (3.60) yields

$$\left(i\hbar\frac{d}{dt_{1}} - t\left(\mathbf{r}_{1}\right) + e\int d\underline{3}V\left(\underline{1},\underline{3}\right)\left(\rho_{\mathrm{ext}}\left(\underline{3}\right) + ei\hbar G\left(\underline{3},\underline{3}^{+}\right)\right) + \frac{i\hbar e}{m}\left\langle\hat{\mathbf{A}}\left(\underline{1}\right)\right\rangle\nabla\left(\underline{1}\right)\right)G\left(\underline{1},\underline{2}\right)$$
$$= \delta\left(\underline{1},\underline{2}\right) + \int d\underline{3}u\left(\underline{1},\underline{3}\right)G\left(\underline{3},\underline{2}\right) - ei\hbar\frac{\delta G\left(\underline{1},\underline{2}\right)}{\delta\rho_{\mathrm{ext}}\left(\underline{1}^{+}\right)} - \frac{\left(i\hbar\right)^{2}e}{m}\sum_{i=1}^{3}\partial_{i}\left(\underline{1}\right)\frac{\delta G\left(\underline{1},\underline{2}\right)}{\delta J_{i,\mathrm{ext}}\left(\underline{1}^{+}\right)}. \tag{3.69}$$

To proceed further, one has assume that contour Green's function has an unique inverse

$$\int d\underline{3}G^{-1}\left(\underline{1},\underline{3}\right)G\left(\underline{3},\underline{2}\right) = \int d\underline{3}G\left(\underline{1},\underline{3}\right)G^{-1}\left(\underline{3},\underline{2}\right) = \delta\left(\underline{1},\underline{2}\right). \tag{3.70}$$

This assumption is possible only if the influence of initial correlations (existing before $\hat{H}_{\mathrm{int}}$ is turned on) on the system is negligible. In other words, the system has to have no memory of its state before t_0 [60, 90]. The necessary condition for this to happen, is that the initial time t_0 has to be equal $-\infty$. Maximal time t_{m} can be also shifted $+\infty$, and now the time contour goes from $-\infty \rightarrow +\infty$ and then back from $+\infty \rightarrow -\infty$.

Shifting the initial time to $-\infty$ is not a sufficient condition as one can imagine a system that is initially in an ordered state (ferromagnetic, superconductor) and

perturbation is not strong enough to disorder that state. Then, even after an infinite time, the system will stay in the initial state. This is why the validity of the assumption that the initial correlations are negligible, depends on the properties of a particular system. In this work, laser diodes are investigated in their steady-state only, which obviously satisfy condition of no memory of the initial state. A more detailed discussion of initial correlations can be found in [60, 87, 90]. A Green's function theory which takes initial correlations into account is described in [95, 96].

The functional derivative terms in Eq. (3.69) can be replaced by a so-called self-energy $\Sigma\left(\underline{1},\underline{2}\right)$ defined as

$$\Sigma\left(\underline{1},\underline{2}\right)=\Sigma_{\mathrm{L}}\left(\underline{1},\underline{2}\right)+\Sigma_{\mathrm{T}}\left(\underline{1},\underline{2}\right), \tag{3.71}$$

where the longitudinal self-energy Σ_{L} is

$$\Sigma_{\mathrm{L}}\left(\underline{1},\underline{2}\right)=-ei\hbar\int d\underline{3}\frac{\delta G\left(\underline{1},\underline{3}\right)}{\delta\rho_{\mathrm{ext}}\left(\underline{1}^{+}\right)}G^{-1}\left(\underline{3},\underline{2}\right), \tag{3.72}$$

and the transverse self-energy Σ_{T} is

$$\Sigma_{\mathrm{T}}\left(\underline{1},\underline{2}\right)=-\frac{\left(i\hbar\right)^{2}e}{m}\sum_{i=1}^{3}\partial_{i}\left(\underline{1}\right)\frac{\delta G\left(\underline{1},\underline{2}\right)}{\delta J_{i,\mathrm{ext}}\left(\underline{1}^{+}\right)}G^{-1}\left(\underline{3},\underline{2}\right). \tag{3.73}$$

With the above definitions, Eq. (3.69) becomes

$$\begin{aligned}&\left(i\hbar\frac{d}{dt_{1}}-t\left(\underline{1}\right)+eU\left(\underline{1}\right)+\frac{i\hbar e}{m}\left\langle\hat{\mathbf{A}}\left(\underline{1}\right)\right\rangle\nabla\left(\underline{1}\right)\right)G\left(\underline{1},\underline{2}\right)\\&=\delta\left(\underline{1},\underline{2}\right)+\int d\underline{3}\left(u\left(\underline{1},\underline{3}\right)+\Sigma\left(\underline{1},\underline{3}\right)\right)G\left(\underline{3},\underline{2}\right).\end{aligned} \tag{3.74}$$

If the self-energy Σ in Eq. (3.74) is expressed by an infinite series containing consecutive powers of Green's functions, then equation (3.74) is called the Dyson equation. The inverse Green's function $G^{-1}\left(\underline{1},\underline{2}\right)$ is

$$\begin{aligned}G^{-1}\left(\underline{1},\underline{2}\right)&=\left(i\hbar\frac{d}{dt_{1}}-t\left(\underline{1}\right)+eU_{\mathrm{eff}}\left(\underline{1}\right)+\frac{i\hbar e}{m}\left\langle\hat{\mathbf{A}}\left(\underline{1}\right)\right\rangle\nabla\left(\underline{1}\right)\right)\delta\left(\underline{1},\underline{2}\right)\\&-u\left(\underline{1},\underline{2}\right)-\Sigma\left(\underline{1},\underline{2}\right),\end{aligned} \tag{3.75}$$

where U_{eff} defined as

$$U_{\mathrm{eff}}\left(\underline{1}\right)=\int d\underline{3}V\left(\underline{1},\underline{3}\right)\left(\rho_{\mathrm{ext}}\left(\underline{3}\right)+\left\langle\hat{\rho}\left(\underline{3}\right)\right\rangle\right), \tag{3.76}$$

is the effective potential acting on the particle. It is a sum of two potentials: potential created by the external sources ρ_{ext}, and a potential from the averaged density of all electrons present in the system $\left\langle\hat{\rho}\left(\underline{1}\right)\right\rangle=-e\left\langle\hat{n}_{\mathrm{p}}\left(\underline{1}\right)\right\rangle$. The averaged electron density can be expressed by Green's function, by combining formulas for the statistical

average of particle density (3.21) and the definition of the contour Green's function (3.25)

$$\langle \hat{\rho}\left(\underline{1}\right)\rangle = -e\left\langle \hat{n}_{\mathrm{p}}\left(\underline{1}\right)\right\rangle = e\left\langle T_{\mathrm{c}}\left[\hat{\Psi}\left(\underline{1}\right)\hat{\Psi}^{\dagger}\left(\underline{1}^{+}\right)\right]\right\rangle = ei\hbar G\left(\underline{1},\underline{1}^{+}\right). \tag{3.77}$$

The Dyson equation (3.74) is in differential form, but it can also be stated in the integral form. To get the integral form one can define G_0 as

$$\left(i\hbar\frac{d}{dt_1} - t\left(\underline{1}\right) + eU_{\mathrm{eff}}\left(\underline{1}\right) + \frac{i\hbar e}{m}\left\langle \hat{\mathbf{A}}\left(\underline{1}\right)\right\rangle \nabla\left(\underline{1}\right)\right) G_0\left(\underline{1},\underline{2}\right) = \delta\left(\underline{1},\underline{2}\right). \tag{3.78}$$

With the above definition of G_0, the integral form of the Dyson equation is

$$G\left(\underline{1},\underline{2}\right) = G_0\left(\underline{1},\underline{2}\right) + \int d\underline{3}\int d\underline{4}\int d\underline{3}G_0\left(\underline{1},\underline{3}\right)\left(u\left(\underline{3},\underline{4}\right) + \Sigma\left(\underline{3},\underline{4}\right)\right)G\left(\underline{4},\underline{2}\right), \tag{3.79}$$

which can easily be proven to be correct by applying

$$\left(i\hbar\frac{d}{dt_1} - t\left(\underline{1}\right) + eU_{\mathrm{eff}}\left(\underline{1}\right) + \frac{i\hbar e}{m}\left\langle \hat{\mathbf{A}}\left(\underline{1}\right)\right\rangle \nabla\left(\underline{1}\right)\right)$$

to both sides of Eq. (3.79) and then using the definition of G_0.

Longitudinal self-energy

The longitudinal self-energy is responsible for electron-electron interaction via the Coulomb potential.

Under the assumption that U_{eff} does not depend on external current $\mathbf{J}_{\mathrm{ext}}$ i.e., $\delta U_{\mathrm{eff}}/\delta J_{\mathrm{ext},i} = 0$, the longitudinal self-energy Σ_{L} can be expressed as

$$\Sigma_{\mathrm{L}}\left(\underline{1},\underline{2}\right) = -i\hbar\int d\underline{3}\int d\underline{4}G\left(\underline{1},\underline{3}\right)\gamma\left(\underline{3},\underline{2},\underline{4}\right)W\left(\underline{4},\underline{1}^{+}\right), \tag{3.80}$$

where

$$\text{longitudinal vertex function:}\quad \gamma\left(\underline{1},\underline{2},\underline{3}\right) = \frac{\delta G^{-1}\left(\underline{1},\underline{2}\right)}{\delta U_{\mathrm{eff}}\left(\underline{3}\right)}, \tag{3.81}$$

$$\text{screened Coulomb potential:}\quad W\left(\underline{1},\underline{2}\right) = \frac{\delta U_{\mathrm{eff}}\left(\underline{1}\right)}{\delta \rho_{\mathrm{ext}}\left(\underline{2}\right)}, \tag{3.82}$$

$$\text{longitudinal polarization function:}\quad p\left(\underline{1},\underline{2}\right) = \frac{\delta\left\langle \hat{\rho}\left(\underline{1}\right)\right\rangle}{\delta U_{\mathrm{eff}}\left(\underline{2}\right)}. \tag{3.83}$$

The screened Coulomb potential (plasmon Green's function) $W\left(\underline{1},\underline{2}\right)$ can be obtained by solving the following equation

$$W\left(\underline{1},\underline{2}\right) = V\left(\underline{1},\underline{2}\right) + \int d\underline{3}\int d\underline{4}V(\underline{1},\underline{3})p\left(\underline{3},\underline{4}\right)W\left(\underline{4},\underline{2}\right). \tag{3.84}$$

One should remember that, although both $W(\underline{1},\underline{2})$ and $V(\underline{1},\underline{2})$ are written as functions of $\underline{1} = (\mathbf{r}_1, \sigma_1, t_1, b_1)$, none of them have actual spin dependence. Equation (3.84) is very similar to the integral Dyson equation (3.79), where the Coulomb potential is the zeroth order term which is modified (screened) by the longitudinal polarization $p(\underline{1},\underline{2})$, which in turn is analogous to a self-energy term in the Dyson equation.

By acting with the Laplace operator on both sides of Eq. (3.84), using

$$V(\underline{1},\underline{2}) = \frac{1}{4\pi\epsilon_0}\frac{1}{|\mathbf{r}_1 - \mathbf{r}_2|}\delta(\underline{t}_1, \underline{t}_2), \tag{3.85}$$

for the Coulomb potential and the following property of the Dirac delta function

$$\nabla^2(\mathbf{r}_1)\frac{1}{|\mathbf{r}_1 - \mathbf{r}_2|} = -4\pi\delta(\mathbf{r}_1 - \mathbf{r}_2), \tag{3.86}$$

one can get the equation for a screened Coulomb potential which is analogous to the differential Dyson equation (3.74)

$$-\epsilon_0\nabla^2(\mathbf{r}_1)W\left(\widetilde{\underline{3}},\widetilde{\underline{2}}\right) = \delta\left(\widetilde{\underline{1}},\widetilde{\underline{2}}\right) + \int d\widetilde{\underline{3}}\,\widetilde{p}\left(\widetilde{\underline{1}},\widetilde{\underline{3}}\right)W\left(\widetilde{\underline{3}},\widetilde{\underline{2}}\right). \tag{3.87}$$

Notational convention used in the above equation is

$$\begin{gathered}\widetilde{\underline{k}} = \{\mathbf{r}_k, \underline{t}_k\} = \{\mathbf{r}_k, t_k, b_k\},\\ \int d\widetilde{\underline{k}} = \int d^3r_k \int d\underline{t}_k = \sum_b b\int d^3r_k\int dt_b,\\ \delta\left(\widetilde{\underline{1}},\widetilde{\underline{2}}\right) = \delta(\underline{t}_1,\underline{t}_2)\,\delta(\mathbf{r}_1 - \mathbf{r}_2),\end{gathered} \tag{3.88}$$

and the term $\widetilde{p}\left(\widetilde{\underline{1}},\widetilde{\underline{2}}\right)$ is defined as

$$\widetilde{p}\left(\widetilde{\underline{1}},\widetilde{\underline{2}}\right) = \sum_{\sigma_1\sigma_2} p(\underline{1},\underline{2}). \tag{3.89}$$

The two remaining equations for $p(\underline{1},\underline{2})$ and $\gamma(\underline{1},\underline{2},\underline{3})$ are

$$p(\underline{1},\underline{2}) = -ei\hbar\int d\underline{3}\int d\underline{4}\,G(\underline{1},\underline{3})\,\gamma(\underline{3},\underline{4},\underline{2})\,G\left(\underline{4},\underline{1}^+\right), \tag{3.90}$$

and

$$\begin{aligned}\gamma(\underline{1},\underline{2},\underline{3}) &= e\delta(\underline{1},\underline{2})\,\delta(\underline{1},\underline{3})\\ &+ \int d\underline{4}\int d\underline{5}\int d\underline{6}\int d\underline{7}\frac{\delta\Sigma_{\mathrm{L}}(\underline{1},\underline{2})}{\delta G(\underline{4},\underline{5})}G(\underline{4},\underline{6})\,\gamma(\underline{6},\underline{7},\underline{3})\,G(\underline{7},\underline{5}).\end{aligned} \tag{3.91}$$

Equations (3.80), (3.84), (3.90), and (3.91) allow to express longitudinal self-energy as an infinite series containing only Green's functions G. This series can

be evaluated as follows: to the first order $\gamma(\underline{1},\underline{2},\underline{3}) = -\delta(\underline{1},\underline{2})\,\delta(\underline{1},\underline{3})$. This value is inserted into equation for $p(\underline{1},\underline{2})$, and both $\gamma(\underline{1},\underline{2},\underline{3})$ and $p(\underline{1},\underline{2})$ are used to evaluate the first order of $W(\underline{1},\underline{2})$. The values of $p(\underline{1},\underline{2})$ and $W(\underline{1},\underline{2})$ are inserted into equation for the longitudinal self-energy (3.80) to obtain the first order of $\Sigma_{\mathrm{L}}(\underline{1},\underline{2})$. The first order self-energy, $\Sigma_{\mathrm{L}}(\underline{1},\underline{2})$ and the first order $\gamma(\underline{1},\underline{2},\underline{3})$ are used to calculate the second order correction to $\gamma(\underline{1},\underline{2},\underline{3})$. The procedure repeats itself up to the desired order.

Transverse self-energy

The transverse self-energy describes electron-photon interaction. The procedure of calculating transverse self-energy is analogous to the procedure that led to the expressions for the longitudinal self-energy.

In analogy to the effective potential $U_{\mathrm{eff}}(\underline{1})$, the effective vector potential is defined as

$$A_{i,\mathrm{eff}}(\underline{1}) = \left\langle \hat{A}_i(\underline{1}) \right\rangle, \tag{3.92}$$

and it is assumed that $\delta A_{i,\mathrm{eff}}/\delta J_{i,\mathrm{ext}} = 0$.

The equation for transverse self-energy is

$$\Sigma_{\mathrm{T}}(\underline{1},\underline{2}) = i\hbar \int d\underline{3} \int d\underline{4} \sum_{i,j=1}^{3} \left(\frac{i\hbar e}{m} \partial_i(\mathbf{r}_1) \right) G(\underline{1},\underline{3})\,\Gamma_j(\underline{3},\underline{2},\underline{4})\,D_{j,i}\left(\underline{4},\underline{1}^{+}\right), \tag{3.93}$$

where

$$\text{transverse vertex function:} \quad \Gamma_i(\underline{1},\underline{2},\underline{3}) = -\mu_0 \frac{\delta G^{-1}(\underline{1},\underline{2})}{\delta A_{i,\mathrm{eff}}(\underline{3})}, \tag{3.94}$$

$$\text{photon Green's function:} \quad D_{i,j}(\underline{1},\underline{2}) = -\frac{1}{\mu_0} \frac{\delta A_{i,\mathrm{eff}}(\underline{1})}{\delta J_{j,\mathrm{ext}}(\underline{2})}, \tag{3.95}$$

$$\text{transverse polarization function:} \quad P_{i,j}(\underline{1},\underline{2}) = -\mu_0 \frac{\delta \left\langle \hat{J}_i^{\mathrm{T}}(\underline{1}) \right\rangle}{\delta A_{j,\mathrm{eff}}(\underline{2})}, \tag{3.96}$$

Similarly, as in the case of the screened Coulomb potential, the photon Green's function $D_{i,j}(\underline{1},\underline{2})$ does not depend on the spin index. In the expression for the transverse polarization function (3.96), $\hat{J}_i^{\mathrm{T}}$ is the transverse current defined as

$$\hat{J}_i^{\mathrm{T}}(\underline{1}) = \sum_{j=1}^{3} \int d\underline{2}\,\delta_{i,j}^{\mathrm{T}}(\underline{1},\underline{2})\,\hat{J}_j(\underline{2}), \tag{3.97}$$

where $\delta_{i,j}^{\mathrm{T}}(\underline{1},\underline{2})$ is the transverse delta function

$$\delta_{i,j}^{\mathrm{T}}(\underline{1},\underline{2}) = \left[\delta_{i,j}\delta(\mathbf{r}_1 - \mathbf{r}_2) + \frac{1}{4\pi} \partial_i(\mathbf{r}_1)\,\partial_j(\mathbf{r}_1) \frac{1}{|\mathbf{r}_1 - \mathbf{r}_2|} \right] \delta_{\sigma_1,\sigma_2}\delta(\underline{t}_1,\underline{t}_2). \tag{3.98}$$

Average value of the paramagnetic current operator (3.39) is expressed by the electron Green's function as

$$\begin{aligned}\left\langle \hat{J}_i\left(\underline{1}\right)\right\rangle &= \frac{e\hbar}{2mi}\lim_{\underline{2}\to\underline{1}}\left(\partial_i\left(\underline{1}\right)-\partial_i\left(\underline{2}\right)\right)\left\langle \hat{\Psi}^\dagger\left(\underline{1}\right)\hat{\Psi}\left(\underline{2}\right)\right\rangle \\ &= -i\hbar\Pi_i\left(\underline{1},\underline{1}^+\right)G\left(\underline{1},\underline{1}^+\right), \end{aligned} \tag{3.99}$$

where

$$\Pi_i\left(\underline{1},\underline{2}\right) = \frac{e\hbar}{2mi}\left(\partial_i\left(\underline{1}\right)-\partial_i\left(\underline{2}\right)\right). \tag{3.100}$$

The photon Green's function can be evaluated directly from Eq. (3.95)

$$D_{i,j}\left(\underline{1},\underline{2}\right) = \frac{1}{i\hbar\mu_0}\left(\left\langle T_{\mathrm{c}}\left[\hat{A}_i\left(\underline{1}\right)\hat{A}_j\left(\underline{2}\right)\right]\right\rangle - \left\langle \hat{A}_i\left(\underline{1}\right)\right\rangle\left\langle \hat{A}_j\left(\underline{2}\right)\right\rangle\right), \tag{3.101}$$

or calculated by solving the differential equation

$$\left(\nabla^2\left(\mathbf{r}_1\right)-\frac{1}{c^2}\frac{d^2}{dt_1^2}\right)D_{i,j}\left(\widetilde{\underline{1}},\widetilde{\underline{2}}\right) = \delta^{\mathrm{T}}_{i,j}\left(\widetilde{\underline{1}},\widetilde{\underline{2}}\right)+\int d\widetilde{\underline{3}}\widetilde{P}_{i,k}\left(\widetilde{\underline{1}},\widetilde{\underline{3}}\right)D_{k,j}\left(\widetilde{\underline{3}},\widetilde{\underline{2}}\right), \tag{3.102}$$

where

$$\widetilde{P}_{i,k}\left(\widetilde{\underline{1}},\widetilde{\underline{2}}\right) = \sum_{\sigma_1,\sigma_2}P_{i,k}\left(\underline{1},\underline{2}\right), \tag{3.103}$$

and $\delta^{\mathrm{T}}_{i,j}\left(\widetilde{\underline{1}},\widetilde{\underline{2}}\right)$ is defined analogously to $\delta^{\mathrm{T}}_{i,j}\left(\underline{1},\underline{2}\right)$, but without $\delta_{\sigma_1,\sigma_2}$ on the RHS in Eq. (3.98). From now on, Eq. (3.102) will be referred to as the photon Dyson equation. The equation for the photon Green's function can be also expressed in terms of integral equation

$$D_{i,j}\left(\underline{1},\underline{2}\right) = D^0_{i,j}\left(\underline{1},\underline{2}\right)+\sum_{k,l=1}^{3}\int d\underline{3}\int d\underline{4}D^0_{i,k}\left(\underline{1},\underline{3}\right)P_{k,l}\left(\underline{3},\underline{4}\right)D_{l,j}\left(\underline{4},\underline{2}\right), \tag{3.104}$$

where $D^0_{i,j}\left(\underline{1},\underline{2}\right)$ satisfies

$$\left(\nabla^2\left(\mathbf{r}_1\right)-\frac{1}{c^2}\frac{d^2}{dt_1^2}\right)D^0_{i,j}\left(\widetilde{\underline{1}},\widetilde{\underline{2}}\right) = \delta^{\mathrm{T}}_{i,j}\left(\widetilde{\underline{1}},\widetilde{\underline{2}}\right). \tag{3.105}$$

Validity of Eq. (3.104) can be checked by acting on it with $\left(\nabla^2\left(\mathbf{r}_1\right)-\frac{1}{c^2}\frac{d^2}{dt_1^2}\right)$ and using definition of $D^0_{i,j}\left(\underline{1},\underline{2}\right)$.

The transverse vertex function Γ_i is determined using the following equation

$$\begin{aligned}\Gamma_i\left(\underline{1},\underline{2},\underline{3}\right) &= \frac{i\hbar e\mu_0}{m}\delta\left(\underline{1},\underline{3}\right)\partial_i\left(\underline{1}\right)\delta\left(\underline{1},\underline{2}\right) \\ &+\int d\underline{4}\int d\underline{5}\int d\underline{6}\int d\underline{7}\frac{\delta\Sigma_{\mathrm{T}}\left(\underline{1},\underline{2}\right)}{\delta G\left(\underline{4},\underline{5}\right)}G\left(\underline{4},\underline{6}\right)\Gamma_i\left(\underline{6},\underline{7},\underline{3}\right)G\left(\underline{7},\underline{5}\right), \end{aligned} \tag{3.106}$$

and the equation for transverse polarization is

$$P_{i,j}\left(\underline{1},\underline{2}\right) = i\hbar \sum_{k=1}^{3} \int d\underline{3} \int d\underline{4} \int d\underline{5} \delta^{\mathrm{T}}_{i,k}\left(\underline{1},\underline{3}\right) \times \Pi_k\left(\underline{3},\underline{3}^{+}\right) G\left(\underline{3},\underline{4}\right) \Gamma_j\left(\underline{4},\underline{5},\underline{2}\right) G\left(\underline{5},\underline{3}^{+}\right). \tag{3.107}$$

The equations for the longitudinal (3.80) and transverse (3.93) self-energies along with all six supplementary equations for the polarization, vertex function, etc. allow, at least in principle, to account for all electrostatic (through screening of Coulomb potential) and electromagnetic (through interaction with photons) many-body interactions caused by electromagnetic field, up to an arbitrary order.

3.3.4 Static ion lattice, ionized impurities, and phonons

During derivations of the Dyson equation, the interaction of electrons with the ion lattice as well as possible impurities, was neglected. The derivation of interaction between electrons and ion lattice is a complex task. A very detailed description of how to include an ion lattice and phonons in the functional derivative approach can be found in [92].

In this work, the influence of static ion lattice, ionized impurities, and phonons is included only at the very basic level. The most important terms for accurate description of a laser diode are added "by hand" to the previously derived equations.

The direct influence of a static ion lattice and ionized dopants is taken into account by adding single-particle potential to the single-particle Hamiltonian. The explicit form of term t in the Hamiltonian (3.34) is

$$t\left(\mathbf{r}\right) = t'\left(\mathbf{r}\right) + e^2 \int d^3r' V(\mathbf{r},\mathbf{r}') \left(N_{\mathrm{A}}\left(\mathbf{r}'\right) - N_{\mathrm{D}}\left(\mathbf{r}'\right)\right), \tag{3.108}$$

where the second term in above equation is the potential due to ionized dopants and $t'\left(\mathbf{r}\right)$ consists of a sum of kinetic energy and an ion lattice single-particle potential without the spin mixing term

$$t'\left(\mathbf{r}\right) = -\frac{\hbar^2}{2m}\nabla^2 - eV_{\mathrm{l}}\left(\mathbf{r}\right). \tag{3.109}$$

The spin mixing term u has only one component – part of the ion lattice potential that is responsible for spin-orbit interactions

$$u\left(\mathbf{r},\sigma,\sigma'\right) = -eV_{\mathrm{so}}\left(\mathbf{r},\sigma,\sigma'\right). \tag{3.110}$$

Another effect which the static ion lattice introduces, is additional screening. This screening is taken into account in a simplest possible way: by multiplying vacuum permittivity ϵ_0 by the relative static permittivity ϵ_{s} whenever electrostatic interactions are considered, and by relative high frequency permittivity ϵ_∞ whenever the electrodynamic effects are considered.

Finally, the interactions with phonon waves will introduce a self-energy term similar to the transverse self-energy (which contains electron-photon interaction). The exact form of this electron-phonon self-energy is discussed in the next chapter along with a more detailed formulation of other self-energy terms.

Chapter 4

Application of NEGF to a laser diode

In this chapter, the formalism discussed in Chapter 3 is used to derive equations describing a laser diode that are suitable for numerical implementation.

Section 4.1 provides a more detailed description of the laser diode system under consideration, and it explains reasons for the most important assumptions necessary to simplify the general equations from the previous section.

In Section 4.2 the contour Dyson equation is converted into a real-time equation. Green's functions are expanded in a discrete basis to allow for a convenient numerical implementation.

The next section introduces the concept of quasiparticle electrons and holes. It provides formulas connecting Green's function written in discrete basis to physical quantities such as electron/hole densities and quasiparticle current densities.

In the final section of this chapter, the electron-photon interaction self-energy given by Eq. (3.93) is calculated for the case of edge-emitting laser. This section also includes a short description of electron-phonon self-energy [97], and the phenomenological Golizadeh self-energy [98].

4.1 Description of the system

The system considered in this work, is an edge-emitting laser diode based on a quantum well. It is in a non-equilibrium steady-state. In the light emission direction x, it is a Fabry-Perot (FP) resonator with two selective mirrors. The mirrors are assumed to reflect only light with a specific frequency ω_{m}, and are perfectly transparent for all other frequencies. In the transverse plane $y - z$, it is a layered structure grown in the z direction with at least one quantum well among the layers.

The system has to be described differently when dealing with optical quantities and differently when dealing with electrical quantities. This is necessary because the quasiparticles (electrons and holes) have substantially shorter wavelengths than electromagnetic field from the visible spectrum. Because of this, for the particles, a significant length scale is of the order of a nanometer while for photons this scale is

in a micrometer range. Without this separation, the electrical part of the simulation would have to a contain huge, and computationally intensive region which would be mostly irrelevant.

For the purpose of the electrical part of the simulator, the system consists only of the portion of the resonator that is in the close vicinity of the quantum well. It is assumed that this system is infinite and macroscopically uniform in the transverse plane $x-y$, but non-uniform in the z direction (crystal growth direction). It forms a $p-i-n$ junction (in z direction) with quantum wells in the intrinsic region.

In the optical part of the equations, the system consist of a full Fabry-Perot resonator and vacuum around it. It is assumed that the laser operates in one transverse mode (fundamental mode) only, and that the electric field of the fundamental mode is polarized in the y direction.

4.2 The real-time Dyson equation in discrete basis

To preform any meaningful calculations, the abstract Dyson equation (3.74) has to be rewritten as set of equations containing only real times and then written in a basis suitable for numerical implementation. In this section, with the help of contour algebra from Appendix B, the Dyson equation (3.74) is converted into a set of equations containing only real times. Next, the discrete basis is introduced. It consists of a product of rapidly varying functions as well as slowly varying envelope functions. At the end of this section, the Dyson equation is formulated in mentioned basis and boundary conditions are imposed.

4.2.1 The Dyson equation for real-time functions

Using the contour algebra described in Appendix B, the full contour Dyson equation (3.74) can be converted into four real-time equations for lesser, greater, advanced, and retarded Green's functions. However, only the equation for the retarded Green's function is necessary, and other three Green's functions can be obtained from the retarded Green's function. The equations which allow to obtain advanced, lesser, and greater Green's functions from the retarded Green's function will be called supplementary equations.

Because the external charges and currents are not physically present in the system under consideration, they are set to zero at this point. It is also assumed that in the steady-state, the average of vector potential $\left\langle \hat{\mathbf{A}} \right\rangle = 0$ [55]. With this assumption, the inverse of contour Green's function (3.75) becomes

$$G^{-1}\left(\mathbf{r}_1\sigma_1\underline{t}_1,\mathbf{r}_2\sigma_2\underline{t}_2\right) = \left[\left(i\hbar\frac{\partial}{\partial t_1} - t\left(\mathbf{r}_1\right) + eU_{\text{eff}}\left(\mathbf{r}_1,t_1\right)\right)\delta_{\sigma_1,\sigma_2} - u\left(\mathbf{r}_1,\sigma_1,\sigma_2\right)\right] \times \delta\left(\mathbf{r}_1-\mathbf{r}_2\right)\delta\left(\underline{t}_1,\underline{t}_2\right) - \Sigma\left(\mathbf{r}_1\sigma_1\underline{t}_1,\mathbf{r}_2\sigma_2\underline{t}_2\right), \tag{4.1}$$

The effective potential U_{eff} can be expressed by electron density n_{p} only

$$eU_{\text{eff}}\left(\rho_{\text{ext}}=0\right)=-e^{2}i\hbar\sum_{\sigma_3}\int d^{3}r_{3}V(\mathbf{r}_{1},\mathbf{r}_{3})G\left(\mathbf{r}_{3}\sigma_{3}\underline{t}_{1},\mathbf{r}_{3}\sigma_{3}\underline{t}_{1}^{+}\right)$$
$$=-e^{2}\sum_{\sigma_3}\int d^{3}r_{3}V(\mathbf{r}_{1},\mathbf{r}_{3})i\hbar G^{<}\left(\mathbf{r}_{3}\sigma_{3}t_{1},\mathbf{r}_{3}\sigma_{3}t_{1}\right)=-e^{2}\int d^{3}r_{3}V(\mathbf{r}_{1},\mathbf{r}_{3})n_{\text{p}}\left(\mathbf{r}_{3}\right), \tag{4.2}$$

where the limit of contour Green's function is calculated using Eq. (B.43), and the total electron density n_{p} does not depend on time because the steady-state condition is assumed. Using Eq. (3.108) to explicitly write $t\left(\mathbf{r}_{1}\right)$ and $u\left(\mathbf{r}_{1}\right)$, the effective potential can be combined with the potential coming from ionized dopants

$$-t\left(\mathbf{r}_{1}\right)+eU_{\text{eff}}\left(\mathbf{r}_{1},t_{1},\rho_{ext}=0\right)=\frac{\hbar^{2}}{2m}\nabla^{2}\left(\mathbf{r}_{1}\right)+eV_{\text{I}}\left(\mathbf{r}_{1}\right)$$
$$-e^{2}\int d^{3}r'V(\mathbf{r}_{1},\mathbf{r}_{3})\left(n_{\text{p}}\left(\mathbf{r}_{3},t_{1}\right)+N_{\text{A}}\left(\mathbf{r}_{3}\right)-N_{\text{D}}\left(\mathbf{r}_{3}\right)\right). \tag{4.3}$$

Now, one can define the total electrostatic potential V_{P} as

$$V_{\text{P}}=-e\int d^{3}r'V(\mathbf{r}_{1},\mathbf{r}_{3})\left(n_{\text{p}}\left(\mathbf{r}_{3},t_{1}\right)+N_{\text{A}}\left(\mathbf{r}_{3}\right)-N_{\text{D}}\left(\mathbf{r}_{3}\right)\right), \tag{4.4}$$

which is a solution of the electrostatic Poisson equation

$$\epsilon_{0}\sum_{i}\partial_{i}\left[\epsilon_{\text{s}}\left(\mathbf{r}\right)\partial_{i}V_{\text{P}}\left(\mathbf{r}\right)\right]=e\left(n_{\text{p}}\left(\mathbf{r}\right)+N_{\text{A}}\left(\mathbf{r}\right)-N_{\text{D}}\left(\mathbf{r}\right)\right), \tag{4.5}$$

where the static relative permittivity $\epsilon_{\text{s}}\left(\mathbf{r}\right)$ is added to account for ion lattice screening.

Inserting Eq. (4.1) into Eq. (3.70), and taking the retarded component of the resulting equation yields the final Dyson equation for retarded Green's function

$$\left(i\hbar\frac{\partial}{\partial t_{1}}+\frac{\hbar^{2}}{2m}\nabla^{2}\left(\mathbf{r}_{1}\right)+eV_{\text{P}}\left(\mathbf{r}_{1}\right)+eV_{\text{I}}\left(\mathbf{r}_{1}\right)\right)G^{\text{R}}\left(\mathbf{r}_{1}\sigma_{1}t_{1},\mathbf{r}_{2}\sigma_{2}t_{2}\right)$$
$$+\sum_{\sigma_3}eV_{\text{so}}\left(\mathbf{r}_{1},\sigma_{1},\sigma_{3}\right)G^{\text{R}}\left(\mathbf{r}_{1}\sigma_{3}t_{1},\mathbf{r}_{2}\sigma_{2}t_{2}\right)=\delta_{\sigma_{1},\sigma_{2}}\delta\left(\mathbf{r}_{1}-\mathbf{r}_{2}\right)\delta\left(t_{1}-t_{2}\right)$$
$$+\sum_{\sigma_3}\int d^{3}r_{3}\int dt_{3}\Sigma^{\text{R}}\left(\mathbf{r}_{1}\sigma_{1}t_{1},\mathbf{r}_{3}\sigma_{3}t_{3}\right)G^{\text{R}}\left(\mathbf{r}_{3}\sigma_{3}t_{3},\mathbf{r}_{2}\sigma_{2}t_{2}\right). \tag{4.6}$$

The advanced Green's function can be calculated from the retarded Green's function using Eqs. (3.31), (3.30), and definitions of lesser and greater Green's functions given by Eq. (3.27)

$$
\begin{aligned}
G^{\mathrm{A}}(1,2) &= -\theta(t_2-t_1)\left[\frac{1}{i\hbar}\left\langle\hat{\Psi}(1)\,\hat{\Psi}^{\dagger}(2)\right\rangle+\frac{1}{i\hbar}\left\langle\hat{\Psi}^{\dagger}(2)\,\hat{\Psi}(1)\right\rangle\right] \\
&= \left(\theta(t_2-t_1)\left[\frac{1}{i\hbar}\left\langle\hat{\Psi}(2)\,\hat{\Psi}^{\dagger}(1)\right\rangle+\frac{1}{i\hbar}\left\langle\hat{\Psi}^{\dagger}(1)\,\hat{\Psi}(2)\right\rangle\right]\right)^{*} \\
&= \left(\theta(t_2-t_1)\left[G^{>}(2,1)-G^{<}(2,1)\right]\right)^{*} = \left[G^{\mathrm{R}}(2,1)\right]^{*} = \left[G^{\mathrm{R}}(1,2)\right]^{\dagger}. \qquad (4.7)
\end{aligned}
$$

The equation for lesser Green's function can be calculated from Eq. (3.70) with the inverse Green's function defined by (3.75). All components ($<$, $>$, R, A) of the functions present in those equations, such as delta function $\delta(\underline{1},\underline{2})$, or inverse Green's function $G^{-1}(\underline{1},\underline{2})$, are calculated using the contour algebra from Appendix B.

By taking lesser ($<$) component of Eq. (3.70) one gets

$$
0 = \int d4\left(\left(G^{-1}\right)^{\mathrm{R}}(3,4)\,G^{<}(4,2)+\left(G^{-1}\right)^{<}(3,4)\,G^{\mathrm{A}}(4,2)\right). \qquad (4.8)
$$

Acting with $\int d\underline{3}G^{\mathrm{R}}(\underline{1},\underline{3})$ on both sides of Eq. (4.8), gives

$$
\begin{aligned}
G^{<}(\underline{1},\underline{2}) &= -\int d3\int d4 G^{\mathrm{R}}(1,3)\left(G^{-1}\right)^{<}(3,4)\,G^{\mathrm{A}}(4,2) \\
&= \int d3\int d4 G^{\mathrm{R}}(1,3)\,\Sigma^{<}(3,4)\,G^{\mathrm{A}}(4,2). \qquad (4.9)
\end{aligned}
$$

In the derivation of above formula, the existence of non-zero homogenous lesser Green's function was neglected, i.e., the lesser Green's function that satisfy

$$
\int d3\left[G^{-1}\right]^{\mathrm{R}}(1,3)\,G_{\mathrm{h}}^{<}(3,2)=0, \qquad (4.10)
$$

is always zero $G_{\mathrm{h}}^{<}(3,2)=0$. If such a solution existed, it would have to be added to Eq. (4.9). This is because during derivation of Eq. (4.9), information of the homogenous part of the solution $G_{\mathrm{h}}^{<}$ was lost after acting with $\int d\underline{3}G^{\mathrm{R}}(\underline{1},\underline{3})$ on both sides of Eq. (4.8). However, the existence of a homogenous solution would have violated the basic assumption about Green's function having an unique inverse (3.70) that was made in Chapter 3. The homogenous solution could have always been added to the retarded Green's function and the retarded component of Eq. (3.70) would not be true. The homogenous solution is directly connected to initial correlations [87, 99] which are neglected in this work.

Finally, knowing G^{R}, G^{A}, and $G^{<}$, the equation for $G^{>}$ can be obtained by rearranging Eq. (B.11) or (B.12)

$$
G^{>}(1,2) = G^{\mathrm{R}}(1,2)-G^{\mathrm{A}}(1,2)+G^{<}(1,2). \qquad (4.11)
$$

Equations (4.6), (4.7), (4.9), and (4.11), together with equations for the retarded and lesser self-energies Σ^{R}, $\Sigma^{<}$, and the Poisson equation (4.5), form a complete set of equations describing the system.

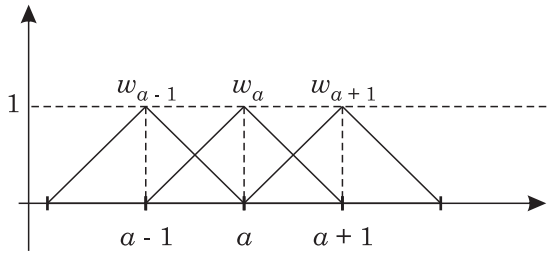

Figure 4.1: Tent-shaped functions.

4.2.2 Discrete basis and temporal Fourier transform

To perform any numerical calculations, all equations have to be written is some discrete basis. It was stated in Section 4.1 that for electrical part of the simulator, the system is assumed to be infinite and macroscopically uniform in the transverse plane $x - y$. This implies that the basis in the transverse plane can consist of plane waves. Since in the crystal growth direction z, the system is nonuniform even macroscopically, the plane wave basis cannot be used for this dimension. Finally, on the microscopic scale, the crystal is non-uniform in all three directions, and the basis should take this fact into account, as well.

The basis used in this work is chosen to be the same as in [51]. It consists of a product of fast varying (over the crystal primitive cell) zone-center Bloch functions u_α, slowly varying plane waves in the transverse direction, and functions w_a which are slowly varying in the crystal growth direction z

$$f_{\mathbf{k}_\mathrm{t},\alpha',a}(\mathbf{R}) = \frac{1}{\sqrt{A}} e^{i\mathbf{k}_\mathrm{t}\mathbf{r}_\mathrm{t}} w_a(z)\, u_{\alpha'}(\mathbf{r}_\mathrm{c}). \tag{4.12}$$

In the above equation $\mathbf{r} = (\mathbf{r}_\mathrm{t}, z)$ is the macroscopic position, $\mathbf{r}_\mathrm{c}$ is microscopic position vector, $\mathbf{R} = \mathbf{r} + \mathbf{r}_\mathrm{c}$ is the total position (macroscopic + microscopic), $\mathbf{k}_\mathrm{t}$ is the transverse wavevector, w_a is the localized basis in z direction, and A is the transverse surface. The fast changing basis Bloch functions $u_{\alpha'}(\mathbf{r}_\mathrm{c})$ are indexed by Greek indexes with primes $\alpha', \beta', ...$ (but never σ' as σ is reserved for spin). Bloch functions and spins combined (when combined they will be referred to as bands), with $\alpha, \beta, ...$, i.e., $\alpha = \{\alpha', \sigma\}$, and slowly changing functions $w_a(z)$ with Latin symbols $a, b, ...$

The functions $w_a(z)$ are chosen to be tent-shaped functions equal to 1 at position point z_a and going linearly to 0 at adjacent z_{a-1} and z_{a+1} points. Functions w_a are presented in Fig. 4.1.

Basis (4.12) is obviously non-orthogonal because functions w_a are non-orthogonal. Whenever dealing with non-orthogonal set of functions, it is necessary to introduce also a bi-orthogonal set $v_a(z)$ [97]. Bi-orthogonal function set $v_a(z)$ is defined as

$$\int dz w_a(z)\, v_b^*(z) = \delta_{a,b}. \tag{4.13}$$

A detailed description of the properties of non-orthogonal and bi-orthogonal sets is presented [97]. In this work, the exact form of bi-orthogonal set $v_a(z)$ and its

properties are irrelevant – the only important fact is that such basis always exists and satisfies Eq. (4.13).

The rapidly varying Bloch functions $u_\alpha(\mathbf{r}_c)$ are unknown as their form is very complex and depends on the static ion lattice potential. However their exact form is not necessary as fast varying coordinates $\mathbf{r}_c$ will be integrated out, leaving the matrix elements $\langle u_{\alpha'}|h|u_{\beta'}\rangle$, where h is a single-particle Hamiltonian. Those matrix elements are well known in optoelectronics [70, 27, 64], and their values are determined from experimental measurements.

Because the system is macroscopically uniform in the transverse plane, all double position functions (such as Green's functions and self-energies) become functions of the difference of transverse positions

$$F(\mathbf{R}_1,\mathbf{R}_2) = F(\mathbf{r}_{1,\mathrm{c}}\mathbf{r}_{1,\mathrm{t}}z_1, \mathbf{r}_{2,\mathrm{c}}\mathbf{r}_{2,\mathrm{t}}z_2) \to F(\mathbf{r}_{1,\mathrm{c}}z_1, \mathbf{r}_{2,\mathrm{c}}z_2, \mathbf{r}_{1,\mathrm{t}}-\mathbf{r}_{2,\mathrm{t}}). \tag{4.14}$$

Similarly, because the system is in the steady-state, all double time function become functions of time difference only, $F(t_1,t_2) \to F(t_1-t_2)$. The temporal Fourier transform can be taken with respect to (t_1-t_2) to shift functions from the time difference domain to the energy domain. The temporal Fourier transform and inverse temporal Fourier transform are defined as

$$F(t_1-t_2) = \frac{1}{2\pi\hbar}\int dE e^{-i\frac{E}{\hbar}(t_1-t_2)}F(E), \tag{4.15}$$

$$F(E) = \int d(t_1-t_2)\, e^{i\frac{E}{\hbar}(t_1-t_2)}F(t_1-t_2). \tag{4.16}$$

4.2.3 Discretization of the Dyson equation

Using the basis provided by Eq. (4.12) and the temporal Fourier transform given by Eq. (4.15), any Green's function or self-energy can be written as

$$\begin{aligned} F(1,2) = \frac{1}{2\pi\hbar}\int dE e^{-i\frac{E}{\hbar}(t_1-t_2)}\frac{1}{A}\sum_{\mathbf{k}_t}\sum_{\alpha',\beta'}\sum_{a,b} e^{i\mathbf{k}_\mathrm{t}(\mathbf{r}_{1,\mathrm{t}}-\mathbf{r}_{2,\mathrm{t}})} \\ \times w_a(z_1)\, w_b^*(z_2)\, u_{\alpha'}(\mathbf{r}_{1,\mathrm{c}})\, u_{\beta'}^*(\mathbf{r}_{2,\mathrm{c}})\, F_{\alpha a,\beta b}(\mathbf{k}_\mathrm{t},E), \end{aligned} \tag{4.17}$$

where F can be any Green's function or self-energy, and $\alpha=\{\alpha',\sigma_1\}$, $\beta=\{\beta',\sigma_2\}$. Functions $F_{\alpha a,\beta b}(\mathbf{k}_\mathrm{t},E)$ can be viewed as matrices parametrized by $\mathbf{k}_\mathrm{t}$ and E with number of elements equal to the number of bands times the number of spatial grid points in the z direction. They can be calculated using the formula

$$\begin{aligned} F_{\alpha a,\beta b}(\mathbf{k}_\mathrm{t},E) = \int d(t_1-t_2)\, e^{i\frac{E}{\hbar}(t_1-t_2)}\int d^2(r_{1,\mathrm{t}}-r_{2,\mathrm{t}})\, e^{-i\mathbf{k}_\mathrm{t}(\mathbf{r}_{1,\mathrm{t}}-\mathbf{r}_{2,\mathrm{t}})} \\ \times\frac{1}{V_c^2}\int d^3r_{1,\mathrm{c}}\int d^3r_{2,\mathrm{c}} u_{\alpha'}^*(\mathbf{r}_{1,\mathrm{c}})\, u_{\beta'}(\mathbf{r}_{2,\mathrm{c}})\int dz_1\int dz_2 v_a^*(z_1)\, v_b(z_2)\, F(1,2), \end{aligned} \tag{4.18}$$

where V_c is the volume of a primitive cell.

The formula (4.17) can be used to expand all Green's functions and self-energies in Eqs. (4.6), (4.7), (4.9), and (4.11). After integrating out the rapidly changing variables $\mathbf{r}_c$, Eqs. (4.6), (4.7), (4.9), and (4.11) become a set of four matrix equations

$$\mathbf{G}^{\mathrm{R}}\left(\mathbf{k}_{\mathrm{t}}, E\right) = \left[\mathbf{E} - \mathbf{H}\left(\mathbf{k}_{\mathrm{t}}\right) - \mathbf{\Sigma}'^{\mathrm{R}}\left(\mathbf{k}_{\mathrm{t}}, E\right)\right]^{-1}, \tag{4.19}$$

$$\mathbf{G}^{<}\left(\mathbf{k}_{\mathrm{t}}, E\right) = \mathbf{G}^{\mathrm{R}}\left(\mathbf{k}_{\mathrm{t}}, E\right) \mathbf{\Sigma}'^{<}\left(\mathbf{k}_{\mathrm{t}}, E\right) \mathbf{G}^{\mathrm{A}}\left(\mathbf{k}_{\mathrm{t}}, E\right), \tag{4.20}$$

$$\mathbf{G}^{\mathrm{A}}\left(\mathbf{k}_{\mathrm{t}}, E\right) = \left[\mathbf{G}^{\mathrm{R}}\left(\mathbf{k}_{\mathrm{t}}, E\right)\right]^{\dagger}, \tag{4.21}$$

$$\mathbf{G}^{>}\left(\mathbf{k}_{\mathrm{t}}, E\right) = \mathbf{G}^{\mathrm{R}}\left(\mathbf{k}_{\mathrm{t}}, E\right) - \mathbf{G}^{\mathrm{A}}\left(\mathbf{k}_{\mathrm{t}}, E\right) + \mathbf{G}^{<}\left(\mathbf{k}_{\mathrm{t}}, E\right). \tag{4.22}$$

In the above equations, $\mathbf{E} = E\mathbf{S}$ and $\mathbf{\Sigma}'^{(\mathrm{A,R,<})} = \mathbf{S}\mathbf{\Sigma}^{(\mathrm{A,R,<})}\mathbf{S}$. For brevity, in most of the calculations the prime sign is dropped. The Hamiltonian and $\mathbf{S}$ matrix are

$$S_{\alpha a,\beta b} = \delta_{\alpha,\beta} \int dz w_a^*\left(z\right) w_b\left(z\right), \tag{4.23}$$

$$H_{\alpha a,\beta b} = \int dz w_a^*\left(z\right) \left(h_{\alpha,\beta}\left(\mathbf{k}_{\mathrm{t}}, z\right) - eV_{\mathrm{P}}\left(z\right)\delta_{\alpha,\beta}\right) w_b\left(z\right). \tag{4.24}$$

The single-particle Hamiltonian $h_{\alpha,\beta}\left(\mathbf{k}_t, z\right)$ is defined as

$$\begin{aligned} h_{\alpha,\beta}\left(\mathbf{k}_{\mathrm{t}}, z\right) = \frac{1}{A} \int d^2 r_{\mathrm{t}} e^{-i\mathbf{k}_{\mathrm{t}}\mathbf{r}_{\mathrm{t}}} \frac{1}{V_{\mathrm{c}}} \int d^3 r_{\mathrm{c}} u_{\alpha'}^*\left(\mathbf{r}_{\mathrm{c}}\right) \\ \times \left(t'(\mathbf{r}_{\mathrm{c}}, \mathbf{r}_{\mathrm{t}}, z)\delta_{\sigma_1,\sigma_2} + u\left(\mathbf{r}_{\mathrm{c}}, \mathbf{r}_{\mathrm{t}}, \sigma_1, \sigma_2\right)\right) u_{\beta'}\left(\mathbf{r}_{\mathrm{c}}\right) e^{i\mathbf{k}_{\mathrm{t}}\mathbf{r}_{\mathrm{t}}}, \end{aligned} \tag{4.25}$$

where $\alpha = \{\alpha', \sigma_1\}$, $\beta = \{\beta', \sigma_2\}$, and Hamiltonian elements t' and u are discussed in Subsection 3.3.4. The Poisson potential $V_{\mathrm{P}}\left(z\right)$ is the solution of the 1-D Poisson equation in the macroscopic coordinates. The Poisson equation in the macroscopic coordinates can be obtained from the general Poisson equation (4.5) by integrating out the rapidly varying variables, and noticing that because the system is macroscopically invariant in the transverse plane, the potential can change only in the z direction. The final form of the Poisson equation is

$$\epsilon_0 \partial_z \left[\epsilon_{\mathrm{s}}\left(z\right) \partial_z V_{\mathrm{P}}\left(z\right)\right] = e\left(n\left(z\right) - p\left(z\right) + N_{\mathrm{A}}\left(z\right) - N_{\mathrm{D}}\left(z\right)\right). \tag{4.26}$$

Because the system under consideration is a heterostructure the Hamiltonian (4.25) will have discontinuities and additional heterointerface conditions have to be specified. For example, for a simple effective mass Hamiltonian the usual conditions at $z = z_i$ are [70, 27]

$$\frac{1}{m_{\mathrm{eff}}\left(z_i^+\right)} \frac{d}{dz} w\left(z\right)\Big|_{z=z_i^+} = \frac{1}{m_{\mathrm{eff}}\left(z_i^-\right)} \frac{d}{dz} w\left(z\right)\Big|_{z=z_i^-}, \tag{4.27}$$

where m_{eff} is position a dependent effective mass. In general those conditions can be arbitrary as long as the Hamiltonian remains Hermitian [27]. The exact method of

how to calculate the Hamiltonian form Eq. (4.24) and discussion of the heterinterface conditions can be found in [100, 101].

It is worth noticing that the Hamiltonian in Eq. (4.25) as well as all Green's functions and self-energies in Eqs. (4.19)-(4.22) are now written in basis which is a direct product of rapidly varying Bloch functions and spin functions. This is not a unique choice, and sometimes it is more convenient to use basis which is a linear combination of the direct product base. For example, for III-V semiconductors the most important fast varying Bloch functions are called [27] $|s\rangle$, $|p_x\rangle$, $|p_y\rangle$, and $|p_z\rangle$ because they have the same symmetry as s and p orbitals. However, because of presence of the spin-orbit interaction, the Hamiltonian is most often written in the total angular momentum basis [29, 30, 27, 31, 102] which is a linear combination of $|s\rangle \left|\frac{1}{2}, \pm\frac{1}{2}\right\rangle$, $|p_x\rangle \left|\frac{1}{2}, \pm\frac{1}{2}\right\rangle$, $|p_y\rangle \left|\frac{1}{2}, \pm\frac{1}{2}\right\rangle$, and $|p_z\rangle \left|\frac{1}{2}, \pm\frac{1}{2}\right\rangle$, where $\left|\frac{1}{2}, \pm\frac{1}{2}\right\rangle$ are spin functions. The use of the total angular momentum basis allows one to simplify the form of Hamiltonian and hence to get a better overview of the problem (for example to choose good numerical parameters for the calculations).

In case a different basis is used, the final equations (4.19)-(4.22) do not change, and the only difference is in the form of the Hamiltonian (4.25). The generalization of Eq. (4.25) for different basis is straight forward

$$h_{\alpha,\beta}\left(\mathbf{k}_{\mathrm{t}}, z\right) = \frac{1}{A}\int d^2 r_{\mathrm{t}} e^{-i\mathbf{k}_{\mathrm{t}}\mathbf{r}_{\mathrm{t}}} \left\langle \alpha \left| t' + u \right| \beta \right\rangle e^{i\mathbf{k}_{\mathrm{t}}\mathbf{r}_{\mathrm{t}}}.$$

In fact, one can assume from the beginning that the basis in which the Green's functions are expanded is a total angular momentum basis (or any other linear combination of the direct product base). However, in this work the direct product base is used because of the didactic reasons. Calculations in the direct product base are conceptually simpler (especially during calculation of the transverse polarization in Section 4.4 and Appendix E) and do not result in the loss of generality.

Equations (4.19)-(4.22) form a complete set of discretized equations. However to solve them, proper boundary conditions have to be set. The boundary conditions for the NEGF technique used in this work have been described for orthogonal basis in [103, 90, 99] and for non-orthogonal basis in [97].

The major idea is that the device is surrounded from both sides (in the z direction) by two semi-infinite leads. Each of the leads is in equilibrium but with different quasi-Fermi level. Because of the difference between quasi-Fermi levels of the leads, the device which is in between them is in the non-equilibrium state.

The leads are described by the same single-particle Hamiltonian as the device (4.24). Because the leads are in equilibrium, the electrostatic potential is constant there. In the left lead it is equal to the potential at the left end of the device, and in the right lead it is the same as potential at the right end of the device.

It is assumed that there are no realistic many-body interactions in the leads. The only allowed scattering mechanism in the leads is phenomenological scattering via so-called Büttiker probes [104, 105]. Because of that, the leads have self-energies in the form of Büttiker probes

$$\mathbf{\Sigma}^{\mathrm{R}} = \left[\mathbf{\Sigma}^{\mathrm{A}}\right]^{\dagger} = i\eta\mathbf{S}, \tag{4.28}$$

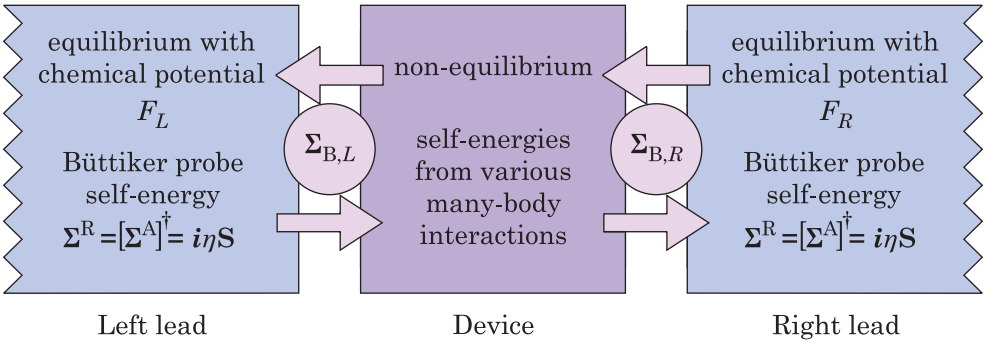

Figure 4.2: Separation of the system into interacting device, and non-interacting leads. The leads are in equilibrium, each with a different quasi-Fermi level (chemical potential) F. The realistic many-body interactions are present only in the device region, while the leads contain a phenomenological scattering in form of Büttiker probe self-energies. The influence of the leads on the device is expressed by the boundary self-energies $\Sigma_{\mathrm{B},L}$ and $\Sigma_{\mathrm{B},L}$ which are added to other self-energies in the device region.

where η is small real number, or they have no self-energies at all ($\eta = 0$). With the self-energy of the leads given by Eq. (4.28), all influence of leads on the device can be described by the boundary self-energies $\mathbf{\Sigma}^{\mathrm{R}}_{\mathrm{B}}$ and $\mathbf{\Sigma}^{<}_{\mathrm{B}}$, which are added to other self-energies in Eqs. (4.19) and (4.20).

The general idea of this method is presented in Fig. 4.2. Detailed calculations and final formulas for boundary self-energies can be found in Appendix D.

4.3 Quasiparticles and physical observables

The first part of this section introduces, common for semiconductor physics, the idea of quasiparticles. It provides formulas allowing to obtain carrier and current densities, and a local density of states using Green's functions. In the second part of this section the formula for the divergence of current is shown and it is used to formulate current-conservation condition as well as derive the formula for power emitted due to electron-hole recombination.

4.3.1 Conduction and valence bands

When dealing with transport in semiconductors, it is convenient to introduce quasiparticles: *electrons* and *holes*. A qusiparticle electron is an electron in a state that is above the bandgap energy of the semiconductor and a quasiparticle hole is a missing electron from below the bandgap energy. Bands which have states above bandgap energy are called conduction bands (usually labeled as CB) and bands below the bandgap are valence bands (VB). From now on, the electrons (real particles) will be called *particle electrons* and quasiparticle electrons and holes will be called just electrons and holes. More information about quasiparticles can be found in [70, 27, 78].

Here, the concept of quaisparticles is illustrated using an example of carrier density. It is shown how quasiparticle densities are related to the particle density.

Because all single-particle functions can be expanded in a basis made of zone-center functions $u_\alpha(\mathbf{r}_\mathrm{c})$, the field operators can also be expanded in this basis, for example

$$\hat{\Psi}(\mathbf{R},\sigma) = \sum_\alpha u_\alpha(\mathbf{r}_\mathrm{c})\,\hat{\Psi}_\alpha(\mathbf{r}), \tag{4.29}$$

where the band index α incorporates the spin index σ. The field operator is defined as

$$\hat{\Psi}_\alpha(\mathbf{r}) = \sum_a F_a(\mathbf{r})\,\hat{c}_{a,\alpha}, \tag{4.30}$$

where $F_a(\mathbf{r})$ is some complete basis of functions that depend on macroscopic position vector, and $\hat{c}_{a,\alpha}$ is the annihilation operator of a particle in state a in band α.

The total density of particle electrons expanded in Bloch's functions basis is

$$n_\mathrm{p}(\mathbf{R}) = \sum_{\alpha,\beta\in \text{ all bands}} u_{\alpha'}(\mathbf{r}_\mathrm{c})\,u^*_{\beta'}(\mathbf{r}_\mathrm{c})\left\langle \hat{\Psi}_\alpha(\mathbf{r})\,\hat{\Psi}^\dagger_\beta(\mathbf{r})\right\rangle. \tag{4.31}$$

After integrating out the fast varying variables, the above equation becomes

$$n_\mathrm{p}(\mathbf{r}) = \sum_{\alpha\in \text{ all bands}} \left\langle \hat{\Psi}_\alpha(\mathbf{r})\,\hat{\Psi}^\dagger_\alpha(\mathbf{r})\right\rangle. \tag{4.32}$$

Quasiparticle electrons are electrons located in the conduction band, and therefore the quasiparticle electron density is

$$n(\mathbf{r}) = \sum_{\alpha\in\mathrm{CB}} \left\langle \hat{\Psi}_\alpha(\mathbf{r})\,\hat{\Psi}^\dagger_\alpha(\mathbf{r})\right\rangle. \tag{4.33}$$

The hole density is defined as "negative" electron density in the valence band

$$p(\mathbf{r}) = -\sum_{\alpha\in\mathrm{VB}} \left\langle \hat{\Psi}_\alpha(\mathbf{r})\,\hat{\Psi}^\dagger_\alpha(\mathbf{r})\right\rangle = \sum_{\alpha\in\mathrm{VB}} \left\langle \hat{\Psi}^\dagger_\alpha(\mathbf{r})\,\hat{\Psi}_\alpha(\mathbf{r})\right\rangle. \tag{4.34}$$

Insertion of Eqs. (4.33) and (4.34) into Eq. (4.32) yields a relation between particle and quasiparticle densities

$$n_\mathrm{p}(\mathbf{r}) = \sum_{\alpha\in \text{ all bands}} \left\langle \hat{\Psi}_\alpha(\mathbf{r})\,\hat{\Psi}^\dagger_\alpha(\mathbf{r})\right\rangle = n(\mathbf{r}) - p(\mathbf{r}). \tag{4.35}$$

Similarly, one can define a quasiparticle local density of states and quasiparticle currents.

4.3.2 Charge and current densities

The particle electron density can be obtained from Green's function using formula

$$n_{\mathrm{p}}\left(\mathbf{R},t\right)=\sum_{\sigma}\left\langle \hat{\Psi}^{\dagger}\left(\mathbf{R}\sigma t\right)\hat{\Psi}\left(\mathbf{R}\sigma t\right)\right\rangle =-i\hbar\sum_{\sigma}G^{<}\left(\mathbf{R}\sigma t,\mathbf{R}\sigma t^{+}\right). \tag{4.36}$$

After expanding the above formula in basis (4.12), integrating out the rapidly varying coordinates and taking a temporal Fourier transform, the equation for quasiparticle electron and hole density is

$$n\left(z_{a},E\right)=\frac{i\hbar}{A}\sum_{\mathbf{k}_{\mathrm{t}}}\sum_{\alpha\in\mathrm{CB}}G^{<}_{\alpha a,\alpha a}\left(\mathbf{k}_{\mathrm{t}},E\right), \tag{4.37}$$

$$p\left(z_{a},E\right)=-\frac{i\hbar}{A}\sum_{\mathbf{k}_{\mathrm{t}}}\sum_{\alpha\in\mathrm{VB}}G^{>}_{\alpha a,\alpha a}\left(\mathbf{k}_{\mathrm{t}},E\right). \tag{4.38}$$

The total quasiparticle densities are calculated by integrating formulas (4.37) and (4.38) over the energy divided by $2\pi\hbar$. For example for the total electron density is

$$n\left(z_{a}\right)=\int\frac{dE}{2\pi\hbar}n\left(z_{a},E\right). \tag{4.39}$$

In equilibrium, the fluctuation-dissipation theorem states that lesser and greater Green's functions are connected by the following relation [90]

$$G^{>}\left(E\right)=-e^{\beta\left(E-F\right)}G^{<}\left(E\right), \tag{4.40}$$

which together with Eq. (4.11) yields

$$G^{<}\left(E\right)=-f\left(E-F\right)\left(G^{\mathrm{R}}\left(E\right)-G^{\mathrm{A}}\left(E\right)\right), \tag{4.41}$$

$$G^{>}\left(E\right)=f\left(F-E\right)\left(G^{\mathrm{R}}\left(E\right)-G^{\mathrm{A}}\left(E\right)\right), \tag{4.42}$$

where $f\left(E-F\right)$ is the Fermi-Dirac distribution function and F is a quasi-Fermi level. In a non-equilibrium state, the above two formulas are also valid, but the quasi-Fermi level has to be position dependent. With spatially varying quasi-Fermi level, one can insert Eq. (4.41), (4.42) into Eqs. (4.37), (4.38) to define a local density of states (LDOS)

$$\mathfrak{D}_{\mathrm{n}(p)}\left(E,z_{a}\right)=-\frac{i}{2\pi}\frac{1}{A}\sum_{\mathbf{k}_{\mathrm{t}}}\sum_{\alpha\in\mathrm{CB}(VB)}\left(G^{\mathrm{R}}_{\alpha a,\alpha a}\left(\mathbf{k}_{\mathrm{t}},E\right)-G^{\mathrm{A}}_{\alpha a,\alpha a}\left(\mathbf{k}_{\mathrm{t}},E\right)\right), \tag{4.43}$$

where the summation is done over conduction bands (CB) for electrons, and over valence bands (VB) for holes. Now, the electron and hole densities can be written as

$$n\left(z_a\right)=\int dEf\left(E-F\left(z_a\right)\right)\mathfrak{D}_{\mathrm{n}}\left(E,z_a\right), \tag{4.44}$$

$$p\left(z_a\right)=\int dEf\left(F\left(z_a\right)-E\right)\mathfrak{D}_{\mathrm{p}}\left(E,z_a\right). \tag{4.45}$$

The general formula for the particle current (of particle electrons) is

$$\begin{aligned}\mathbf{J}\left(\mathbf{R},t\right)&=\sum_{\sigma}\frac{i\hbar}{2m}\left(\nabla\left(\mathbf{R}\right)-\nabla\left(\mathbf{R}^{+}\right)\right)\left\langle\hat{\Psi}^{\dagger}\left(\mathbf{R}\sigma t\right)\hat{\Psi}\left(\mathbf{R}^{+}\sigma t\right)\right\rangle\\&=\sum_{\sigma}\frac{\hbar^2}{2m}\left(\nabla\left(\mathbf{R}\right)-\nabla\left(\mathbf{R}^{+}\right)\right)G^{<}\left(\mathbf{R}\sigma t,\mathbf{R}^{+}\sigma t^{+}\right).\end{aligned} \tag{4.46}$$

Similarly, as in case of density, the particle current can be separated into quasiparticle electron and hole currents. The formula for quasiparticle currents, expressed in the basis (4.12) is [97, 90, 99]

$$\begin{aligned}J_{\mathrm{n(p)}}\left(z_a\to z_{a+1},E\right)=(-)\frac{1}{A}\sum_{\mathbf{k}_{\mathrm{t}}}\sum_{\alpha\in\mathrm{CB}(VB)}\left(\left(H_{\alpha a,\alpha a+1}\left(\mathbf{k}_{\mathrm{t}}\right)-E_{\alpha a,\alpha a+1}\right)\right.\\\left.\times G^{<(>)}_{\alpha a+1,\alpha a}\left(\mathbf{k}_{\mathrm{t}},E\right)-\left(H_{\alpha a+1,\alpha a}\left(\mathbf{k}_{\mathrm{t}}\right)-E_{\alpha a+1,\alpha a}\right)G^{<(>)}_{\alpha a,\alpha a+1}\left(\mathbf{k}_{\mathrm{t}},E\right)\right).\end{aligned} \tag{4.47}$$

4.3.3 Current conservation and power absorption/emission.

Divergence of quasiparticle current is given by the following equation [99, 97, 90]

$$\begin{aligned}\partial_z J_{\mathrm{n(p)}}\left(z_a,E\right)=(-)\frac{1}{A\Delta_a}\sum_{\mathbf{k}_{\mathrm{t}}}\sum_{\alpha\in\mathrm{CB}(VB)}\left[\mathbf{\Sigma}^{\mathrm{R}}\left(\mathbf{k}_{\mathrm{t}},E\right)\mathbf{G}^{<(>)}\left(\mathbf{k}_{\mathrm{t}},E\right)\right.\\+\mathbf{\Sigma}^{<(>)}\left(\mathbf{k}_{\mathrm{t}},E\right)\mathbf{G}^{\mathrm{A}}\left(\mathbf{k}_{\mathrm{t}},E\right)-\mathbf{G}^{\mathrm{R}}\left(\mathbf{k}_{\mathrm{t}},E\right)\mathbf{\Sigma}^{<(>)}\left(\mathbf{k}_{\mathrm{t}},E\right)\\\left.-\mathbf{G}^{<(>)}\left(\mathbf{k}_{\mathrm{t}},E\right)\mathbf{\Sigma}^{\mathrm{A}}\left(\mathbf{k}_{\mathrm{t}},E\right)\right]_{\alpha a,\alpha a},\end{aligned} \tag{4.48}$$

where $\Delta_a=\left(z_{a+1}-z_{a-1}\right)/2$.

The formula for the current divergence (4.48) is used in NEGF simulations for two purposes. First, because the system in a steady-state, the divergence of the total electric current given by

$$\partial_z J\left(z_a\right)=\int\frac{dE}{2\pi\hbar}\left(e\partial_z J_{\mathrm{p}}\left(z_a,E\right)-e\partial_z J_{\mathrm{n}}\left(z_a,E\right)\right), \tag{4.49}$$

has to be zero for every grid point a.

The above condition can also be formulated in terms of a particle electron current

$$\partial_z J(z_a) = \int \frac{dE}{2\pi\hbar} \frac{e}{A\Delta_a} \sum_{\mathbf{k}_\mathrm{t}} \sum_{\alpha \in \text{ all bands}} \left[\boldsymbol{\Sigma}^\mathrm{R}(\mathbf{k}_\mathrm{t}, E) \mathbf{G}^<(\mathbf{k}_\mathrm{t}, E) \right.$$
$$+ \boldsymbol{\Sigma}^<(\mathbf{k}_\mathrm{t}, E) \mathbf{G}^\mathrm{A}(\mathbf{k}_\mathrm{t}, E) - \mathbf{G}^\mathrm{R}(\mathbf{k}_\mathrm{t}, E) \boldsymbol{\Sigma}^<(\mathbf{k}_\mathrm{t}, E)$$
$$\left. - \mathbf{G}^<(\mathbf{k}_\mathrm{t}, E) \boldsymbol{\Sigma}^\mathrm{A}(\mathbf{k}_\mathrm{t}, E) \right]_{\alpha a, \alpha a} = 0. \tag{4.50}$$

The second use for the current divergence formula, is that it allows one to calculate the recombination rates due to particular scattering mechanisms. The recombination rate is connected to the divergence of a particle current by [70]

$$R = A \int dz \partial_z J_\mathrm{n}(z), \tag{4.51}$$

where A is a cross-section of the device.

Because the self-energies are additive, Eq. (4.48) can be broken into a sum of divergences due to different scattering mechanisms. In particular, one can take only the divergence due to a radiative generation/recombination.

One can assume that the radiative generation/recombination self-energy $\boldsymbol{\Sigma}_\mathrm{rad}$ can be further broken into a sum of self-energies which generate/recombine electron-hole pairs with a particular energy $\hbar\omega_m$

$$\boldsymbol{\Sigma}_\mathrm{rad} = \sum_m \boldsymbol{\Sigma}_{\omega_m}. \tag{4.52}$$

With the above formula, one can obtain an equation for absorbed/emitted power due to the generation/recombination self-energy $\boldsymbol{\Sigma}_\mathrm{rad}$

$$P(\omega_m) = \hbar\omega_m R(\omega_m) = \hbar\omega_m A \int dz \partial_z J_{\mathrm{n},m}(z), \tag{4.53}$$

where $\partial_z J_{\mathrm{n},m}(z)$ is calculated using Eq. (4.48) with $\boldsymbol{\Sigma} = \boldsymbol{\Sigma}_{\omega_m}$.

4.4 Self-energies

Because of the computational limitations, in this work there are only three types of scattering present: electron-photon, electron-optical phonon, and phenomenological scattering.

The electron-photon scattering self-energy for the edge-emitting laser is responsible for stimulated and spontaneous emission of the light and it is the crucial element of this simulator. Formula for this self-energy is derived by solving Eqs. (3.93), (3.102), (3.106), and (3.107) for the Fabry-Perot resonator.

Scattering due to interaction with polar optical phonons is non-elastic i.e., carriers scattered by the phonons either increase or decrease their energy by the amount equal to the energy of the phonon. Inclusion of this scattering mechanism is very important because it allow carriers to change their energy within the same band, while traveling through the device – this process is known as thermalisation.

The phenomenological Golizadeh scattering self-energy [98] serves as a simple substitution of an electron-electron self-energy, which itself is too demanding computationally. The most important reason to include this self-energy is to broaden the very fine energy levels inside the quantum well.

4.4.1 Electron-photon scattering

Electron-photon self-energy is given by Eq. (3.93) which is coupled to Eq. (3.102) for the photon Green's function, Eq. (3.106) for the transverse vertex function, and Eq. (3.107) for the transverse polarization.

The first order approximation of the electron-photon self-energy is calculated as follows. The first step is to approximate Eq. (3.107) for transverse polarization with its first order term. Next, the approximated transverse vertex function is inserted into Eq. (3.107) to obtain the first order transverse polarization. This polarization is then used to calculate the photon Green's function using Eq. (3.102). Finally, the polarization and the photon Green's function are inserted into Eq. (3.93), which the gives the first order term of electron-photon self-energy.

Because it is assumed that the electric field is polarized in the y direction only, the transverse vertex function possesses only the y component, and the polarization and photon Green's function tensors have only (y, y) components

$$\Gamma_i = \delta_{i,y}\Gamma, \tag{4.54}$$

$$P_{i,j} = \delta_{i,y}\delta_{j,y}P, \tag{4.55}$$

$$D_{i,j} = \delta_{i,y}\delta_{j,y}D. \tag{4.56}$$

The transverse polarization is defined as a functional derivative from the transverse current, which creates a problematic transverse delta function in Eq. (3.107). In general, the transverse part of some quantity is a part with a vanishing divergence. Because in this work it is assumed that system is in a steady-state, divergence of the total current is always zero and thus the total current is equal to the transverse current. Because of that, the transverse delta $\delta^{\mathrm{T}}_{i,j}(\mathbf{r}_1, \mathbf{r}_2)$ in Eq. (3.107) can be replaced with a regular (contour) delta function $\delta_{i,j}\delta(\mathbf{r}_1 - \mathbf{r}_2)$.

In the first order approximation, the vertex function in Eq. (3.107) is approximated by its first order term

$$\Gamma(\underline{1}, \underline{2}, \underline{3}) = \frac{i\hbar e\mu_0}{m}\delta(\underline{1}, \underline{3})\,\partial_y(\underline{1})\,\delta(\underline{1}, \underline{2}), \tag{4.57}$$

and the polarization becomes

$$\begin{aligned} P(\underline{1}, \underline{2}) = &-\frac{i\hbar^3 e^2\mu_0}{2m^2}\left(\partial_y(\underline{1}) - \partial_y\left(\underline{1}^+\right)\right) \\ &\times \left[\partial_y(\underline{2})\,G(\underline{1}, \underline{2})\right] G\left(\underline{2}, \underline{1}^+\right). \end{aligned} \tag{4.58}$$

It is assumed that the wavevectors of photons present in the system are much smaller than wavevectors of quasiparticles, and the momentum matrix element defined as

$$\frac{1}{V_{\mathrm{c}}}\int d^3 r_{\mathrm{c}} u^*_{\alpha'}\left(\mathbf{r}_{\mathrm{c}}\right)\partial_y u_{\beta'}\left(\mathbf{r}_{\mathrm{c}}\right)\delta_{\sigma_\alpha,\sigma_\beta} = \frac{i}{\hbar}p^y_{\alpha,\beta} = \frac{i}{\hbar}p_{\alpha,\beta}, \tag{4.59}$$

is much larger then the quasiparticle wavevector. With above assumptions, formula for the (y,y) component of the lesser and greater polarization averaged over primitive cell, summed over spin indices, and Fourier transformed to the frequency (energy) domain is

$$\begin{aligned} &P^{\mathrm{av},\lessgtr}\left(\mathbf{r}_a,\mathbf{r}_b,\hbar\omega\right) = \delta\left(\mathbf{r}_{a,\mathrm{t}}-\mathbf{r}_{b,\mathrm{t}}\right)P^{\mathrm{av},\lessgtr}\left(z_a,z_b,\hbar\omega\right) \\ &= \delta\left(\mathbf{r}_{a,\mathrm{t}}-\mathbf{r}_{b,\mathrm{t}}\right)\frac{e^2\mu_0}{im^2}\int\frac{dE}{2\pi}\frac{1}{A}\sum_{\mathbf{k}_{\mathrm{t}}}\sum_{\alpha,\beta,\mu,\nu}G^{\lessgtr}_{\alpha a,\beta b}\left(\mathbf{k}_{\mathrm{t}},E+\hbar\omega\right) \\ &\times p^*_{\alpha,\nu}p_{\beta,\mu}G^{\gtrless}_{\mu b,\nu a}\left(\mathbf{k}_{\mathrm{t}},E\right). \end{aligned} \tag{4.60}$$

A detailed derivation of the average polarization in Eq. (4.60) from general formula (4.58), with all intermediate steps is shown in Section E.1 in Appendix E.

One should also remember that if the Hamiltonian (4.25) is not written in a direct product base (product of Bloch functions and spin functions), then the momentum matrix $p_{\alpha,\beta}$ also has to be written in the same basis as the Hamiltonian (in Eq. (4.59) the momentum matrix is written in the direct product base). The generalization is straight forward: $\mathbf{p}_{\alpha,\beta} = \langle\alpha\left|\hat{\mathbf{p}}\right|\beta\rangle$, where $\hat{\mathbf{p}}$ is momentum operator, and $|\alpha\rangle$ is the basis in which the Hamiltonian is written.

The retarded and advanced components of polarization can be calculated from the lesser and greater components using formulas (B.9) and (B.10) (with singular part $f\left(t\right)=0$). In practice, only the formula for retarded polarization is necessary, and the application of temporal Fourier transform to Eq. (B.10) gives

$$\begin{aligned} P^R\left(E\right) &= \mathrm{Pr}\int\frac{dE'}{2\pi}i\frac{P^{>}\left(E'\right)-P^{<}\left(E'\right)}{E'-E} \\ &+\frac{P^{>}\left(E\right)-P^{<}\left(E\right)}{2}, \end{aligned} \tag{4.61}$$

where Pr indicates principal value of the integral. The above equation is valid for any double contour time function for which the singular part is equal to zero. Using the properties of contour functions from Appendix B, it can be shown that

$$P^{>}\left(E\right)-P^{<}\left(E\right) = P^R\left(E\right)-\left[P^R\left(E\right)\right]^* = 2i\mathrm{Im}P^R\left(E\right), \tag{4.62}$$

and thus the first term in Eq. (4.61) is purely real while the second is purely imaginary.

The next step is to obtain the equation for retarded photon Green's function from the general contour equation (3.102).

The photon Green's functions posses properties very similar to the electron Green's functions, in particular they satisfy equations similar to Eqs. (4.7), (4.9), (4.11) with the transverse polarization functions instead of self-energies [55, 106]

$$D^{\mathrm{A}}_{i,j}(1,2) = \left[D^{\mathrm{R}}_{i,j}(1,2)\right]^{\dagger}, \tag{4.63}$$

$$D^{\lessgtr}_{i,j}(1,2) = \sum_{k,l}\int d3d4 D^{\mathrm{R}}_{i,k}(1,3)\, P^{\lessgtr}_{k,l}(3,4)\, D^{\mathrm{A}}_{l,j}(4,3), \tag{4.64}$$

$$D^{>}_{i,j}(1,2) = D^{\mathrm{R}}_{i,j}(1,2) - D^{\mathrm{A}}_{i,j}(1,2) + D^{<}_{i,j}(1,2). \tag{4.65}$$

The above equations can be derived similarly to analogous equations for the electron Green's functions by using Eqs. (3.101), (3.102), and contour algebra from Appendix B. To derive Eq. (4.64), it has to be assumed that the homogenous photon Green's function is zero (this is the same assumption that has been done for electron Green's functions). In general, the homogenous solution corresponds to the vacuum-induced part of a photon Green's function, while the non-homogenous solution corresponds to the medium-induced part of photon Green's function [106]. In lasers, the medium-induced emission is dominant and therefore the homogenous solution is neglected.

Applying the contour algebra from Appendix B to Eq. (3.102), and using Eq. (4.60) yields

$$\left(\nabla^2(\mathbf{r}_1) + n_{\mathrm{b}}^2(\mathbf{r}_1)\frac{\omega^2}{c^2}\right) D^{\mathrm{R}}(\mathbf{r}_1,\mathbf{r}_2,\omega) = \delta(\mathbf{r}_1-\mathbf{r}_2) + \int_{V_{\mathrm{D}}} d^3r_3 \delta(\mathbf{r}_{1,\mathrm{t}}-\mathbf{r}_{3,\mathrm{t}}) P^{\mathrm{av,R}}(z_1,z_3,\hbar\omega)\, D^{\mathrm{R}}(\mathbf{r}_3,\mathbf{r}_2,\omega), \tag{4.66}$$

where $\int_{V_{\mathrm{D}}}$ indicates that the integral is taken over the whole volume of the FP cavity, and $n_{\mathrm{b}} = \sqrt{\epsilon_\infty}$ is added to take into account screening due ion lattice.

By replacing the polarization $P^{\mathrm{av,R}}(z_1,z_2,\hbar\omega)$ in Eq. (4.66) with some approximate formula proportional to delta function $\delta(z_1-z_2)$, integral on the RHS of Eq. (4.66) is eliminated, and the polarization can be added to the refractive index. Such approximation is justified if the function $P^{\mathrm{av,R}}(z_1,z_2,\hbar\omega)$ has a peak at $z_1=z_2$ and decreases to zero when $|z_1-z_2|$ increases. Additionally, it has to decrease rapidly on a length scale small in comparison to the length scale on which D^{R} varies. Because D^{R} varies on the length scale of a micrometer, $P^{\mathrm{av,R}}$ has to decrease to zero when $|z_1-z_2|$ is not larger than few nanometers.

By numerically calculating the polarization from Eq. (4.60), it can be shown that $P^{\mathrm{av,R}}(z_1,z_2,\hbar\omega)$ has significant non-zero values as long as z_1 and z_2 are in the area where population of carriers is inverted. Outside of that region polarization is very small and can be considered to be zero. Because the active region (quantum well) is a few nanometers long, the approximation by delta function is justified. Thus, for a

system with a one active region the following replacement is made

$$P^{\mathrm{av,R}}\left(z_1,z_2,\hbar\omega\right)\rightarrow\delta\left(z_1-z_2\right)\int_{\mathrm{QW}}dz_3 \\ \times P^{\mathrm{av,R}}\left(z_3,z_3,\hbar\omega\right)=\delta\left(z_1-z_2\right)P_{\mathrm{QW}}^{\mathrm{av,R}}\left(\hbar\omega\right), \tag{4.67}$$

for z_1, z_2 inside the active region, and

$$P^{\mathrm{av,R}}\left(z_1,z_2,\hbar\omega\right)\rightarrow 0, \tag{4.68}$$

when z_1, z_2 are outside the active region. This approximation can be easily generalized to a multiple quantum well system in which case the equation for the retarded photon Green's function becomes

$$\left(\nabla^2\left(\mathbf{r}_1\right)+n^2\left(\mathbf{r}_1\right)\frac{\omega^2}{c^2}\right)D^{\mathrm{R}}\left(\mathbf{r}_1,\mathbf{r}_2,\omega\right)=\delta(\mathbf{r}_1-\mathbf{r}_2), \tag{4.69}$$

where the total refractive index n is

$$n^2\left(\mathbf{r}\right)=n_{\mathrm{b}}^2\left(\mathbf{r}\right)-\frac{c^2}{\omega^2}P_{\mathrm{QW}}^{\mathrm{av,R}}\left(\hbar\omega,\mathbf{r}\right), \tag{4.70}$$

and

$$P_{\mathrm{QW}}^{\mathrm{av,R}}\left(\mathbf{r},\hbar\omega\right)=\begin{cases}P_{\mathrm{QW},i}^{\mathrm{av,R}}\left(\hbar\omega\right)=\int_{\mathrm{QW},i}dz_3P^{\mathrm{av,R}}\left(z_3,z_3,\hbar\omega\right) & \text{for } \mathbf{r}\in V_{\mathrm{QW},i}\\ 0 & \text{otherwise}\end{cases}, \tag{4.71}$$

Here $V_{\mathrm{QW},i}$ is the volume of the ith quantum well. Equation (4.70) allows one to easily connect the averaged polarization with material gain. The real part of $\frac{c^2}{\omega^2}P_{\mathrm{QW}}^{\mathrm{av,R}}$ can usually be assumed to be much smaller than n_{b}^2 and

$$\mathrm{Im}n=-\frac{c^2}{2n_{\mathrm{b}}\omega^2}\mathrm{Im}P_{\mathrm{QW}}^{\mathrm{av,R}}=-\frac{c^2}{4n_{\mathrm{b}}\omega^2}\left(P_{\mathrm{QW}}^{\mathrm{av},>}-P_{\mathrm{QW}}^{\mathrm{av},<}\right), \tag{4.72}$$

Substitution of the above formula into the definition of material gain given by Eq. (2.1) allows one to express material gain by the transverse polarization functions

$$g=-2\frac{\omega}{c}\mathrm{Im}n=\frac{c}{\omega n_{\mathrm{b}}}\mathrm{Im}P_{\mathrm{QW}}^{\mathrm{av,R}}=\frac{c}{2\omega n_{\mathrm{b}}}\left(P_{\mathrm{QW}}^{\mathrm{av},>}-P_{\mathrm{QW}}^{\mathrm{av},<}\right). \tag{4.73}$$

With the assumption that most power is propagating in the fundamental mode, the general solution of Eq. (4.69) for a Fabry-Perot laser can be written as [71]

$$D^{\mathrm{R}}\left(\mathbf{r}_1,\mathbf{r}_2,\omega\right)=D_{\mathrm{x}}^{\mathrm{R}}\left(x_1,x_2,\omega\right)\phi\left(y_1,z_1\right)\phi^*\left(y_2,z_2\right), \tag{4.74}$$

where function ϕ is fundamental eigenmode of a 2-D scalar Helmholtz equation

$$\left(\partial_y^2+\partial_z^2+n^2\left(y,z,\omega\right)\frac{\omega^2}{c^2}\right)\phi\left(y,z\right)=k_{\mathrm{eff}}^2\left(\omega\right)\phi\left(y,z\right), \tag{4.75}$$

and $D_{\mathrm{x}}^{\mathrm{R}}\left(x_1, x_2, \omega\right)$ satisfies

$$\left(\partial_{x_1}^2 + k_{\mathrm{eff}}^2\left(\omega\right)\right) D_{\mathrm{x}}^{\mathrm{R}}\left(x_1, x_2, \omega\right) = \delta\left(x_1 - x_2\right). \tag{4.76}$$

Equation (4.75) can easily be solved numerically with the boundary condition $\phi\left(y, z\right) = 0$ at the boundary of a computation window. The most popular methods to solve this kind of Helmholtz equation are finite difference method [107] and finite elements method [100].

It is assumed that the FP laser has a left mirror at $x = -L_{\mathrm{x}}/2$, and a right mirror at $x = L_{\mathrm{x}}/2$. Inside the laser cavity, the propagation constant is $k_{\mathrm{eff}} = n_{\mathrm{eff}}\frac{\omega}{c}$, and both mirrors possess the same reflectivity coefficient r.

The solution of Eq. (4.76) can be obtained analytically [71, 54, 55], and inside the laser cavity $(-\frac{L_{\mathrm{x}}}{2} < x < \frac{L_{\mathrm{x}}}{2})$ it is

$$\begin{aligned} &D_{\mathrm{x}}^{\mathrm{R}}\left(x_1, x_2\right) = \theta\left(x_1 - x_2\right) F\left(x_1\right) F\left(-x_2\right) \\ &+ \theta\left(x_2 - x_1\right) F\left(x_2\right) F\left(-x_1\right), \end{aligned} \tag{4.77}$$

where

$$F\left(x\right) = \frac{e^{ik_{\mathrm{eff}}x} + r_{\mathrm{b}}e^{-ik_{\mathrm{eff}}x}}{\sqrt{2ik_{\mathrm{eff}}\left(1 + r_{\mathrm{b}}^2\right)}}, \tag{4.78}$$

and

$$r_{\mathrm{b}} = e^{ik_{\mathrm{eff}}L_{\mathrm{x}}}r. \tag{4.79}$$

Lesser and greater photon Green's function are obtained by substituting the retarded photon Green's function and the lesser/greater transverse polarizations into Eq. (4.64)

$$\begin{aligned} &D^{\lessgtr}\left(\mathbf{r}_1, \mathbf{r}_2, \omega\right) = \int d^3r_3 d^3r_4 D^{\mathrm{R}}\left(\mathbf{r}_1, \mathbf{r}_3, \omega\right) \\ &\times P^{\lessgtr}\left(\mathbf{r}_3, \mathbf{r}_4, \omega\right)\left[D^{\mathrm{R}}\left(\mathbf{r}_2, \mathbf{r}_4, \omega\right)\right]^* \\ &= \int_{L_{\mathrm{x}}} dx_3 D_{\mathrm{x}}^{\mathrm{R}}\left(x_1, x_3, \omega\right)\left[D_{\mathrm{x}}^{\mathrm{R}}\left(x_2, x_3, \omega\right)\right]^* \phi\left(y_1, z_1\right) \\ &\times \phi^*\left(y_2, z_2\right) \sum_i P_{\mathrm{QW},i}^{\mathrm{av},\lessgtr}\left(\omega\right) \int_{A_{\mathrm{QW},i}} dy_3 dz_3 \left|\phi\left(y_3, z_3\right)\right|^2, \end{aligned} \tag{4.80}$$

where $\int_{L_{\mathrm{x}}}$ means that this integration is done over the laser cavity only. For the integral $\int_{A_{\mathrm{QW},i}}$ the integration is done over the surface of ith quantum well.

For the system to be uniform in the transverse direction, the photon Green's function can only depend on the difference of transverse coordinates $x_1 - x_2$ and $y_1 - y_2$. From Eq. (4.80) one can see that $D^{\lessgtr}\left(\mathbf{r}_1, \mathbf{r}_2, \omega\right)$ has no such dependence. To deal with this problem, the photon Green's function is averaged over x and y i.e., the following replacement is made

$$\int_{L_x} dx_3 D_x^R(x_1, x_3, \omega) \left[D_x^R(x_2, x_3, \omega)\right]^*$$

$$\downarrow$$

$$\frac{1}{L_x}\int_{L_x} dx_1 \int_{L_x} dx_2 D_x^R(x_1, x_2, \omega) \left[D_x^R(x_1, x_2, \omega)\right]^*, \tag{4.81}$$

$$\phi(y,z) \to \bar{\phi}(z) = \frac{1}{L_y}\int dy \phi(y,z). \tag{4.82}$$

The average of the product of two photon Green's functions can be calculated analytically to be

$$\frac{1}{L_x}\int_{L_x} dx_1 \int_{L_x} dx_1 D_x^R(x_1, x_2, \omega) \left[D_x^R(x_1, x_2, \omega)\right]^* = \frac{2I(k_{eff})}{\left|2ik_{eff}(1+r_b^2)\right|^2}, \tag{4.83}$$

where $I = \sum_{i=1}^{9} I_i$ is

$$I_1 = \frac{1}{2\mathrm{Im}k_{eff}}\left(e^{\mathrm{Im}k_{eff}L_x}\frac{\sinh(\mathrm{Im}k_{eff}L_x)}{\mathrm{Im}k_{eff}L_x} - 1\right), \tag{4.84}$$

$$I_2 = -\frac{|r_b|^4}{2\mathrm{Im}k_{eff}}\left(e^{\text{-}\mathrm{Im}k_{eff}L_x}\frac{\sinh(\mathrm{Im}k_{eff}L_x)}{\mathrm{Im}k_{eff}L_x} - 1\right), \tag{4.85}$$

$$I_3 = |r_b|^2 L\left(\frac{\sinh(\mathrm{Im}k_{eff}L_x)}{\mathrm{Im}k_{eff}L_x}\right)^2, \tag{4.86}$$

$$I_4 = \mathrm{Re}\left[\frac{ir_b}{\mathrm{Re}k_{eff}}\left(e^{-i\mathrm{Re}k_{eff}L_x}\frac{\sinh(\mathrm{Im}k_{eff}L_x)}{\mathrm{Im}k_{eff}L_x} - \frac{\sin(k_{eff}^* L_x)}{k_{eff}^* L_x}\right)\right], \tag{4.87}$$

$$I_5 = \mathrm{Re}\left[\frac{r_b^*}{\mathrm{Im}k_{eff}}\left(e^{\mathrm{Im}k_{eff}L_x}\frac{\sin(\mathrm{Re}k_{eff}L_x)}{\mathrm{Re}k_{eff}L_x} - \frac{\sin(k_{eff}L_x)}{k_{eff}L_x}\right)\right], \tag{4.88}$$

$$I_6 = \mathrm{Re}\left[\frac{r_b^*|r_b|^2}{\mathrm{Im}k_{eff}}\left(\frac{\sin(k_{eff}^* L_x)}{k_{eff}^* L_x} - e^{-\mathrm{Im}k_{eff}L}\frac{\sin(\mathrm{Re}k_{eff}L_x)}{\mathrm{Re}k_{eff}L_x}\right)\right], \tag{4.89}$$

$$I_7 = \mathrm{Re}\left[\frac{i|r_b|^2}{\mathrm{Re}k_{eff}}\left(e^{-i\mathrm{Re}k_{eff}L_x}\frac{\sin(\mathrm{Re}k_{eff}L_x)}{\mathrm{Re}k_{eff}L_x} - \frac{\sin(2\mathrm{Re}k_{eff}L_x)}{2\mathrm{Re}k_{eff}L_x}\right)\right], \tag{4.90}$$

$$I_8 = \mathrm{Re}\left[\frac{i(r_b^*)^2}{\mathrm{Re}k_{eff}}\left(1 - e^{i\mathrm{Re}k_{eff}L_x}\frac{\sin(\mathrm{Re}k_{eff}L_x)}{\mathrm{Re}k_{eff}L_x}\right)\right], \tag{4.91}$$

$$I_9 = \mathrm{Re}\left[\frac{ir_b^*|r_b|^2}{\mathrm{Re}k_{eff}}\left(e^{-i\mathrm{Re}k_{eff}L_x}\frac{\sinh(\mathrm{Im}k_{eff}L_x)}{\mathrm{Im}k_{eff}L_x} - \frac{\sin(k_{eff}L_x)}{k_{eff}L_x}\right)\right]. \tag{4.92}$$

The final formula for the lesser and greater photon Green's functions is then

$$D^{\lessgtr}(z_1, z_2, \omega) = \frac{I}{2\left|k_{\text{eff}}\right|^2 \left|(1+r_{\text{b}}^2)\right|^2} \bar{\phi}(z_1)\, \bar{\phi}^*(z_2) \times \sum_i P_{\text{QW},i}^{\text{av},\lessgtr}(\omega) \int_{A_{\text{QW},i}} dy_3 dz_3 \left|\phi(y_3, z_3)\right|^2. \tag{4.93}$$

Detailed analysis of the term $1/\left|(1+r_{\text{b}}^2)\right|^2$ reveals that it has local maximums at resonance frequencies for which

$$\text{Re}\left(k_{\text{eff}}(\omega)\right) = \frac{l\pi - \text{ph}(r)}{L_{\text{x}}}, \tag{4.94}$$

where l is an integer number, $\text{ph}(r)$ is a phase of the reflection coefficient. Additionally, it has singularities when the total gain is equal to the total losses through the mirrors. It occurs when

$$\text{Im}\left(k_{\text{eff}}(\omega)\right) \to \frac{1}{2L_{\text{x}}} \ln \frac{1}{|r|^2}, \tag{4.95}$$

which is the usual laser threshold condition. In general, the spectrum of $D^{\lessgtr}(\omega)$ has very sharp peaks at the resonance frequencies. With the increasing bias voltage across the junction, the height of those peaks increases and their widths decrease – they tend to be delta function peaks. To properly implement those functions numerically, a very fine numerical grid would be necessary – consisting of at least tens of thousands points.

To get around this problem, the $D^{\lessgtr}(\omega)$ is approximated by the following expression

$$D^{\text{av},\lessgtr}(\omega) = \sum_m \theta\left(|\omega - \omega_m| - \frac{\Delta\omega_m}{2}\right) D^{\lessgtr}(\omega_m), \tag{4.96}$$

where ω_m are frequencies of the peaks and $\Delta\omega_m$ are widths of the peaks at half-maximum (FWHMs).

Assuming that the phase of reflection coefficient is small and can be neglected, and that the real part of effective refractive index depends weakly on frequency so that $\text{Re}\left(n_{\text{eff}}(\omega)\right)$ can be approximated by its value at some ω_0 which was chosen to be the lasing frequency, formulas for the peak values and FWHMs are

$$\omega_m = \frac{l_m \pi c}{\text{Re}\left(n_{\text{eff}}(\omega_0)\right) L_{\text{x}}}, \tag{4.97}$$

$$\Delta\omega_m = \frac{|r|^{-2} e^{g(\omega_m)L_{\text{x}}} - 1}{\sqrt{2} L_{\text{x}} \text{Re}\left(n_{\text{eff}}(\omega_0)\right)/c}. \tag{4.98}$$

The formula for FWHM is obtained by expansion of the denominator $1/\left|(1+r_{\text{b}}^2)\right|^2$ in Eq. (4.93) in Taylor series around resonance frequencies ω_m. This approximation

is accurate only for sharp and narrow peaks – as long as the majority of the peak can be described by the second order Taylor series. The accuracy of this approximation increases as gain approaches its threshold value (peaks become narrower and higher). However, in the real systems the gain never reaches its threshold value and formula (4.98) might need some tuning.

Finally, inserting the approximated transverse vertex function from Eq. (4.57) into Eq. (3.93) gives

$$\Sigma\left(\underline{1},\underline{2}\right)=\frac{i\mu_0 e^2\hbar^3}{m^2}\left[\partial_y\left(\underline{1}\right)\partial_y\left(\underline{2}\right)G\left(\underline{1},\underline{2}\right)\right]D\left(\underline{2},\underline{1}\right). \tag{4.99}$$

The calculated dependence of $D^{\mathrm{av},\lessgtr}$ on z_1 and z_2 is very weak and therefore the function $\bar{\phi}\left(z\right)$ present in formula (4.93) for lesser and greater photon Green's functions is replaced with its value in the middle of the structure. Equation (4.99) is written in basis (4.12) in a similar way as it was done for polarization (4.60). Detailed calculations are provided in Section E.2 in Appendix E.2

$$\begin{aligned}
&\boldsymbol{\Sigma}'^{\lessgtr}\left(\mathbf{k}_{\mathrm{t}},E\right)=\mathbf{S}\boldsymbol{\Sigma}^{\lessgtr}\mathbf{S}\\
&=i\mu_0\left(\frac{e}{m}\right)^2\int_{-\infty}^{+\infty}\frac{d\left(\hbar\omega\right)}{2\pi}D^{\mathrm{av},\gtrless}\left(\omega\right)\mathbf{p}\mathbf{G}^{\lessgtr}\left(\mathbf{k}_{\mathrm{t}},E+\hbar\omega\right)\mathbf{p}\\
&=i\mu_0\left(\frac{e}{m}\right)^2\int_{0}^{\infty}\frac{d\left(\hbar\omega\right)}{2\pi}\mathbf{p}\left(D^{\mathrm{av},\gtrless}\left(\hbar\omega\right)\mathbf{G}^{\lessgtr}\left(\mathbf{k}_{\mathrm{t}},E+\hbar\omega\right)-D^{\mathrm{av},\lessgtr}\left(\hbar\omega\right)\mathbf{G}^{\lessgtr}\left(\mathbf{k}_{\mathrm{t}},E-\hbar\omega\right)\right)\mathbf{p}\\
&=\frac{i\mu_0\hbar}{2\pi}\left(\frac{e}{m}\right)^2\sum_m\mathbf{p}\left(D^{\gtrless}\left(\omega_m\right)\Delta\omega_m\mathbf{G}^{\lessgtr}\left(\mathbf{k}_{\mathrm{t}},E+\hbar\omega_m\right)-D^{\lessgtr}\left(\omega_m\right)\Delta\omega_m\mathbf{G}^{\lessgtr}\left(\mathbf{k}_{\mathrm{t}},E-\hbar\omega_m\right)\right)\mathbf{p}.
\end{aligned} \tag{4.100}$$

where $\omega_m>0$, and

$$p_{\alpha a,\beta b}=p_{\alpha,\beta}\int dz w_a^*\left(z\right)w_b\left(z\right). \tag{4.101}$$

The retarded and advanced self-energy are obtained from lesser and greater self-energy using Eq. (4.61) and (B.9), where the term containing principal value of the integral is small and can be ignored [99, 51]

$$\boldsymbol{\Sigma}'^{\mathrm{R}}\left(E\right)=\frac{\boldsymbol{\Sigma}'^{>}\left(E\right)-\boldsymbol{\Sigma}'^{<}\left(E\right)}{2}, \tag{4.102}$$

$$\boldsymbol{\Sigma}'^{\mathrm{A}}\left(E\right)=\boldsymbol{\Sigma}'^{R}\left(E\right)-\left(\boldsymbol{\Sigma}'^{>}\left(E\right)-\boldsymbol{\Sigma}'^{<}\left(E\right)\right)=-\frac{\boldsymbol{\Sigma}'^{>}\left(E\right)-\boldsymbol{\Sigma}'^{<}\left(E\right)}{2}, \tag{4.103}$$

Additionally, the lesser photon Green's function corresponds to emission while the greater is responsible for absorption. In lasers, emission is much greater than absorption and the greater photon Green's function $D^{>}$ is therefore neglected.

4.4.2 Electron-phonon scattering

Although there are many types of phonons present in the III-V semiconductor, in this work only the interaction with longitudinal optical phonons is taken into account. This is because scattering by polar optical phonons in strongly inelastic. As it is shown in Chapter 6, inelastic scattering has a very significant influence on the performance of the laser.

The polar optical phonons are modeled with the Fröhlich approach [108], and contrary to electrons and photons, the phonons are assumed to be in constant equilibrium. It is also assumed that phonons in the layered structure can be approximated by phonons from the bulk structure. Material parameters such as relative electric permittivity are set to have identical values in all layers.

The general formula for the first order electron-phonon scattering self-energy is [97, 90, 99]

$$\Sigma'^{\lessgtr}_{\mu m,\nu n}\left(\mathbf{k}_{\mathrm{t}},E\right)=\frac{e^{2}\hbar\omega_{\mathrm{LO}}}{2\epsilon_{0}}\left(\frac{1}{\epsilon_{\infty}}-\frac{1}{\epsilon_{\mathrm{s}}}\right)\frac{1}{A}\sum_{\mathbf{q}_{\mathrm{t}}}F\left(q_{\mathrm{t}},\Delta_{m,n},k_{\mathrm{t}},q_{0}\right)$$
$$\times\left(\mathbf{S}\left(N_{\mathrm{LO}}\mathbf{G}^{\lessgtr}\left(\mathbf{q}_{\mathrm{t}},E\mp\hbar\omega_{\mathrm{LO}}\right)+\left(N_{\mathrm{LO}}+1\right)\mathbf{G}^{\lessgtr}\left(\mathbf{q}_{\mathrm{t}},E\pm\hbar\omega_{\mathrm{LO}}\right)\right)\mathbf{S}\right)_{\mu m,\nu n}. \quad (4.104)$$

In the above formula $\hbar\omega_{\mathrm{LO}}$ is the energy of a longitudinal optical phonon, N_{LO} is the average number of phonons determined from the following formula

$$N_{\mathrm{LO}}=\frac{1}{e^{\hbar\omega_{\mathrm{LO}}/kT}-1}, \quad (4.105)$$

and the function F is

$$F\left(q_{\mathrm{t}},\Delta_{m,n},k_{\mathrm{t}},q_{0}\right)=\int_{0}^{2\pi/a}dq_{z}\cos\left(q_{z}\Delta_{m,n}\right)\left(\frac{1}{\left(\left(q_{z}^{2}+q_{\mathrm{t}}^{2}+q_{0}^{2}+k_{\mathrm{t}}^{2}\right)^{2}-4k_{\mathrm{t}}^{2}q_{\mathrm{t}}^{2}\right)^{1/2}}\right.$$
$$\left.-q_{0}^{2}\frac{q_{z}^{2}+q_{\mathrm{t}}^{2}+q_{0}^{2}+k_{\mathrm{t}}^{2}}{\left(\left(q_{z}^{2}+q_{\mathrm{t}}^{2}+q_{0}^{2}+k_{\mathrm{t}}^{2}\right)^{2}-4k_{\mathrm{t}}^{2}q_{\mathrm{t}}^{2}\right)^{3/2}}\right). \quad (4.106)$$

In Eq. (4.106), q_0 is the Debye screening length [109] which is taken to be a constant parameter, $\Delta_{m,n}=z_m-z_n$, and a is a lattice constant. Retarded and advanced self-energy can be calculated from lesser and greater self-energies by using formulas (4.102) and (4.103).

4.4.3 Golizadeh scattering

Due to the numerical limitations, no electron-electron scattering other than Hartree term is present. However, addition of some simplified substitute of electron-electron self-energy is necessary because energy levels inside the quantum well are very narrow

(on energy scale) and some broadening mechanism is necessary to avoid very fine energy grids. Numerical experiments showed that electron-phonon self-energy is not enough to broaden confined levels inside the quantum well.

In [98, 51], it is argued that the second order electron-electron self-energy (assuming that the scattering is elastic) has a general form $\Sigma_{i,j} = D_{i,j}G_{i,j}$, where i, j are position nodes and $D_{i,j}$ is a complicated term depending on the Green's function itself. The complicated term $D_{i,j}$ can be replaced by $d\delta_{i,j}$, where d is a constant "scattering strength". In non-orthogonal basis this leads to the following form of self-energy

$$\mathbf{\Sigma}'^{\lessgtr,\mathrm{R,A}}\left(\mathbf{k}_\mathrm{t}, E\right) = d\mathbf{S}\mathbf{G}^{\lessgtr,\mathrm{R,A}}_{\mathrm{diag}}\left(\mathbf{k}_\mathrm{t}, E\right)\mathbf{S}, \tag{4.107}$$

where $\mathbf{G}_{\mathrm{diag}}$ is a Green's function with diagonal elements only.

Chapter 5

Numerical implementation

This chapter presents a detailed description of numerical implementation of the theory developed in the previous chapters. The first section describes a creation of numerical grids for position, energy, and wavevector. It provides a method of creating energy and wavevector grids which do not violate the current conservation condition given by Eq. (4.49).

The general structure of the simulator is presented in Section 5.2. This section includes a flow diagram and discussion of convergence criteria. Numerical approach and the boundary conditions for the 1-D Poisson equation (4.26) are discussed in Section 5.3. The last section describes an application of the bisection method to deal with numerically unstable calculation of the photon Green's function.

5.1 Numerical grids of position, energy, and wavevector

The determination of a good position grid is fairly simple. The discrete basis given by Eq. (4.12) allows for non-uniform spatial grids. Spatial grid can have more nodes inside and around the quantum well region, and less nodes everywhere else. Contrary to drift-diffusion models, current is conserved for any choice of the grid.

In general, a higher number of nodes (shorter distance between adjacent nodes) makes calculations more accurate. However, one needs to remember that it was assumed that slowly varying functions (which are described at the nodes of the grid) are approximated as constant over primitive cell. For III-V semiconductors the length of the primitive cell in the z direction is equal to half of the lattice constant which is roughly $a/2 \approx 0.27$ nm. Thus, if the simulation requires a spatial grid with a step significantly shorter than 0.27 nm then, even with a very dense grid, the results are meaningless since it means that supposedly slowly varying functions vary significantly over primitive cell.

Because of the current conservation condition given by Eq. (4.50), the energy grid is more difficult to determine than the spatial grid. The four self-energies used in this work (electron-photon, electron-phonon, Golizadeh, and boundary self-energy) all satisfy the mentioned condition in the case of continuous values of energy. In case

of discrete values of energy, condition (4.50) becomes violated whenever self-energy is proportional to Green's function with energy which is not located on the energy grid. For example self-energies from Eqs. (4.100) and (4.104) have the following general form

$$\mathbf{\Sigma}\left(k_{\mathrm{t}}, E_j\right) \sim \mathbf{G}\left(k_{\mathrm{t}}, E_j \pm \hbar\omega\right). \tag{5.1}$$

In general, the energy $E_j \pm \hbar\omega$ will not be located exactly on the energy grid point and Green's function for this value of energy has to be calculated as a linear combination of Green's functions at the adjacent energy points $E_i < E_j \pm \hbar\omega < E_{i+1}$.

In the case of electron-photon interaction self-energy (4.100), the problem is avoided by assuming that the laser operates at one frequency ω_m only. This is equivalent to the assumption that the mirrors reflect only light with frequency ω_m and are perfectly transparent for all other frequencies. Such structure can be viewed as an ideal distributed Bragg reflector laser. The energy grid consists of two regions with the same constant step: one for the valence band, and another for the conduction band. The energy grid is constructed in a way that for all significant energy levels in the valence band E (those which are occupied by carriers inside quantum well), energies $E_j + \hbar\omega_m$ are located exactly at grid points in the conduction band.

Additionally, if electron-phonon self-energy (4.104) is present, the constant step ΔE in both regions of the energy grid is chosen to satisfy

$$\frac{\hbar\omega_{\mathrm{LO}}}{\Delta E} = n \qquad n = 1, 2, 3, \ldots, \tag{5.2}$$

where $\hbar\omega_{\mathrm{LO}}$ is the energy of the optical phonon. Choice of the constant step satisfying Eq. (5.2) assures that energies $E_i \pm \hbar\omega_{\mathrm{LO}}$ are located exactly at the nodes of the energy grid.

As for the lower and upper boundaries of the energy grid, they should be chosen in such a way that the energy grid will cover all energies for which the values of the carrier density are significant. In addition, the energy grid should cover the region just below the lowest level of the valence band edge, and just above the highest level of the conduction band edge even if there are no carriers there. This is because of the existence of ballistic current [90, 99]. In terms of energy, the ballistic current starts just below the lowest valence band edge (hole current) and above the highest level of the conduction band edge (electron current). In both cases, it has the form of a relatively sharp peak (on the energy scale) which goes to zero after approximately 0.2 eV from the respective band edge. However, when ballistic current can be neglected (for example when recombination current is orders of magnitude larger), it is sufficient for the energy grid to cover only the region where the carrier density is significant.

As mentioned before, for the purpose of electric calculations, the device is considered to be infinite in the transverse plane and thus summation over the wavevector can be replaced by an integral

$$\frac{1}{A}\sum_{\mathbf{k}_{\mathrm{t}}} \to \frac{1}{(2\pi)^2}\int_0^{k_{\max}} k_{\mathrm{t}} dk_{\mathrm{t}} \int_0^{2\pi} d\phi_k. \tag{5.3}$$

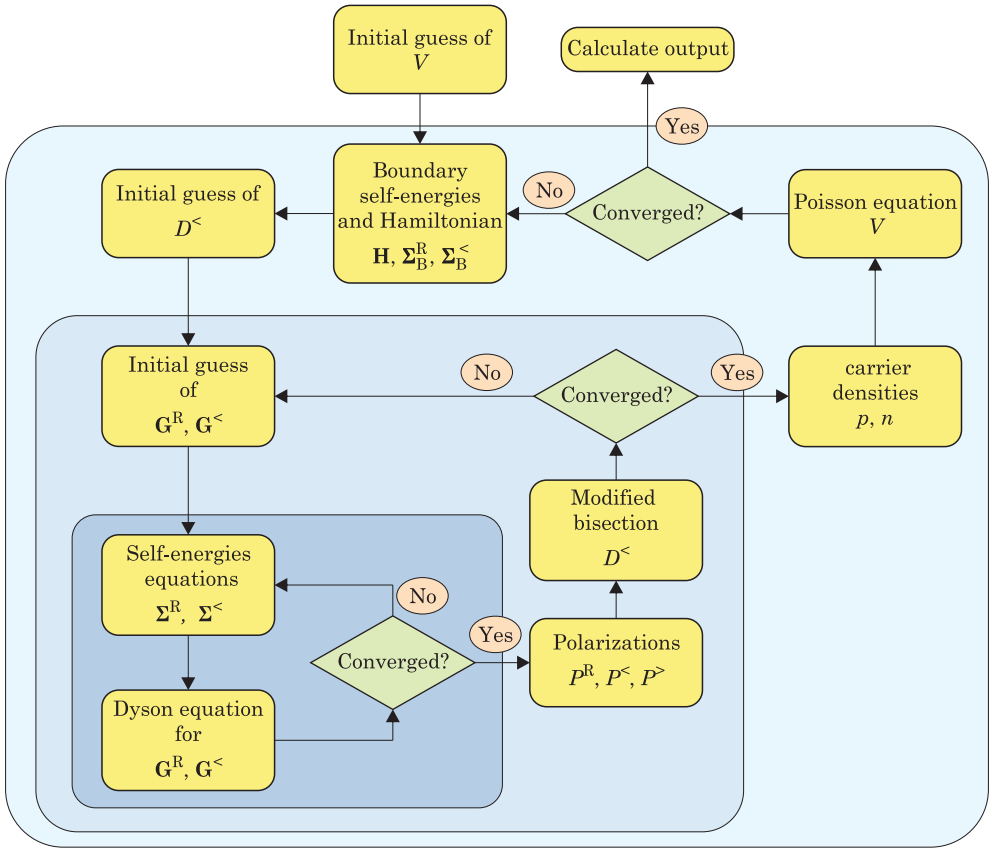

Figure 5.1: Flow diagram of the simulator. The three major loops are indicated with boxes with different shades of blue.

To reduce computation time and memory requirements, it is assumed in this work that the Hamiltonian and all self-energies are isotropic (are functions of k_{t} only) and integration over angle ϕ_k is just equal to multiplication by 2π

$$\frac{1}{(2\pi)^2}\int k_{\mathrm{t}}dk_{\mathrm{t}}\int d\phi_k = \frac{1}{2\pi}\int k_{\mathrm{t}}dk_{\mathrm{t}}. \tag{5.4}$$

The simplest possible Hamiltonian – the effective mass Hamiltonian is already isotropic and no additional approximations are necessary. More complicated Hamiltonian models: 4×4, and 6×6 Luttinger-Kohn Hamiltonians [70, 27, 24] can be approximated as isotropic, by setting Luttinger parameters γ_2 and γ_3 to be equal.

The grid for k_{t} is taken to be uniform spanning from 0 to some k_{max}. The value of wavevector k_{max} depends on the curvature of the bands – flatter bands need larger values. It is also worth mentioning that a dense wavevector grid is necessary to remove sharp ripples in spectral currents and quasiparticle densities plots, which are caused by numerical integration over k_{t}.

5.2 General structure of the code

The calculation scheme of the simulator is presented in Fig. 5.1. It starts with an initial guess of the electrostatic potential form V_{P} present in Eqs. (4.19) and (4.26). The initial guess is obtained by determining the applied voltage bias, doping concentrations, and by using the depletion region approximation described in [70].

Next, the initial guess of potential is used to calculate the single-particle Hamiltonian from Eq. (4.24) and boundary self-energies using Eqs. (D.16) and (D.26).

The next step is the initial guess of $D^<$. After all approximations of photon Green's function, $D^<$ is just a real, positive number. The value of initial guess of $D^<$ is not crucial as the algorithm is not very sensitive to initial values and converges even if it differs from the real solution by many orders of magnitude. Initial guess of Green's functions is obtained by solving Eqs. (4.19)-(4.22) with boundary self-energy only (the only one which does not depend on Green's function).

The initial Green's functions are used to calculate self-energies (Golizadeh, phonon, and photon), which are again inserted into Eqs. (4.19)-(4.22) to update Green's functions. This loop continues until the convergence criteria described in Section 5.5 are met. When it happens, Green's functions are used to calculate polarizations using Eqs. (4.60) and (4.61). Polarizations allow to update photon Green's function $D^<$, which is used instead of the initial guess of $D^<$. Unfortunately, this loop does not allow for self-consistent calculations i.e., if a new $D^<$ is calculated directly from Eq. (4.93) and inserted into Eq. (4.100) for electron-photon self-energy the procedure does not converge. Instead, the bisection method is used to obtain convergence. This procedure is described in detail in Section 5.4.

When the second loop converges, electron and hole densities are calculated using Eqs. (4.37) and (4.38). Updated carrier densities are inserted into the Poison equation (4.26), allowing update of the electrostatic potential. Updated electrostatic potential is used to update Hamiltonian, and the procedure repeats itself. When convergence is reached, the desired output is calculated from Green's functions.

5.3 Method of solving the Poisson equation

The Poisson equation (4.26) has to be supplemented with proper boundary conditions. In this work, boundary conditions (BC) are chosen to be Neumann boundary conditions

$$\partial_z V_{\mathrm{P}}|_{z=z_1} = \partial_z V_{\mathrm{P}}|_{z=z_N} = 0, \tag{5.5}$$

where z_1 is the first grid point and z_N is the last grid point in the device. These BC are consistent with the assumption that the potential inside the leads is constant.

Equation (4.26) is discretized by using basis functions w_a shown in Fig. 4.1. After discretization, it has the following form

$$\mathbf{KV} = \text{-}\mathbf{M}\boldsymbol{\rho}\,(\mathbf{V}), \tag{5.6}$$

where matrices $\mathbf{K}$ and $\mathbf{M}$ are defined as

$$K_{i,j} = \epsilon_0 \int dz w_i(z)\, \partial_z \epsilon_{\mathrm{s}}(z)\, \partial_z w_j(z)\,, \tag{5.7}$$

$$M_{i,j} = \int dz w_i(z)\, w_j(z)\,, \tag{5.8}$$

and vectors $\mathbf{V}$ and $\boldsymbol{\rho}$ are

$$\rho_i = -e\left(n(z_i) - p(z_i) + N_{\mathrm{A}}(z_i) - N_{\mathrm{D}}(z_i)\right) \tag{5.9}$$

$$V_i = V_{\mathrm{P}}(z_i)\,. \tag{5.10}$$

To calculate elements of matrix $\mathbf{K}$, additional boundary conditions on interfaces (where ϵ_{s} is discontinuous) have to be specified. Because the electric field vector is orientated in the z direction, the boundary condition at the interface is [70]

$$\epsilon_{\mathrm{s}}\left(z^+\right) \partial_z V\left(z^+\right) = \epsilon_{\mathrm{s}}\left(z^-\right) \partial_z V\left(z^-\right). \tag{5.11}$$

This is exactly the same interface condition as in the case of an effective mass Hamiltonian with ϵ_{s} instead of $1/m_{\mathrm{c(v)}}$ or Luttinger parameters in the case of more complicated Hamiltonians. A detailed description of how to calculate elements in Eq. (5.7) with boundary conditions given by Eq. (5.11) can be found in [100, 101].

Equation (5.6) has to solved self-consistently with the Dyson equation. Unfortunately, with Neumann boundary conditions given by Eq. (5.5), matrix $\mathbf{K}$ is singular and Eq. (5.6) has no solutions. Singularity of the matrix is caused solely by the Neumann boundary conditions and not by the discretization method. For example, discretization of the Poisson equation with the finite difference also leads to the singular matrix [99].

Although Eq. (5.11) has no exact solutions, it can be solved approximately. A very good description of how to deal with this problem is presented in [99]. After calculating of n and p (with potential V_{P}), those functions are modeled with the Fermi-Dirac distribution with position dependent quasi-Fermi levels of electrons (F_{n}) and holes (F_{p}). Quasi-Fermi levels are found by inverting the following equations

$$n\,(p)\,(z_i) = N_{\mathrm{c(v)}}(z_i)\, F_{\frac{1}{2}}\left((-)\,\frac{F_{\mathrm{n(p)}}(z_i) - \left(E_{\mathrm{c(v)}}(z_i) - eV_{\mathrm{P}}(z_i)\right)}{kT}\right), \tag{5.12}$$

where

$$N_{\mathrm{c(v)}} = 2\left(\frac{m_{\mathrm{c(v)}}(z_i)\, ekT}{2\pi\hbar^2}\right)^{\frac{3}{2}}, \tag{5.13}$$

$F_{\frac{1}{2}}(x)$ is a Fermi-Dirac integral [70], $E_{\mathrm{c}(v)}$ is the bandedge of conduction (valence band), and $m_{\mathrm{c(v)}}$ is the conduction (valence) band effective mass. When the Hamiltonian of the system has more than one valence band, for example if the Hamiltonian is a 4×4 Luttinger-Kohn Hamiltonian [70], better equation for modeling the hole distribution is

$$p = p_{\mathrm{hh}} + p_{\mathrm{lh}}, \tag{5.14}$$

where

$$p_{\mathrm{hh(lh)}}\left(z_i\right) = N_{\mathrm{hh(lh)}}\left(z_i\right) F_{\frac{1}{2}}\left(-\frac{F_{\mathrm{p}}\left(z_i\right) - \left(E_{\mathrm{hh(lh)}}\left(z_i\right) - eV_{\mathrm{P}}\left(z_i\right)\right)}{kT}\right). \tag{5.15}$$

Exact values of material parameters (such as effective masses and bandedges) in Eqs. (5.12) and (5.15) are not crucial here, however they have to resemble those of the real structure being modeled.

After F_{n} and F_{p} are extracted, equations (5.12) and (5.15) are inserted into Eq. (5.6). This time however, quasi-Fermi levels are fixed (equal to the values extracted in the previous step) and V_{P} is assumed to be variable. This results in the following equation non-linear equation

$$\mathbf{f}\left(\mathbf{V}\right) = \mathbf{K}\mathbf{V} + \mathbf{M}\boldsymbol{\rho}(\mathbf{V}) = \mathbf{0}. \tag{5.16}$$

The above equation is then solved with the Newton-Raphson method. The Jacobian necessary for the Newton-Rhapson method is calculated analytically using properties of Fermi-Dirac integral [70].

5.4 Application of bisection to an unstable photon Green's function loop

The reason why the middle loop from Fig. 5.1 is unstable, is the singularity in Eq. (4.93). Equation (4.93) is well defined for modal gain

$$g_{\mathrm{mod}} = \mathrm{Im}\left(k_{\mathrm{eff}}\left(\omega\right)\right)/2 < \frac{1}{2L_{\mathrm{x}}} \ln \frac{1}{\left|r\right|^2},$$

approaches infinity $(+\infty)$ when

$$\mathrm{Im}\left(k_{\mathrm{eff}}\left(\omega\right)\right) \to \frac{1}{2L_{\mathrm{x}}} \ln \frac{1}{\left|r\right|^2},$$

and becomes meaningless when

$$\mathrm{Im}\left(k_{\mathrm{eff}}\left(\omega\right)\right) > \frac{1}{2L_{\mathrm{x}}} \ln \frac{1}{\left|r\right|^2}.$$

As explained in Chapter 2, g_{mod} can never physically reach or exceed threshold $g_{\mathrm{th}} = \frac{2}{L_{\mathrm{x}}} \ln \frac{1}{|r|}$. However, during intermediate steps in steady-state calculations this happens i.e., sometimes g_{mod} calculated from Green's functions is too big, and $D^{<}$ cannot be calculated. Numerical experiments have shown that no matter how good the initial guess of $D^{<}$ is, self-consistent calculations will always lead at some point to g_{mod} larger than g_{th}.

If it is assumed that the laser operates in one mode only $D^{<}(\omega_m) = D^{<}$, this problem can be solved by bisection method. Initially, it is assumed that the real value of $D^{<}$ is located somewhere in the range $[D^{<}_{\min}, D^{<}_{\max}] = [0, +\infty]$. The bisection method is used for the following equation

$$D^{<}_{\mathrm{c}}\left(D^{<}_{\mathrm{i}}\right) - D^{<}_{\mathrm{i}} = 0, \tag{5.17}$$

where $D^{<}_{\mathrm{i}}$ is the value from the previous step (in the first step it is the initial guess) and $D^{<}_{\mathrm{c}}$ is calculated using formula (4.93) after solving the Dyson equation (most inner loop in Fig. 5.1) with electron-photon self-energy containing $D^{<}_{\mathrm{i}}$. At each step of the bisection method, after solving the Dyson equation, g_{mod} is calculated and checked if it is smaller than g_{th}. If it is smaller, then $D^{<}_{\mathrm{c}}$ is calculated using Eq. (4.93) and bisection is used to determine new $D^{<}_{\mathrm{i}}$, $D^{<}_{\min}$, and $D^{<}_{\max}$. If it is not, then it means that $D^{<}_{\mathrm{i}}$ is too big and new $D^{<}_{\mathrm{i}}$and $D^{<}_{\max}$ are determined to be $D^{<}_{\mathrm{i,new}} = \left(D^{<}_{\mathrm{i}} + D^{<}_{\min}\right)/2$, $D^{<}_{\mathrm{max,new}} = D^{<}_{\mathrm{i}}$.

5.5 Convergence criteria and numerical simplifications

As can be seen from Fig. 5.1 there are three major loops: most outer Poisson loop, middle photon loop, and inner Green's function loop.

The most inner loop (the Dyson equation) usually requires many iterations (hundreds) to reach convergence. The most intuitive convergence condition is to require that relative change of quasiparticle densities and currents between iterations are smaller than some error criterion parameter. For example the criteria for electrons are

$$\frac{\|\mathbf{n} - \mathbf{n}_{\mathrm{prev}}\|}{\|\mathbf{n}\|} < \epsilon_{\mathrm{n}}, \tag{5.18}$$

$$\frac{\|\mathbf{J}_{\mathrm{n}} - \mathbf{J}_{\mathrm{n,prev}}\|}{\|\mathbf{J}\|} < \epsilon_{\mathrm{J}}, \tag{5.19}$$

where $n_i = n(z_i)$, $J_{\mathrm{n},i} = J_{\mathrm{n}}(z_i)$, and $\|\|$ is a norm (for example infinity or an Euclidean norm). Though intuitive, the conditions (5.18) and (5.19) are not optimal. This is because there are $N_k \times N_E$ Green's functions and only a small subset of all Green's functions requires many loops to converge, while others usually converge in 2-5 iterations. If conditions (5.18) and (5.19) are used, all $N_k \times N_E$ Green's functions have to be iterated many times. It is much better to set the convergence criteria for every (k_i, E_i) separately

$$\frac{\|\mathbf{n}(k_i, E_j) - \mathbf{n}_{\mathrm{prev}}(k_i, E_j)\|}{n_{\mathrm{ref}}} < \epsilon_{\mathrm{n}}, \tag{5.20}$$

$$\frac{\|\mathbf{J}(k_i, E_j) - \mathbf{J}_{\mathrm{prev}}(k_i, E_j)\|}{J_{\mathrm{ref}}} < \epsilon_{\mathrm{J}}. \tag{5.21}$$

where $n_{\text{ref}} = \max\left(\|\mathbf{n}\left(k_i, E_j\right)\|\right)$ and $J_{\text{ref}} = \max\left(\|\mathbf{J}\left(k_i, E_j\right)\|\right)$. The conditions for hole density and current are analogous to (5.20) and (5.21). Note that in the denominators of conditions (5.20) and (5.21) there are reference values instead of just $\|\mathbf{n}\left(k_i, E_j\right)\|$ and $\|\mathbf{J}\left(k_i, E_j\right)\|$. This is because for some (k_i, E_i) where carrier and/or current densities should be zero (for example in the bandgap), numerical round-off error causes the values of $\mathbf{n}$ and/or $\mathbf{J}$ to be not exactly zero, but still orders of magnitude less than any significant value. For such (k_i, E_i), it might happen that the calculations never converge (the result is just a numerical noise). The denominators n_{ref} and J_{ref} assure that for such (k_i, E_i) the convergence criteria are satisfied immediately. That is, even if the error $\|\mathbf{n}\left(k_i, E_j\right) - \mathbf{n}_{\text{prev}}\left(k_i, E_j\right)\|$ is always significant in relation to $\|\mathbf{n}\left(k_i, E_j\right)\|$, in relation to n_{ref} it is much smaller than convergence parameter ϵ_{n}.

For the middle loop, there are two possible convergence conditions

$$\frac{\left|D_{\text{c}}^{<}\left(D_{\text{i}}^{<}\right) - D_{\text{i}}^{<}\right|}{D_{\text{i}}^{<}} < \epsilon_{\text{D}}, \tag{5.22}$$

or

$$\frac{\left|D_{\text{max}}^{<} - D_{\text{min}}^{<}\right|}{D_{\text{i}}^{<}} < \epsilon_{\text{D}}. \tag{5.23}$$

The number of steps to reach convergence with the bisection method depends linearly on the desired precision ϵ_{D}.

If the initial guess of the Poisson equation is obtained from the depletion region approximation [70], the outer loop usually requires only a few steps to converge. The convergence condition used in this work is

$$\frac{\|\mathbf{V} - \mathbf{V}_{\text{prev}}\|}{\|\mathbf{V}\|} < \epsilon_{\text{V}}, \tag{5.24}$$

with $V_i = V_{\text{P}}\left(z_i\right)$.

To ease the computational burden, three major approximations are done.

First, only block-diagonal and a limited number of block-off-diagonals of Green's functions and self-energies are calculated and stored (where block size is the number of bands of the Hamiltonian). Physically, this corresponds to limiting the range of many-body interactions. For example, by leaving only 2 off-diagonals (1 above and 1 below the diagonal) the range is limited to $\Delta = z_{i+1} - z_i$.

Second, if the Hamiltonian from Eq. (4.24) does not have conduction-valence band coupling elements, then the Green's functions and consequently the self-energies will not have conduction-valence band elements either. In that case, memory and time requirements can be reduced by introducing separate conduction band Green's functions and valence band Green's functions instead of solving the Dyson equation for the full Green's function (conduction + valence bands). The Dyson equation is then solved separately for conduction and valence bands. For example, for the simplest effective mass Hamiltonian having the following form [70]

$$h = \begin{bmatrix} h_{\mathrm{c}} & 0 & 0 & 0 \\ 0 & h_{\mathrm{c}} & 0 & 0 \\ 0 & 0 & h_{\mathrm{v}} & 0 \\ 0 & 0 & 0 & h_{\mathrm{v}} \end{bmatrix}, \tag{5.25}$$

$$h_{\mathrm{c(v)}} = (-)\left(-\frac{\hbar^2}{2m_0}\frac{\partial}{\partial z}\frac{1}{m_{\mathrm{c(v)}}(z)}\frac{\partial}{\partial z} + \frac{\hbar^2 k_{\mathrm{t}}^2}{2m_0}\right), \tag{5.26}$$

and a spatial grid with 100 points, a single 400×400 Green's function matrix is reduced to 4 100×100 matrices. In the case where there are also no spin coupling terms, as it is in the Hamiltonian from Eq. (5.25), it is enough to solve equations only for one spin orientation only (2 100×100 matrices) and multiply the final results (carrier densities etc.) by 2.

A final simplification is made after noticing that for relatively low voltages, the carrier density modification induced by electron-photon and electron-phonon interactions is small. Because the electrostatic potential depends only on carrier densities, calculations with electron-photon and electron-phonon interaction self-energies and without them give approximately the same value of electrostatic potential. When this is the case, initial calculations to obtain the potential profile across the device can be performed without those interactions. The electrostatic potential determined in this way, is then used as the initial guess in full calculations (with all interactions), and, for this step, only one or two iterations with the Poisson equation (third loop) are necessary.

Chapter 6

Sample results and conclusions

This chapter presents a sample of possibilities of the simulator. Calculations are performed on an exemplary standard single-well $Al_{0.2}Ga_{0.8}As/GaAs$ edge-emitting laser. The first section provides electrical and optical results for the system without electron-phonon interaction present. The results include carrier densities, current densities, local density of states and modal gain. In addition to the current and carrier density plots, contour plots presenting spectral distributions of the carrier and current densities are shown.

In the second section, based on the contour plot of current density, it is argued why any realistic simulation has to include inelastic scattering mechanism (such as scattering by longitudinal optical phonons). Calculations for a system with optical phonons are presented and compared with calculations for a system without phonons.

The last two sections of this chapter include final remarks and conclusions about the theory presented in this work. A path for future development of the model is discussed.

6.1 System without phonons

The system under consideration is an $Al_{0.2}Ga_{0.8}As/GaAs$ edge-emitting laser. It is 300 μm long, with two mirrors having identical reflection coefficients $r^2 = 0.33$. The geometry of the laser is presented in Fig. 6.1 and in Tab. 6.1. Material parameters used in simulation are listed in Tab. 6.2. Intraband transitions were neglected transitions by assuming that intraband momentum matrix element $p_{c,c} = p_{v,v} = 0$.

Lasing frequency is chosen to be fixed at $\hbar\omega = 1.506$ eV. It corresponds to a wavelength $\lambda = 0.82$ μm.

Wavevector k is discretized with 125 uniformly distributed points, with $k_{\min} = 0$ and $k_{\max} = 1$ nm^{-1}. The hole effective mass is taken to be much smaller than the commonly accepted value – this allows one to significantly reduce wavevector grid and thus computation time and memory required. Energy grid has a total of 1000 points, 500 hundred for the valence and 500 for the conduction band. The minimal value of energy on the energy grid is $E_{\min} = -0.41$ eV and maximal is $E_{\max} = 1.7$ eV. Such choice of minimal and maximal values of energy grid does not cover energies in

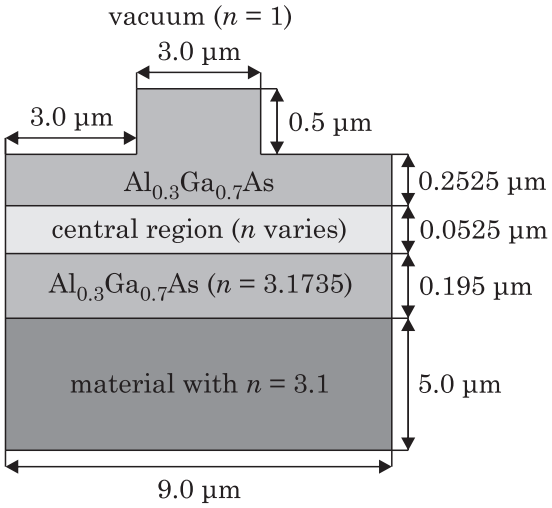

Figure 6.1: Geometry of the simulated laser. Central region consists of many layers which are given in Tab. 6.1. Reprinted with permission from [110]. Copyright 2012, American Institute of Physics.

thickness [nm]	material	doping [m^{-3}]
15	$Al_{0.3}Ga_{0.7}As$	$n - 10^{25}$
7.5	$Al_{0.3}Ga_{0.7}As$	–
7.5	GaAs	–
7.5	$Al_{0.3}Ga_{0.7}As$	–
15	$Al_{0.3}Ga_{0.7}As$	$p - 10^{25}$

Table 6.1: Characteristics of the central region. Reprinted with permission from [110]. Copyright 2012, American Institute of Physics.

parameter	symbol [unit]	well	barriers
electron mass	m_e [m_0]	0.067	0.084
hole mass	m_h [m_0]	0.1	0.117
CB bandedge	V_{CB} [eV]	1.59	1.85
VB bandedge	V_{VB} [eV]	0.164	0
Golizadeh const.	d [eV^2]	$1.96 \cdot 10^{-4}$	
Debye screening length	q_0 [nm^{-1}]	0.2	
lattice constant	a [nm]	0.5653	0.5655
high dielectric const.	$\epsilon_\infty[\epsilon_0]$	10.89	10.07
stat. dielectric const.	$\epsilon_s[\epsilon_0]$	13.1	11.69
momentum matrix	$p_{c,v}[\mathrm{kg} \cdot \frac{\mathrm{m}}{\mathrm{s}}]$	$9.68 \cdot 10^{-25}$	$9.42 \cdot 10^{-25}$

Table 6.2: Parameters used in the simulation.

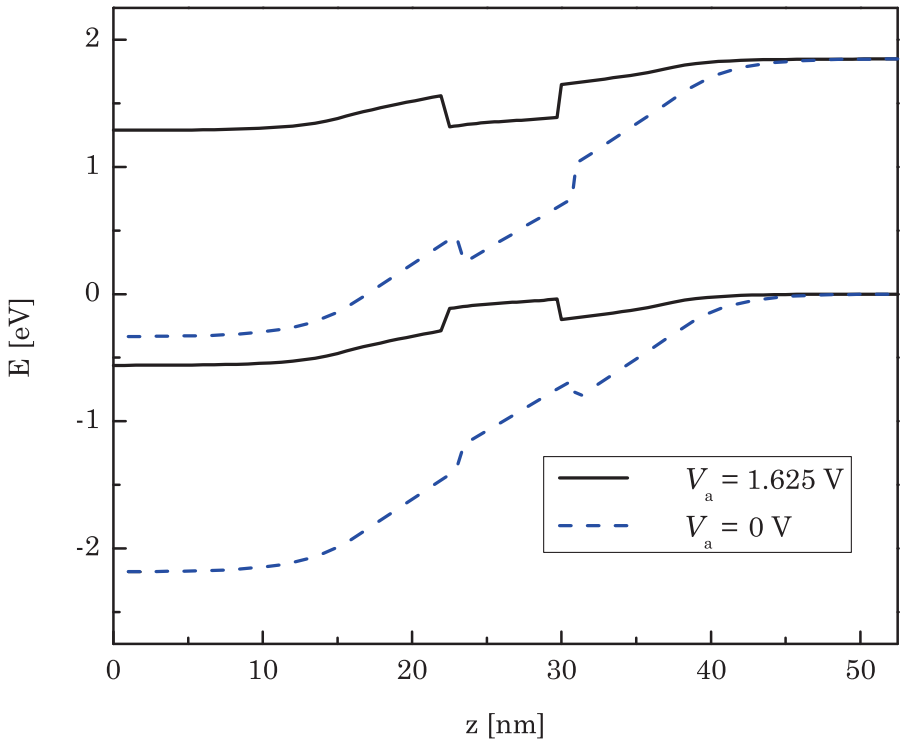

Figure 6.2: Bandedge profile for applied voltage bias and for $V_a = 1.625$ V and for $V_a = 0$ V (equilibrium). The applied forward bias flattens the bandedge profile which allows for the formation of confined states inside the quantum well region.

which the ballistic current is located. However, this is acceptable since the ballistic current is much smaller than the current due to electron-hole recombination and thus the ballistic current can be safely neglected.

Spatial grid is taken to be nonuniform one, consisting of 92 points with denser distribution around the quantum well region and less dense in the barriers.

The plots presented in this section were obtained for applied forward bias $V_a = 1.625$ V. The applied bias counters the built-in electric field and flattens the bandedge profile. The comparison of bandedge profile of the system in equilibrium and under bias is presented in Fig. 6.2.

One of the biggest advantages of the Green's function technique is that it allows one to obtain spectral characteristics of carriers and current densities as well as local density of states (LDOS).

Figure 6.3a shows a contour plot of LDOS. Different structure of density of states inside and outside of the quantum well is clearly visible. LDOS for a few selected position points presented in Fig. 6.3b reveals that far away form the quantum well the density of states resembles density of states of a bulk system [70] i.e., it increases as square root of energy. Inside the quantum well, density of states becomes a step function characteristic for a 2-D system.

One can see that the LDOS function in Fig. 6.3 collapses for very small (negative) values and for very high values (not shown) of energy. This is caused by finite range

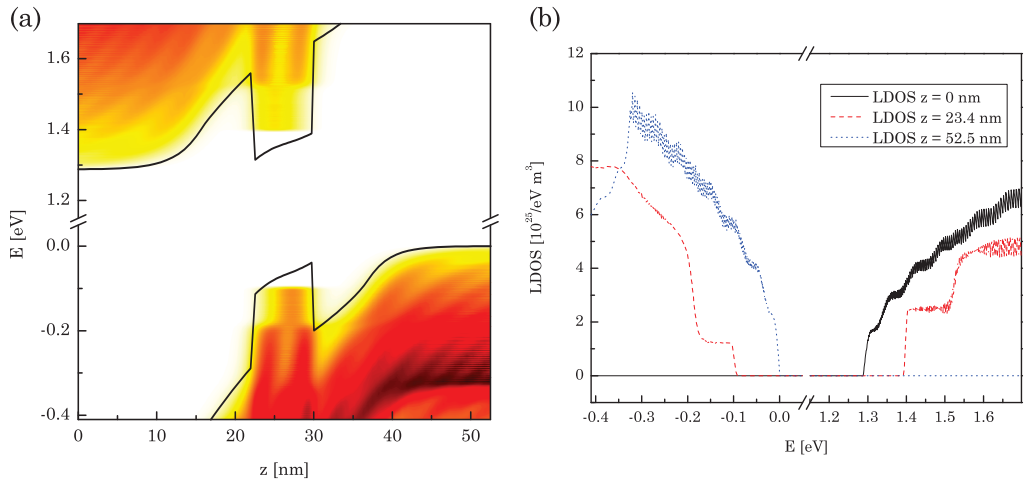

Figure 6.3: LDOS for $V_a = 1.625$ V. On the left-hand side the contour plot (a) clearly shows different structure of density of states inside and outside of the quantum well. The LDOS for three selected positions points is shown in plot (b). LDOS far away from the quantum well resemble square root dependency of a bulk material [70]. Inside the quantum well, density of states behaves like density of states of a 2-D structure [70]. For extreme values of the energy, LDOS collapses and becomes inaccurate. It is caused by insufficient rage of k_t in the numerical calculations, but has no influence on the physical results as long as those states remain unoccupied.

of inverse wavevector k_t. This collapse does not influence physical quantities as long as states for which this collapse occur remain unoccupied. LDOS (and also other quantities) have characteristic ripples caused by numerical integration over k_t. Those can be removed or at least reduced by making k_t grid more dense.

The local density of states for $k_t = 0$ presented in Fig. 6.4 gives further insight into the distribution of states inside the device. It shows a characteristic stripe pattern which is caused by superposition of injected states and states reflected form the bandedge. The first and second confined levels are clearly visible inside the quantum well. Because the LDOS inside the quantum well is very sharply peaked, the energy grid has to be very dense in that region. This sharp peaks are major reason for inclusion of phenomenological scattering. The electron-photon scattering or even electron-phonon is not enough to sufficiently broaden the states inside the quantum well and extremely dense energy grid would be necessary (at least tens of thousands points).

Figure 6.5 shows spectral and spatial distributions of carrier densities. In Fig. 6.5b, inversion of population is clearly visible in the quantum well region. The central region (quantum well) has an inversion of population which creates the material gain and allows for lasing action to occur. This region is not electrically neutral (locally) which reduces the gain because it is proportional to the smaller value of electron and hole densities. This mismatch is not observed in the conventional gain models [70, 27, 24, 64] which use the flat band approximation. The gain model considered

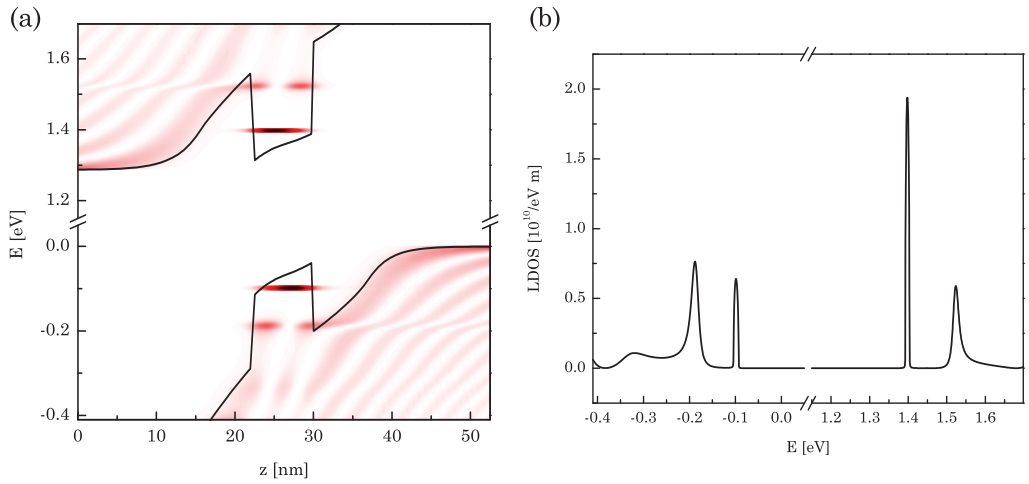

Figure 6.4: LDOS at $k_t = 0$ for $V_a = 1.625$ V. The contour plot (a) shows characteristic stripe pattern due to superposition of injected states and states reflected from the potential edge. Inside the quantum well region the first and the second quantum levels are clearly visible in both the conduction and valence bands. Plot (b) shows the LDOS for $z = 23.4$ nm (inside the quantum well). The fundamental energy levels are better confined and thus are more sharply peaked in comparison to second levels in the well.

in this work does not approximate potential profile as flat – this can be seen in Fig. 6.2.

Carrier densities at the edges of the structure have the same values as doping concentrations which assures that the leads are electrically neutral and hence the potential profile inside them is flat.

The current flowing through the device is shown in Fig. 6.6. Figure 6.6a shows electron current flowing from the n-side and hole current flowing from the p-side. Both currents are terminated in the quantum well where the electron-hole recombination and emission take place. These spectral currents are very sharply peaked and the distance between the peaks is roughly equal to energy of emitted photons. It is clear from Fig. 6.6a that the quantum tunneling plays an important role in delivering the current to the quantum well. Figure 6.6b proves that the total current (electron + hole) is conserved.

Finally, Fig. 6.7 shows the modal gain for three different voltages with and without the stimulated emission. Because the gain is a purely electric quantity (it is related to polarization) it can be calculated even if the electromagnetic field is not present. Figure 6.7a shows the modal gain without electron-photon coupling. The gain increases as the voltage bias (and thus inversion of population) increases with the slight shift of a gain peak. Each of the gain curves rises rapidly at $E = 1.4575$ eV – roughly the bandgap energy, reaches a peak value, and then drops to negative values (not shown on the pictures). With electron-photon interaction, gain at the lasing frequency is suppressed below its threshold level which can be determined

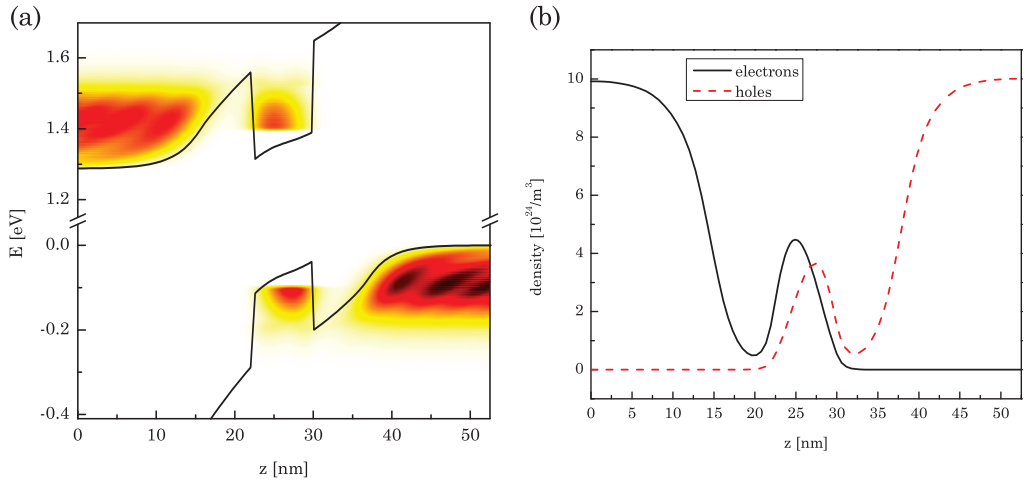

Figure 6.5: Carrier densities for $V_a = 1.625$ V. The contour plot (a) shows spectral distribution of carriers and plot (b) shows spatial distributions of carrier densities. Due to deviation of bandedge profile from flat band profile the peaks of electron and hole densities inside quantum well do not occur at the same point in space. This effect reduces the material gain of the well and is not taken into account in majority of conventional laser models [70, 27, 72, 24].

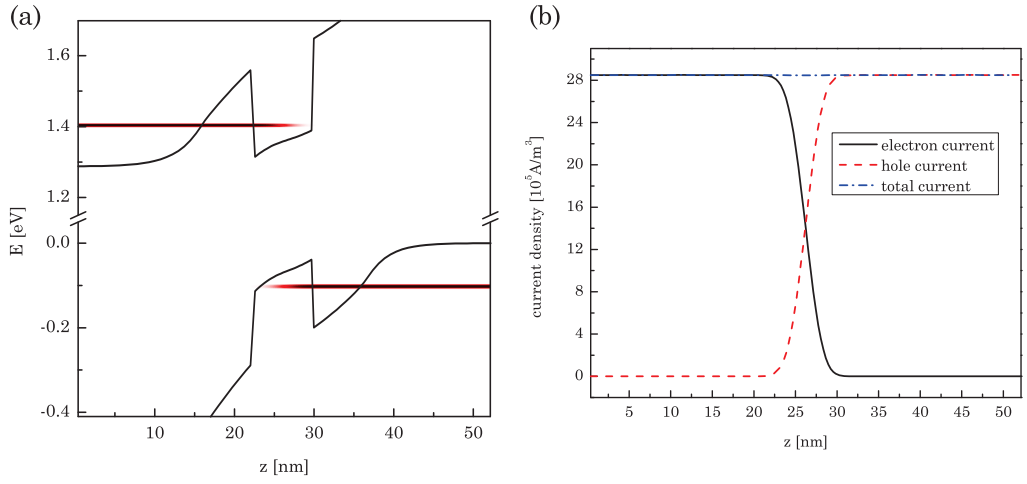

Figure 6.6: Current densities for $V_a = 1.625$ V. The contour plot (a) shows spectral current consisting of two very sharp peaks (on the energy scale). The distance between the peaks in roughly equal to the energy of emitted light. It is clearly visible that the quantum tunneling is an important mechanism of delivering current to the quantum well where the recombination takes place. The plot presenting spatial dependency of current densities (b) shows that the total current is indeed conversed.

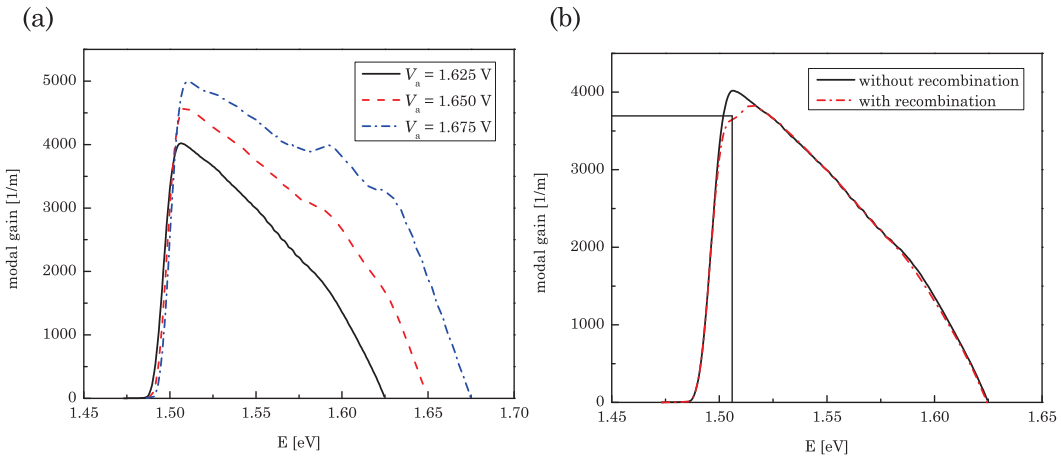

Figure 6.7: The plot on the left-hand side (a) shows the modal gain for a few selected applied voltages before electron-photon interaction is turned on. Plot (b) shows a comparison of the modal gain with and without electron-photon interaction for $V_a = 1.625$ V. The vertical line indicates the lasing frequency and the horizontal one indicates threshold gain value. Electron-photon interaction reduces the value of the modal gain (at the lasing frequency) so that after interaction is turned on the modal gain is slightly below the threshold gain.

from the condition

$$g_{\text{th}} = \frac{2}{L_{\text{x}}} \ln \frac{1}{r}. \tag{6.1}$$

6.2 System with phonons

Figure 6.6a shows one of the major shortcoming of not including phonons or any other thermalization mechanism into the simulation. Without phonons, the only way the current can be delivered to the quantum well is via quantum tunneling effect. One can imagine an extreme case when with the increasing applied bias V_a, the potential profile eventually becomes flat. When this happens, all levels in the quantum well are below (or above in case of holes) bandedge of the barrier and the current cannot be delivered via quantum tunneling effect. This concept is shown in Fig. 6.8. This means that if the quantum tunneling was the only way to deliver the current to the quantum well, for large enough potentials there would be no emission at all. Because such effect is not observed in experiments, the model has to be expanded to include a thermalization mechanism (inelastic scattering).

Addition of inelastic scattering by phonons allows for the current to flow with a high energy and then when it is in the quantum well region to get to the lower energy levels through the inelastic scattering.

The most significant difference after addition of the electron-phonon interaction is a change in current characteristics. Figure 6.9 shows spectral current of a system

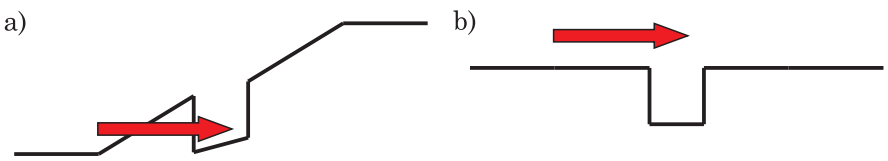

Figure 6.8: For moderate values of applied bias (a), the current can be delivered to the quantum well via quantum tunneling. For large voltages (b), the current flows above the well and without inelastic scattering mechanism it cannot flow into the quantum well.

voltage [V]	gain [1/m]
1.625	4019
1.6375	4282
1.65	4483
1.675	4666

Table 6.3: Values of gain at the lasing frequency before turning on electron-photon interaction.

with the electron-phonon scattering present. Now, the current flows in a much wider energy range. It consists of sharp peaks (on the energy scale). The peaks are separated by $\hbar\omega_{\mathrm{LO}}$ – energy of longitudinal optical phonons.

Figure 6.10 shows the power and current for four different values of the applied voltage for the system with and without phonons. With the phonons present, much more current can reach the quantum well and recombine, hence the stimulated emission is stronger than in the model without phonons.

From Fig. 6.10 one can see that for the system without phonons, with increasing voltage, the current first increases and then starts to decrease. This happens because of the change of the shape of bandedge profile. Although the gain increases, the barrier potential which the current has to tunnel through, also increases which results in a decreased current. This artificial effect is avoided by including inelastic scattering. With the phonons present, the current can be delivered to the deep levels of the quantum well not only by the quantum tunneling mechanism but also by the inelastic scattering inside the quantum well.

Finally, the $I-V$ characteristics in Fig. 6.10 do not show the regular exponential dependency because the only recombination mechanism is through the emission of photons with a particular energy $\hbar\omega = 1.5086$ eV. The scattering strength (and thus the current) is proportional to the value of the modal gain (calculated before the electron-photon interaction is taken into account) at this energy. In general, the gain peak increases exponentially with the applied voltage, however the gain value for a particular frequency does not increases exponentially as can be seen from Tab. 6.3 and Fig. 6.7b.

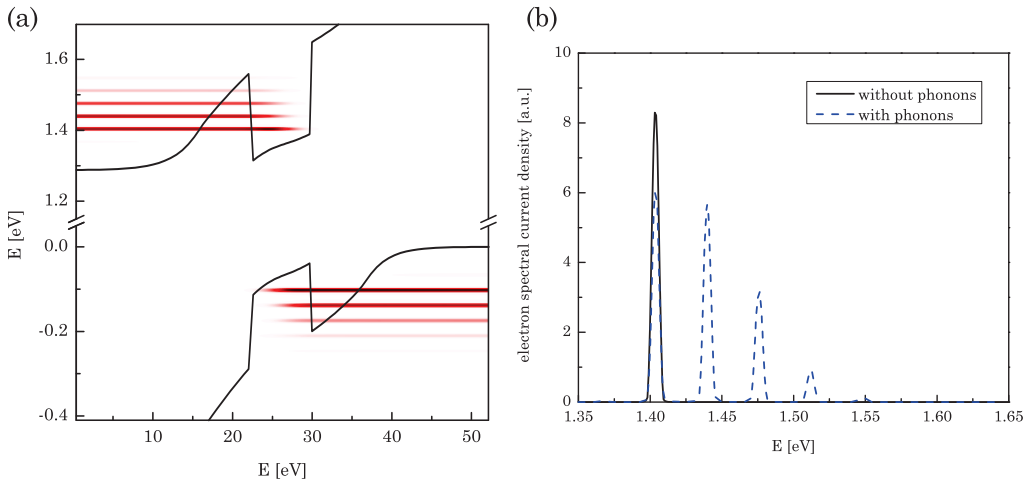

Figure 6.9: Current characteristics for applied voltage $V_a = 1.625$ V. Figure (a) shows a contour plot of spectral current density with electron-phonon coupling. Inelastic electron-phonon scattering allows for the current to flow in much wider energy range that in the case without electron-phonon scattering. Plot (b) contains a comparison of the spectral electron current for $z = 0.375$ nm for the model with and without electron-phonon interaction. The distance between the current peaks is roughly equal to the energy of longitudinal optical phonons.

6.3 Summary

This work presents a complete description of a fully quantum mechanical model of a semiconductor laser under the steady-state conditions. Equations necessary to simulate a laser diode were derived straight from the microscopic theory. In comparison to usual simulation techniques, the model presented here requires only a couple of most fundamental material parameters such as parameters of the Hamiltonian or electric permittivity.

Because NEGF equations are derived from the microscopic theory, they are much more fundamental that the commonly used equations to describe semiconductor lasers. Because of its quantum nature, this formalism naturally includes the quantum tunneling. Unlike in the popular drift-diffusion methods, carriers and currents are energy dependent and the effect of spectral distributions of those quantities on the characteristics of the laser can be investigated. For example, the stimulated emission depends not only on the number of carriers in the quantum well but also on their spectral distribution. The drift-diffusion models can only use the effective mass Hamiltonian to describe the dynamics of quasiparticles. Although in this work only the effective mass Hamiltonian was used, NEGF technique is fully capable of using much more complex Hamiltonians to describe the dynamics of carriers. Finally, the gain model presented here, naturally takes into account the complex shape of the bandedge. This is a significant improvement over the usual flat-band approximation which not only assumes that the bandedge profile is flat but also makes an artificial

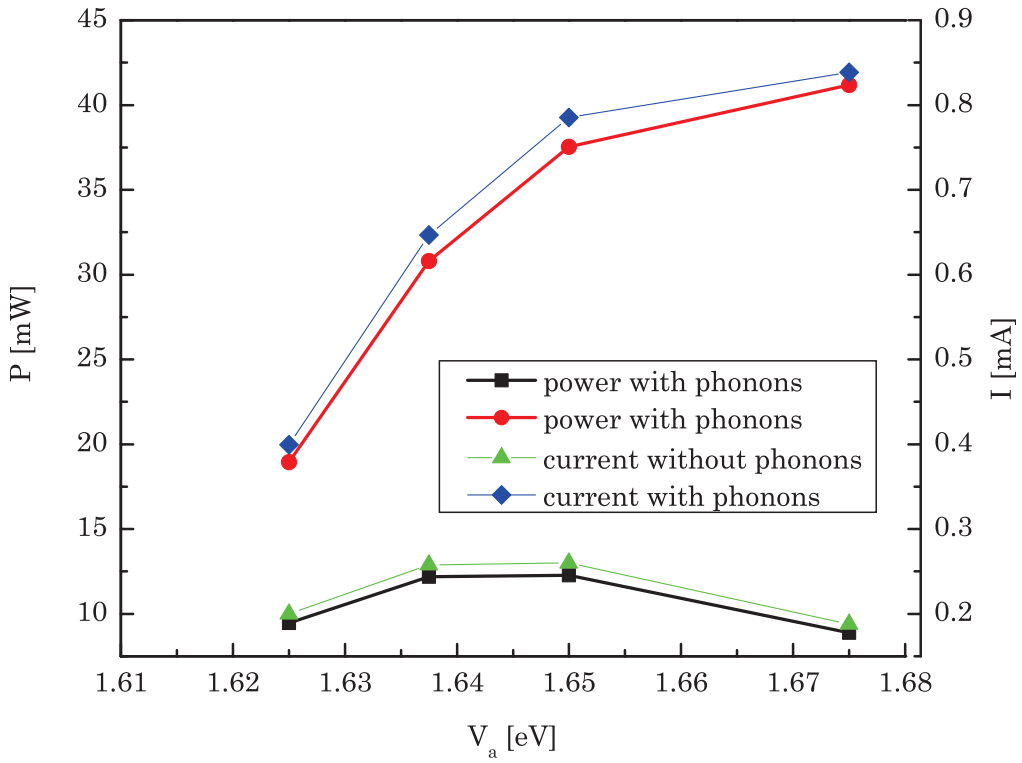

Figure 6.10: Current and emitted power as a function of applied bias for a system with and without phonons. Addition of inelastic scattering mechanism greatly increases both current and the power output.

distinction between the 2-D quantum well states and 3-D bulk states.

In general, the technique presented in this work is able to capture much more of the complex processes occurring in a laser diode. However, the increased accuracy of this model comes at a price. Even after the significant simplifications, the computational burden and memory requirements are enormous. Additionally, inclusion of every scattering mechanism significantly increases the computation time. Because of the fundamental nature of the NEGF technique, some scattering mechanisms cannot be omitted even in a simplest simulations. At the same time, it is very difficult to model scattering mechanisms phenomenologically.

6.4 Further development

To make NEGF applicable for engineering use it is necessary to reduce the computation time and complexity without loosing too much of the accuracy. The most urgent improvement is to decrease the number of steps necessary for convergence of the Dyson equation – self-energy loop. At this point for some values of input parameters, in the most extreme cases this loop needs ten of thousands iterations to converge. This reduction can probably be done by improving the initial guess and by improving the method of updating the solution during iterations.

The simulator should also be expanded to be able to take into account more longitudinal modes. Although the presence of other modes is not desirable in laser diodes, they are always present and have an influence on the performance of the lasers. However, in this work it was assumed that the stimulated emission occurs at a single frequency only i.e., that the mirrors reflect only photons at this single frequency and are perfectly transparent for all other frequencies. This quite artificial assumption is forced only by numerical difficulties – the theory presented here is fully capable of taking into account more than one mode. Because the bisection method used in this work cannot be expanded to solve for more than one mode, a completely new algorithm has to be developed.

The complete laser simulator should also possess other major types of scattering: Shockley-Read-Hall, Auger, spontaneous emission, and possibly more types of inelastic scattering.

Although the spontaneous emission is included in the electron-photon self-energy derived in this work, because of the limitation of the emission to the single frequency only, the spontaneous emission is also limited to this one frequency. Addition of the spontaneous emission for the other frequencies without adding the stimulated emission is straight forward. The limitation of the stimulated emission was achieved by setting the photon Green's function to zero at all frequencies other than the desired lasing frequency. If the spontaneous emission is to be included, instead of setting photon Green's function to zero at other frequencies, one has to replace them with a photon Green's function of a free photon field. The free photon Green's function is easy to calculate and can quite realistically represent spontaneous emission [51]. The spontaneous emission was not taken into account in this work solely due to already too large computational burden.

The Auger recombination can be obtained as a second order electron-electron interaction combined with the phonons. The second order process would require much more computational power because the scattering self-energy is proportional to the product of two Green's functions and can involve up to 4 integrals (2 over k_t and 2 over E). The Auger recombination also requires a Hamiltonian which can accurately describe distant energy bands and that is accurate for large values of the inverse wavevector k_t. Obviously the $\mathbf{k}\cdot\mathbf{p}$ and effective mass Hamiltonian do not meet those requirements and would have to be replaced by either the Hamiltonian obtained from the ab initio calculations or by the effective orbital Hamiltonian. Taking into account all the above arguments, it is clear that the Auger recombination self-energy has to be modeled phenomenologically rather than derived from the first principles.

Contrary to the Auger recombination, the Shockley-Read-Hall (SHR) recombination is a first order process and it is much more plausible that it can be included in the simulation in the near future. The addition of SHR will require a microscopic model of the impurities and an additional very fine energy grid inside the bandgap to cover the energy levels of the impurities.

Because the optical part of the problem is determined solely by the solution of the photon Green's function for the particular geometry of the laser, it should be relatively easy to simulate other types of lasers such as VCSEL or DFB lasers.

Finally, for the most practical calculations it is not enough to assume that the transport of carriers occurs in one dimension only, and that the current flows only in the vicinity of the quantum well. However it is very doubtful that this approach can be expanded to encompass a second dimension or to even have one dimension but a few micrometers long. In the future, this method should be somehow merged with the drift-diffusion method. Then, the NEGF formalism could be used for the region in the vicinity of the active region where the high accuracy is necessary and a drift-diffusion model would be used to simulate behavior far away from the active region.

Due to the early stage of development of our model and all the mentioned above shortcomings, the device simulated in this chapter is a very simplistic one and thus a fair comparison with experiment is not possible at this stage. A reasonable comparison with experiment will be possible to make after further improvement of the numerical procedures. More efficient numerical routines will allow to use Hamiltonian with realistic effective mass of the holes (or even more complex Luttinger-Kohn Hamiltonian) and addition of the SHR and Auger recombination mechanisms (even if modeled phonomenologically).

Appendix A

Pictures of quantum mechanics

In transport theory, one has to deal with time-dependent systems. The standard formulation of the Schrödinger equation (also called the Schrödinger picture) is very convenient when dealing with static problems where the Hamiltonian of the system is not explicitly time-dependent. One can easily get rid of time from the state vectors and deal with a static problem only. However, when considering time dependent phenomena, such simplification is not possible and the Schrödinger picture is not the best approach anymore. For time-dependent Hamiltonians two methods have been developed: the Heisenberg picture and the interaction picture. In the interaction picture, part of the time dependency is moved into operators, while in the Heisenberg picture all of the time dependency is in the operators, making the state vectors time independent. Although this topic is very basic and both pictures are usually described in quantum mechanics textbooks, they are often introduced without proper motivation or justification. This short appendix provides the most important facts and derivations concerning both types of pictures.

In the first section, two different time evolution operators are introduced. In the second section, time evolution operators are used to define the interaction and Heisenberg pictures, as well as connections between them. At the end of the second section, the time evolution of quantum statistical ensemble is considered.

A.1 Time evolution operators

The time dependent Schrödinger equation is

$$i\hbar\frac{\partial}{\partial t}\left|\Psi\left(t\right)\right\rangle = \hat{H}\left(t\right)\left|\Psi\left(t\right)\right\rangle, \tag{A.1}$$

where the Hamiltonian can be separated into time independent and time dependent parts

$$\hat{H}\left(t\right) = \hat{H}_0 + \hat{H}_{\text{int}}\left(t\right). \tag{A.2}$$

One can assume that state $\left|\Psi\left(t\right)\right\rangle$ can be expressed by the action of time evolution operator $\hat{U}$ operating on that state at some reference time t_0

$$|\Psi(t)\rangle = \hat{U}(t,t_0)\,|\Psi(t_0)\rangle\,. \tag{A.3}$$

It is assumed that the evolution operator is unitary so that it does not change the length of the vector state on which it operates, and that it can evolve the vector state both forward and backward in time. With those assumptions and the definition (A.3), one can immediately specify properties of $\hat{U}$

$$\hat{U}^{\dagger}(t_1,t_2) = \hat{U}^{-1}(t_1,t_2)\,, \tag{A.4}$$

$$\hat{U}(t,t) = \hat{1}, \tag{A.5}$$

$$\hat{U}^{-1}(t_1,t_2) = \hat{U}(t_2,t_1)\,, \tag{A.6}$$

$$\hat{U}(t_1,t_2) = \hat{U}(t_1,t_3)\,\hat{U}(t_3,t_2)\,. \tag{A.7}$$

Substitution of (A.3) into the Schrödinger equation (A.1) gives

$$i\hbar\frac{d}{dt}\hat{U}(t,t_0)\,|\Psi(t_0)\rangle = \hat{H}(t)\,\hat{U}(t,t_0)\,|\Psi(t_0)\rangle\,,$$

and

$$i\hbar\frac{d}{dt}\hat{U}(t,t_0) = \left(\hat{H}_0 + \hat{H}_{\text{int}}(t)\right)\hat{U}(t,t_0)\,. \tag{A.8}$$

To find solutions of the evolution equation (A.8), it will be assumed that the evolution operator $\hat{U}$ can be written as

$$\hat{U}(t,t_0) = e^{-\frac{i}{\hbar}\hat{H}_0(t-t_0)}\hat{S}(t,t_0)\,, \tag{A.9}$$

which can always be done since nothing is assumed about operator $\hat{S}$. Operator $\hat{S}$ is called the interaction picture time evolution operator – the reason for this name is explained in the next section when the interaction picture is defined. By inserting formula (A.9) into Eqs. (A.4)-(A.7), it can be shown that operator $\hat{S}$ has exactly the same properties as operator $\hat{U}$.

To obtain the equation of motion for operator $\hat{S}$, Eq. (A.9) is substituted into Eq. (A.8)

$$i\hbar\frac{d}{dt}\hat{U}(t,t_0) = \hat{H}_0 e^{-\frac{i}{\hbar}\hat{H}_0(t-t_0)}\hat{S}(t,t_0) + \hat{H}_{\text{int}}(t)\,e^{-\frac{i}{\hbar}\hat{H}_0(t-t_0)}\hat{S}(t,t_0)\,. \tag{A.10}$$

Taking the time derivative of the Eq. (A.9) gives

$$i\hbar\frac{d}{dt}\hat{U}(t,t_0) = \hat{H}_0 e^{-\frac{i}{\hbar}\hat{H}_0(t-t_0)}\hat{S}(t,t_0) + i\hbar e^{-\frac{i}{\hbar}\hat{H}_0(t-t_0)}\partial_t\hat{S}(t,t_0)\,. \tag{A.11}$$

When combined, the last two equations give the formula for $\hat{S}$

$$i\hbar\frac{d}{dt}\hat{S}(t,t_0) = \hat{H}_{\text{int,I}}(t)\,\hat{S}(t,t_0)\,, \tag{A.12}$$

where

$$\hat{H}_{\mathrm{int,I}}(t) = e^{\frac{i}{\hbar}\hat{H}_0(t-t_0)}\hat{H}_{\mathrm{int}}(t)\, e^{-\frac{i}{\hbar}\hat{H}_0(t-t_0)}. \tag{A.13}$$

Formal integration of Eq. (A.12) from t_0 to t, with initial condition $\hat{U}(t_0,t_0) = \hat{1} \Rightarrow \hat{S}(t_0,t_0) = \hat{1}$ gives

$$\hat{S}(t,t_0) = \hat{1} - \frac{i}{\hbar}\int_{t_0}^{t} dt' \hat{H}_{\mathrm{int,I}}(t')\,\hat{S}(t',t_0)\,. \tag{A.14}$$

The solution of the above equation is described in detail in [85]. The overall result can be represented as following series

$$\begin{aligned}
\hat{S}(t,t_0) &= \sum_{n=0}^{\infty}\left(-\frac{i}{\hbar}\right)^n \frac{1}{n!}\int_{t_0}^{t} dt_1 \int_{t_0}^{t_1} dt_2 \ldots \int_{t_0}^{t_{n-1}} dt_n \hat{H}_{\mathrm{int,I}}(t_1)\,\hat{H}_{\mathrm{int,I}}(t_2)\ldots\hat{H}_{\mathrm{int,I}}(t_n) \\
&= \sum_{n=0}^{\infty}\left(-\frac{i}{\hbar}\right)^n \frac{1}{n!}\int_{t_0}^{t} dt_1 \ldots \int_{t_0}^{t} dt_n T_+\left[\hat{H}_{\mathrm{int,I}}(t_1)\ldots\hat{H}_{\mathrm{int,I}}(t_n)\right] \\
&= T_+\left[\exp\left(-\frac{i}{\hbar}\int_{t_0}^{t} dt' \hat{H}_{\mathrm{int,I}}(t')\right)\right],
\end{aligned} \tag{A.15}$$

where T_+ is the positive time-ordering operator

$$T_+\left[\hat{A}(t_1)\,\hat{B}(t_2)\right] = \theta(t_1-t_2)\,\hat{A}(t_1)\,\hat{B}(t_2) + \theta(t_2-t_1)\,\hat{B}(t_2)\,\hat{A}(t_1)\,, \tag{A.16}$$

which orders operators from left to right with decreasing time arguments (higher times are to the left).

One can also take the Hermitian adjoint of both sides of Eq. (A.12) to get the equation of motion for the adjoint operator $\hat{S}^\dagger$

$$-i\hbar\frac{d}{dt}\hat{S}^\dagger(t,t_0) = \hat{S}^\dagger(t,t_0)\,\hat{H}_{\mathrm{int,I}}(t)\,. \tag{A.17}$$

The solution of the adjointed equation is obtained in a similar way as the solution of the original equation, it is

$$\begin{aligned}
\hat{S}^\dagger(t,t_0) &= \sum_{n=0}^{\infty}\left(\frac{i}{\hbar}\right)^n \frac{1}{n!}\int_{t_0}^{t} dt_1 \ldots \int_{t_0}^{t} dt_n T_-\left[\hat{H}_{\mathrm{int,I}}(t_1)\ldots\hat{H}_{\mathrm{int,I}}(t_n)\right] \\
&= T_-\left[\exp\left(\frac{i}{\hbar}\int_{t_0}^{t} dt' \hat{H}_{\mathrm{int,I}}(t')\right)\right] = T_-\left[\exp\left(-\frac{i}{\hbar}\int_{t}^{t_0} dt' \hat{H}_{\mathrm{int,I}}(t')\right)\right],
\end{aligned} \tag{A.18}$$

where T_- orders operators from left to right with increasing time arguments (lower times are to the left).

A.2 Interaction and Heisenberg pictures

To avoid confusion, the following notational convention is used to distinguish between pictures: "I" subscript indicates the interaction picture, "H" subscript indicates the Heisenberg picture, no subscript means the Schrödinger picture.

In the previous subsection, times t and t_0 were completely arbitrary. At this point it is assumed that $t_0 < t$ and that the time dependent part of the Hamiltonian (A.2) is turned on at t_0

$$\hat{H}(t) = \begin{cases} \hat{H}_0 & \text{for } t < t_0 \\ \hat{H}_0 + \hat{H}_{\text{int}}(t) & \text{for } t \geq t_0 \end{cases}.$$

A state vector in the interaction picture is defined as

$$|\Psi_{\text{I}}(t)\rangle = e^{\frac{i}{\hbar}\hat{H}_0(t-t_0)} |\Psi(t)\rangle. \tag{A.19}$$

Such defined state vector has the same length in both Schrödinger and interaction pictures because the operator $e^{\frac{i}{\hbar}\hat{H}_0(t-t_0)}$ is unitary. Average value of any operator $\hat{O}(t)$ is

$$\left\langle \hat{O}(t) \right\rangle = \left\langle \Psi(t) \left| \hat{O}(t) \right| \Psi(t) \right\rangle = \left\langle \Psi_{\text{I}}(t) \left| e^{\frac{i}{\hbar}\hat{H}_0(t-t_0)} \hat{O}(t) e^{-\frac{i}{\hbar}\hat{H}_0(t-t_0)} \right| \Psi_{\text{I}}(t) \right\rangle, \tag{A.20}$$

so any operator (even explicitly time-dependent) $\hat{O}(t)$ in the interaction picture takes the following form

$$\hat{O}_{\text{I}}(t) = e^{\frac{i}{\hbar}\hat{H}_0(t-t_0)} \hat{O}(t) e^{-\frac{i}{\hbar}\hat{H}_0(t-t_0)}. \tag{A.21}$$

A state vector in the Heisenberg picture is defined as a state vector at a reference time t_0

$$|\Psi_{\text{H}}\rangle = |\Psi(t_0)\rangle = \hat{U}^{-1}(t, t_0) |\Psi(t)\rangle = \hat{S}^{-1}(t, t_0) |\Psi_{\text{I}}(t)\rangle. \tag{A.22}$$

With this definition of the Heisenberg picture, it is clear why the operator $\hat{S}$ is called the interaction picture evolution operator – it can evolve states between the interaction and the Heisenberg pictures similarly as evolution operator $\hat{U}$ evolves states between the Schrödinger and Heisenberg pictures.

The average value of an operator $\hat{O}(t)$ can be now written as

$$\begin{aligned} \left\langle \hat{O}(t) \right\rangle &= \left\langle \Psi(t) \left| \hat{O}(t) \right| \Psi(t) \right\rangle = \left\langle \Psi_{\text{H}} \left| \hat{U}^{\dagger}(t, t_0) \hat{O}(t) \hat{U}(t, t_0) \right| \Psi_{\text{H}} \right\rangle \\ &= \left\langle \Psi_{\text{H}} \left| \hat{S}^{\dagger}(t, t_0) \hat{O}_{\text{I}}(t) \hat{S}(t, t_0) \right| \Psi_{\text{H}} \right\rangle, \end{aligned} \tag{A.23}$$

hence the operator in the Heisenberg is

$$\hat{O}_{\text{H}}(t) = \hat{U}^{\dagger}(t, t_0) \hat{O}(t) \hat{U}(t, t_0) = \hat{S}^{\dagger}(t, t_0) \hat{O}_{\text{I}}(t) \hat{S}(t, t_0). \tag{A.24}$$

Because in the Heisenberg picture, vector states are time-independent and all time dependency is moved to the operators, it is useful to have equation of motion for operator in this picture. It can be done by taking the time derivative of Eq. (A.24), and utilizing equation of motion for the time evolution operator (A.8). The final formula for the equation of motion of operator in the Heisenberg picture, also called the Heisenberg equation of motion, is

$$i\hbar\frac{d}{dt}\hat{O}_{\mathrm{H}}(t)=\left[\hat{O}_{\mathrm{H}}(t),\hat{H}_{\mathrm{H}}(t)\right]_{-}+i\hbar\left[\frac{\partial}{\partial t}\hat{O}(t)\right]_{\mathrm{H}}, \tag{A.25}$$

where $[]_-$ is a commutator, and the last term in square brackets means that for an operator which is explicitly time dependent, one has to first take the time derivative of the operator in the Schrödinger picture and then transform the result into the Heisenberg picture using the evolution operator $\hat{U}^{\dagger}(t,t_0)$.

For nonzero temperatures, the following form of density operator in the Schrödinger picture is assumed

$$\hat{\rho}(t)=\sum_k|\Psi_k(t)\rangle P\left(|\Psi_k(t_0)\rangle\right)\langle\Psi_k(t)|, \tag{A.26}$$

where $|\Psi_k(t)\rangle$ is a complete, orthonormal set of states, and $P\left(|\Psi_k(t_0)\rangle\right)$ is the classical probability of the system being in state k. With this form of the density operator, it is assumed that the classical probability does not change in time and such stays "frozen" at t_0. Physically, this means that heat reservoir changes slowly enough that its evolution in time can be ignored.

Using equation (A.3), the density operator can be written as

$$\hat{\rho}(t)=\hat{U}(t,t_0)\,\hat{\rho}_0\hat{U}^{\dagger}(t,t_0), \tag{A.27}$$

where $\hat{\rho}_0$ is defined as

$$\begin{aligned}\hat{\rho}_0=\hat{\rho}(t_0)&=\sum_k|\Psi_k(t_0)\rangle P\left(|\Psi_k(t_0)\rangle\right)\langle\Psi_k(t_0)|\\&=\sum_k|\Psi_{k,\mathrm{H}}\rangle P\left(|\Psi_{k,\mathrm{H}}\rangle\right)\langle\Psi_{k,\mathrm{H}}|.\end{aligned} \tag{A.28}$$

The average value of operator $\hat{O}$ is therefore

$$\begin{aligned}&\left\langle\hat{O}(t)\right\rangle=\mathrm{Tr}\left[\hat{\rho}(t)\,\hat{O}(t)\right]=\mathrm{Tr}\left[\hat{U}(t,t_0)\,\hat{\rho}_0\hat{U}^{\dagger}(t,t_0)\,\hat{O}(t)\right]\\&=\mathrm{Tr}\left[\hat{\rho}_0\hat{U}^{\dagger}(t,t_0)\,\hat{O}(t)\,\hat{U}(t,t_0)\right]=\mathrm{Tr}\left[\hat{\rho}_0\hat{S}^{\dagger}(t,t_0)\,\hat{O}_{\mathrm{I}}(t)\,\hat{S}(t,t_0)\right]\\&=\left\langle\hat{S}^{\dagger}(t,t_0)\,\hat{O}_{\mathrm{I}}(t)\,\hat{S}(t,t_0)\right\rangle_0=\left\langle\hat{O}_{\mathrm{H}}(t)\right\rangle_0,\end{aligned} \tag{A.29}$$

where subscript 0 next to the bracket $\langle\rangle$ denotes that the average is taken with the density operator ρ_0 (Heisenberg picture).

Appendix B

Contour algebra

Although it is very convenient to use contour notation during the derivation of the Dyson equation and related formulas for self-energies, to obtain any meaningful results it is necessary to switch back to the real-time. This procedure is non-trivial whenever two or more double-time functions are under the same integral over contour time.

In this appendix, a method of evaluating contour integrals is shown, contour-time step and delta functions are defined, and a limit of function in the contour sense is discussed.

The time contour consists of an upper branch specified by the argument $b = +1$ going from t_0 to $t_\mathrm{m} > t_0$, and a lower branch where $b = -1$ which goes back from t_m to t_0. In general, values of t_0 and t_m can be arbitrary as long as t_0 is smaller than t_m, including $t_0 = -\infty$ and $t_\mathrm{m} = +\infty$. Contour time consists of a set of two numbers: one for the value of time and another to indicate the branch $\underline{t} = \{t, b\}$. Integration over the contour is defined as

$$\int d\underline{t} = \int_{t_0}^{t_\mathrm{m}} dt_{+1} + \int_{t_\mathrm{m}}^{t_0} dt_{-1} = \sum_{b\in\{+1,-1\}} b \int_{t_0}^{t_\mathrm{m}} dt_b \tag{B.1}$$

For any double-time function $A(\underline{t}_1, \underline{t}_2)$ described on a contour, four distinct components can be defined

$$\begin{aligned}
\text{lesser: } & A^{<}(t_1, t_2) \text{ for } b_1 = +1\ b_2 = -1, \\
\text{greater: } & A^{>}(t_1, t_2) \text{ for } b_1 = -1\ b_2 = +1, \\
\text{time ordered: } & A^{\mathrm{t}}(t_1, t_2) \text{ for } b_1 = +1\ b_2 = +1, \\
\text{anti-time ordered: } & A^{\bar{\mathrm{t}}}(t_1, t_2) \text{ for } b_1 = -1\ b_2 = -1.
\end{aligned} \tag{B.2}$$

An arbitrary function $A(\underline{t}_1, \underline{t}_2)$ defined on a contour (known as a contour function) becomes a lesser (greater) function when the first argument is before (after) the second in the contour sense, and time ordered (anti-time ordered) when both arguments are on the upper (lower) branch.

Contour-time functions present in the Dyson equation and in all the supplementary equations have a very specific form which limits the number of independent components of any relevant contour-time function

$$A\left(\underline{t}_1,\underline{t}_2\right)=A_1\left(\underline{t}_1,\underline{t}_2\right)+A_2\left(\underline{t}_1,\underline{t}_2\right), \tag{B.3}$$

where A_1 and A_2 are contour functions with the following properties

$$\begin{aligned}
&A_1^{<}\left(t_1,t_2\right)\ \text{arbitrary},\\
&A_1^{>}\left(t_1,t_2\right)\ \text{arbitrary},\\
&A_1^{\mathrm{t}}\left(t_1,t_2\right)=\theta\left(t_1-t_2\right)A_1^{>}\left(t_1,t_2\right)+\theta\left(t_2-t_1\right)A_1^{<}\left(t_1,t_2\right),\\
&A_1^{\bar{\mathrm{t}}}\left(t_1,t_2\right)=\theta\left(t_2-t_1\right)A_1^{>}\left(t_1,t_2\right)+\theta\left(t_1-t_2\right)A_1^{<}\left(t_1,t_2\right),
\end{aligned} \tag{B.4}$$

and

$$\begin{aligned}
&A_2^{<}\left(t_1,t_2\right)=0,\\
&A_2^{>}\left(t_1,t_2\right)=0,\\
&A_2^{\mathrm{t}}\left(t_1,t_2\right)=\delta\left(t_1-t_2\right)f\left(t_2\right),\\
&A_2^{\bar{\mathrm{t}}}\left(t_1,t_2\right)=-\delta\left(t_1-t_2\right)f\left(t_2\right),\\
&f\left(t_2\right)\ \text{arbitrary}.
\end{aligned} \tag{B.5}$$

It can be seen from the definition of the contour Green's function that it has the same properties as A_1. Because all other double time functions are related to Green's function (they are functionals of Green's function) they also posses the same general form as A_1. The presence of A_2 is to accommodate singular behavior originating from $\frac{d}{dt_1}A_1\left(\underline{t}_1,\underline{t}_2\right)$ and the contour delta function, both present in the Dyson equation.

Using Eqs. (B.3), (B.4), and (B.5) one can show that the double-time function $A\left(\underline{t}_1,\underline{t}_2\right)$ also has following the property

$$\begin{aligned}
&A^{\bar{\mathrm{t}}}\left(t_1,t_2\right)-A^{<}\left(t_1,t_2\right)=\left(A_1^{\bar{\mathrm{t}}}\left(t_1,t_2\right)+A_2^{\bar{\mathrm{t}}}\left(t_1,t_2\right)\right)\\
&-\left(A_1^{<}\left(t_1,t_2\right)+A_2^{<}\left(t_1,t_2\right)\right)=\theta\left(t_2-t_1\right)\left(A_1^{>}\left(t_1,t_2\right)-A_1^{<}\left(t_1,t_2\right)\right)\\
&-\delta\left(t_1-t_2\right)f\left(t_2\right)=A^{>}\left(t_1,t_2\right)-A^{\mathrm{t}}\left(t_1,t_2\right).
\end{aligned} \tag{B.6}$$

Although time and anti-time ordered functions can be obtained directly from contour functions by specifying branches of time arguments, usually it is more convenient to work with retarded and advanced functions. The major reason is that the final formulas for calculating contour integrals have simpler forms if retarded and advanced functions are used instead of time and anti-time ordered functions. Retarded and advanced functions are defined as

$$\text{advanced:}\quad A^{\mathrm{A}}\left(t_1,t_2\right)=A^{<}\left(t_1,t_2\right)-A^{\bar{\mathrm{t}}}\left(t_1,t_2\right), \tag{B.7}$$

$$\text{retarded:}\quad A^{\mathrm{R}}\left(t_1,t_2\right)=A^{\mathrm{t}}\left(t_1,t_2\right)-A^{<}\left(t_1,t_2\right). \tag{B.8}$$

Equation (B.6) allows one to express the retarded and advanced components as

$$A^{\mathrm{A}}(t_1,t_2) = -\theta(t_2-t_1)\left(A_1^{>}(t_1,t_2) - A_1^{<}(t_1,t_2)\right) + \delta(t_1-t_2)\, f(t_2)\,, \tag{B.9}$$

$$A^{\mathrm{R}}(t_1,t_2) = \theta(t_1-t_2)\left(A_1^{>}(t_1,t_2) - A_1^{<}(t_1,t_2)\right) + \delta(t_1-t_2)\, f(t_2)\,. \tag{B.10}$$

With the definitions of advanced component (B.7), retarded component (B.8), and Eq. (B.6), time and anti-time ordered functions can be expressed as

$$A^{\mathrm{t}}(t_1,t_2) = A^{<}(t_1,t_2) + A^{\mathrm{R}}(t_1,t_2) = A^{>}(t_1,t_2) + A^{\mathrm{A}}(t_1,t_2) \tag{B.11}$$

$$A^{\bar{\mathrm{t}}}(t_1,t_2) = A^{<}(t_1,t_2) - A^{\mathrm{A}}(t_1,t_2) = A^{>}(t_1,t_2) - A^{\mathrm{R}}(t_1,t_2) \tag{B.12}$$

It is also useful to have contour step and delta functions. A step function is defined as

$$\theta(\underline{t}_1,\underline{t}_2) = \begin{cases} 1 & \text{for } \underline{t}_1 > \underline{t}_2 \text{ on time contour} \\ 0 & \text{for } \underline{t}_1 < \underline{t}_2 \text{ on time contour} \end{cases}. \tag{B.13}$$

Its explicit form is obtained by specifying branches of arguments $\underline{t}_1$ and $\underline{t}_2$ and using equations (B.7) and (B.8) for retarded and advanced components to get

$$\theta^{<}(t_1,t_2) = 0, \tag{B.14}$$

$$\theta^{>}(t_1,t_2) = 1, \tag{B.15}$$

$$\theta^{\mathrm{t}}(t_1,t_2) = \theta(t_1-t_2)\,, \tag{B.16}$$

$$\theta^{\bar{\mathrm{t}}}(t_1,t_2) = -\theta(t_2-t_1)\,, \tag{B.17}$$

$$\theta^{\mathrm{R}}(t_1,t_2) = \theta(t_1-t_2)\,, \tag{B.18}$$

$$\theta^{\mathrm{A}}(t_1,t_2) = -\theta(t_2-t_1)\,. \tag{B.19}$$

From the above equations, one can see that the step function is a function described by Eq. (B.3) with $A_1^{<} = 0$, $A_1^{>} = 1$, and $f = 0$.

A regular delta function can be defined as a derivative of a step function. A contour delta function can be defined analogously, but instead of a normal step function, a contour step function (B.13) is used

$$\delta(\underline{t}_1,\underline{t}_2) = \frac{d}{dt_1}\theta(\underline{t}_1,\underline{t}_2)\,, \tag{B.20}$$

whose explicit form is

$$\delta^{<}(t_1,t_2) = 0, \tag{B.21}$$

$$\delta^{>}(t_1,t_2) = 0, \tag{B.22}$$

$$\delta^{\mathrm{t}}(t_1,t_2) = \delta(t_1-t_2)\,, \tag{B.23}$$

$$\delta^{\bar{\mathrm{t}}}(t_1,t_2) = -\delta(t_1-t_2)\,, \tag{B.24}$$

$$\delta^{\mathrm{R}}(t_1,t_2) = \delta(t_1-t_2)\,, \tag{B.25}$$

$$\delta^{\mathrm{A}}(t_1,t_2) = -\delta(t_1-t_2)\,. \tag{B.26}$$

It is easy to see that this is also a function satisfying Eq. (B.3) with $A_1^< = 0$, $A_1^> = 0$, and $f = 1$.

The simplest, and most important contour integral is of the following form

$$C\left(\underline{t}_1, \underline{t}_2\right) = \int d\underline{t}_3 A\left(\underline{t}_1, \underline{t}_3\right) B\left(\underline{t}_3, \underline{t}_2\right). \tag{B.27}$$

The goal is to calculate all real-time components of C (lesser, greater, retarded, and advanced) using only the real-time components of A and B.

The lesser component of C can be calculated by breaking the contour integral into an integral over the upper branch and over the lower branch according to Eq. (B.1). After the integral is broken, contour functions can be replaced by proper real-time components

$$\begin{aligned}
C^<\left(t_1, t_2\right) &= \int d\underline{t}_3 A\left(t_{1,+1}, \underline{t}_3\right) B\left(\underline{t}_3, t_{2,-1}\right) \\
&= \int_{t_0}^{t_\mathrm{m}} dt_{3,+1} A\left(t_{1,+1}, t_{3,+1}\right) B\left(t_{3,+1}, t_{2,-1}\right) - \int_{t_0}^{t_\mathrm{m}} dt_{3,-1} A\left(t_{1,+1}, t_{3,-1}\right) B\left(t_{3,-1}, t_{2,-1}\right) \\
&= \int_{t_0}^{t_\mathrm{m}} dt_3 A^\mathrm{t}\left(t_1, t_3\right) B^<\left(t_3, t_2\right) + \int_{t_\mathrm{m}}^{t_0} dt_3 A^<\left(t_1, t_3\right) B^{\bar{\mathrm{t}}}\left(t_3, t_2\right) \\
&= \int_{t_0}^{t_\mathrm{m}} dt_3 \left(A^\mathrm{t}\left(t_1, t_3\right) B^<\left(t_3, t_2\right) - A^<\left(t_1, t_3\right) B^{\bar{\mathrm{t}}}\left(t_3, t_2\right)\right).
\end{aligned} \tag{B.28}$$

Equations (B.11) and (B.12) can be used to replace time and anti-time ordered functions with advanced and retarded components

$$\begin{aligned}
C^<\left(t_1, t_2\right) &= \int_{t_0}^{t_\mathrm{m}} dt_3 \left(A^<\left(t_1, t_2\right) B^<\left(t_1, t_2\right) + A^\mathrm{R}\left(t_1, t_2\right) B^<\left(t_1, t_2\right)\right. \\
&\left. - A^<\left(t_1, t_2\right) B^<\left(t_1, t_2\right) + A^<\left(t_1, t_2\right) B^\mathrm{A}\left(t_1, t_2\right)\right) \\
&= \int_{t_0}^{t_\mathrm{m}} dt_3 \left(A^\mathrm{R}\left(t_1, t_3\right) B^<\left(t_3, t_2\right) + A^<\left(t_1, t_3\right) B^\mathrm{A}\left(t_3, t_2\right)\right).
\end{aligned} \tag{B.29}$$

A similar procedure can be done for the greater component to get

$$C^>\left(t_1, t_2\right) = \int_{t_0}^{t_\mathrm{m}} dt_3 \left(A^\mathrm{R}\left(t_1, t_3\right) B^>\left(t_3, t_2\right) + A^>\left(t_1, t_3\right) B^\mathrm{A}\left(t_3, t_2\right)\right). \tag{B.30}$$

To derive formulas for advanced and retarded functions, first it is necessary to have formulas for time and anti-time ordered components. Again, they are obtained in the same way as for the lesser component

$$C^{\mathrm{t}}(t_1,t_2) = \int_{t_0}^{t_\mathrm{m}} dt_3 \left(A^{\mathrm{R}}(t_1,t_3)\, B^{>}(t_3,t_2) + A^{<}(t_1,t_3)\, B^{\mathrm{A}}(t_3,t_2) + A^{\mathrm{R}}(t_1,t_3)\, B^{\mathrm{A}}(t_3,t_2) \right), \tag{B.31}$$

$$C^{\bar{\mathrm{t}}}(t_1,t_2) = \int_{t_0}^{t_\mathrm{m}} dt_3 \left(A^{\mathrm{R}}(t_1,t_3)\, B^{<}(t_3,t_1) + A^{>}(t_1,t_3)\, B^{\mathrm{A}}(t_3,t_2) - A^{\mathrm{R}}(t_1,t_3)\, B^{\mathrm{A}}(t_3,t_2) \right). \tag{B.32}$$

Using definitions of advanced (B.7) and retarded (B.8) functions, and formulas (B.29), (B.30), (B.31), and (B.32), the final formulas for advanced and retarded components are

$$C^{\mathrm{A}}(t_1,t_2) = C^{<}(t_1,t_2) - C^{\bar{\mathrm{t}}}(t_1,t_2) = \int_{t_0}^{t_\mathrm{m}} dt_3 A^{\mathrm{A}}(t_1,t_3)\, B^{\mathrm{A}}(t_3,t_2), \tag{B.33}$$

$$C^{\mathrm{R}}(t_1,t_2) = C^{\mathrm{t}}(t_1,t_2) - C^{<}(t_1,t_2) = \int_{t_0}^{t_\mathrm{m}} dt_3 A^{\mathrm{R}}(t_1,t_3)\, B^{\mathrm{R}}(t_3,t_2). \tag{B.34}$$

The complete set of equations necessary to evaluate integral (B.27) is

$$C^{<}(t_1,t_2) = \int_{t_0}^{t_\mathrm{m}} dt_3 \left(A^{\mathrm{R}}(t_1,t_3)\, B^{<}(t_3,t_2) + A^{<}(t_1,t_3)\, B^{\mathrm{A}}(t_3,t_2) \right), \tag{B.35}$$

$$C^{>}(t_1,t_2) = \int_{t_0}^{t_\mathrm{m}} dt_3 \left(A^{\mathrm{R}}(t_1,t_3)\, B^{>}(t_3,t_2) + A^{>}(t_1,t_3)\, B^{\mathrm{A}}(t_3,t_2) \right), \tag{B.36}$$

$$C^{\mathrm{A}}(t_1,t_2) = \int_{t_0}^{t_\mathrm{m}} dt_3 A^{\mathrm{A}}(t_1,t_3)\, B^{\mathrm{A}}(t_3,t_2), \tag{B.37}$$

$$C^{\mathrm{R}}(t_1,t_2) = \int_{t_0}^{t_\mathrm{m}} dt_3 A^{\mathrm{R}}(t_1,t_3)\, B^{\mathrm{R}}(t_3,t_2). \tag{B.38}$$

If one needs, for example the time-ordered component C^{t}, then after calculating $C^{<}$, $C^{>}$, C^{A}, and C^{R}, Eq. (B.11) can be used to get the time-ordered component.

One can easily see now why retarded and advanced functions are better choices than time and anti-time ordered functions. The advanced and retarded components

of integral (B.27) are expressed only by advanced and retarded components of functions under the integral (A and B). If, instead of choosing lesser, greater, advanced, and retarded functions to describe the integral (B.27), one chooses lesser, greater, time and anti-time ordered functions, they will also form a complete set of four equations. However, the equations for time and anti-time ordered components will be expressed not only by time and anti-time ordered functions A and B but also by the lesser and greater components of A and B. For example, $C^{\mathrm{t}} = A^{\mathrm{t}}B^{\mathrm{t}} - A^{<}B^{>}$.

By setting $A\left(\underline{t}_1, \underline{t}_3\right) = \delta\left(\underline{t}_1, \underline{t}_3\right)$ and $B\left(\underline{t}_3, \underline{t}_2\right) = C\left(\underline{t}_3, \underline{t}_2\right)$, and using equations form the frame above, one can also easily show that contour delta function has the following property

$$C\left(\underline{t}_1, \underline{t}_2\right) = \int d\underline{t}_3 \delta\left(\underline{t}_1, \underline{t}_3\right) C\left(\underline{t}_3, \underline{t}_2\right). \tag{B.39}$$

Finally, more complicated contour time integrals present in the Dyson equation can be expressed by equations derived for the basic integral (B.27). For example, the retarded component of

$$D\left(\underline{t}_1, \underline{t}_2\right) = \int d\underline{t}_3 \int d\underline{t}_4 A\left(\underline{t}_1, \underline{t}_3\right) B\left(\underline{t}_3, \underline{t}_4\right) C\left(\underline{t}_4, \underline{t}_2\right), \tag{B.40}$$

can be obtained by applying formula (B.38) to contour integral over $\underline{t}_3$ only, and then using the same formula to get the retarded component of integral over $\underline{t}_4$

$$\begin{aligned} D^{\mathrm{R}}\left(t_1, t_2\right) &= \int_{t_0}^{t_{\mathrm{m}}} dt_3 A^{\mathrm{R}}\left(t_1, t_3\right) \left[\int d\underline{t}_4 B\left(\underline{t}_3, \underline{t}_4\right) C\left(\underline{t}_4, \underline{t}_2\right)\right]^{\mathrm{R}} \\ &= \int_{t_0}^{t_{\mathrm{m}}} dt_3 \int_{t_0}^{t_{\mathrm{m}}} dt_4 A^{\mathrm{R}}\left(t_1, t_3\right) B^{\mathrm{R}}\left(t_3, t_4\right) C^{\mathrm{R}}\left(t_4, t_2\right). \end{aligned} \tag{B.41}$$

The contour time limit frequently encountered in the Dyson equation has the following form

$$A\left(\underline{t}_1, \underline{t}_1^{+}\right) = \lim_{\underline{t}_2 \to \underline{t}_1^{+}} A\left(\underline{t}_1, \underline{t}_2\right). \tag{B.42}$$

The meaning of this expression is that value t_2 is approaching or equal to t_1 but $\underline{t}_2$ remains further on the contour than $\underline{t}_1$. This situation can occur in three cases: when both times are on the upper branch and the value of t_2 is infinitesimally larger than t_1; when both are on the lower branch and t_2 is infinitesimally smaller than t_1; and finally when $\underline{t}_1$ is on the upper branch, $\underline{t}_2$ on lower branch and they both have the same values $t_2 = t_1$ or $t_2 \to t_1$. Inspection of equations (B.3), (B.4), and (B.5) immediately reveals that all three cases lead to the same result

$$A\left(\underline{t}_1, \underline{t}_1^{+}\right) = A^{<}\left(t_1, t_1\right), \tag{B.43}$$

and thus the limit $A\left(\underline{t}_1, \underline{t}_1^{+}\right)$ is well defined. Similarly one can introduce and evaluate other limits such as $A\left(\underline{t}_1^{+}, \underline{t}_1\right)$, $A\left(\underline{t}_1^{-}, \underline{t}_1\right)$, etc.

Appendix C

Functional derivative technique

This appendix contains intermediate calculations for Subsection 3.3.3. All notation used here is explained in Chapter 3.

C.1 Functional derivatives of Green's function over external sources

To calculate the functional derivative of

$$G\left(\underline{1},\underline{2}\right)=\frac{1}{i\hbar}\frac{\left\langle T_{\mathrm{c}}\left[\hat{S}_{\mathrm{c}}\hat{\Psi}_{\mathrm{I}}\left(\underline{1}\right)\hat{\Psi}_{\mathrm{I}}^{\dagger}\left(\underline{2}\right)\right]\right\rangle}{\left\langle \hat{S}_{\mathrm{c}}\right\rangle}, \tag{C.1}$$

over $\rho_{\mathrm{ext}}\left(\underline{1}\right)$ and $\mathbf{J}_{\mathrm{ext}}\left(\underline{1}\right)$ it is necessary to evaluate variation δG as a function of variations $\delta\rho_{\mathrm{ext}}$ and $\delta\mathbf{J}_{\mathrm{ext}}$. To do this it is best to start by evaluating variation the $\delta\hat{S}_{\mathrm{c}}$.

The perturbation Hamiltonian $\left(\hat{H}_{\mathrm{int,I}}\right)$ in the interaction picture is

$$\begin{aligned}\hat{H}_{\mathrm{int,I}}(\underline{t})=\sum_{\sigma}\int d^{3}r\left(\rho_{\mathrm{ext}}\left(\mathbf{r},\sigma,\underline{t}\right)\sum_{\sigma'}\int d^{3}r'V\left(\mathbf{r}-\mathbf{r}'\right)\left[-e\hat{\Psi}_{\mathrm{I}}^{\dagger}\left(\mathbf{r}',\sigma',\underline{t}\right)\hat{\Psi}_{\mathrm{I}}\left(\mathbf{r}',\sigma',\underline{t}\right)\right]\right.\\ \left.-\mathbf{J}_{\mathrm{ext}}\left(\mathbf{r},\sigma,\underline{t}\right)\hat{\mathbf{A}}_{\mathrm{I}}\left(\mathbf{r},\underline{t}\right)+\hat{H}_{\mathrm{k}}\left(\rho_{\mathrm{ext}}\left(\mathbf{r},\sigma,\underline{t}\right),\mathbf{J}_{\mathrm{ext}}\left(\mathbf{r},\sigma,\underline{t}\right)\right)\right),\end{aligned} \tag{C.2}$$

where $\hat{H}_{\mathrm{k}}$ does not contain any quantum mechanical operators, and the source terms are formally different on different branches of time contour: $\rho_{\mathrm{ext}}\left(t,+1\right)\neq\rho_{\mathrm{ext}}\left(\underline{t},-1\right)$ and $\mathbf{J}_{\mathrm{ext}}\left(t,+1\right)\neq\mathbf{J}_{\mathrm{ext}}\left(t,-1\right)$. With the above form of the Hamiltonian operator $\hat{S}_{\mathrm{c}}$ becomes

$$\begin{aligned}\hat{S}_{\mathrm{c}} &= T_{\mathrm{c}}\left[\exp\left(-\frac{i}{\hbar}\int d\underline{t}'\hat{H}_{\mathrm{int,I}}(\underline{t}')\right)\right]\\ &= T_{\mathrm{c}}\left[\exp\left(-\frac{i}{\hbar}\int d\underline{1}\left(-e\rho_{\mathrm{ext}}\left(\underline{1}\right)\int d\underline{2}V(\underline{1},\underline{2})\hat{\Psi}_{\mathrm{I}}^{\dagger}\left(\underline{2}^{+}\right)\hat{\Psi}_{\mathrm{I}}\left(\underline{2}\right)\right.\right.\right.\\ &\left.\left.\left.-\mathbf{J}_{\mathrm{ext}}\left(\underline{1}\right)\hat{\mathbf{A}}_{\mathrm{I}}\left(\underline{1}\right)+\hat{H}_{\mathrm{k}}\left(\rho_{\mathrm{ext}}\left(\underline{1}\right),\mathbf{J}_{\mathrm{ext}}\left(\underline{1}\right)\right)\right)\right)\right]. \end{aligned} \tag{C.3}$$

Its first variation with respect to ρ_{ext} and $J_{i,\mathrm{ext}}$ is

$$\begin{aligned}\delta\hat{S}_{\mathrm{c}} &= T_{\mathrm{c}}\left[\hat{S}_{\mathrm{c}}\frac{1}{i\hbar}\left(-e\int d\underline{1}\int d\underline{2}V(\underline{1},\underline{2})\delta\rho_{\mathrm{ext}}\left(\underline{1}\right)\hat{\Psi}_{\mathrm{I}}^{\dagger}\left(\underline{2}^{+}\right)\hat{\Psi}_{\mathrm{I}}\left(\underline{2}\right)\right.\right.\\ &-\sum_{i=1}^{3}\int d\underline{1}\delta J_{i,\mathrm{ext}}\left(\underline{1}\right)\hat{A}_{i,\mathrm{I}}\left(\underline{1}\right)+\int d\underline{1}\frac{\delta\hat{H}_{\mathrm{k}}}{\delta\rho_{\mathrm{ext}}\left(\underline{1}\right)}\delta\rho_{\mathrm{ext}}\left(\underline{1}\right)\\ &\left.\left.+\sum_{i=1}^{3}\int d\underline{1}\frac{\delta\hat{H}_{\mathrm{k}}}{\delta J_{i,\mathrm{ext}}\left(\underline{1}\right)}\delta J_{i,\mathrm{ext}}\left(\underline{1}\right)\right)\right]. \end{aligned} \tag{C.4}$$

With the variation of $\hat{S}_{\mathrm{c}}$, one can calculate the variation of G in analogous way one would calculate the regular differential. The variation of G is

$$\begin{aligned}\delta G\left(\underline{1},\underline{2}\right) &= \delta G_{\mathrm{A}}\left(\underline{1},\underline{2}\right)+\delta G_{\mathrm{B}}\left(\underline{1},\underline{2}\right)\\ &= -\frac{1}{i\hbar}\frac{\left\langle\delta\hat{S}_{\mathrm{c}}\right\rangle}{\left\langle\hat{S}_{\mathrm{c}}\right\rangle}\frac{\left\langle T_{\mathrm{c}}\left[\hat{S}_{\mathrm{c}}\hat{\Psi}_{\mathrm{I}}\left(\underline{1}\right)\hat{\Psi}_{\mathrm{I}}^{\dagger}\left(\underline{2}\right)\right]\right\rangle}{\left\langle\hat{S}_{\mathrm{c}}\right\rangle}\\ &+\frac{1}{i\hbar}\frac{\left\langle T_{\mathrm{c}}\left[\delta\hat{S}_{\mathrm{c}}\hat{\Psi}_{\mathrm{I}}\left(\underline{1}\right)\hat{\Psi}_{\mathrm{I}}^{\dagger}\left(\underline{2}\right)\right]\right\rangle}{\left\langle\hat{S}_{\mathrm{c}}\right\rangle}, \end{aligned} \tag{C.5}$$

where δG_{A} and δG_{B} can be evaluated using Eq. (C.4) to obtain

$$\begin{aligned}\delta G_{\mathrm{A}}\left(\underline{1},\underline{2}\right) &= -\left(-\frac{e}{i\hbar}\int d\underline{3}\int d\underline{4}V(\underline{3},\underline{4})\delta\rho_{\mathrm{ext}}\left(\underline{3}\right)\frac{\left\langle T_{\mathrm{c}}\left[\hat{S}_{\mathrm{c}}\hat{\Psi}_{\mathrm{I}}^{\dagger}\left(\underline{4}^{+}\right)\hat{\Psi}_{\mathrm{I}}\left(\underline{4}\right)\right]\right\rangle}{\left\langle\hat{S}_{\mathrm{c}}\right\rangle}\right.\\ &-\frac{1}{i\hbar}\sum_{i=1}^{3}\int d\underline{3}\delta J_{i,\mathrm{ext}}\left(\underline{3}\right)\frac{\left\langle T_{\mathrm{c}}\left[\hat{S}_{\mathrm{c}}\hat{A}_{i,\mathrm{I}}\left(\underline{3}\right)\right]\right\rangle}{\left\langle\hat{S}_{\mathrm{c}}\right\rangle}+\int d\underline{3}\frac{\delta\hat{H}_{\mathrm{k}}}{\delta\rho_{\mathrm{ext}}\left(\underline{3}\right)}\delta\rho_{\mathrm{ext}}\left(\underline{3}\right)\\ &\left.+\sum_{i=1}^{3}\int d\underline{3}\frac{\delta\hat{H}_{\mathrm{k}}}{\delta J_{i,\mathrm{ext}}\left(\underline{3}\right)}\delta J_{i,\mathrm{ext}}\left(\underline{3}\right)\right)\frac{1}{i\hbar}\frac{\left\langle T_{\mathrm{c}}\left[\hat{S}_{\mathrm{c}}\hat{\Psi}_{\mathrm{I}}\left(\underline{1}\right)\hat{\Psi}_{\mathrm{I}}^{\dagger}\left(\underline{2}\right)\right]\right\rangle}{\left\langle\hat{S}_{\mathrm{c}}\right\rangle}, \end{aligned} \tag{C.6}$$

and

$$\delta G_{\mathrm{B}}\left(\underline{1},\underline{2}\right)=-e\left(\frac{1}{i\hbar}\right)^{2}\int d\underline{3}\int d\underline{4}V\left(\underline{3},\underline{4}\right)\frac{\left\langle T_{\mathrm{c}}\left[\hat{S}_{\mathrm{c}}\hat{\Psi}_{\mathrm{I}}^{\dagger}\left(\underline{4}^{+}\right)\hat{\Psi}_{\mathrm{I}}\left(\underline{4}\right)\hat{\Psi}_{\mathrm{I}}\left(\underline{1}\right)\hat{\Psi}_{\mathrm{I}}^{\dagger}\left(\underline{2}\right)\right]\right\rangle}{\left\langle \hat{S}_{\mathrm{c}}\right\rangle}\delta\rho_{\mathrm{ext}}\left(\underline{3}\right)$$
$$-\left(\frac{1}{i\hbar}\right)^{2}\sum_{i=1}^{3}\int d\underline{3}\delta J_{i,\mathrm{ext}}\left(\underline{3}\right)\frac{\left\langle T_{\mathrm{c}}\left[\hat{S}_{\mathrm{c}}\hat{A}_{i,\mathrm{I}}\left(\underline{3}\right)\hat{\Psi}_{\mathrm{I}}\left(\underline{1}\right)\hat{\Psi}_{\mathrm{I}}^{\dagger}\left(\underline{2}\right)\right]\right\rangle}{\left\langle \hat{S}_{\mathrm{c}}\right\rangle}$$
$$+\left(\int d\underline{3}\frac{\delta\hat{H}_{\mathrm{k}}}{\delta\rho_{\mathrm{ext}}\left(\underline{3}\right)}\delta\rho_{\mathrm{ext}}\left(\underline{3}\right)+\sum_{i=1}^{3}\int d\underline{3}\frac{\delta\hat{H}_{\mathrm{k}}}{\delta J_{i,\mathrm{ext}}\left(\underline{3}\right)}\delta J_{i,\mathrm{ext}}\left(\underline{3}\right)\right)\frac{1}{i\hbar}\frac{\left\langle T_{\mathrm{c}}\left[\hat{S}_{\mathrm{c}}\hat{\Psi}_{\mathrm{I}}\left(\underline{1}\right)\hat{\Psi}_{\mathrm{I}}^{\dagger}\left(\underline{2}\right)\right]\right\rangle}{\left\langle \hat{S}_{\mathrm{c}}\right\rangle}. \tag{C.7}$$

Summation of $\delta G_{\mathrm{A}}\left(\underline{1},\underline{2}\right)$ and $\delta G_{\mathrm{B}}\left(\underline{1},\underline{2}\right)$ gives the total variation of G with respect to ρ_{ext} and $\mathbf{J}_{\mathrm{ext}}$. One can easily see that the contributions from $\hat{H}_{\mathrm{k}}$ (kinetic energy of the externally controlled sources) in $\delta G_{\mathrm{A}}\left(\underline{1},\underline{2}\right)$ and $\delta G_{\mathrm{B}}\left(\underline{1},\underline{2}\right)$ are the same but with different signs, and after the summation they cancel each other. This confirms what was said in Subsection 3.3.1, that the exact form of $\hat{H}_{\mathrm{k}}$ has no influence on the calculations presented here.

The variation $\delta G\left(\underline{1},\underline{2}\right)$ can now be used to calculate the functional derivative of $G\left(\underline{1},\underline{2}\right)$ over $\rho_{\mathrm{ext}}\left(\underline{3}\right)$ and $\mathbf{J}_{\mathrm{ext}}\left(\underline{3}\right)$

$$\frac{\delta G\left(\underline{1},\underline{2}\right)}{\delta\rho_{\mathrm{ext}}\left(\underline{3}\right)}=-e\int d\underline{4}V\left(\underline{3},\underline{4}\right)G\left(\underline{4},\underline{4}^{+}\right)G\left(\underline{1},\underline{2}\right)$$
$$-e\left(\frac{1}{i\hbar}\right)^{2}\int d\underline{3}V\left(\underline{1},\underline{3}\right)\left\langle T_{\mathrm{c}}\left[\hat{\Psi}^{\dagger}\left(\underline{4}^{+}\right)\hat{\Psi}\left(\underline{4}\right)\hat{\Psi}\left(\underline{1}\right)\hat{\Psi}^{\dagger}\left(\underline{2}\right)\right]\right\rangle, \tag{C.8}$$

$$\frac{\delta G\left(\underline{1},\underline{2}\right)}{\delta J_{i,\mathrm{ext}}\left(\underline{3}\right)}=\frac{1}{i\hbar}\left\langle \hat{A}_{i}\left(\underline{3}\right)\right\rangle G\left(\underline{1},\underline{2}\right)-\left(\frac{1}{i\hbar}\right)^{2}\left\langle T_{\mathrm{c}}\left[\hat{A}_{i}\left(\underline{3}\right)\hat{\Psi}\left(\underline{1}\right)\hat{\Psi}^{\dagger}\left(\underline{2}\right)\right]\right\rangle. \tag{C.9}$$

C.2 Derivation of the longitudinal self-energy and related terms

With the definition of inverse Green's function (3.70), one may calculate the functional derivative from the delta function and substitute this delta function with Eq. (3.70) to obtain

$$0=\frac{\delta}{\delta B_{\mathrm{ext}}\left(\underline{3}\right)}\delta\left(\underline{1},\underline{2}\right)=\frac{\delta\int d\underline{4}G\left(\underline{1},\underline{4}\right)G^{-1}\left(\underline{4},\underline{2}\right)}{\delta B_{\mathrm{ext}}\left(\underline{3}\right)}=$$
$$=\int d\underline{4}\frac{\delta G\left(\underline{1},\underline{4}\right)}{\delta B_{\mathrm{ext}}\left(\underline{3}\right)}G^{-1}\left(\underline{4},\underline{2}\right)+\int d\underline{4}G\left(\underline{1},\underline{4}\right)\frac{\delta G^{-1}\left(\underline{4},\underline{2}\right)}{\delta B_{\mathrm{ext}}\left(\underline{3}\right)}, \tag{C.10}$$

where B_{ext} can be any of the external sources ρ_{ext} or $J_{i,\text{ext}}$. With the above formula, the derivative in the equation for longitudinal self-energy (3.80) can be shifted from G to G^{-1}

$$\Sigma_{\text{L}}\left(\underline{1},\underline{2}\right)=-ei\hbar\int d\underline{3}\frac{\delta G\left(\underline{1},\underline{3}\right)}{\delta\rho_{\text{ext}}\left(\underline{1}^{+}\right)}G^{-1}\left(\underline{3},\underline{2}\right)=ei\hbar\int d\underline{3}G\left(\underline{1},\underline{3}\right)\frac{\delta G^{-1}\left(\underline{3},\underline{2}\right)}{\delta\rho_{\text{ext}}\left(\underline{1}^{+}\right)}, \quad \text{(C.11)}$$

Under the assumption that $\delta U_{\text{eff}}/\delta J_{i,\text{ext}}=0$, the equation for longitudinal self-energy can be further rearranged

$$\begin{aligned}\Sigma_{\text{L}}\left(\underline{1},\underline{2}\right)&=ei\hbar\int d\underline{3}\int d\underline{4}G\left(\underline{1},\underline{3}\right)\frac{\delta G^{-1}\left(\underline{3},\underline{2}\right)}{\delta U_{\text{eff}}\left(\underline{4}\right)}\frac{\delta U_{\text{eff}}\left(\underline{4}\right)}{\delta\rho_{\text{ext}}\left(\underline{1}^{+}\right)}\\&=ei\hbar\int d\underline{3}\int d\underline{4}G\left(\underline{1},\underline{3}\right)\gamma\left(\underline{3},\underline{2},\underline{4}\right)W\left(\underline{4},\underline{1}^{+}\right).\end{aligned} \quad \text{(C.12)}$$

The equation for the screened Coulomb potential W (3.84) can be derived using only the definition of W (3.82), effective potential U_{eff} (3.76) and chain rule for functional derivative (analogous to the chain rule for regular derivative)

$$\begin{aligned}W\left(\underline{1},\underline{2}\right)&=\frac{\delta U_{\text{eff}}\left(\underline{1}\right)}{\delta\rho_{\text{ext}}\left(\underline{2}\right)}=V\left(\underline{1},\underline{2}\right)+\int d\underline{3}\int d\underline{4}V(\underline{1},\underline{3})\frac{\langle\hat{\rho}\left(\underline{1}\right)\rangle}{\delta U_{\text{eff}}\left(\underline{4}\right)}\frac{\delta U_{\text{eff}}\left(\underline{4}\right)}{\delta\rho_{\text{ext}}\left(\underline{2}\right)}\\&=V\left(\underline{1},\underline{2}\right)+\int d\underline{3}\int d\underline{4}V(\underline{1},\underline{3})p\left(\underline{3},\underline{4}\right)W\left(\underline{4},\underline{2}\right).\end{aligned} \quad \text{(C.13)}$$

Finally, equations for the longitudinal polarization p and longitudinal vertex function γ are derived using the definitions of p, γ, Σ_{L},$\langle\hat{\rho}\left(\underline{1}\right)\rangle$ and the chain rule

$$\begin{aligned}&p\left(\underline{1},\underline{2}\right)=\frac{\delta\left\langle\hat{\rho}\left(\underline{1}\right)\right\rangle}{\delta U_{\text{eff}}\left(\underline{2}\right)}=ei\hbar\frac{\delta G\left(\underline{1},\underline{1}^{+}\right)}{\delta U_{\text{eff}}\left(\underline{2}\right)}=ei\hbar\int d\underline{3}\int d\underline{4}\frac{\delta G\left(\underline{1},\underline{3}\right)}{\delta U_{\text{eff}}\left(\underline{2}\right)}G^{-1}\left(\underline{3},\underline{4}\right)G\left(\underline{4},\underline{1}^{+}\right)\\&=-ei\hbar\int d\underline{3}\int d\underline{4}G\left(\underline{1},\underline{3}\right)\frac{\delta G^{-1}\left(\underline{3},\underline{4}\right)}{\delta U_{\text{eff}}\left(\underline{2}\right)}G\left(\underline{4},\underline{1}^{+}\right)=-ei\hbar\int d\underline{3}\int d\underline{4}G\left(\underline{1},\underline{3}\right)\gamma\left(\underline{3},\underline{4},\underline{2}\right)G\left(\underline{4},\underline{1}^{+}\right),\end{aligned} \quad \text{(C.14)}$$

$$\begin{aligned}&\gamma\left(\underline{1},\underline{2},\underline{3}\right)=\frac{\delta G^{-1}\left(\underline{1},\underline{2}\right)}{\delta U_{\text{eff}}\left(\underline{3}\right)}=e\delta\left(\underline{1},\underline{2}\right)\delta\left(\underline{1},\underline{3}\right)-\frac{\delta\Sigma_{\text{L}}\left(\underline{1},\underline{2}\right)}{\delta U_{\text{eff}}\left(\underline{3}\right)}\\&=e\delta\left(\underline{1},\underline{2}\right)\delta\left(\underline{1},\underline{3}\right)-\int d\underline{4}\int d\underline{5}\frac{\delta\Sigma_{\text{L}}\left(\underline{1},\underline{2}\right)}{\delta G\left(\underline{4},\underline{5}\right)}\frac{\delta G\left(\underline{4},\underline{5}\right)}{\delta U_{\text{eff}}\left(\underline{3}\right)}\\&=e\delta\left(\underline{1},\underline{2}\right)\delta\left(\underline{1},\underline{3}\right)-\int d\underline{4}\int d\underline{5}\frac{\delta\Sigma_{\text{L}}\left(\underline{1},\underline{2}\right)}{\delta G\left(\underline{4},\underline{5}\right)}\int d\underline{6}\int d\underline{7}\frac{\delta G\left(\underline{4},\underline{6}\right)}{\delta U_{\text{eff}}\left(\underline{3}\right)}G^{-1}\left(\underline{6},\underline{7}\right)G\left(\underline{7},\underline{5}\right)\\&=e\delta\left(\underline{1},\underline{2}\right)\delta\left(\underline{1},\underline{3}\right)+\int d\underline{4}\int d\underline{5}\frac{\delta\Sigma_{\text{L}}\left(\underline{1},\underline{2}\right)}{\delta G\left(\underline{4},\underline{5}\right)}\int d\underline{6}\int d\underline{7}G\left(\underline{4},\underline{6}\right)\frac{\delta G^{-1}\left(\underline{6},\underline{7}\right)}{\delta U_{\text{eff}}\left(\underline{3}\right)}G\left(\underline{7},\underline{5}\right)\\&=e\delta\left(\underline{1},\underline{2}\right)\delta\left(\underline{1},\underline{3}\right)+\int d\underline{4}\int d\underline{5}\int d\underline{6}\int d\underline{7}\frac{\delta\Sigma_{\text{L}}\left(\underline{1},\underline{2}\right)}{\delta G\left(\underline{4},\underline{5}\right)}G\left(\underline{4},\underline{6}\right)\gamma\left(\underline{6},\underline{7},\underline{3}\right)G\left(\underline{7},\underline{5}\right).\end{aligned} \quad \text{(C.15)}$$

C.3 Derivation of the transverse self-energy and related terms

The formula for the transverse self-energy (3.93) is derived exactly the same way as the formula for the longitudinal self-energy: first, with the help of Eq. (C.10), the functional derivative is shifted from G to G^{-1} and then, under assumption that $\delta\left\langle \hat{A}_i\left(\underline{1}\right)\right\rangle/\delta J_{i,\mathrm{ext}}=0$, the chain rule is used

$$\begin{aligned}
\Sigma_{\mathrm{T}}\left(\underline{1},\underline{2}\right) &= -\frac{e}{m}\left(i\hbar\right)^2\sum_{i=1}^{3}\partial_i\left(\underline{1}\right)\int d\underline{3}\frac{\delta G\left(\underline{1},\underline{3}\right)}{\delta J_{i,\mathrm{ext}}\left(\underline{1}^+\right)}G^{-1}\left(\underline{3},\underline{2}\right)\\
&= i\hbar\sum_{i=1}^{3}\left(\frac{ie\hbar}{m}\partial_i\left(\underline{1}\right)\right)\int d\underline{3}G\left(\underline{1},\underline{3}\right)\frac{\delta G^{-1}\left(\underline{3},\underline{2}\right)}{\delta J_{i,\mathrm{ext}}\left(\underline{1}^+\right)}\\
&= i\hbar\int d\underline{3}\int d\underline{4}\sum_{i,j=1}^{3}\left(\frac{ie\hbar}{m}\partial_i\left(\underline{1}\right)\right)G\left(\underline{1},\underline{3}\right)\frac{\delta G^{-1}\left(\underline{3},\underline{2}\right)}{\delta\left\langle \hat{A}_j\left(\underline{4}\right)\right\rangle}\frac{\delta\left\langle \hat{A}_j\left(\underline{4}\right)\right\rangle}{\delta J_{i,\mathrm{ext}}\left(\underline{1}^+\right)}\\
&= i\hbar\int d\underline{3}\int d\underline{4}\sum_{i,j=1}^{3}\left(\frac{i\hbar e}{m}\partial_i\left(\underline{1}\right)\right)G\left(\underline{1},\underline{3}\right)\Gamma_j\left(\underline{3},\underline{2},\underline{4}\right)D_{j,i}\left(\underline{4},\underline{1}^+\right).
\end{aligned}\tag{C.16}$$

Photon Green's function can be calculated by direct evaluation of the derivative in (3.95). The variation of $\left\langle \hat{A}_i\left(\underline{1}\right)\right\rangle$ with respect to external current $J_{j,\mathrm{ext}}\left(\underline{2}\right)$ is calculated in the same as the variation of Green's function given by Eqs. (C.6) and (C.7)

$$\begin{aligned}
\delta\left\langle \hat{A}_i\left(\underline{1}\right)\right\rangle &= -\frac{\left\langle T_{\mathrm{c}}\left[\delta\hat{S}_{\mathrm{c}}\right]\right\rangle}{\left\langle \hat{S}_{\mathrm{c}}\right\rangle}\frac{\left\langle T_{\mathrm{c}}\left[\hat{S}_{\mathrm{c}}\hat{A}_{i,\mathrm{I}}\left(\underline{1}\right)\right]\right\rangle}{\left\langle \hat{S}_{\mathrm{c}}\right\rangle}+\frac{\left\langle T_{\mathrm{c}}\left[\delta\hat{S}_{\mathrm{c}}\hat{A}_{i,\mathrm{I}}\left(\underline{3}\right)\right]\right\rangle}{\left\langle \hat{S}_{\mathrm{c}}\right\rangle}\\
&= \frac{1}{i\hbar}\sum_{j=1}^{3}\int d\underline{2}\left\langle \hat{A}_j\left(\underline{2}\right)\right\rangle\left\langle \hat{A}_i\left(\underline{1}\right)\right\rangle\delta J_{j,\mathrm{ext}}\left(\underline{2}\right)\\
&- \frac{1}{i\hbar}\sum_{j=1}^{3}\int d\underline{2}\left\langle T_{\mathrm{c}}\left[\hat{A}_j\left(\underline{2}\right)\hat{A}_i\left(\underline{1}\right)\right]\right\rangle\delta J_{j,\mathrm{ext}}\left(\underline{2}\right)\\
&+ \left(\text{terms dependent only on }\delta\rho_{\mathrm{ext}}\right).
\end{aligned}\tag{C.17}$$

Combination of definition of photon Green's function (3.95) and Eq. (C.17) gives the following formula for photon Green's function

$$D_{i,j}\left(\underline{1},\underline{2}\right)=-\frac{1}{\mu_0}\frac{\delta\left\langle \hat{A}_i\left(\underline{1}\right)\right\rangle}{\delta J_{j,\mathrm{ext}}\left(\underline{2}\right)}=\frac{1}{i\hbar\mu_0}\left(\left\langle T_{\mathrm{c}}\left[\hat{A}_j\left(\underline{2}\right)\hat{A}_i\left(\underline{1}\right)\right]\right\rangle-\left\langle \hat{A}_j\left(\underline{2}\right)\right\rangle\left\langle \hat{A}_i\left(\underline{1}\right)\right\rangle\right).\tag{C.18}$$

The first step to obtain Eq. (3.102) for $D_{i,j}\left(\underline{1},\underline{2}\right)$, is to use the equation of motion for an operator in the Heisenberg picture (A.25) to calculate the second derivative (regular) of the vector field operator $\hat{\mathbf{A}}$ over time

$$\frac{d^2\hat{A}_i}{dt^2}=\frac{d}{dt}\left(\frac{d\hat{A}_i}{dt}\right)=\frac{1}{i\hbar}\left[\frac{d\hat{A}_i}{dt},\hat{H}\right]_-, \tag{C.19}$$

where it is assumed that $\hat{\mathbf{A}}$ does not have explicit time dependence causing the last term in equation (A.25) to vanish. For brevity, here the following notation is used

$$\hat{A}_i\left(t\right)=\hat{A}_i, \tag{C.20}$$

$$\frac{d\hat{A}_i\left(t\right)}{dt}=\dot{\hat{A}}_i. \tag{C.21}$$

Using the definition of the Hamiltonian from Subsection 3.3.1, the second derivative of $\hat{A}_i$ is

$$\begin{aligned}i\hbar\frac{d^2\hat{A}_i\left(\mathbf{r}\right)}{dt^2}&=\frac{1}{2}\int d^3r'\left(\epsilon_0\left[\dot{\hat{A}}_i\left(\mathbf{r}\right),\dot{\hat{A}}_i\left(\mathbf{r}'\right)^2\right]_-+\frac{1}{\mu_0}\left[\dot{\hat{A}}_i\left(\mathbf{r}\right),\left(\nabla\times\hat{\mathbf{A}}\left(\mathbf{r}'\right)\right)^2\right]_-\right)\\&-\sum_{j=1}^{3}\sum_{\sigma'}\int d^3r'\left(\hat{J}_j\left(\mathbf{r}',\sigma'\right)+J_{j,\text{ext}}\left(\mathbf{r}',\sigma'\right)\right)\left[\dot{\hat{A}}_i\left(\mathbf{r}\right),\hat{A}_j\left(\mathbf{r}'\right)\right].\end{aligned} \tag{C.22}$$

The commutation relations for $\dot{\hat{A}}_i$ and $\hat{A}_i$ are [63]

$$\left[\hat{A}_i\left(\mathbf{r}\right),\hat{A}_j\left(\mathbf{r}'\right)\right]_-=\left[\dot{\hat{A}}_i\left(\mathbf{r}\right),\dot{\hat{A}}_j\left(\mathbf{r}'\right)\right]_-=0, \tag{C.23}$$

$$\epsilon_0\left[\hat{A}_i\left(\mathbf{r}\right),\dot{\hat{A}}_j\left(\mathbf{r}'\right)\right]_-=i\hbar\left[\delta_{i,j}\delta(\mathbf{r}-\mathbf{r}')+\frac{1}{4\pi}\partial_i\left(\mathbf{r}\right)\partial_j\left(\mathbf{r}\right)\frac{1}{\left|\mathbf{r}-\mathbf{r}'\right|}\right]=i\hbar\delta^{\mathrm{T}}_{i,j}(\mathbf{r}-\mathbf{r}'). \tag{C.24}$$

The commutator $\left[\dot{\hat{A}}_i\left(\mathbf{r}\right),\left(\nabla\times\hat{\mathbf{A}}\left(\mathbf{r}'\right)\right)^2\right]_-$ can be calculated using commutation relations (C.23), (C.24), and the definition of the curl operator $\nabla\times$

$$\left(\nabla\times\hat{\mathbf{A}}\left(\mathbf{r}\right)\right)_i=e_{i,l,m}\partial_l\hat{A}_m\left(\mathbf{r}\right), \tag{C.25}$$

where $e_{i,l,m}$ is a Levi-Civita symbol. This approach yields

$$\begin{aligned}&\left[\dot{\hat{A}}_n\left(\mathbf{r}\right),\left(\nabla\times\hat{\mathbf{A}}\left(\mathbf{r}'\right)\right)^2\right]_-=\left[\dot{\hat{A}}_n\left(\mathbf{r}\right),\left(\nabla\times\hat{\mathbf{A}}\left(\mathbf{r}'\right)\right)_i\right]_-\left(\nabla\times\hat{\mathbf{A}}\left(\mathbf{r}'\right)\right)_i\\&+\left(\nabla\times\hat{\mathbf{A}}\left(\mathbf{r}'\right)\right)_i\left[\dot{\hat{A}}_n\left(\mathbf{r}\right),\left(\nabla\times\hat{\mathbf{A}}\left(\mathbf{r}'\right)\right)_i\right]\\&=e_{i,l,m}e_{i,\alpha,\beta}\left(\left[\dot{\hat{A}}_n\left(\mathbf{r}\right),\partial_l\hat{A}_m\left(\mathbf{r}'\right)\right]_-\partial_\alpha\dot{\hat{A}}_\beta\left(\mathbf{r}'\right)+\left(\partial_\alpha\dot{\hat{A}}_\beta\left(\mathbf{r}'\right)\right)\left[\dot{\hat{A}}_n\left(\mathbf{r}\right),\partial_l\hat{A}_m\left(\mathbf{r}'\right)\right]_-\right)\\&=\frac{2\hbar}{i\epsilon_0}\left(\partial_\alpha\left(\mathbf{r}'\right)\delta(\mathbf{r}'-\mathbf{r})\partial_\alpha\left(\mathbf{r}'\right)\hat{A}_n\left(\mathbf{r}'\right)-\partial_\beta\left(\mathbf{r}'\right)\delta(\mathbf{r}'-\mathbf{r})\partial_n\left(\mathbf{r}'\right)\hat{A}_\beta\left(\mathbf{r}'\right)\right).\end{aligned} \tag{C.26}$$

After integration over $\mathbf{r}'$, the above formula becomes

$$\begin{aligned}
&\int d^3r' \left[\dot{\hat{A}}_n (\mathbf{r}) , \left(\nabla \times \hat{\mathbf{A}} (\mathbf{r}') \right)^2 \right]_- = \\
&= \frac{2\hbar}{i\epsilon_0} \int d^3r' \left(\partial_\alpha (\mathbf{r}') \delta(\mathbf{r}' - \mathbf{r}) \partial_\alpha (\mathbf{r}') \hat{A}_n (\mathbf{r}') - \partial_\beta (\mathbf{r}') \delta(\mathbf{r}' - \mathbf{r}) \partial_n (\mathbf{r}') \hat{A}_\beta (\mathbf{r}') \right) = \\
&= -\frac{2\hbar}{i\epsilon_0} \int d^3r' \delta(\mathbf{r}' - \mathbf{r}) \left(\partial_\alpha (\mathbf{r}') \partial_\alpha (\mathbf{r}') \hat{A}_n (\mathbf{r}') - \partial_n (\mathbf{r}') \partial_\beta (\mathbf{r}') \hat{A}_\beta (\mathbf{r}') \right) = \\
&= \frac{2i\hbar}{\epsilon_0} \partial_\alpha (\mathbf{r}) \partial_\alpha (\mathbf{r}) \hat{A}_n (\mathbf{r}) = \frac{2i\hbar}{\epsilon_0} \nabla^2 \hat{A}_n (\mathbf{r}) . \qquad \text{(C.27)}
\end{aligned}$$

Combination of Eqs. (C.27), (C.23), (C.24) and the initial equation for the second time derivative of $\hat{\mathbf{A}}$ (C.22) gives

$$\frac{d^2 \hat{A}_i (\mathbf{r})}{dt^2} = \frac{1}{\epsilon_0 \mu_0} + \left(\nabla^2 \hat{A}_i (\mathbf{r}) + \mu_0 \sum_j \sum_{\sigma'} \int d^3r' \delta^{\mathrm{T}}_{i,j} (\mathbf{r} - \mathbf{r}') \left(\hat{J}_j (\mathbf{r}', \sigma') + J_{j,\mathrm{ext}} (\mathbf{r}', \sigma') \right) \right) . \qquad \text{(C.28)}$$

Going back to full contour notation, one may write

$$\left(\nabla^2 (\underline{1}) - \epsilon_0 \mu_0 \frac{d^2}{dt^2} \right) \left\langle \hat{A}_i (\underline{1}) \right\rangle = -\mu_0 \sum_{\sigma_1} \left\langle \hat{J}^{\mathrm{T}}_i (\underline{1}) \right\rangle - \mu_0 \int d\underline{2} \delta^{\mathrm{T}}_{i,j} (\mathbf{r}_1 - \mathbf{r}_2) \delta (\underline{t}_1, \underline{t}_2) J_{j,\mathrm{ext}} (\underline{2}) , \qquad \text{(C.29)}$$

and by taking the functional derivative with respect to $J_{i,\mathrm{ext}} (\underline{2})$ on both sides of eqn. (C.29) and using the chain rule on the RHS, one gets

$$\begin{aligned}
&\left(\nabla^2 (\underline{1}) - \epsilon_0 \mu_0 \frac{d^2}{dt_1^2} \right) \frac{\delta \left\langle \hat{A}_i (\underline{1}) \right\rangle}{\delta J_{j,\mathrm{ext}} (\underline{2})} = -\mu_0 \delta^{\mathrm{T}}_{i,j} (\mathbf{r}_1 - \mathbf{r}_2) \delta (\underline{t}_1, \underline{t}_2) \\
&- \mu_0 \sum_{\sigma_1} \sum_{k=1}^{3} \int d\underline{3} \frac{\delta \left\langle \hat{J}^{\mathrm{T}}_i (\underline{1}) \right\rangle}{\delta \left\langle \hat{A}_k (\underline{3}) \right\rangle} \frac{\delta \left\langle \hat{A}_k (\underline{3}) \right\rangle}{\delta \left\langle \hat{J}^{\mathrm{T}}_j (\underline{2}) \right\rangle} . \qquad \text{(C.30)}
\end{aligned}$$

After using the definitions of transverse vertex function (3.94), transverse self-energy (3.94), photon Green's function (3.95), and notation (3.88), Eq. (C.30) becomes

$$\left(\nabla^2 (\underline{1}) - \frac{1}{c^2} \frac{d^2}{dt_1^2} \right) D_{i,j} \left(\widetilde{\underline{1}}, \widetilde{\underline{2}} \right) = \delta^T_{i,j} \left(\widetilde{\underline{1}}, \widetilde{\underline{2}} \right) + \int d\widetilde{\underline{3}} \widetilde{P}_{i,k} \left(\widetilde{\underline{1}}, \widetilde{\underline{3}} \right) D_{k,j} \left(\widetilde{\underline{3}}, \widetilde{\underline{2}} \right) . \qquad \text{(C.31)}$$

Final formulas for the transverse polarization (3.107) and the transverse vertex function (3.107) are calculated from their definitions by using the chain rule in exactly the same way as it is done for their longitudinal counterparts.

Appendix D

Boundary self-energies

This appendix presents a method of imposing open boundary conditions on the Dyson equation. The method presented here has been described for the case of an orthogonal basis in [103, 90, 99] and for a a non-orthogonal basis in [97]. The major idea behind this method in presented in Fig. D.1. The infinite system (in the z direction) is separated into two semi-infinite leads and a finite device. It is assumed that both leads are in equilibrium but with different quasi-Fermi levels. The difference between the quasi-Fermi levels creates a non-equilibrium state in the device. It is also assumed that inside the leads there are no realistic many-body interactions and the only allowed scattering mechanism in the leads is phenomenological scattering via so-called Büttiker probes [104, 105].

With the above assumptions about the leads, it is possible to solve the Dyson equation for the device region only. The whole influence of the leads on the device can be taken into account by adding additional boundary self-energies to the device region. The exact method of calculation of these boundary self-energies is presented below.

The Dyson equation and three supplementary equations for the whole system (the device + semi-infinite leads) are

$$\mathbf{t}^{\mathrm{R}}\mathbf{G}^{\mathrm{R}} = \mathbf{1}, \tag{D.1}$$

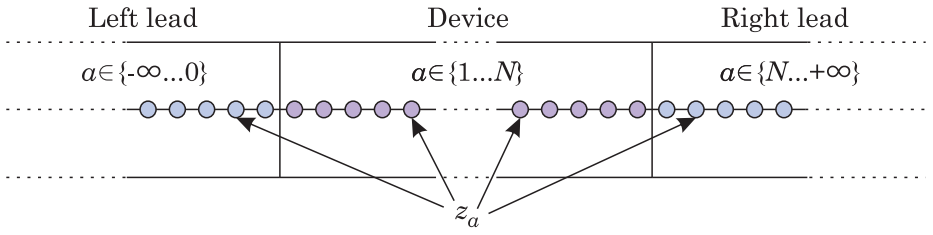

Figure D.1: Separation of the infinite system into the finite device and two quasi-infinite leads. The nodes of the spatial grid in the left lead are numbered from $-\infty$ to 0, in the device from 1 to N, and in the right lead from $N+1$ to $+\infty$.

$$\mathbf{G}^{<} = \mathbf{G}^{\mathrm{R}}\mathbf{\Sigma}^{<}\mathbf{G}^{\mathrm{A}}, \tag{D.2}$$

$$\mathbf{G}^{\mathrm{A}} = \left[\mathbf{G}^{\mathrm{R}}\right]^{\dagger}, \tag{D.3}$$

$$\mathbf{G}^{>} = \mathbf{G}^{\mathrm{R}} - \mathbf{G}^{\mathrm{A}} + \mathbf{G}^{<}, \tag{D.4}$$

where $\mathbf{1}$ is a unit matrix of infinite dimension (leads are infinite), and $\mathbf{t}$ is the inverse of the retarded Green's function

$$\mathbf{t}^{\mathrm{R}} = \left[\mathbf{G}^{\mathrm{R}}\right]^{-1} = \mathbf{E} - \mathbf{H}\left(\mathbf{k}_t, E\right) - \mathbf{\Sigma}^{\mathrm{R}}\left(\mathbf{k}_t, E\right). \tag{D.5}$$

All matrices in Eqs. (D.1)-(D.4) can be written as matrices containing submatrices corresponding to each region (leads and device). For example, the retarded Green's function is

$$\mathbf{G}^{\mathrm{R}} = \begin{pmatrix} \mathbf{G}^{\mathrm{R}}_{LL,LL} & \mathbf{G}^{\mathrm{R}}_{LL,D} & \mathbf{G}^{\mathrm{R}}_{LL,RL} \\ \mathbf{G}^{\mathrm{R}}_{D,LL} & \mathbf{G}^{\mathrm{R}}_{D,D} & \mathbf{G}^{\mathrm{R}}_{D,RL} \\ \mathbf{G}^{\mathrm{R}}_{RL,LL} & \mathbf{G}^{\mathrm{R}}_{RL,D} & \mathbf{G}^{\mathrm{R}}_{RL,RL} \end{pmatrix}, \tag{D.6}$$

where indices are defined as: LL – left lead, RL – right lead, D – device.

The goal is to derive equations which allow to calculate Green's function in the device region: $\mathbf{G}^{\mathrm{R}}_{D,D}$, $\mathbf{G}^{\mathrm{A}}_{D,D}$, $\mathbf{G}^{<}_{D,D}$, $\mathbf{G}^{>}_{D,D}$. From the block diagonal form of the Green's function of the whole system (D.6), and Eqs. (D.3), (D.4), one can see that the equations for the device part of the greater and advanced Greens functions are

$$\mathbf{G}^{\mathrm{A}}_{D,D} = \left[\mathbf{G}^{\mathrm{R}}_{D,D}\right]^{\dagger}, \tag{D.7}$$

$$\mathbf{G}^{>}_{D,D} = \mathbf{G}^{\mathrm{R}}_{D,D} - \mathbf{G}^{\mathrm{A}}_{D,D} + \mathbf{G}^{<}_{D,D}. \tag{D.8}$$

It is assumed that there is no direct interaction between leads, and thus the $\mathbf{t}^{\mathrm{R}}$ matrix is

$$\mathbf{t}^{\mathrm{R}} = \begin{pmatrix} \mathbf{t}^{\mathrm{R}}_{LL,LL} & \mathbf{t}^{\mathrm{R}}_{LL,D} & \mathbf{0}_{LL,RL} \\ \mathbf{t}^{\mathrm{R}}_{D,LL} & \mathbf{t}^{\mathrm{R}}_{D,D} & \mathbf{t}^{\mathrm{R}}_{D,RL} \\ \mathbf{0}_{RL,LL} & \mathbf{t}^{\mathrm{R}}_{RL,D} & \mathbf{t}^{\mathrm{R}}_{RL,RL} \end{pmatrix}. \tag{D.9}$$

Inserting Eq. (D.6) and Eq. (D.9) into the Dyson equation (D.1) gives 9 equations, of which the relevant ones are

$$\mathbf{t}^{\mathrm{R}}_{D,LL}\mathbf{G}^{\mathrm{R}}_{LL,D} + \mathbf{t}^{\mathrm{R}}_{D,D}\mathbf{G}^{\mathrm{R}}_{D,D} + \mathbf{t}^{\mathrm{R}}_{D,RL}\mathbf{G}^{\mathrm{R}}_{RL,D} = \mathbf{1}_{D,D}, \tag{D.10}$$

$$\mathbf{t}^{\mathrm{R}}_{L,D}\mathbf{G}^{\mathrm{R}}_{D,D} + \mathbf{t}^{\mathrm{R}}_{L,L}\mathbf{G}^{\mathrm{R}}_{L,D} = \mathbf{0}_{L,D}, \tag{D.11}$$

where Eq. (D.11) represents two equations (one for each lead) with index $L = \{RL, LL\}$. Equation (D.11) can be rearranged to get

$$\mathbf{G}^{\mathrm{R}}_{L,D} = -\left[\mathbf{t}^{\mathrm{R}}_{L,L}\right]^{-1}\mathbf{t}^{\mathrm{R}}_{L,D}\mathbf{G}^{\mathrm{R}}_{D,D} = -\mathbf{g}^{\mathrm{R}}_{L,L}\mathbf{t}^{\mathrm{R}}_{L,D}\mathbf{G}^{\mathrm{R}}_{D,D}, \tag{D.12}$$

where the retarded Green's function of the lead is defined as

$$\mathbf{t}^{\mathrm{R}}_{L,L}\mathbf{g}^{\mathrm{R}}_{L,L} = \mathbf{1}_{L,L}. \tag{D.13}$$

Small $\mathbf{g}^{\mathrm{R}}$ as well as $\mathbf{g}^{\mathrm{A}}$, and $\mathbf{g}^{<}$, are Green's functions of leads when they are disconnected from the rest of the system (both the device and the other lead). Equation (D.12) can be inserted into Eq. (D.10) to get the Dyson equation for the device region only

$$\left(\mathbf{t}^{\mathrm{R}}_{D,D} - \mathbf{t}^{\mathrm{R}}_{D,LL}\mathbf{g}^{\mathrm{R}}_{LL,LL}\mathbf{t}^{\mathrm{R}}_{LL,D} - \mathbf{t}^{\mathrm{R}}_{D,RL}\mathbf{g}^{\mathrm{R}}_{RL,RL}\mathbf{t}^{\mathrm{R}}_{RL,D}\right)\mathbf{G}^{\mathrm{R}}_{D,D} = \mathbf{1}_{D,D}. \tag{D.14}$$

Using Eq. (D.5), the above equation can be expressed as

$$\mathbf{G}^{\mathrm{R}}_{D,D} = \left[\mathbf{E}_{D,D} - \mathbf{H}_{D,D} - \mathbf{\Sigma}^{\mathrm{R}}_{D,D} - \mathbf{\Sigma}^{\mathrm{B,R}}_{D,D}\right]^{-1}, \tag{D.15}$$

where the retarded boundary self-energy for the device is

$$\mathbf{\Sigma}^{\mathrm{B,R}}_{D,D} = \mathbf{\Sigma}^{\mathrm{BL,R}}_{D,D} + \mathbf{\Sigma}^{\mathrm{BR,R}}_{D,D} = \mathbf{t}^{\mathrm{R}}_{D,LL}\mathbf{g}^{\mathrm{R}}_{LL,LL}\mathbf{t}^{\mathrm{R}}_{LL,D} + \mathbf{t}^{\mathrm{R}}_{D,RL}\mathbf{g}^{\mathrm{R}}_{RL,RL}\mathbf{t}^{\mathrm{R}}_{RL,D}. \tag{D.16}$$

In general, the boundary self-energy $\mathbf{\Sigma}^{\mathrm{B,R}}_{D,D}$ is going to be dependent on $\mathbf{G}^{\mathrm{R}}_{D,D}$ because terms $\mathbf{t}^{\mathrm{R}}_{D,LL}$, $\mathbf{t}^{\mathrm{R}}_{LL,D}$, $\mathbf{t}^{\mathrm{R}}_{D,RL}$, and $\mathbf{t}^{\mathrm{R}}_{RL,D}$ contain device-lead self-energies $\mathbf{\Sigma}^{\mathrm{R}}_{D,LL}$, $\mathbf{\Sigma}^{\mathrm{R}}_{LL,D}$, $\mathbf{\Sigma}^{\mathrm{R}}_{D,RL}$, and $\mathbf{\Sigma}^{\mathrm{R}}_{RL,D}$ which are dependent on $\mathbf{G}^{\mathrm{R}}_{D,D}$. However, here it is assumed that all device-lead (lesser, greater, advanced, and retarded) self-energies are equal to zero, so all boundary self-energies can be calculated independently of Green's functions.

To calculate the lesser boundary self-energy, one needs expressions for $\mathbf{G}^{\mathrm{A}}_{LL,D}$, $\mathbf{G}^{\mathrm{A}}_{RL,D}$, $\mathbf{G}^{\mathrm{R}}_{D,LL}$, and $\mathbf{G}^{\mathrm{R}}_{D,RL}$. The formula for $\mathbf{G}^{\mathrm{R}}_{D,LL}$ and $\mathbf{G}^{\mathrm{R}}_{D,RL}$ is obtained from the same matrix equation as Eq. (D.11)

$$\mathbf{G}^{\mathrm{R}}_{D,L} = -\mathbf{G}^{\mathrm{R}}_{D,D}\mathbf{t}^{\mathrm{R}}_{D,L}\mathbf{g}^{\mathrm{R}}_{L,L}. \tag{D.17}$$

To get formula for $\mathbf{G}^{\mathrm{A}}_{LL,D}$ and $\mathbf{G}^{\mathrm{A}}_{RL,D}$, one can use the relation given by Eq. (4.21)

$$\mathbf{G}^{\mathrm{A}}_{L,D} = \left[\mathbf{G}^{\mathrm{R}}_{D,L}\right]^{\dagger} = -\left[\mathbf{g}^{\mathrm{R}}_{L,L}\right]^{\dagger}\left[\mathbf{t}^{\mathrm{R}}_{L,D}\right]^{\dagger}\left[\mathbf{G}^{\mathrm{R}}_{D,D}\right]^{\dagger} = -\mathbf{g}^{\mathrm{A}}_{L,L}\left[\mathbf{t}^{\mathrm{R}}_{L,D}\right]^{\dagger}\mathbf{G}^{\mathrm{A}}_{D,D}, \tag{D.18}$$

where the advanced Green's function of the lead is

$$\mathbf{g}^{\mathrm{A}}_{L,L} = \left[\mathbf{g}^{\mathrm{R}}_{L,L}\right]^{\dagger}. \tag{D.19}$$

Keeping in mind that all lead-device and left lead-right lead self-energies are zero, the lesser self-energy reduces to

$$\mathbf{\Sigma}^{<} = \begin{pmatrix} \mathbf{\Sigma}^{<}_{LL,LL} & \mathbf{0}_{LL,D} & \mathbf{0}_{LL,RL} \\ \mathbf{0}_{D,LL} & \mathbf{\Sigma}^{<}_{D,D} & \mathbf{0}_{D,RL} \\ \mathbf{0}_{RL,LL} & \mathbf{0}_{RL,D} & \mathbf{\Sigma}^{<}_{RL,RL} \end{pmatrix}, \tag{D.20}$$

and, using Eq. (D.2) for the lesser Green's function, one gets

$$\begin{aligned}\mathbf{G}^{<}_{D,D} &= \mathbf{G}^{\mathrm{R}}_{D,D}\mathbf{\Sigma}^{<}_{D,D}\mathbf{G}^{\mathrm{A}}_{D,D} \\ &+ \mathbf{G}^{\mathrm{R}}_{D,LL}\mathbf{\Sigma}^{<}_{LL,LL}\mathbf{G}^{\mathrm{A}}_{LL,D} + \mathbf{G}^{\mathrm{R}}_{D,RL}\mathbf{\Sigma}^{<}_{RL,RL}\mathbf{G}^{\mathrm{A}}_{RL,D}.\end{aligned} \tag{D.21}$$

The left lead component of Eq. (D.21) is

$$\begin{aligned}&\mathbf{G}^{\mathrm{R}}_{D,LL}\mathbf{\Sigma}^{<}_{LL,LL}\mathbf{G}^{\mathrm{A}}_{LL,D} \\ &= \mathbf{G}^{\mathrm{R}}_{D,D}\mathbf{t}^{\mathrm{R}}_{D,LL}\mathbf{g}^{\mathrm{R}}_{LL,LL}\mathbf{\Sigma}^{<}_{LL,LL}\mathbf{g}^{\mathrm{A}}_{LL,LL}\left[\mathbf{t}^{\mathrm{R}}_{LL,D}\right]^{\dagger}\mathbf{G}^{\mathrm{A}}_{D,D} \\ &= \mathbf{G}^{\mathrm{R}}_{D,D}\mathbf{t}^{\mathrm{R}}_{D,LL}\mathbf{g}^{<}_{LL,LL}\left[\mathbf{t}^{\mathrm{R}}_{LL,D}\right]^{\dagger}\mathbf{G}^{\mathrm{A}}_{D,D},\end{aligned} \tag{D.22}$$

and the right lead term is

$$\mathbf{G}^{\mathrm{R}}_{D,RL}\mathbf{\Sigma}^{<}_{RL,RL}\mathbf{G}^{\mathrm{A}}_{RL,D} = \mathbf{G}^{\mathrm{R}}_{D,D}\mathbf{t}^{\mathrm{R}}_{D,RL}\mathbf{g}^{<}_{RL,RL}\left[\mathbf{t}^{\mathrm{R}}_{RL,D}\right]^{\dagger}\mathbf{G}^{\mathrm{A}}_{D,D}, \tag{D.23}$$

where the lesser Green's function of the lead is

$$\mathbf{g}^{<}_{L,L} = \mathbf{g}^{\mathrm{R}}_{L,L}\mathbf{\Sigma}^{<}_{L,L}\mathbf{g}^{\mathrm{A}}_{L,L}. \tag{D.24}$$

Inserting Eqs. (D.22) and (D.23) into Eq. (D.21) gives the final formula for the lesser Green's function of the device

$$\mathbf{G}^{<}_{D,D} = \mathbf{G}^{\mathrm{R}}_{D,D}\left(\mathbf{\Sigma}^{<}_{D,D} + \mathbf{\Sigma}^{B,<}_{D,D}\right)\mathbf{G}^{\mathrm{A}}_{D,D}, \tag{D.25}$$

where

$$\mathbf{\Sigma}^{\mathrm{B},<}_{D,D} = \mathbf{\Sigma}^{\mathrm{BL},<}_{D,D} + \mathbf{\Sigma}^{\mathrm{BR},<}_{D,D} = \mathbf{t}^{\mathrm{R}}_{D,LL}\mathbf{g}^{<}_{LL,LL}\left[\mathbf{t}^{\mathrm{R}}_{LL,D}\right]^{\dagger} + \mathbf{t}^{\mathrm{R}}_{D,RL}\mathbf{g}^{<}_{RL,RL}\left[\mathbf{t}^{\mathrm{R}}_{RL,D}\right]^{\dagger}. \tag{D.26}$$

In the following derivation of $\mathbf{\Sigma}^{\mathrm{B,R}}_{D,D}$ and $\mathbf{\Sigma}^{\mathrm{B},<}_{D,D}$ it is assumed that both $\mathbf{E}$ and $\mathbf{H}$ are non-zero only at elements corresponding to nodes $(a-1,a)$, (a,a), and $(a,a+1)$ – those matrices are block-tridiagonal where the dimension of the block is determined by the type of Hamiltonian used. In general, when dealing with Hamiltonians with larger number of off-diagonals, one can always introduce virtual nodes made of two or more real nodes. For example, assume that 2-band Hamiltonian with 100 nodes has 1 main diagonal and 4 off-diagonals each made of 2×2 sub-matrices. The number of off-diagonals may be reduced from 4 to 2 by interpreting this Hamiltonian as 4-band with 50 virtual nodes. Now, the diagonal and 2 off-diagonals are each made of 4×4 sub-matrices because each virtual node contains 2 real nodes.

Numbering method for spatial nodes in the whole system (device + leads) is shown in Fig. D.1. For the left lead-device interface, elements $\mathbf{t}^{\mathrm{R}}_{LL,D}$ and $\mathbf{t}^{\mathrm{R}}_{D,LL}$ have the following form

$$\mathbf{t}^{\mathrm{R}}_{LL,D} = \begin{pmatrix} \vdots & \vdots & & \vdots \\ \vdots & \vdots & & \vdots \\ \mathbf{0} & \mathbf{0} & \cdots & \mathbf{0} \\ \mathbf{t}^{\mathrm{R}}_{0,1} & \mathbf{0} & \cdots & \mathbf{0} \end{pmatrix}, \tag{D.27}$$

and

$$\mathbf{t}^{\mathrm{R}}_{D,LL} = \begin{pmatrix} \cdots & \cdots & \mathbf{0} & \mathbf{t}^{\mathrm{R}}_{1,0} \\ \cdots & \cdots & \mathbf{0} & \mathbf{0} \\ & & \vdots & \vdots \\ \cdots & \cdots & \mathbf{0} & \mathbf{0} \end{pmatrix}, \tag{D.28}$$

where $\mathbf{t}^{\mathrm{R}}_{0,1} = \mathbf{E}_{0,1} - \mathbf{H}_{0,1}$, and $\mathbf{t}^{\mathrm{R}}_{1,0} = \mathbf{E}_{1,0} - \mathbf{H}_{1,0}$. The elements $\mathbf{E}_{a,b}$ and $\mathbf{H}_{a,b}$ are submatrices of the full matrices $\mathbf{E}$, $\mathbf{H}$ from Eq. (D.5), corresponding to the particular grid points a, b. The terms $\mathbf{t}^{\mathrm{R}}_{LL,D}$ and $\mathbf{t}^{\mathrm{R}}_{D,LL}$ have such form because it is assumed that there are no lead-device self-energies, and all other elements of $\mathbf{t}^{\mathrm{R}}$ are block-tridiagonal. Inserting Eqs. (D.27) and (D.28) into Eq. (D.16) gives the following equation for the left boundary self-energy

$$\begin{aligned}
\boldsymbol{\Sigma}^{\mathrm{BL,R}}_{D,D} &= \mathbf{t}^{\mathrm{R}}_{D,LL}\mathbf{g}^{\mathrm{R}}_{LL,LL}\mathbf{t}^{\mathrm{R}}_{LL,D} \\
&= \begin{pmatrix} \cdots & \cdots & \mathbf{0} & \mathbf{t}^{\mathrm{R}}_{1,0} \\ \cdots & \cdots & \mathbf{0} & \mathbf{0} \\ & & \vdots & \vdots \\ \cdots & \cdots & \mathbf{0} & \mathbf{0} \end{pmatrix} \begin{pmatrix} \ddots & & \vdots & \vdots \\ & \ddots & \vdots & \vdots \\ \cdots & \cdots & \mathbf{g}^{\mathrm{R}}_{-1,-1} & \mathbf{g}^{\mathrm{R}}_{-1,0} \\ \cdots & \cdots & \mathbf{g}^{\mathrm{R}}_{0,-1} & \mathbf{g}^{\mathrm{R}}_{0,0} \end{pmatrix} \begin{pmatrix} \vdots & \vdots & & \vdots \\ \vdots & \vdots & & \vdots \\ \mathbf{0} & \mathbf{0} & \cdots & \mathbf{0} \\ \mathbf{t}^{\mathrm{R}}_{0,1} & \mathbf{0} & \cdots & \mathbf{0} \end{pmatrix} \\
&= \begin{pmatrix} \cdots & \cdots & \mathbf{t}^{\mathrm{R}}_{1,0}\mathbf{g}^{\mathrm{R}}_{0,-1} & \mathbf{t}^{\mathrm{R}}_{1,0}\mathbf{g}^{\mathrm{R}}_{0,0} \\ \cdots & \cdots & \mathbf{0} & \mathbf{0} \\ & & \vdots & \vdots \\ \cdots & \cdots & \mathbf{0} & \mathbf{0} \end{pmatrix} \begin{pmatrix} \vdots & \vdots & & \vdots \\ \vdots & \vdots & & \vdots \\ \mathbf{0} & \mathbf{0} & \cdots & \mathbf{0} \\ \mathbf{t}^{\mathrm{R}}_{0,1} & \mathbf{0} & \cdots & \mathbf{0} \end{pmatrix} \\
&= \begin{pmatrix} \mathbf{t}^{\mathrm{R}}_{1,0}\mathbf{g}^{\mathrm{R}}_{0,0}\mathbf{t}^{\mathrm{R}}_{0,1} & \mathbf{0} & \cdots & \mathbf{0} \\ \mathbf{0} & \mathbf{0} & \cdots & \mathbf{0} \\ \vdots & \vdots & \ddots & \vdots \\ \mathbf{0} & \mathbf{0} & \cdots & \mathbf{0} \end{pmatrix}.
\end{aligned} \tag{D.29}$$

A similar procedure is done for the right lead, this time

$$\mathbf{t}^{\mathrm{R}}_{D,RL} = \begin{pmatrix} \vdots & \vdots & & \vdots \\ \vdots & \vdots & & \vdots \\ \mathbf{0} & \mathbf{0} & \cdots & \mathbf{0} \\ \mathbf{t}^{\mathrm{R}}_{N,N+1} & \mathbf{0} & \cdots & \mathbf{0} \end{pmatrix}, \tag{D.30}$$

$$\mathbf{t}^{\mathrm{R}}_{RL,R} = \begin{pmatrix} \cdots & \cdots & \mathbf{0} & \mathbf{t}^{\mathrm{R}}_{N+1,1} \\ \cdots & \cdots & \mathbf{0} & \mathbf{0} \\ & & \vdots & \vdots \\ \cdots & \cdots & \mathbf{0} & \mathbf{0} \end{pmatrix}, \tag{D.31}$$

and the full retarded boundary self-energy becomes

$$\mathbf{\Sigma}^{\mathrm{B,R}}_{D,D} = \begin{pmatrix} \mathbf{t}^{\mathrm{R}}_{1,0}\mathbf{g}^{\mathrm{R}}_{0,0}\mathbf{t}^{\mathrm{R}}_{0,1} & \mathbf{0} & \cdots & \mathbf{0} & \mathbf{0} \\ \mathbf{0} & \mathbf{0} & \cdots & \mathbf{0} & \mathbf{0} \\ \vdots & \vdots & \ddots & \vdots & \vdots \\ \mathbf{0} & \mathbf{0} & \cdots & \mathbf{0} & \mathbf{0} \\ \mathbf{0} & \mathbf{0} & \cdots & \mathbf{0} & \mathbf{t}^{\mathrm{R}}_{N,N+1}\mathbf{g}^{\mathrm{R}}_{N+1,N+1}\mathbf{t}^{\mathrm{R}}_{N+1,N} \end{pmatrix}. \tag{D.32}$$

Exactly the same procedure is repeated for $\mathbf{\Sigma}^{\mathrm{B},<}_{D,D}$, given by Eq. (D.26). Because there are no lead-device self-energies, $\mathbf{t}^{\mathrm{R}}_{a,b} = \left[\mathbf{t}^{\mathrm{R}}\right]^{\dagger}_{a,b}$ for all (a,b) at the lead-device interfaces $((1,0),\,(0,1),\,(N+1,N),\,(N,N+1))$, and the final equation for $\mathbf{\Sigma}^{\mathrm{B},<}_{D,D}$ is the same as Eq. (D.32) but with $\mathbf{g}^{<}$ instead of $\mathbf{g}^{\mathrm{R}}$.

Because leads are in equilibrium, $\mathbf{g}^{<}_{0,0}$ and $\mathbf{g}^{<}_{N+1,N+1}$ can be calculated from $\mathbf{g}^{\mathrm{R}}_{0,0}$ and $\mathbf{g}^{\mathrm{R}}_{N+1,N+1}$ using the fluctuation-dissipation theorem [97, 90]. The lesser Green's functions in the leads are

$$\mathbf{g}^{<}_{0,0}\left(E\right) = -f\left(E - F_L\right)\left(\mathbf{g}^{\mathrm{R}}_{0,0} - \left[\mathbf{g}^{\mathrm{R}}_{0,0}\right]^{\dagger}\right) \tag{D.33}$$

for the left lead, and

$$\mathbf{g}^{<}_{N+1,N+1}\left(E\right) = -f\left(E - F_R\right)\left(\mathbf{g}^{\mathrm{R}}_{N+1,N+1} - \left[\mathbf{g}^{\mathrm{R}}_{N+1,N+1}\right]^{\dagger}\right), \tag{D.34}$$

for the right lead. In the above equations, $f\left(E\right)$ is a Fermi-Dirac distribution function, F_L the quasi-Fermi level (chemical potential) of the left lead, and F_R the quasi-Fermi level of the right lead.

To get the final formulas for $\mathbf{\Sigma}^{\mathrm{B,R}}_{D,D}$ and $\mathbf{\Sigma}^{\mathrm{B},<}_{D,D}$, one still has to calculate the retarded Green's functions of the leads $\mathbf{g}^{\mathrm{R}}_{0,0}$ and $\mathbf{g}^{\mathrm{R}}_{N+1,N+1}$. Retarded Greens functions are calculated using formula (D.13). The single-particle Hamiltonian in this equation is the same as the one in the device but with constant potential. For the left lead this potential is equal to the potential at the first node of the device, and for the right lead it is the same as the potential at last node of the device. As mentioned before, the retarded self-energy in the leads is assumed to have form of Büttiker probe

$$\mathbf{\Sigma}^{\mathrm{R}}_{L,L} = \left[\mathbf{\Sigma}^{\mathrm{A}}_{L,L}\right]^{\dagger} = i\eta\mathbf{S}_{L,L}, \tag{D.35}$$

where η is a small real number or zero. With the above definition, the Dyson equation for the retarded Green's function in the lead (D.13) becomes

$$\mathbf{t}^{\mathrm{R}}_{L,L}\mathbf{g}^{\mathrm{R}}_{L,L} = \left(\mathbf{E}_{L,L} - \mathbf{H}_{L,L} - i\eta\mathbf{S}_{L,L}\right)\mathbf{g}^{\mathrm{R}}_{L,L} = \mathbf{1}. \tag{D.36}$$

Under the assumption that all nodes in the leads are uniformly distributed and $\mathbf{E}$, $\mathbf{H}$, and $\mathbf{\Sigma}^{\mathrm{R}}$, are the same on every node of the lead, Eq. (D.36) can be written as

$$
\begin{aligned}
&\mathbf{t}^{\mathrm{R}}_{LL,LL}\mathbf{g}^{\mathrm{R}}_{LL,LL} = \\
&= \begin{pmatrix} \ddots & \vdots & \vdots & \vdots & \vdots \\ \cdots & \mathbf{D} & \mathbf{T}_{\mathrm{U}} & \mathbf{0} & \mathbf{0} \\ \cdots & \mathbf{T}_{\mathrm{L}} & \mathbf{D} & \mathbf{T}_{\mathrm{U}} & \mathbf{0} \\ \cdots & \mathbf{0} & \mathbf{T}_{\mathrm{L}} & \mathbf{D} & \mathbf{T}_{\mathrm{U}} \\ \cdots & \mathbf{0} & \mathbf{0} & \mathbf{T}_{\mathrm{L}} & \mathbf{D} \end{pmatrix} \begin{pmatrix} \ddots & \vdots & \vdots & \vdots \\ \cdots & \mathbf{g}^{\mathrm{R}}_{-2,-2} & \mathbf{g}^{\mathrm{R}}_{-2,-1} & \mathbf{g}^{\mathrm{R}}_{-2,0} \\ \cdots & \mathbf{g}^{\mathrm{R}}_{-1,-2} & \mathbf{g}^{\mathrm{R}}_{-1,-1} & \mathbf{g}^{\mathrm{R}}_{-1,0} \\ \cdots & \mathbf{g}^{\mathrm{R}}_{0,-2} & \mathbf{g}^{\mathrm{R}}_{0,-1} & \mathbf{g}^{\mathrm{R}}_{0,0} \end{pmatrix} \\
&= \begin{pmatrix} \ddots & & \vdots & \vdots & \vdots \\ & \ddots & \mathbf{0} & \mathbf{0} & \mathbf{0} \\ \cdots & \mathbf{0} & \mathbf{1} & \mathbf{0} & \mathbf{0} \\ \cdots & \mathbf{0} & \mathbf{0} & \mathbf{1} & \mathbf{0} \\ \cdots & \mathbf{0} & \mathbf{0} & \mathbf{0} & \mathbf{1} \end{pmatrix},
\end{aligned} \tag{D.37}
$$

where $\mathbf{D} = \mathbf{t}^{\mathrm{R}}_{0,0}$, $\mathbf{T}_{\mathrm{L}} = \mathbf{t}^{\mathrm{R}}_{0,-1}$, $\mathbf{T}_{\mathrm{U}} = \mathbf{t}^{\mathrm{R}}_{-1,0}$.

The following two equations can be extracted form Eq. (D.37)

$$\mathbf{T}_{\mathrm{L}}\mathbf{g}^{\mathrm{R}}_{-1,0} + \mathbf{D}\mathbf{g}^{\mathrm{R}}_{0,0} = \mathbf{1}, \tag{D.38}$$

and

$$\mathbf{T}_{\mathrm{L}}\mathbf{g}^{\mathrm{R}}_{a-2,a} + \mathbf{D}\mathbf{g}^{\mathrm{R}}_{a-1,i} + \mathbf{T}_{\mathrm{U}}\mathbf{g}^{\mathrm{R}}_{a,a} = \mathbf{0}, \qquad (a \leq 0)\,. \tag{D.39}$$

To construct solutions satisfying Eq. (D.39) one can use functions $\boldsymbol{\phi}_a$ satisfying the following equations

$$\begin{pmatrix} \ddots & \vdots & \vdots & \vdots & \vdots \\ \cdots & \mathbf{D} & \mathbf{T}_{\mathrm{U}} & \mathbf{0} & \mathbf{0} \\ \cdots & \mathbf{T}_{\mathrm{L}} & \mathbf{D} & \mathbf{T}_{\mathrm{U}} & \mathbf{0} \\ \cdots & \mathbf{0} & \mathbf{T}_{\mathrm{L}} & \mathbf{D} & \mathbf{T}_{\mathrm{U}} \\ \cdots & \mathbf{0} & \mathbf{0} & \mathbf{T}_{\mathrm{L}} & \mathbf{D} \end{pmatrix} \begin{pmatrix} \vdots \\ \boldsymbol{\phi}_{-3} \\ \boldsymbol{\phi}_{-2} \\ \boldsymbol{\phi}_{-1} \\ \boldsymbol{\phi}_{0} \end{pmatrix} = \begin{pmatrix} \vdots \\ \mathbf{0}_{\mathrm{V}} \\ \mathbf{0}_{\mathrm{V}} \\ \mathbf{0}_{\mathrm{V}} \\ \mathbf{0}_{\mathrm{V}} \end{pmatrix}, \tag{D.40}$$

and

$$\mathbf{T}_{\mathrm{L}}\boldsymbol{\phi}_{a-2} + \mathbf{D}\boldsymbol{\phi}_{a-1} + \mathbf{T}_{\mathrm{U}}\boldsymbol{\phi}_{a} = \mathbf{0}_{\mathrm{V}}. \tag{D.41}$$

If matrices $\mathbf{D}$, $\mathbf{T}_{\mathrm{L}}$, $\mathbf{T}_{\mathrm{U}}$, $\mathbf{0}$ are $n \times n$ matrices, then $\boldsymbol{\phi}_a$ and $\mathbf{0}_{\mathrm{V}}$ are $n \times 1$ vectors, where the "V" subscript was added to distinguish between zero matrices and zero vectors. Because the distance between adjacent nodes is constant and equal to Δ, vectors $\boldsymbol{\phi}_a$ have to be periodic

$$\boldsymbol{\phi}_a = \boldsymbol{\phi}_0 e^{ik(z_a - z_0)} = \boldsymbol{\phi}_0 e^{-aik\Delta}, \tag{D.42}$$

where k is constant, and

$$\boldsymbol{\phi}_{a-1} = \boldsymbol{\phi}_a e^{-ik\Delta}, \tag{D.43}$$

$$\boldsymbol{\phi}_{a-2} = \boldsymbol{\phi}_a e^{-2ik\Delta} = \boldsymbol{\phi}_{a-1} e^{-ik\Delta}. \tag{D.44}$$

Inserting the two above results into Eq. (D.41) leads to set of equations for $\boldsymbol{\phi}_a$

$$\begin{cases} \mathbf{T}_{\mathrm{L}} \boldsymbol{\phi}_{a-1} e^{-ik\Delta} + \mathbf{D}\boldsymbol{\phi}_a e^{-ik\Delta} + \mathbf{T}_{\mathrm{U}} \boldsymbol{\phi}_a = \mathbf{0}_{\mathrm{V}} \\ \phi_0 = \boldsymbol{\phi}_{a-1} e^{ik\Delta} \end{cases}, \tag{D.45}$$

which in matrix form is

$$\begin{pmatrix} \mathbf{D} & \mathbf{T}_{\mathrm{L}} \\ \mathbf{1} & \mathbf{0} \end{pmatrix} \begin{pmatrix} \boldsymbol{\phi}_a \\ \boldsymbol{\phi}_{a-1} \end{pmatrix} = e^{ik\Delta} \begin{pmatrix} -\mathbf{T}_{\mathrm{U}} & \mathbf{1} \\ \mathbf{0} & \mathbf{1} \end{pmatrix} \begin{pmatrix} \boldsymbol{\phi}_a \\ \boldsymbol{\phi}_{a-1} \end{pmatrix}. \tag{D.46}$$

The above equation can be rearranged into an eigenequation for $\left(\boldsymbol{\phi}_a, \boldsymbol{\phi}_{a-1}\right)$

$$\begin{pmatrix} -\mathbf{T}_{\mathrm{U}} & \mathbf{0} \\ \mathbf{0} & \mathbf{1} \end{pmatrix}^{-1} \begin{pmatrix} \mathbf{D} & \mathbf{T}_{\mathrm{L}} \\ \mathbf{1} & \mathbf{0} \end{pmatrix} \begin{pmatrix} \boldsymbol{\phi}_a \\ \boldsymbol{\phi}_{a-1} \end{pmatrix} = e^{ik\Delta} \begin{pmatrix} \boldsymbol{\phi}_a \\ \boldsymbol{\phi}_{a-1} \end{pmatrix}. \tag{D.47}$$

In general there are $2n$ solutions of Eq. (D.47), of which only n will be used to construct the retarded Green's function. The condition for choosing the right solutions is shown later but for now it is assumed that the proper solutions are chosen. The retarded Green's function satisfying Eq. (D.39) and its Hermitian adjoint is

$$\mathbf{g}^{\mathrm{R}}_{a,b} = \boldsymbol{\Phi} \mathbf{e}^{\mathbf{ik(z_a - z_0)}} \tilde{\mathbf{g}}^{\mathrm{R}} \left[\mathbf{e}^{\mathbf{ik(z_b - z_0)}}\right]^{\dagger} \boldsymbol{\Phi}^{\dagger} \qquad (a < b \leq 0). \tag{D.48}$$

In the above equation, $\boldsymbol{\Phi}$ is an $n \times n$ matrix which holds n proper eigenvectors $\boldsymbol{\phi}_0$ ($\boldsymbol{\phi}_a$ with $a = 0$) of Eq. (D.47)

$$\boldsymbol{\Phi} = \left[\boldsymbol{\phi}_0^1, \boldsymbol{\phi}_0^2, \ldots, \boldsymbol{\phi}_0^n\right]. \tag{D.49}$$

$\mathbf{e}^{\mathbf{ik(z_a - z_0)}}$ is an $n \times n$ matrix whose elements are

$$\left[\mathbf{e}^{\mathbf{ik(z_a - z_0)}}\right]_{\mu,\nu} = \delta_{\mu,\nu} e^{ik_\mu (z_a - z_0)}, \tag{D.50}$$

where μ is an eigenvalue number, and $\tilde{\mathbf{g}}^{\mathrm{R}}$ is an $n \times n$ matrix yet to be determined.

Validity of (D.48) can be checked by inserting it into Eq. (D.39) and its adjoint. To determine $\tilde{\mathbf{g}}^{\mathrm{R}}$, formula (D.48) is inserted into eq. (D.38) to get

$$\mathbf{T}_{\mathrm{L}} \boldsymbol{\Phi} \mathbf{e}^{-\mathbf{ik\Delta}} \tilde{\mathbf{g}}^{\mathrm{R}} \boldsymbol{\Phi}^{\dagger} + \mathbf{D} \boldsymbol{\Phi} \tilde{\mathbf{g}}^{\mathrm{R}} \boldsymbol{\Phi}^{\dagger} = \mathbf{1}, \tag{D.51}$$

which can be rearranged to obtain the final formula for $\tilde{\mathbf{g}}^{\mathrm{R}}$

$$\tilde{\mathbf{g}}^{\mathrm{R}} = \left[\boldsymbol{\Phi}^{\dagger} \mathbf{T}_{\mathrm{L}} \boldsymbol{\Phi} \mathbf{e}^{-\mathbf{ik\Delta}} + \boldsymbol{\Phi}^{\dagger} \mathbf{D} \boldsymbol{\Phi}\right]^{-1}. \tag{D.52}$$

Combination of Eqs. (D.52) and (D.47) gives the final equation for the retarded Green's function of the left lead

$$\mathbf{g}^{\mathrm{R}}_{a,b} = \boldsymbol{\Phi} \mathbf{e}^{\mathbf{ik(z_a - z_0)}} \left[\boldsymbol{\Phi}^{\dagger} \mathbf{T}_{\mathrm{L}} \boldsymbol{\Phi} \mathbf{e}^{-\mathbf{ik\Delta}} + \boldsymbol{\Phi}^{\dagger} \mathbf{D} \boldsymbol{\Phi}\right]^{-1} \left[\mathbf{e}^{\mathbf{ik(z_b - z_0)}}\right]^{\dagger} \boldsymbol{\Phi}^{\dagger}. \tag{D.53}$$

The equation for $\mathbf{g}^{\mathrm{R}}_{0,0}$ necessary to calculate boundary self-energy of the left lead is

$$\mathbf{g}^{\mathrm{R}}_{0,0} = \left[\mathbf{T}_{\mathrm{L}}\mathbf{\Phi}\mathbf{e}^{-\mathbf{ik\Delta}}\mathbf{\Phi}^{-1} + \mathbf{D}\right]^{-1}. \tag{D.54}$$

To determine which eigenvectors of Eq. (D.47) should be used to construct the retarded Green's function, one can take Eq. (D.48) and set a and b to be 0 to get

$$\tilde{\mathbf{g}}^{\mathrm{R}}\mathbf{\Phi}^{\dagger} = \mathbf{\Phi}^{-1}\mathbf{g}^{\mathrm{R}}_{0,0}. \tag{D.55}$$

The above result can be again inserted into Eq. (D.48), but this time for arbitrary a and $b = 0$, to get

$$\mathbf{g}^{\mathrm{R}}_{a,0} = \mathbf{\Phi}\mathbf{e}^{\mathbf{aik\Delta}}\mathbf{\Phi}^{-1}\mathbf{g}^{\mathrm{R}}_{0,0}. \tag{D.56}$$

Retarded Green's function should decrease to zero with increasing distance Δa and thus the condition for choosing proper eigenvalues is

$$\left|e^{ik_\mu \Delta}\right| > 1. \tag{D.57}$$

In the case that $\mathbf{\Sigma}^{\mathrm{R}}_{LL,LL} = \mathbf{\Sigma}^{\mathrm{A}}_{LL,LL} = \mathbf{0}$, the Dyson equations for the retarded and the advanced Green's function are identical, and the above condition cannot always be used because there are cases when $\left|e^{ik_\mu \Delta}\right| = 1$. In this case, half the solutions of Eq. (D.47) correspond to the retarded Green's function and another half to the advanced Green's function. To choose the solutions corresponding to the retarded Green's function one has to refer to the physical interpretation of the retarded Green's function [88, 111].

The retarded Green's function $\mathbf{g}^{\mathrm{R}}_{a,b}$ describes propagation of perturbation originating at $z = z_b$ and terminating at $z = z_a$. Because Eq. (D.48) is valid for $a < b$ only, the solutions corresponding to the retarded Green's function, are waves propagating from right to left i.e., solutions for which $\frac{dE}{dk_\mu} < 0$.

The procedure of finding the retarded Green's function for right lead is analogous, and thus only major points are shown. For right lead one has

$$\mathbf{t}^{\mathrm{R}}_{RL,RL}\mathbf{g}^{\mathrm{R}}_{RL} = \begin{pmatrix} \mathbf{D} & \mathbf{T}_{\mathrm{U}} & \mathbf{0} & \mathbf{0} & \cdots \\ \mathbf{T}_{\mathrm{L}} & \mathbf{D} & \mathbf{T}_{\mathrm{U}} & \mathbf{0} & \cdots \\ \mathbf{0} & \mathbf{T}_{\mathrm{L}} & \mathbf{D} & \mathbf{T}_{\mathrm{U}} & \cdots \\ \mathbf{0} & \mathbf{0} & \mathbf{T}_{\mathrm{L}} & \mathbf{D} & \cdots \\ \vdots & \vdots & \vdots & \vdots & \ddots \end{pmatrix} \begin{pmatrix} \mathbf{g}^{\mathrm{R}}_{N+1,N+1} & \mathbf{g}^{\mathrm{R}}_{N+1,N+2} & \mathbf{g}^{\mathrm{R}}_{N+1,N+3} & \cdots \\ \mathbf{g}^{\mathrm{R}}_{N+2,N+1} & \mathbf{g}^{\mathrm{R}}_{N+2,N+2} & \mathbf{g}^{\mathrm{R}}_{N+2,N+3} & \cdots \\ \mathbf{g}^{\mathrm{R}}_{N+3,N+1} & \mathbf{g}^{\mathrm{R}}_{N+3,N+2} & \mathbf{g}^{\mathrm{R}}_{N+3,N+3} & \cdots \\ \vdots & \vdots & \vdots & \ddots \end{pmatrix}$$

$$= \begin{pmatrix} \mathbf{1} & \mathbf{0} & \mathbf{0} & \mathbf{0} & \cdots \\ \mathbf{0} & \mathbf{1} & \mathbf{0} & \mathbf{0} & \cdots \\ \mathbf{0} & \mathbf{0} & \mathbf{1} & \mathbf{0} & \cdots \\ \mathbf{0} & \mathbf{0} & \mathbf{0} & \ddots & \\ \vdots & \vdots & \vdots & & \ddots \end{pmatrix}, \tag{D.58}$$

where $\mathbf{D} = \mathbf{t}^{\mathrm{R}}_{N+1,N+1}$, $\mathbf{T}_{\mathrm{L}} = \mathbf{t}^{\mathrm{R}}_{N+2,N+1}$, and $\mathbf{T}_{\mathrm{U}} = \mathbf{t}^{\mathrm{R}}_{N+1,N+2}$. It gives two equations analogous to (D.38) and (D.39)

$$\mathbf{T}_{\mathrm{U}}\mathbf{g}^{\mathrm{R}}_{N+2,N+1} + \mathbf{D}\mathbf{g}^{\mathrm{R}}_{N+1,N+1} = \mathbf{1}, \tag{D.59}$$

$$\mathbf{T}_{\mathrm{L}}\mathbf{g}^{\mathrm{R}}_{a,a} + \mathbf{D}\mathbf{g}^{\mathrm{R}}_{a+1,a} + \mathbf{T}_{\mathrm{U}}\mathbf{g}^{\mathrm{R}}_{a+2,a} = \mathbf{0} \qquad (a \geq N+1)\,. \tag{D.60}$$

This time vectors $\boldsymbol{\phi}_a$ satisfy

$$\boldsymbol{\phi}_a = \boldsymbol{\phi}_{N+1} e^{ik(z_a - z_{N+1})} = \boldsymbol{\phi}_{N+1} e^{aik\Delta}, \tag{D.61}$$

and the eigenequation for $\left(\boldsymbol{\phi}_a, \boldsymbol{\phi}_{a+1}\right)$ is

$$\begin{pmatrix} -\mathbf{T}_{\mathrm{L}} & \mathbf{0} \\ \mathbf{0} & \mathbf{1} \end{pmatrix}^{-1} \begin{pmatrix} \mathbf{D} & \mathbf{T}_{\mathrm{U}} \\ \mathbf{1} & \mathbf{0} \end{pmatrix} \begin{pmatrix} \boldsymbol{\phi}_a \\ \boldsymbol{\phi}_{a+1} \end{pmatrix} = e^{-ik\Delta} \begin{pmatrix} \boldsymbol{\phi}_a \\ \boldsymbol{\phi}_{a+1} \end{pmatrix}. \tag{D.62}$$

Solution of Eq. (D.60) constructed from functions $\boldsymbol{\phi}_a$ is

$$\mathbf{g}^{\mathrm{R}}_{a,b} = \boldsymbol{\Phi}\mathbf{e}^{\mathbf{ik(z_a - z_{N+1})}}\tilde{\mathbf{g}}^{R}\left[\mathbf{e}^{\mathbf{ik(z_b - z_{N+1})}}\right]^{\dagger}\boldsymbol{\Phi}^{\dagger} \qquad (a > b \geq N+1)\,, \tag{D.63}$$

and $\tilde{\mathbf{g}}^{\mathrm{R}}$ is

$$\tilde{\mathbf{g}}^{\mathrm{R}} = \left[\boldsymbol{\Phi}^{\dagger}\mathbf{T}_{\mathrm{U}}\boldsymbol{\Phi}\mathbf{e}^{\mathbf{ik\Delta}} + \boldsymbol{\Phi}^{\dagger}\mathbf{D}\boldsymbol{\Phi}\right]^{-1}. \tag{D.64}$$

Finally, the retarded Green's function necessary to calculate right boundary self-energy is

$$\mathbf{g}^{\mathrm{R}}_{N+1,N+1} = \left[\mathbf{T}_{\mathrm{U}}\boldsymbol{\Phi}\mathbf{e}^{\mathbf{ik\Delta}}\boldsymbol{\Phi}^{-1} + \mathbf{D}\right]^{-1}. \tag{D.65}$$

The condition for physical eigenvalues is derived by inserting Eq. (D.65) into Eq. (D.63) and taking $a = b = N+1$ which results in

$$\tilde{\mathbf{g}}^{\mathrm{R}}\boldsymbol{\Phi}^{\dagger} = \boldsymbol{\Phi}^{-1}\mathbf{g}^{\mathrm{R}}_{N+1,N+1}. \tag{D.66}$$

Equation (D.66) is inserted again into Eq. (D.63) for $b = N+1$ which gives

$$\mathbf{g}^{\mathrm{R}}_{a,N+1} = \boldsymbol{\Phi}\mathbf{e}^{\mathbf{aik\Delta}}\boldsymbol{\Phi}^{-1}\mathbf{g}^{\mathrm{R}}_{N+1,N+1}, \tag{D.67}$$

and, because the retarded Green's function should decrease to zero with increasing distance Δa, the condition for choosing proper eigenvalues is

$$\left|e^{ik_\mu \Delta}\right| < 1. \tag{D.68}$$

In the case that$\boldsymbol{\Sigma}^{\mathrm{R}}_{LL,LL} = \boldsymbol{\Sigma}^{\mathrm{A}}_{LL,LL} = \mathbf{0}$, one can use the same reasoning as for the left lead to see that solutions corresponding to the retarded Green's function are waves propagating from left to right i.e., solutions for which $\frac{dE}{dk_\mu} > 0$.

Appendix E

Polarization and electron-photon self-energy

This appendix presents all intermediate steps between the general formulas for transverse self-energy (3.93) and transverse polarization (3.107), and their final forms given by Eqs. (4.100) and (4.60).

E.1 Transverse polarization

In the first order approximation, the transverse vertex function in Eq. (3.106) is approximated by its first order term

$$\Gamma_i\left(\underline{1},\underline{2},\underline{3}\right)=\frac{i\hbar e\mu_0}{m}\delta\left(\underline{1},\underline{3}\right)\partial_i\left(\underline{1}\right)\delta\left(\underline{1},\underline{2}\right). \tag{E.1}$$

Under the assumption that all currents are transverse (this assumption is discussed in Subsection 4.4.1), the transverse delta function in Eq. (3.107) can be replaced with the regular delta function. Insertion of Eq. (E.1) into Eq. (3.107) yields

$$\begin{aligned}
&P_{i,j}\left(\underline{1},\underline{2}\right)=i\hbar\int d\underline{4}\int d\underline{5}\Pi_i\left(\underline{1},\underline{1}^+\right)G\left(\underline{1},\underline{4}\right)\frac{i\hbar e\mu_0}{m}\delta\left(\underline{4},\underline{5}\right)\partial_j\left(\underline{4}\right)\delta\left(\underline{4},\underline{2}\right)G\left(\underline{5},\underline{1}^+\right)\\
&=-\frac{\hbar^2 e\mu_0}{m}\int d\underline{4}\Pi_i\left(\underline{1},\underline{1}^+\right)G\left(\underline{1},\underline{4}\right)\frac{i\hbar e\mu_0}{m}\partial_j\left(\underline{4}\right)\delta\left(\underline{4},\underline{2}\right)G\left(\underline{4},\underline{1}^+\right)\\
&=-\frac{\hbar^2 e\mu_0}{m}\int d\underline{4}\Pi_i\left(\underline{1},\underline{1}^+\right)G\left(\underline{1},\underline{4}\right)\left(\left[\partial_j\left(\underline{4}\right)\delta\left(\underline{4},\underline{2}\right)\right]G\left(\underline{4},\underline{1}^+\right)+\delta\left(\underline{4},\underline{2}\right)\partial_j\left(\underline{4}\right)G\left(\underline{4},\underline{1}^+\right)\right)\\
&=-\frac{\hbar^2 e\mu_0}{m}\Pi_i\left(\underline{1},\underline{1}^+\right)\left(-\left[\partial_j\left(\underline{2}\right)G\left(\underline{1},\underline{2}\right)\right]G\left(\underline{2},\underline{1}^+\right)\right.\\
&\left.-G\left(\underline{1},\underline{2}\right)\partial_j\left(\underline{2}\right)G\left(\underline{2},\underline{1}^+\right)+G\left(\underline{1},\underline{2}\right)\partial_j\left(\underline{2}\right)G\left(\underline{2},\underline{1}^+\right)\right)\\
&=\frac{\hbar^2 e\mu_0}{m}\Pi_i\left(\underline{1},\underline{1}^+\right)\left[\partial_j\left(\underline{2}\right)G\left(\underline{1},\underline{2}\right)\right]G\left(\underline{2},\underline{1}^+\right)\\
&=-\frac{i\hbar^3 e^2\mu_0}{2m^2}\left(\partial_i\left(\underline{1}\right)-\partial_i\left(\underline{1}^+\right)\right)\left[\partial_j\left(\underline{2}\right)G\left(\underline{1},\underline{2}\right)\right]G\left(\underline{2},\underline{1}^+\right).
\end{aligned} \tag{E.2}$$

The Green's functions are then expanded in basis (4.12), and the (y,y) component of the transverse polarization is

$$
\begin{aligned}
P_{y,y}\left(\underline{1},\underline{2}\right) &= -\frac{i\hbar^3 e^2\mu_0}{2m^2}\frac{1}{A^2}\sum_{\mathbf{k}_\mathrm{t},\mathbf{k}_\mathrm{t}^{'}}\sum_{\alpha,\beta,\mu,\nu}\sum_{a,b,m,n}\delta_{\sigma_1,\sigma_\alpha}\delta_{\sigma_1,\sigma_\nu}\delta_{\sigma_2,\sigma_\beta}\delta_{\sigma_2,\sigma_\mu}\\
&\times G_{\alpha a,\beta b}\left(\mathbf{k}_\mathrm{t},\underline{t}_1-\underline{t}_2\right)G_{\mu m,\nu n}\left(\mathbf{k}_\mathrm{t}^{'},\underline{t}_2-\underline{t}_1\right)w_a\left(z_1\right)w_b^*\left(z_2\right)w_m\left(z_2\right)w_n^*\left(z_1\right)\\
&\times\left(\partial_{y_1}-\partial_{y_{1^+}}\right)\left[\partial_{y_2}e^{i\mathbf{k}_\mathrm{t}\left(\mathbf{r}_{1,\mathrm{t}}-\mathbf{r}_{2,\mathrm{t}}\right)}u_{\alpha'}\left(\mathbf{r}_{1,\mathrm{c}}\right)u_{\beta'}^*\left(\mathbf{r}_{2,\mathrm{c}}\right)\right]e^{i\mathbf{k}_\mathrm{t}^{'}\left(\mathbf{r}_{2,\mathrm{t}}-\mathbf{r}_{1^+,\mathrm{t}}\right)}u_{\mu'}\left(\mathbf{r}_{2,\mathrm{c}}\right)u_{\nu'}^*\left(\mathbf{r}_{1^+,\mathrm{c}}\right),
\end{aligned}
\tag{E.3}
$$

where $\alpha=\{\alpha',\sigma_\alpha\}$ etc. The average polarization is obtained by integrating Eq. (E.3) over the primitive cell, summing over spin indices σ_1, σ_2, and applying a Fourier transform with respect to $(\mathbf{r}_{1,\mathrm{t}}-\mathbf{r}_{2,\mathrm{t}})$

$$
P^{av}\left(z_1,z_2,\mathbf{q}_\mathrm{t},\underline{t}_1-\underline{t}_2\right)=\sum_{\sigma_1,\sigma_2}\int d^2\left(r_{1,\mathrm{t}}-r_{2,\mathrm{t}}\right)e^{-i\mathbf{q}_\mathrm{t}\left(\mathbf{r}_{1,\mathrm{t}}-\mathbf{r}_{2,\mathrm{t}}\right)}\frac{1}{V_\mathrm{c}^2}\int d^3r_{1,\mathrm{c}}\int d^3r_{2,\mathrm{c}}P_{y,y}\left(\underline{1},\underline{2}\right).
\tag{E.4}
$$

The last term in Eq. (E.3), call it X, is

$$
\begin{aligned}
X &= \left(\partial_{y_1}-\partial_{y_{1^+}}\right)e^{i\mathbf{k}_\mathrm{t}^{'}\left(\mathbf{r}_{2,\mathrm{t}}-\mathbf{r}_{1^+,\mathrm{t}}\right)}u_{\mu'}\left(\mathbf{r}_{2,\mathrm{c}}\right)u_{\nu'}^*\left(\mathbf{r}_{1^+,\mathrm{c}}\right)\partial_{y_2}e^{i\mathbf{k}_\mathrm{t}\left(\mathbf{r}_{1,\mathrm{t}}-\mathbf{r}_{2,\mathrm{t}}\right)}u_{\alpha'}\left(\mathbf{r}_{1,\mathrm{c}}\right)u_{\beta'}^*\left(\mathbf{r}_{2,\mathrm{c}}\right)\\
&= e^{i\mathbf{k}_\mathrm{t}^{'}\left(\mathbf{r}_{2,\mathrm{t}}-\mathbf{r}_{1^+,\mathrm{t}}\right)}\left(\partial_{y_1}+ik_y^{'}-\partial_{y_{1^+}}\right)u_{\mu'}\left(\mathbf{r}_{2,\mathrm{c}}\right)u_{\nu'}^*\left(\mathbf{r}_{1^+,\mathrm{c}}\right)\\
&\times e^{i\mathbf{k}_\mathrm{t}\left(\mathbf{r}_{1,t}-\mathbf{r}_{2,t}\right)}\left(-ik_y+\partial_{y_2}\right)u_{\alpha'}\left(\mathbf{r}_{1,\mathrm{c}}\right)u_{\beta'}^*\left(\mathbf{r}_{2,\mathrm{c}}\right)\\
&= e^{i\left(\mathbf{k}_\mathrm{t}^{'}-\mathbf{k}_\mathrm{t}\right)\left(\mathbf{r}_{2,\mathrm{t}}-\mathbf{r}_{1,\mathrm{t}}\right)}\left(\partial_{y_1}+ik_y+ik_y^{'}-\partial_{y_{1^+}}\right)\\
&\times u_{\mu'}\left(\mathbf{r}_{2,\mathrm{c}}\right)u_{\nu'}^*\left(\mathbf{r}_{1^+,\mathrm{c}}\right)\left(-ik_{y,t}+\partial_{y_2}\right)u_{\alpha'}\left(\mathbf{r}_{1,\mathrm{c}}\right)u_{\beta'}^*\left(\mathbf{r}_{2,\mathrm{c}}\right)\\
&= e^{i\left(\mathbf{k}_\mathrm{t}-\mathbf{k}_\mathrm{t}^{'}\right)\left(\mathbf{r}_{1,\mathrm{t}}-\mathbf{r}_{2,\mathrm{t}}\right)}\left\{\left(ik_y+ik_y^{'}\right)u_{\mu'}\left(\mathbf{r}_{2,\mathrm{c}}\right)u_{\nu'}^*\left(\mathbf{r}_{1,\mathrm{c}}\right)\left(-ik_y+\partial_{y_2}\right)u_{\alpha'}\left(\mathbf{r}_{1,\mathrm{c}}\right)u_{\beta'}^*\left(\mathbf{r}_{2,\mathrm{c}}\right)\right.\\
&+ u_{\mu'}\left(\mathbf{r}_{2,\mathrm{c}}\right)u_{\nu'}^*\left(\mathbf{r}_{1,\mathrm{c}}\right)\left(-ik_y+\partial_{y_2}\right)\left[\partial_{y_1}u_{\alpha'}\left(\mathbf{r}_{1,\mathrm{c}}\right)\right]u_{\beta'}^*\left(\mathbf{r}_{2,\mathrm{c}}\right)\\
&\left.-u_{\mu'}\left(\mathbf{r}_{2,\mathrm{c}}\right)\left[\partial_{y_1}u_{\nu'}^*\left(\mathbf{r}_{1,\mathrm{c}}\right)\right]\left(-ik_y+\partial_{y_2}\right)u_{\alpha'}\left(\mathbf{r}_{1,\mathrm{c}}\right)u_{\beta'}^*\left(\mathbf{r}_{2,\mathrm{c}}\right)\right\}.
\end{aligned}
\tag{E.5}
$$

The momentum matrix is defined as

$$
p_{\alpha,\beta}^i=\frac{1}{V_\mathrm{c}}\int d^3r_\mathrm{c}u_{\alpha'}^*\left(\mathbf{r}_\mathrm{c}\right)\frac{\hbar}{i}\partial_i u_{\beta'}\left(\mathbf{r}_\mathrm{c}\right)\delta_{\sigma_\alpha,\sigma_\beta}.
\tag{E.6}
$$

The above formula for y component gives

$$
\frac{1}{V_\mathrm{c}}\int d^3r_\mathrm{c}u_\alpha^*\left(\mathbf{r}_\mathrm{c}\right)\partial_y u_\beta\left(\mathbf{r}_\mathrm{c}\right)\delta_{\sigma_\alpha,\sigma_\beta}=\frac{i}{\hbar}p_{\alpha,\beta}^y=\frac{i}{\hbar}p_{\alpha,\beta},
\tag{E.7}
$$

$$
\frac{1}{V_\mathrm{c}}\int d^3r_\mathrm{c}u_\alpha\left(\mathbf{r}_\mathrm{c}\right)\partial_y u_\beta^*\left(\mathbf{r}_\mathrm{c}\right)\delta_{\sigma_\alpha,\sigma_\beta}=-\frac{i}{\hbar}p_{\alpha,\beta}^*.
\tag{E.8}
$$

With the above definitions of the momentum matrix, the formula (E.5) averaged over the primitive cell is

$$\begin{aligned}
&\sum_{\sigma_1,\sigma_2}\int d^2\left(r_{1,\mathrm{t}}-r_{2,\mathrm{t}}\right)e^{-i\mathbf{q}_\mathrm{t}\left(\mathbf{r}_{1,\mathrm{t}}-\mathbf{r}_{2,\mathrm{t}}\right)}\frac{1}{V_\mathrm{c}^2}\int d^3r_{1,\mathrm{c}}\int d^3r_{2,\mathrm{c}}\delta_{\sigma_1,\sigma_\alpha}\delta_{\sigma_1,\sigma_\nu}\delta_{\sigma_2,\sigma_\beta}\delta_{\sigma_2,\sigma_\mu}X\\
&=\int d^2\left(r_{1,\mathrm{t}}-r_{2,\mathrm{t}}\right)e^{i\left(\mathbf{k}_\mathrm{t}-\mathbf{k}_\mathrm{t}^{'}-\mathbf{q}_t\right)\left(\mathbf{r}_{1,\mathrm{t}}-\mathbf{r}_{2,\mathrm{t}}\right)}\left(\left(ik_y+ik_y^{'}\right)\left(-ik_y-\frac{i}{\hbar}p^*_{\mu,\beta}\right)\delta_{\nu,\alpha}\right.\\
&\left.+\left(-ik_y-\frac{i}{\hbar}p^*_{\mu,\beta}\right)\frac{i}{\hbar}p_{\nu,\alpha}-\left(-ik_y-\frac{i}{\hbar}p^*_{\mu,\beta}\right)\left(-\frac{i}{\hbar}p^*_{\alpha,\nu}\right)\right)\\
&=\delta_{\mathbf{k}_\mathrm{t}^{'},\mathbf{k}_\mathrm{t}-\mathbf{q}_\mathrm{t}}\left(-ik_y-\frac{i}{\hbar}p^*_{\mu,\beta}\right)\left(\left(ik_y+ik_y^{'}\right)\delta_{\nu,\alpha}+\frac{i}{\hbar}p_{\nu,\alpha}+\frac{i}{\hbar}p_{\nu,\alpha}\right). \qquad \text{(E.9)}
\end{aligned}$$

Plugging Eqs. (E.3), and (E.9), into Eq. (E.4) gives

$$\begin{aligned}
&P^{\mathrm{av}}\left(z_1,z_2,\mathbf{q}_t,\underline{t}_1-\underline{t}_2\right)=\frac{i\hbar^3e^2\mu_0}{2m^2}\frac{1}{A}\sum_{\mathbf{k}_\mathrm{t}}\sum_{\alpha,\beta,\mu,\nu}\sum_{a,b,m,n}\\
&\times G_{\alpha a,\beta b}\left(\mathbf{k}_\mathrm{t},\underline{t}_1-\underline{t}_2\right)G_{\mu m,\nu n}\left(\mathbf{k}_\mathrm{t}-\mathbf{q}_\mathrm{t},\underline{t}_2-\underline{t}_1\right)w_a\left(z_1\right)w_b^*\left(z_2\right)w_m\left(z_2\right)w_n^*\left(z_1\right)\\
&\times\left(ik_y+\frac{i}{\hbar}p^*_{\mu,\beta}\right)\left(\left(2ik_y+iq_y\right)\delta_{\nu,\alpha}+\frac{2i}{\hbar}p_{\nu,\alpha}\right). \qquad \text{(E.10)}
\end{aligned}$$

As mentioned in the Subsection 4.4.1, the wavelength of the photons in much greater than the wavelength of the quasiparticles and $q_\mathrm{t}\ll k_\mathrm{t}$. Also $p\gg k_y$, so the terms proportional to p^2 in the above formula are dominating. Taking those facts into account, values of $P^{\mathrm{av}}\left(z_1,z_2,\mathbf{q}_\mathrm{t}\right)$ at the nodes $z_1=z_a$, $z_2=z_b$ can be determined from

$$P^{\mathrm{av}}\left(z_a,z_b,\mathbf{q}_\mathrm{t},\underline{t}_1-\underline{t}_2\right)=-\frac{i\hbar e^2\mu_0}{m^2}\frac{1}{A}\sum_{\mathbf{k}_\mathrm{t}}\sum_{\alpha,\beta,\mu,\nu}G_{\alpha a,\beta b}\left(\mathbf{k}_\mathrm{t},\underline{t}_1-\underline{t}_2\right)p^*_{\alpha,\nu}p_{\beta,\mu}G_{\mu b,\nu a}\left(\mathbf{k}_\mathrm{t},\underline{t}_2-\underline{t}_1\right). \qquad \text{(E.11)}$$

The final formula for the lesser and greater polarizations is obtained by fixing the contour branches of $\underline{t}_1$ and $\underline{t}_2$ in Eq. (E.11), applying a temporal Fourier transform and an inverse spatial Fourier transform with respect to $\mathbf{q}_\mathrm{t}$. The final formula is

$$\begin{aligned}
&P^{\mathrm{av},\lessgtr}\left(\mathbf{r}_a,\mathbf{r}_b,\hbar\omega\right)=-\frac{i\hbar e^2\mu_0}{m^2}\delta\left(\mathbf{r}_{a,\mathrm{t}}-\mathbf{r}_{b,\mathrm{t}}\right)\int\frac{dE}{2\pi}\frac{1}{A}\sum_{\mathbf{k}_\mathrm{t}}\sum_{\alpha,\beta,\mu,\nu}G^{\lessgtr}_{\alpha a,\beta b}\left(\mathbf{k}_\mathrm{t},E+\hbar\omega\right)\\
&\times p^*_{\alpha,\nu}p_{\beta,\mu}G^{\gtrless}_{\mu b,\nu a}\left(\mathbf{k}_\mathrm{t},E\right). \qquad \text{(E.12)}
\end{aligned}$$

E.2 Transverse (electron-photon) self-energy

Approximated transverse vertex function from Eq. (E.1) inserted into the general formula for transverse self-energy (3.93) gives

$$\Sigma\left(\underline{1},\underline{2}\right)=i\hbar\int d\underline{3}\int d\underline{4}\sum_{i,j=1}^{3}\left(\frac{i\hbar e}{m}\partial_{i}\left(\underline{1}\right)\right)G\left(\underline{1},\underline{3}\right)\frac{i\hbar e\mu_{0}}{m}\delta\left(\underline{3},\underline{4}\right)\partial_{j}\left(\underline{3}\right)\delta\left(\underline{3},\underline{2}\right)D_{j,i}\left(\underline{4},\underline{1}^{+}\right)$$
$$=-i\hbar\mu_{0}\left(\frac{e\hbar}{m}\right)^{2}\sum_{i,j=1}^{3}\int d\underline{3}\partial_{i}\left(\underline{1}\right)G\left(\underline{1},\underline{3}\right)\partial_{j}\left(\underline{3}\right)\delta\left(\underline{3},\underline{2}\right)D_{j,i}\left(\underline{3},\underline{1}^{+}\right)$$
$$=-i\hbar\mu_{0}\left(\frac{e\hbar}{m}\right)^{2}\sum_{i,j=1}^{3}\int d\underline{3}\partial_{i}\left(\underline{1}\right)G\left(\underline{1},\underline{3}\right)\left(\left[\partial_{j}\left(\underline{3}\right)\delta\left(\underline{3},\underline{2}\right)\right]+\delta\left(\underline{3},\underline{2}\right)\partial_{j}\left(\underline{3}\right)\right)D_{j,i}\left(\underline{3},\underline{1}^{+}\right)$$
$$=-i\hbar\mu_{0}\left(\frac{e\hbar}{m}\right)^{2}\sum_{i,j=1}^{3}\left(-\partial_{i}\left(\underline{1}\right)\left[\partial_{j}\left(\underline{2}\right)G\left(\underline{1},\underline{2}\right)\right]\right.$$
$$\left.-\partial_{i}\left(\underline{1}\right)G\left(\underline{1},\underline{2}\right)\partial_{j}\left(\underline{2}\right)+\partial_{i}\left(\underline{1}\right)G\left(\underline{1},\underline{3}\right)\partial_{j}\left(\underline{2}\right)\right)D_{j,i}\left(\underline{2},\underline{1}^{+}\right)$$
$$=i\hbar\mu_{0}\left(\frac{e\hbar}{m}\right)^{2}\sum_{i,j=1}^{3}\left[\partial_{i}\left(\underline{1}\right)\partial_{j}\left(\underline{2}\right)G\left(\underline{1},\underline{2}\right)\right]D_{j,i}\left(\underline{2},\underline{1}\right). \tag{E.13}$$

Under the assumption that $D_{j,i}\left(\underline{2},\underline{1}\right)=\delta_{i,y}\delta_{j,y}D\left(z_{2},z_{1},\underline{t}_{2}-\underline{t}_{1}\right)$, the right-hand side of Eq. (E.13) is expanded in the basis (4.12)

$$\Sigma\left(\underline{1},\underline{2}\right)=i\hbar\mu_{0}\left(\frac{e\hbar}{m}\right)^{2}\frac{1}{A}\sum_{\mu,m,\nu,n,\mathbf{k}_{\mathrm{t}}}w_{m}\left(z_{1}\right)w_{n}^{*}\left(z_{2}\right)G_{\mu m,\nu n}\left(\mathbf{k}_{\mathrm{t}},\underline{t}_{1}-\underline{t}_{2}\right)$$
$$\times D\left(z_{2},z_{1},\underline{t}_{2}-\underline{t}_{1}\right)\partial_{y_{1}}\partial_{y_{2}}e^{i\mathbf{k}_{\mathrm{t}}\left(\mathbf{r}_{1,\mathrm{t}}-\mathbf{r}_{2,\mathrm{t}}\right)}u_{\mu'}\left(\mathbf{r}_{1,\mathrm{c}}\right)u_{\nu'}^{*}\left(\mathbf{r}_{2,\mathrm{c}}\right)\delta_{\sigma_{1},\sigma_{\mu}}\delta_{\sigma_{2},\sigma_{\nu}}$$
$$=i\hbar\mu_{0}\left(\frac{e\hbar}{m}\right)^{2}\frac{1}{A}\sum_{\mu,m,\nu,n,\mathbf{k}_{\mathrm{t}}}w_{m}\left(z_{1}\right)w_{n}^{*}\left(z_{2}\right)G_{\mu m,\nu n}\left(\mathbf{k}_{\mathrm{t}},\underline{t}_{1}-\underline{t}_{2}\right)D\left(z_{2},z_{1},\underline{t}_{2}-\underline{t}_{1}\right)$$
$$\times\left(ik_{y}+\partial_{y_{1}}\right)\left(-ik_{y}+\partial_{y_{2}}\right)u_{\mu'}\left(\mathbf{r}_{1,\mathrm{c}}\right)u_{\nu'}^{*}\left(\mathbf{r}_{2,\mathrm{c}}\right)\delta_{\sigma_{1},\sigma_{\mu}}\delta_{\sigma_{2},\sigma_{\nu}}. \tag{E.14}$$

Multiplying both sides from the left by $\frac{1}{V_{\mathrm{c}}}\int d^{3}r_{1,\mathrm{c}}u_{\alpha'}^{*}\left(\mathbf{r}_{1,\mathrm{c}}\right)$, $\frac{1}{V_{\mathrm{c}}}\int d^{3}r_{2,\mathrm{c}}u_{\beta'}\left(\mathbf{r}_{2,\mathrm{c}}\right)$,

and setting $\sigma_1 = \sigma_\alpha$, $\sigma_2 = \sigma_\beta$ gives

$$\begin{aligned}
&\frac{1}{A}\sum_{\mu,m,\nu,n,\mathbf{k}_\mathrm{t}} w_m\left(z_1\right) w_n^*\left(z_2\right) \delta_{\mu,\alpha}\delta_{\nu,\beta}\Sigma_{\mu m,\nu n}\left(\mathbf{k}_\mathrm{t}, \underline{t}_1 - \underline{t}_2\right) \\
&= i\hbar\mu_0\left(\frac{e\hbar}{m}\right)^2 \frac{1}{A}\sum_{\mu,m,\nu,n,\mathbf{k}_\mathrm{t}} w_m\left(z_1\right) w_n^*\left(z_2\right) G_{\alpha m,\beta n}\left(\mathbf{k}_\mathrm{t}, \underline{t}_1 - \underline{t}_2\right) \\
&\times D\left(z_2, z_1, \underline{t}_2 - \underline{t}_1\right) \delta_{\sigma_\alpha,\sigma_\mu}\delta_{\sigma_\beta,\sigma_\nu}\left(k_y^2\delta_{\mu',\alpha'}\delta_{\nu',\beta'}\right. \\
&+ \left(\frac{1}{V_\mathrm{c}}\int d^3 r_{1,\mathrm{c}} u_{\alpha'}^*\left(\mathbf{r}_{1,\mathrm{c}}\right)\partial_{y_1} u_{\mu'}\left(\mathbf{r}_{1,\mathrm{c}}\right)\right)\left(\frac{1}{V_\mathrm{c}}\int d^3 r_{2,\mathrm{c}} u_{\beta'}\left(\mathbf{r}_{2,\mathrm{c}}\right)\partial_{y_2} u_{\nu'}^*\left(\mathbf{r}_{2,\mathrm{c}}\right)\right) \\
&+ \delta_{\mu',\alpha'} i k_y\left(\frac{1}{V_\mathrm{c}}\int d^3 r_{2,\mathrm{c}} u_{\beta'}\left(\mathbf{r}_{2,\mathrm{c}}\right)\partial_{y_2} u_{\nu'}^*\left(\mathbf{r}_{2,\mathrm{c}}\right)\right) \\
&\left.-\delta_{\nu',\beta'} i k_y\left(\frac{1}{V_\mathrm{c}}\int d^3 r_{1,\mathrm{c}} u_{\alpha'}^*\left(\mathbf{r}_{1,\mathrm{c}}\right)\partial_{y_1} u_{\mu'}\left(\mathbf{r}_{1,\mathrm{c}}\right)\right)\right) \\
&= i\hbar\mu_0\left(\frac{e\hbar}{m}\right)^2 \frac{1}{A}\sum_{\mu,m,\nu,n,\mathbf{k}_\mathrm{t}} w_m\left(z_1\right) w_n^*\left(z_2\right) G_{\alpha m,\beta n}\left(\mathbf{k}_\mathrm{t}, \underline{t}_1 - \underline{t}_2\right) D\left(z_2, z_1, \underline{t}_2 - \underline{t}_1\right) \\
&\times\left(k_y^2\delta_{\mu,\alpha}\delta_{\nu,\beta} + \frac{p_{\alpha,\mu}p_{\beta,\nu}^*}{\hbar^2} + \delta_{\mu,\alpha}k_y\frac{p_{\beta,\nu}^*}{\hbar} + \delta_{\nu,\beta}k_y\frac{p_{\alpha,\mu}}{\hbar}\right). \qquad \text{(E.15)}
\end{aligned}$$

Similarly as during calculations of the polarization, only terms proportional to p^2 are left. It is also assumed that $D\left(z_2, z_1, \underline{t}_2 - \underline{t}_1\right)$ is constant for z_1 and z_2 inside the device (this approximation is discussed in Subsection 4.4.1) and after multiplying both sides by $\int dz_1 w_a^*\left(z_1\right)$ and $\int dz_2 w_b\left(z_2\right)$, Eq. (E.15) becomes

$$\begin{aligned}
&\sum_{\mu,m,\nu,n} S_{\alpha a,\mu m}\Sigma_{\mu m,\nu n}\left(\mathbf{k}_\mathrm{t}, \underline{t}_1 - \underline{t}_2\right) S_{\nu n,\beta b} = i\hbar\mu_0\left(\frac{e}{m}\right)^2 \\
&\times p_{\alpha a,\mu m} G_{\mu m,\nu n}\left(\mathbf{k}_\mathrm{t}, \underline{t}_1 - \underline{t}_2\right) p_{\nu n,\beta b} D\left(\underline{t}_2 - \underline{t}_1\right), \qquad \text{(E.16)}
\end{aligned}$$

where

$$p_{\alpha a,\mu m} = p_{\alpha,\mu}\int dz w_a^*\left(z\right) w_b\left(z\right). \qquad \text{(E.17)}$$

Applying of the temporal a Fourier transform to lesser and greater component of transverse self-energy in Eq. (E.16) gives

$$\begin{aligned}
&\sum_{\mu,m,\nu,n} S_{\alpha a,\mu m}\Sigma_{\mu m,\nu n}^{\lessgtr}\left(\mathbf{k}_\mathrm{t}, E\right) S_{\nu n,\beta b} = i\hbar\mu_0\left(\frac{e}{m}\right)^2 \\
&\times\sum_{\mu,m,\nu,n}\int_{-\infty}^{+\infty}\frac{d\left(\hbar\omega\right)}{2\pi} p_{\alpha a,\mu m} G_{\mu m,\nu n}^{\lessgtr}\left(\mathbf{k}_\mathrm{t}, E + \hbar\omega\right) p_{\nu n,\beta b} D^{\gtrless}\left(\hbar\omega\right). \qquad \text{(E.18)}
\end{aligned}$$

The above formula can be also expressed in a compact matrix notation

$$\mathbf{\Sigma}'^{\lessgtr}(\mathbf{k}_{\mathrm{t}}, E) = \mathbf{S}\mathbf{\Sigma}^{\lessgtr}(\mathbf{k}_{\mathrm{t}}, E)\,\mathbf{S} = i\mu_0 \left(\frac{e}{m}\right)^2 \int_{-\infty}^{+\infty} \frac{d(\hbar\omega)}{2\pi} D^{\gtrless}(\hbar\omega)\,\mathbf{p}\mathbf{G}^{\lessgtr}(\mathbf{k}_{\mathrm{t}}, E+\hbar\omega)\,\mathbf{p}. \tag{E.19}$$

By taking a temporal Fourier transform of Eq. (3.101) it can be shown quite generally that

$$D^{\gtrless}_{i,j}(\mathbf{r}_1, \mathbf{r}_2, \hbar\omega) = D^{\lessgtr}_{j,i}(\mathbf{r}_2, \mathbf{r}_1, -\hbar\omega), \tag{E.20}$$

and Eq. (E.19) can be written as

$$\mathbf{\Sigma}'^{\lessgtr}(\mathbf{k}_{\mathrm{t}}, E) = i\mu_0 \left(\frac{e}{m}\right)^2 \int_{0}^{\infty} \frac{d(\hbar\omega)}{2\pi} \mathbf{p}\left(D^{\gtrless}(\hbar\omega)\,\mathbf{G}^{\lessgtr}(\mathbf{k}_{\mathrm{t}}, E+\hbar\omega) - D^{\lessgtr}(\hbar\omega)\,\mathbf{G}^{\lessgtr}(\mathbf{k}_{\mathrm{t}}, E-\hbar\omega)\right)\mathbf{p}. \tag{E.21}$$

Appendix F

List of publications

F.1 Peer reviewed publications

1. J. M. Miloszewski, M. S. Wartak, P. Weetman, and O. Hess, Analysis of linewidth enhancement factor for quantum well structures based on InGaAsN/GaAs material system, *J. Appl. Phys.* 30:063102, 2009

2. J. M. Miloszewski, M. S. Wartak, and P. Weetman, Broad gain spectra of single and multiple InGaAsN quantum well systems, *Phys. Status Solidi B* 246:1697, 2009

3. J. M. Miloszewski and M. S. Wartak, Semiconductor laser simulations using non-equilibrium Green's functions, *J. App. Phys.* 111:053104, 2012

F.2 Conference proceedings

1. J. M. Miloszewski and M. S. Wartak,One Dimensional Model of Semiconductor Laser Based on Quantum Well Using Non-equilibrium Green's Functions Method, *AIP Conf. Proc.* 1368:121, 2011

Bibliography

[1] N. W. Ashcroft and N. D. Mermin. *Solid State Physics*. Harcourt, 1976.

[2] C. Kittel. *Introduction to Solid State Physics*. Wiley, 7 edition, 1996.

[3] R. Stratton. Diffusion of hot and cold electrons in semiconductor barriers. *Phys. Rev.*, 126:2002–2014, 1962.

[4] R. Stratton. Semiconductor current-flow equations (diffusion an degeneracy). *IEEE Trans. Electron Devices*, 19:1288–1292, 1972.

[5] T. Ohtoshi, K. Yamaguchi, C. Nagaoka, T. Uda, Y. Murayama, and N. Chinone. A two-dimensional device simulator of semiconductor lasers. *Solid State Electron.*, 30:627–638, 1987.

[6] S. Seki, T. Yamanaka, and K. Yokoyama. Two-dimensional numerical analysis of current blocking mechanism in InP buried heterostructure lasers. *J. Appl. Phys.*, 71:3572–3578, 1992.

[7] R. F. Kazarinov and M. R. Pinto. Carrier transport in laser heterostructures. *IEEE J. Quantum Electron.*, 30:49–53, 1994.

[8] M. Gault, P. Mawby, A. R. Adams, and M. Towers. Two-dimensional simulation of constricted-mesa InGaAsP/InP buried-heterostructure lasers. *IEEE J. Quantum Electron.*, 30:1691–1700, 1994.

[9] K. B. Kahen. Two-dimensional simulation of laser diodes in the steady state. *IEEE J. Quantum Electron.*, 24:641–651, 1988.

[10] M. Ueno, S. Asada, and S. Kumashiro. Two-dimensional numerical analysis of lasing characteristics for self-aligned structure semiconductor lasers. *IEEE J. Quantum Electron.*, 26:972–981, 1990.

[11] Z.-M. Li, K. M. Dzurko, A. Delâgé, and S. P. McAlister. Self-consistent two-dimensional model of quantum-well semiconductor lasers: Optimization of a GRIN-SCH SQW laser structure. *IEEE J. Quantum Electron.*, 28:792–803, 1992.

[12] M. Ueno, S. Asada, and S. Kumashiro. Two-dimensional analysis of astigmatism in self-aligned structure semiconductor laser. *IEEE J. Quantum Electron.*, 28:1487–1495, 1992.

[13] G.-L. Tan, N. Bewtra, K. Lee, and J. M. Xu. A two-dimensional nonisothermal finite element simulation of laser diodes. *IEEE J. Quantum Electron.*, 29:822–835, 1993.

[14] S. P. McAlister and Z.-M. Li. Two dimensional simulation of quantum-well lasers. In W.W. Chow and M. Osinski, editors, *Physics and Simulation of Optoelectronic Devices II*, volume 2146 of *Proc. SPIE*, pages 162–173, 1994.

[15] A. Champagne, R. Maciejko, and T. Makino. Enhanced carrier injection efficiency from lateral current injection in multiple-quantum-well DFB lasers. *IEEE Photonics Technol. Lett.*, 8:749–751, 1996.

[16] M. Grupen and K. Hess. Simulation of carrier transport and nonlinearities in quantum-well laser diodes. *IEEE J. Quantum Electron.*, 34:120–140, 1998.

[17] M. A. Alam, M. S. Hybertsen, R. K. Smith, and G. A. Baraff. Simulation of semiconductor quantum well lasers. *IEEE Trans. Electron Devices*, 47:1917–1925, 2000.

[18] B. Witzigmann, M.S. Hybertsen, Jr. C.L. Lewis Reynolds, G. L. Belenky, L. Shterengas, and G.E. Shtengel. Microscopic simulation of the temperature dependence of static and dynamic $1.3\mu m$ multi-quantum-well laser performance. *IEEE J. Quantum Electron.*, 39:120–129, 2003.

[19] K. Yokoyama, T. Yamanaka, and S. Seki. Two-dimensional numerical simulator for multielectrode distributed feedback laser diodes. *IEEE J. Quantum Electron.*, 29:856–863, 1993.

[20] A. D. Sadovnikov, X. Li, and W.-P. Huang. A two-dimensional DFB laser model accounting for carrier transport effects. *IEEE J. Quantum Electron.*, 31:1856–1862, 1995.

[21] J. Piprek, D. I. Babić, and J. E. Bower. Simulation and analysis of 1.55 μm double-fused vertical-cavity lasers. *J. Appl. Phys.*, 81:338–3390, 1997.

[22] D. W. Winston and R. E. Hayes. Optoelectronic device simulation of Bragg reflectors and their influence on surface-emitting laser characteristics. *IEEE J. Quantum Electron.*, 34:707–715, 1998.

[23] M. Streiff, A. Witzig, M. Pfeiffer, P. Royo, and W. Fichtner. A comprehensive VCSEL device simulator. *IEEE J. Sel. Topics Quantum Electron.*, 9:879–891, 2003.

[24] J. Piprek. *Semiconductor Optoelectronic Devices*. Academic Press, 2003.

[25] D. Ahn and S. L. Chuang. The theory of strained-layer quantum-well lasers with bandgap renormalization. *IEEE J. Quantum Electron.*, 30:350–365, 1994.

[26] C. Aversa and K. Iizuka. Gain of TE-TM modes in quantum-well laser. *IEEE J. Q*, 28:1864–1873, 1992.

[27] John P. Loehr. *Physics of Strained Quantum Well Lasers*. Kluwer Acadamic Publishers, 1998.

[28] Crosslight Software Inc. *Crosslight Software General Description*, 1 edition, 2003.

[29] T. B. Bahder. Eight-band $\mathbf{k} \cdot \mathbf{p}$ model of strained zinc-blende crystals. *Phys. Rev. B*, 41:11992, 1990.

[30] S. L. Chuang and C. S. Chang. $\mathbf{k} \cdot \mathbf{p}$ method for strained wurtzite semiconductors. *Phys. Rev. B*, 54:2491–2504, 1996.

[31] S. Tomić, E. P. O'Reilly, R. Fehse, S. J. Sweeney, A. R. Adams, A. D. Andreev, S. A. Choulis, T. J. C. Hosea, and H. Riechert. Theoretical and experimental analysis of 1.3-μm InGaAsN/GaAs lasers. *IEEE J. Sel. Top. Quantum Electron.*, 9:1228–1238, 2003.

[32] C. Caroli, R. Combescot, P. Nozieres, and D. Saint-James. Direct calculation of the tunneling current. *J. Phys. C: Solid State Phys.*, 4:916–929, 1971.

[33] G. Kim and G. B. Arnold. Theoretical study of tunneling phenomena in double-barrier quantum-well heterostructures. *Phys. Rev. B*, 38:3252–3236, 1988.

[34] E. V. Anda and F. Flores. The role of inelastic scattering in resonant tunnelling heterostructures. *J. Phys. Condens. Matter*, 3:9087–9101, 1991.

[35] G. Kim, H.-H. Suh, and E.-H. Lee. Green's-function study of the electron tunneling in a double-barrier heterostructure. *Phys. Rev. B*, 52:2632–2639, 1995.

[36] R. K. Lake, G. Klimeck, R. C. Bowen, and D. Jovanovic. Single and multiband modeling of quantum electron transport through layered semiconductor devices. *J. Appl. Phys.*, 81:7845–7869, 1997.

[37] M. Ogawa, T. Sugano, R. Tominaga, and T. Miyoshi. Multi-band simulation of resonant tunneling diodes with scattering e!ects. *Physica B*, 272:167–170, 1999.

[38] C. Rivas, R. Lake, W. R. Frensley, G. Klimeck, P. E. Thompson, K. D. Hobart, S. L. Rommel, and P. R. Berger. Full band modeling of the excess current in a delta-doped silicon tunnel diode. *J. Appl. Phys.*, 94:5005–5013, 2003.

[39] N. Sergueev, A. A. Demkov, and H. Guo. Inelastic resonant tunneling in C_{60} molecular junctions. *Phys. Rev. B*, 75:233418, 2007.

[40] Z. Ren, R. Venugopal, S. Goasguen, S. Datta, and M. S. Lundstrom. nanoMOS 2.5: A two-dimensional simulator for quantum transport in double-gate MOSFETs. *IEEE Trans. Electron Devices*, 50:1914–1925, 2003.

[41] H. Fitriawan, M. Ogawa, S. Souma, and T. Miyoshi. Quantum electron transport modeling in double-gate MOSFETs based on multiband non-equilibrium Green's function method. *Physica E*, 40:245–248, 2007.

[42] A. Martinez, J. R. Barker, A. Svizhenko, M. P. Anantram, and A. Asenov. The impact of random dopant aggregation in source and drain on the performance of ballistic DG nano-MOSFETs: A NEGF study. *IEEE Trans. Nanotechnol.*, 6:438 – 445, 2007.

[43] M. P. Anantram, M. S. Lundstrom, and D. E. Nikonov. Modeling of nanoscale devices. *Proc. IEEE*, 96:1511–1550, 2008.

[44] N. Seoane, A. Martinez, A. R. Brown, J. R. Barker, and A. Asenov. Current variability in Si nanowire MOSFETs due to random dopants in the source/drain regions: A fully 3-D NEGF simulation study. *IEEE Trans. Electron Devices*, 56:1388–1395, 2009.

[45] A. Maiti, A. Svizhenko, and M. P. Anantram. Electronic transport through carbon nanotubes: Effects of structural deformation and tube chirality. *Phys. Rev. Lett.*, 88:126805, 2002.

[46] D. A. Stewart and F. Leonard. Photocurrents in nanotube junctions. *Phys. Rev. Lett.*, 93:107401, 2004.

[47] J. Guo. A quantum-mechanical treatment of phonon scattering in carbon nanotube transistors. *J. Appl. Phys.*, 98:063519, 2005.

[48] J. Guo, M. A. Alam, and Y. Yoon. Theoretical investigation on photoconductivity of single intrinsic carbon nanotubes. *Appl. Phys. Lett.*, 88:133111, 2006.

[49] L. E. Henrickson. Nonequilibrium photocurrent modeling in resonant tunneling photodetectors. *J. Appl. Phys.*, 91:6273–6281, 2002.

[50] O. Kurniawan, P. Bai, and E. P. Li. Non-equilibrium Green's function calculation of optical absorption in nano optoelectronic devices. In *2010 13th International Workshop on Computational Electronics (IWCE)*, 2009.

[51] S. Steiger. *Modelling Nano-LEDs*. PhD thesis, Swiss Federal Institute of Technology Zurich (ETHZ), 2009.

[52] U. Aeberhard and R. H. Morf. Microscopic nonequilibrium theory of quantum well solar cells. *Phys. Rev. B*, 77:125343, 2008.

[53] F Herzel, K. Henneberger, and W. Vogel. The semiconductor laser linewidth: a Green's function approach. *IEEE J. Quantum Electron.*, 29:2891 – 2897, 1993.

[54] F. Jahnke and W. Koch. Many-body theory for semiconductor microcavity laser. *Phys. Rev. A*, 52:1712–1727, 1995.

[55] M. F. Pereira and K. Henneberger. Green's functions theory for semiconductor-quantum-well laser spectra. *Phys. Rev. B*, 53:16485–16496, 1996.

[56] S.-C. Lee and A. Wacker. Nonequilibrium Green's function theory for transport and gain properties of quantum cascade structures. *Phys. Rev. B*, 66:245314, 2002.

[57] P. Weetman and M. S. Wartak. Wigner function modeling of quantum well semiconductor lasers using classical electromagnetic field coupling. *J. Appl. Phys.*, 93:9562 – 9575, 2003.

[58] P. Weetman and M. S. Wartak. Self-consistent model of a nanoscale semiconductor laser using Green and Wigner functions in two bases. *Phys. Rev. B*, 76:035332, 2007.

[59] R. A. Craig. Perturbation expansion for real-time Green's functions. *J. Math. Phys.*, 9:605–611, 1968.

[60] D. F. DuBois. *Lectures in Theoretical Physics, Kinetic Theory*, volume IX C, chapter 14, pages 469–620. Gordon and Breach, New York, 1967.

[61] V. Korenman. Noneqilibrium quantum statistics; application to the laser. *Ann. Phys.*, 39:72–126, 1966.

[62] L. V. Keldysh. Diagram technique for nonequilibrium processes. *Sov. Phys. JETP*, 20:1018–1026, 1965.

[63] L. I. Schiff. *Quantum Mechanics*. McGraw-Hill, New York, 1968.

[64] M. A. Parker. *Physics of Optoelectronics*. CRC Press, 2005.

[65] W. Shockley and W. T. Read. Statistics of the recombinations of holes and electrons. *Phys. Rev.*, 87:835–842, 1952.

[66] R. N. Hall. Electron-hole recombination in germanium. *Ph*, 87:387, 1952.

[67] N. K. Dutta and R. J. Nelso. The case for Auger recombination in $In_{1-x}Ga_xAs_yP_{1-y}$. *J. Appl. Phys.*, 53:74–92, 1981.

[68] A. Sugimura. Band-to-band Auger effect in long wavelength multinary III-V alloy semiconductor lasers. *IEEE J*, QE-18:352–363, 1982.

[69] A. Haug. Auger recombination in direct-gap semiconductors: band-structure effects. *J. Phys. C: Solid State Phys.*, 16:4159–4172, 1983.

[70] S. L. Chuang. *Physics of Optoelectronic Devices*. John Wiley and Sons, New York, 1995.

[71] C. H. Henry. Theory of spontaneous emission noise in open resonators and its application to lasers and optical amplifiers. *J. Lightwave Technol.*, 4:288–297, 1986.

[72] X. Li. *Optoelectronic Devices: Design, Modeling, and Simulation*. Cambridge University Press, 2009.

[73] L. Coldren and S. Corzine. *Diode Lasers and Photonic Integrated Circuits*. Wiley, 1995.

[74] S. Arahira, Y. Matsui, T. Kunii, S. Oshiba, and Y. Ogawa. Transform-limit ed optical short-pulse generation at high repetition rate over 40 GHz from a monolithic passive mode-locked DBR laser diode. *IEEE Photonics Technol. Lett.*, 5:1362–1365, 1993.

[75] Y. Katoh, T. Kunii, Y. Matsui, H. Wada, T. Kamijoh, and Y. Kawai. DBR laser array for WDM system. *Electron. Lett.*, 29:2195–2197, 1993.

[76] K. David, G. Morthier, P. Vankwikelberge, R. G. Baets, T. Wolf, and B. Borchert. Gain-coupled DFB lasers versus index-coupled and phase-shifted DFB lasers: A comparison based on spatial hole burning corrected yield. *IEEE J. Quantum Electron.*, 27:1714–1723, 1991.

[77] J. E. Carroll, J. Whiteaway, and D. Plumb. *Distributed Feedback Semiconductor Lasers*. The Institution of Engineering and Technology, 1998.

[78] G. P. Bava, P. Debernardi, and L. Fratta. Three-dimensional model for vectorial fields in vertical-cavity surface-emitting lasers. *Phys. Rev. A*, 63:023816, 2001.

[79] *Crosslight Software PICS3D User's Manual*, 2003.

[80] *Silvaco ATLAS User's Manual*, 2012.

[81] *Integrated Systems Engineering DESSIS User's Manual*, 2004.

[82] *RSoft Design Group LaserMOD 3.0 User Guide*, 2008.

[83] http://www.nlcstr.com.

[84] http://www.photond.com.

[85] A. L. Fetter and J. D. Walecka. *Quantum Theory of Many-Particle Systems*. McGraw-Hill, New York, 1971.

[86] H. Bruus and K. Flensberg. *Many-Body Quantum Theory in Condensed Matter Physics: An Introduction*. Oxford University Press, 2004.

[87] P. Danielewicz. Quantum theory of nonequilibrium processes, I. *Annals of Physics*, 152:239–304, 1984.

[88] L. P. Kadanoff and G. Baym. *Quantum Statistical Mechanics : Green's Function Methods in Equilibrium and Non-Equilibrium Problems*. Benjamin, New York, 1962.

[89] T. Fujikawa and H. Arai. Nonrelativistic quantum electrodynamic approach to photoemission theory: I. Basic theoretical framework. *J. Elec. Spec. Rel. Phenom.*, 149:61–86, 2005.

[90] M. Luisier. Quantum transport for nanostructures. Technical report, Eidgenossische Technische Hochschule (ETH) Zurich, 2007.

[91] K. Henneberger and V. May. Nonequilibrium Green's functions and kinetic equations for highly excited semiconductors: I. general considerations. *Physica A*, 138:537–556, 1986.

[92] W. Schafer and M. Wegener. *Semiconductor Optics and Transport Phenomena*. Springer, Berlin, 2002.

[93] J. Schwinger. Brownian motion of a quantum oscillator. *J. Math. Phys.*, 2:407–432, 1961.

[94] R. Binder and W. Koch. Nonequilibrium semiconductor dynamics. *Prog. Quant. Electr.*, 19:307–462, 1995.

[95] M. Wagner. Expansions of nonequilibrium Green's functions. *Phys. Rev. B*, 44:6104–6117, 1991.

[96] V. G. Morozow and G. Ropke. The "mixed" Green's function approach to qua kinetics with initial correlations. *Ann. Phys.*, 278:127–177, 1999.

[97] R. K. Lake and R. R. Pandey. *Handbook of semiconductor nanostructures and nanodevices. Vol.3:Spintronics and nanoelectronics*, chapter Non-Equilibrium Green Functions in Electronic Device Modeling. American Scientific Publishers, 2006.

[98] R. Golizadeh-Mojarad and S. Datta. Nonequilibrium Green's function based models for dephasing in quantum transport. *Phys. Rev. B*, 75:081301–081305, 2007.

[99] U. Aeberhard. *A Microscopic Theory of Quantum Well Photovoltaics*. PhD thesis, Swiss Federal Institute of Technology Zurich (ETHZ), 2008.

[100] M. Koshiba. *Optical Waveguide Theory by the Finite Element Method*. Springer, 1993.

[101] R. Ram-Mohan. *Finite Element and Boundary Element Applications in Quantum Mechanics*. Oxford University Press, 2002.

[102] M. A. Parker. *Solid State and Quantum Theory for Optoelectronics*. CRC Press, 2009.

[103] A. Wacker. Semiconductor superlattices: a model system for nonlinear transport. *Phys. Rep.*, 357:1–111, 2002.

[104] M. Büttiker. Role of quantum coherence in series resistors. *Phys. Rev. B*, 33:3020–3026, 1986.

[105] S. Datta. Nanoscale device modeling: the Green's function method. *Superlattices Microstruct.*, 28:253–278, 2000.

[106] F. Richter, M. Florian, and K. Henneberger. Generalized radiation law for excited media in a nonequilibrium steady state. *Phys. Rev. B*, 78:205114, 2008.

[107] M. S. Stern. Semivectorial polarised finite difference method for optical waveguides with arbitrary index profiles. *IEE Proc.: Optoelectron.*, 135:56–63, 1988.

[108] H. Frohlich. Electrons in lattice fields. *Adv. Phys.*, 3:325–361, 1954.

[109] B. K. Ridley. *Quantum Processes in Semiconductors*. Oxford University Press, 2 edition, 1988.

[110] Jacek M. Miloszewski and Marek S. Wartak. Semiconductor laser simulations using non-equilibrium green's functions. *J. Appl. Phys.*, 111:053104, 2012.

[111] S. Datta. *Electronic Transport in Mesoscopic Systems*. Cambridge University Press, Cambridge, 1995.